NASA TECHNICAL NOTE

NASA TN D-7742

NASA TN D-7742

SUBSONIC WIND-TUNNEL INVESTIGATION OF A TWIN-ENGINE ATTACK AIRPLANE MODEL HAVING NONMETRIC POWERED NACELLES

by Vernard E. Lockwood and Aniello Matarazzo

Langley Research Center
Hampton, Va. 23665

NATIONAL AERONAUTICS AND SPACE ADMINISTRATION • WASHINGTON, D. C. • NOVEMBER 1974

1. Report No.	2. Government Accession No.	3. Recipient's Catalog No.
NASA TN D-7742		

4. Title and Subtitle	5. Report Date
SUBSONIC WIND-TUNNEL INVESTIGATION OF A TWIN-ENGINE ATTACK AIRPLANE MODEL HAVING NONMETRIC POWERED NACELLES	November 1974
	6. Performing Organization Code

7. Author(s)	8. Performing Organization Report No.
Vernard E. Lockwood and Aniello Matarazzo	L-9569
	10. Work Unit No. 760-17-01-10

9. Performing Organization Name and Address	11. Contract or Grant No.
NASA Langley Research Center Hampton, Va. 23665	
	13. Type of Report and Period Covered
12. Sponsoring Agency Name and Address	Technical Note
National Aeronautics and Space Administration Washington, D.C. 20546	14. Sponsoring Agency Code

15. Supplementary Notes

Aniello Matarazzo is associated with Fairchild Republic Company, Farmingdale, Long Island, N.Y.

16. Abstract

A 1/10-scale powered model of a twin-engine attack airplane was investigated in the Langley high-speed 7- by 10-foot tunnel. The study was made at several Mach numbers between 0.225 and 0.75 which correspond to Reynolds numbers, based on the mean aerodynamic chord, of 1.35×10^6 and 3.34×10^6. Unheated compressed air was used for jet simulation in the nonmetric engine nacelles which were located ahead of and above the horizontal stabilizer.

17. Key Words (Suggested by Author(s))		18. Distribution Statement
Subsonic flow	Hinge moments	Unclassified – Unlimited
Mach number effects	Ground effects	
Stability and control	Twin-engine attack airplane	
Nacelle blowing		STAR Category 01

19. Security Classif. (of this report)	20. Security Classif. (of this page)	21. No. of Pages	22. Price*
Unclassified	Unclassified	132	$4.75

*For sale by the National Technical Information Service, Springfield, Virginia 22151

SUBSONIC WIND-TUNNEL INVESTIGATION OF A TWIN-ENGINE ATTACK AIRPLANE MODEL HAVING NONMETRIC POWERED NACELLES

By Vernard E. Lockwood and Aniello Matarazzo*
Langley Research Center

SUMMARY

A 1/10-scale powered model of a twin-engine attack airplane was investigated in the Langley high-speed 7- by 10-foot tunnel. The study was made at several Mach numbers between 0.225 and 0.75 which correspond to Reynolds numbers, based on the mean aerodynamic chord, between 1.35×10^6 and 3.34×10^6. Unheated compressed air was used for jet simulation in the nonmetric engine nacelles which were located ahead of and above the horizontal stabilizer. The aerodynamic coefficients were affected most at the lowest Mach number where the thrust coefficients were the greatest. The lift increments resulting from nacelle blowing were all positive but generally decreased as the elevator deflections became more negative. The pitching-moment increments were usually negative for elevator deflections of 0° and -10°, but were positive for elevator deflections of -15° and -25°. The lateral-directional characteristics were only slightly affected by nacelle blowing. Reducing the model height above the ground plane induced nose-down pitching moments and reduced the trim lift coefficients. Nacelle blowing increased the elevator hinge moments for negative elevator deflections; however, nacelle blowing had less effect on the relationship between the model pitching moments and the elevator hinge moments. Nacelle blowing increased the rudder hinge moments when the sideslip angle and rudder deflection were in directions such that the angle between the rudder chord plane and the free stream was increased.

INTRODUCTION

The National Aeronautics and Space Administration has made a wind-tunnel investigation of a 1/10-scale powered model of a subsonic attack airplane. The principal objective of the power testing was to assess the interference effects of the separately mounted propulsion system on the aerodynamic characteristics of the model. The model was equipped with ejector-type engine nacelles using cold air to simulate jet engine flow characteristics. Since the nacelles were supported rigidly and independently from the rest of

*Fairchild Republic Company, Farmingdale, Long Island, N.Y.

the model, thrust measurements could be obtained only by wake survey methods. The maximum thrust coefficients based on such measurements varied from approximately 0.91 at the lowest Mach number to 0.08 at the highest Mach number. Longitudinal stability and control characteristics were obtained from measurements made over an angle-of-attack range which varied from -4° to as high as 17°. Directional stability and control characteristics were obtained from measurements made over a similar angle-of-attack range at sideslip angles of 9° and -9° for the lowest Mach number only.

In the high-lift configuration with trailing-edge flaps deflected 30° and landing gear attached to the model, data were obtained both with and without the ground plane. The ground plane was simulated by installation of a board beneath the model which divided the tunnel test section. With the ground plane in place, the tests were made with the angle of attack held fixed and the model height and elevator deflection varied.

The tests were made in the Langley high-speed 7- by 10-foot tunnel over a Mach number range from 0.225 to 0.75 which corresponds to a variation in Reynolds number based on the wing mean aerodynamic chord from 1.35×10^6 to 3.34×10^6. In addition to the usual six-component balance measurements, elevator and rudder hinge-moment measurements were taken. All data are presented in coefficient form.

SYMBOLS

The coefficients of forces and moments are referred to the stability-axis system. The model moments are referred to a point located on the plane of symmetry longitudinally at 0.25 of the mean aerodynamic chord and vertically at 0.0918 of the mean aerodynamic chord below the model reference line. Measurements and calculations were made in the U.S. Customary Units. They are presented herein in the International System of Units (SI) with the equivalent values given parenthetically in the U.S. Customary Units. The symbols used in this paper are defined as follows:

b	wing span
$\bar{c}$	mean aerodynamic chord
$\bar{c}_e$	elevator moment arm
$\bar{c}_r$	rudder moment arm
C_D	drag coefficient, $\frac{\text{Drag}}{qS}$

$C_{h,e}$ elevator hinge-moment coefficient, $\frac{\text{Elevator hinge moment}}{2\bar{c}_e S_e q_\infty}$

$C_{h,r}$ rudder hinge-moment coefficient, $\frac{\text{Rudder hinge moment}}{2\bar{c}_r S_r q_\infty}$

C_L lift coefficient, $\frac{\text{Lift}}{Sq_\infty}$

$C_{L,trim}$ trim lift coefficient

C_l rolling-moment coefficient, $\frac{\text{Rolling moment}}{Sbq_\infty}$

C_m pitching-moment coefficient, $\frac{\text{Pitching moment}}{S\bar{c}q_\infty}$

C_n yawing-moment coefficient, $\frac{\text{Yawing moment}}{Sbq_\infty}$

$C_{p,ne}$ nacelle exit static-pressure coefficient, $\frac{p_{ne} - p_\infty}{q_\infty}$

C_T gross thrust coefficient of both nacelles, $\left(\frac{2q_{ne}}{q_\infty} + C_{p,ne}\right)\frac{S_{ne}}{S}$

C_Y side-force coefficient, $\frac{\text{Side force}}{Sq_\infty}$

h distance between main wheels and the ground plane with tunnel inoperative

i_n nacelle incidence, positive nose up, deg

M free-stream Mach number

p_{ne} nacelle exit static pressure

$p_{ne,t}$ nacelle exit total pressure

p_∞ free-stream static pressure

q_{ne} nacelle exit dynamic pressure

q_∞ free-stream dynamic pressure

S model reference area

S_e elevator area aft of hinge line

S_{ne} nacelle exit area

S_{ni} nacelle inlet area

S_r rudder area aft of hinge line

α angle of attack of model reference line, deg

β angle of sideslip, deg

γ ratio of specific heats for air, 1.4

δ_e elevator deflection, positive trailing edge down, deg

δ_f flap deflection, positive trailing edge down, deg

δ_r rudder deflection, positive trailing edge to the left, deg

MODEL DESCRIPTION

The model used for this investigation was a 1/10-scale version of a close air support aircraft. Drawings showing dimensions and photographs of the model mounted in the Langley high-speed 7- by 10-foot tunnel are presented in figures 1 to 4; additional dimensions are presented in table I. The model was sting supported by means of a six-component balance. The nonmetric nacelles had air ejectors which were supplied with compressed air through an overhead strut assembly as shown in figure 1. For the ground-effect studies a plywood board spanned the tunnel and was supported by brackets as shown in figure 4.

The model had a low wing with an aspect ratio of 6.0 and a taper ratio of 0.69. The wing had an NACA 6716 airfoil section from the root to 34.2 percent of the semispan from which it varied linearly to an NACA 6713 airfoil section at the tip. In addition, the wing had pylons and landing gear pods as shown in figures 1 and 3. For the landing and takeoff configurations the model used single slotted extensible flaps deflected 30° and landing gear as shown in figures 4(a) and 4(b).

The tail had a horizontal stabilizer and remotely controlled elevator endplated by fins with an adjustable rudder. The right elevator and rudder had electrical strain gages to measure the control surface hinge moments.

The powered nacelles were positioned between the wing and the horizontal tail and were attached to an overhead strut assembly with a pylon as shown in figure 1. A small gap separated the pylon from the fuselage to prevent contact.

Although the ejectors used to simulate the engine flow were similar to those illustrated in figure 1 of reference 1, they were larger and employed 76 nozzles in place of the 177 smaller ones shown in the illustration. The three air passages in the strut for each engine or a total of six supplied air to a common opening in the nacelle support. High pressure unheated air was brought with flexible hoses through the slot openings in the floor of the test section to the overhead sting as shown in figures 3 and 4. Throttle valves attached to the main supply line in the sphere surrounding the test section balanced the flow to the two ejectors, and a valve placed in the single line set the operating level of the ejectors. A pressure tap in each ejector plenum monitored the pressure level in the nacelle. In addition, an eight-tube manifold total-pressure rake indicated pressure at the nacelle exit (see fig. 4(b)). A 20-tube survey rake which contained both static- and total-pressure tubes was utilized to measure the pressures in the thrust calibration since the overall design made direct thrust measurements impractical.

TEST CONDITIONS

The test conditions are presented in the following table:

Mach number	Dynamic pressure		Average stagnation temperature		Reynolds number
	Pa	lb/ft^2	K	^oR	
0.225	3 496.7	73.03	284	511	1.352×10^6
.45	12 549.8	262.11	294	529	2.420
.60	20 135.4	420.54	299	539	2.934
.70	25 188.2	526.07	308	555	3.146
.73	26 611.2	555.79	321	578	3.063
.75	27 620.0	576.86	303	545	3.344

The Reynolds number is based on the mean aerodynamic chord: the lower Reynolds number noted in the table for $M = 0.73$, as compared with $M = 0.70$, results from a higher tunnel operating temperature.

In order to insure turbulent flow in the boundary layer, a 0.254-cm (0.10-in.) wide strip of No. 90 carborundum grains was placed 2.54 cm (1 in.) behind the leading edge of all surfaces. For the fuselage and landing gear pods, the grit was placed 3.81 cm (1.50 in.) aft of the nose. A discussion of transition fixing on the model for testing is given in reference 2. The tests without the ground plane were made by varying the angle of attack at

fixed control surface deflection and constant thrust values. When the model was tested in the presence of the ground plane, the angle of attack was held constant and the height of the model and the elevator deflections were varied.

MEASUREMENTS AND CORRECTIONS

The model was equipped with a six-component strain-gage balance for measuring the forces and moments. The nacelle was supported independently as shown in figure 3(b); consequently, the forces and moments on the nacelle are not included in the measured model data. An accelerometer was installed in the nose of the model for measuring the pitch angle directly. The sideslip angles were obtained by offsetting the sting coupling angles of 9° and -9°. No corrections were applied to the sideslip angle for deflection of the sting and balance under load.

A single static-pressure tube measured the difference in static pressure between the base of the model and the free stream, and this difference in static pressure was used to adjust the axial force to a free-stream condition.

Jet-boundary corrections calculated by the method presented in reference 3 were applied to the data obtained without the ground plane. The corrections to angle of attack and drag coefficient are listed as follows:

$$\alpha_{corrected} = \alpha_{measured} - 0.274C_L$$

$$C_{D,corrected} = C_{D,measured} - 0.00473C_L^2$$

The principal objective of the power testing was to assess the interference effects of the fuselage-mounted propulsion system on the aerodynamic characteristics of the airplane. The thrust coefficient is the accepted correlating parameter since it relates the exiting momentum of the propulsion system to the free-stream momentum. The gross thrust coefficient is defined as

$$C_T = \left(\frac{2q_{ne}}{q_\infty} + C_{p,ne}\right)\frac{S_{ne}}{S}$$

where the nacelle exit dynamic pressure is measured by a total-pressure rake installed for the calibration. Because of the design of the nacelle support system, direct thrust measurements were impractical. The calibration of the right and left nacelles was made with the tunnel in operation at $M = 0.225$ to prevent frost from forming inside the ejector.

By use of the compressible flow equations, the gross thrust coefficient may also be written in terms of the measurable jet exit conditions as

$$C_T = \frac{4S_{ne}}{(\gamma - 1)SM_\infty^2}\left[\left(\frac{p_{ne,t}}{p_\infty}\right)^{\frac{\gamma-1}{\gamma}}\left(\frac{p_{ne}}{p_\infty}\right)^{\frac{1}{\gamma}} - \left(\frac{\gamma + 1}{2\gamma}\right)\left(\frac{p_{ne}}{p_\infty}\right) - \frac{\gamma - 1}{2\gamma}\right]$$

The gross thrust coefficient is a function of the Mach number squared, the ratio of exit total pressure to free-stream static pressure, and the ratio of exit static pressure to free-stream static pressure. For subsonic exit velocities, the static-pressure ratio is taken to be 1; therefore, the thrust coefficient can be computed from the measured nacelle exit total pressure and free-stream static pressure. The result of this computation is shown by the broken line in figure 5. There is good agreement between the two methods of determining thrust coefficient.

The range of thrust coefficients obtained at each Mach number is shown in figure 6. The expected full-scale gross thrust coefficient at various flight conditions are included for comparison. As may be seen from this figure, the investigation encompassed a major part of the airplane flight envelope. The minimum values shown in figure 6 and in the data figures correspond to the momentum in the free stream minus ejector losses.

PRESENTATION OF RESULTS

The data obtained in the investigation are presented in figures 5 to 34, and the following table summarizes these data:

DISCUSSION OF RESULTS

The basic purpose of this investigation was to determine the effect of nacelle blowing on the model characteristics. Since the model was equipped with nonmetric nacelles, the induced effects on the model were of primary interest. The gross thrust coefficient C_T

is used as the blowing parameter. The relationship between values obtained with a 1/10-scale model and those of the full-scale airplane for the maximum thrust condition at various altitudes are shown in figure 6. The airplane idling thrust condition has also been included.

Longitudinal Aerodynamic Characteristics

Flaps neutral.- The pitching-moment data with the flaps in the neutral position shown in figures 7 to 11 indicate that most of the effect of nacelle blowing is dependent on the elevator deflection. These effects are probably also a function of the horizontal-tail incidence which was kept constant at -5° for this investigation. Since the maximum change in the pitching-moment characteristics occurred at low speeds where the thrust coefficients are the greatest, this discussion is restricted to the results obtained at $M = 0.225$. Power induces a negative pitching-moment increment at $\delta_e = 0^{\circ}$ and a positive pitching-moment increment at $\delta_e = -15^{\circ}$. The net result is an increase in elevator effectiveness $C_{m_{\delta e}}$.

A plot of the ratio of $C_{m_{\delta_e}}$ with power to $C_{m_{\delta_e}}$ without power is shown in figure 29 for $C_L \approx 0.5$. The increase in elevator effectiveness is directly proportional to the increase in thrust coefficient and relatively independent of Mach number. Data obtained with the flaps down also show similar increases in elevator effectiveness (fig. 29).

30° flap setting.- Aerodynamic characteristics obtained with various amounts of blowing and elevator deflections at nacelle incidences of 4° and 2° are presented in figures 17 and 18, respectively. Incremental lift, drag, and pitching-moment coefficients obtained from figure 17 where $i_n = 4^{\circ}$ are shown in figure 30 as a function of thrust coefficient for angles of attack of 0° and 10°. The drag increments may be either positive or negative depending on the angle of attack and the elevator deflection. At all elevator deflections the lift-coefficient increments are positive, but as the elevator is deflected negatively (upward into the engine exhaust), the lift generally decreases both with elevator deflection and thrust coefficient. The pitching-moment increments which are negative at $\delta_e = 0^{\circ}$ progressively become more positive as the elevator deflection is increased to -25°. This change in the sign of the pitching-moment increments plus the reduction in lift increments probably was a result of reduced air circulation over the horizontal tail. In addition, the engine efflux may also cause a reaction on the elevator. Both conditions would produce greater trim lift coefficients. The increased effectiveness of the elevator to trim ($\delta_e = -25^{\circ}$) with power is illustrated in figure 31, where $C_{L,trim}$ is increased from 1.17 to 2.03 (or a lift increment of 0.86) with an increase in C_T from 0.03 to 0.61. A change of nacelle incidence to 2° reduced $C_{L,trim}$ from 2.03 to 1.73 at C_T of 0.6. The $C_{L,trim}$ values quoted are with the nonmetric nacelle. With the nacelle attached,

however, the trim lift coefficients may be entirely different because of the lift, drag, and thrust forces transmitted from the nacelle.

30° flap setting in ground effect.- The effects of nacelle blowing in the presence of a ground plane are presented in figure 19 for a limited angle-of-attack range and in figure 20 for the range of elevator deflections at $\alpha = 0^{\circ}$. The power effects on the lift and the pitching-moment coefficients are similar to those obtained without the ground plane. For example, blowing induces a positive lift increment and a negative pitching-moment increment at $\delta_e = 0^{\circ}$, whereas with $\delta_e = -25^{\circ}$ the lift increments are substantially reduced and the pitching-moments increments become more positive resulting in higher trim lift coefficients. Generally, decreasing the model height induces nose-down pitching moments as shown in figures 20 and 32 and thereby reduces the trim lift coefficients (fig. 33). With the thrust coefficient at a value of 0.61 and $\delta_e = -25^{\circ}$, $C_{L,trim}$ was reduced from 2.03 without ground plane to 1.25 at $h/b = 0$. Power-off data likewise show a large reduction in trim lift coefficient with decreased height.

Lateral Stability and Control

The data obtained with the model in sideslip and with the rudder deflected show no significant effects on the rolling- and yawing-moment characteristics when the thrust coefficient was varied.

Control Hinge-Moment Characteristics

The elevator hinge-moment characteristics obtained through the Mach number range for $\delta_f = 0^{\circ}$ are presented in figure 23. The data indicate that the maximum power effects occur at the lowest Mach numbers which correspond to the highest thrust coefficient. These data in conjunction with those obtained with flaps deflected (figs. 24 and 25) show that power reverses the sign of the elevator hinge moments between $\delta_e = 0^{\circ}$ and $\delta_e = -10^{\circ}$. In addition, the magnitude of the power effect increases and the elevator deflection is increased to -25°. A summary plot showing C_m as a function of $C_{h,e}$ for several thrust coefficients and model heights is presented in figure 34. These data correspond to the various elevator deflections at $\alpha \approx 0^{\circ}$. The effect of power on the relationship of $C_{h,e}$ to C_m appears to be relatively small; there is, however, a tendency for the elevator hinge moments to become more positive for a given pitching moment as the model height is reduced.

The power effects on the rudder hinge moments were relatively small compared with the hinge moments resulting from rudder deflection as shown in figure 28. Nacelle blowing increased the magnitude of the hinge moments when the sideslip angle and rudder deflection were in directions such that the angle between the rudder chord plane and the free stream was increased.

CONCLUSIONS

A 1/10-scale powered model of a twin-engine attack airplane was studied in the Langley high-speed 7- by 10-foot tunnel over a Mach number range from 0.225 to 0.75. Two nonmetric air ejector engines were used to simulate the efflux from jet engines. The investigation indicated the following conclusions:

1. As might be expected, the major effect on the aerodynamic coefficients from nacelle blowing occurred at the lowest Mach number where the thrust coefficient was the greatest.

2. At the higher thrust coefficients, the lift increments were all positive but were generally less for negative elevator deflections than for zero deflection.

3. The drag increments were either positive or negative depending on the angle of attack and the elevator deflection.

4. The pitching-moment increments were generally negative for 0° and -10° elevator deflections and positive for elevator deflections of -15° and -25°. An increase in the thrust coefficient from 0.03 to 0.61 increased the trim lift coefficient by a lift increment 0.86 with an elevator deflection of -25°.

5. Reducing the model height above a ground plane induced nose-down pitching moments and thereby decreased the trim lift coefficients.

6. Power generally had only minor effects on the rolling moments, yawing moments, and side forces with the model in sideslip and with the rudder deflected.

7. Power increased the elevator hinge moments for negative elevator deflections; however, there was little effect on the relationship between model pitching moments and the elevator hinge moments.

8. Power increased the rudder hinge moments when the sideslip angle and rudder deflection were in directions such that the angle between the rudder chord plane and the free stream was increased.

Langley Research Center,
National Aeronautics and Space Administration,
Hampton, Va., August 5, 1974.

Page Intentionally Left Blank

REFERENCES

1. Margason, Richard J.; and Gentry, Garl L.: Static Calibration of an Ejector Unit for Simulation of Jet Engines in Small-Scale Wind-Tunnel Models. NASA TN D-3867, 1967.

2. Braslow, Albert L.; Hicks, Raymond M.; and Harris, Roy V., Jr.: Use of Grit-Type Boundary-Layer-Transition Trips on Wind-Tunnel Models. NASA TN D-3579, 1966.

3. Wright, Ray H.; and Barger, Raymond L.: Wind-Tunnel Lift Interference on Sweptback Wings in Rectangular Test Sections With Slotted Top and Bottom Walls. NASA TR R-241, 1966.

TABLE I.- MODEL GEOMETRY

Wing:		
Reference area, m^2 (ft^2)	0.4459	(4.80)
Span, m (ft)	1.6368	(5.37)
Aspect ratio	6.0	
Taper ratio	0.69	
Dihedral angle, deg, for –		
0 to 0.342b/2	0	
0.342b/2 to 1.0b/2	7	
Root chord, m (ft)	0.2944	(0.966)
Tip chord, m (ft)	0.2094	(0.687)
Mean aerodynamic chord, m (ft)	0.2764	(0.907)
Incidence, deg	-1.0	
Geometric twist	0	
Leading-edge sweep angle, deg, for –		
0 to 0.342b/2	0	
0.342b/2 to 1.0b/2	5.75	
Quarter-chord sweep angle, deg, for –		
0 to 0.342b/2	0	
0.342b/2 to 1.0b/2	3.2	
Airfoil section –		
Root to 0.342b/2	NACA 6716	
Tip	NACA 6713	
Flaps:		
Type	Single slotted extensible	
Total area, m^2 (ft^2)	0.0817	(0.88)
Inboard location, fraction of b/2	0.118	
Outboard location, fraction of b/2	0.612	
Ratio of flap chord to wing chord for –		
0.118b/2 to 0.342b/2	0.35	
0.612	0.34	
Fuselage:		
Frontal area, m^2 (ft^2)	0.0232	(0.25)
Length, m (ft)	1.582	(5.19)
Depth (maximum), m (ft)		
Without canopy	0.177	(0.58)
With canopy	0.213	(0.70)
Width (maximum), m (ft)	0.134	(0.44)
Balance chamber area, m^2 (ft^2)	0.00424	(0.0456)

TABLE I.- MODEL GEOMETRY – Concluded

Horizontal tail:		
Area, m^2 (ft^2) –		
Theoretical	0.1096	(1.18)
Exposed	0.0873	(0.94)
Span, m (ft)	0.5730	(1.88)
Aspect ratio	3.00	
Taper ratio	1.0	
Incidence, deg	-5.0	
Dihedral, deg	0	
Chord, m (ft)	0.1917	(0.6292)
Tail length (0.25 wing M.A.C. to 0.25 tail M.A.C.), m (ft)	0.6782	(2.225)
Quarter-chord sweep angle, deg	0	
Airfoil section	NACA $64_{(112)}$A013	
Elevator hinge line, % tail chord	70	
Sweep of elevator hinge line, deg	0	
Elevator area aft of hinge line (per side), m^2 (ft^2)	0.0132	(0.1422)
Centroid of elevator area (aft of hinge line), m (ft)	0.0287	(0.0943)
Elevator moment area (per side), m^3 (ft^3)	0.000380	(0.0134)
Vertical tail:		
Area (total), m^2 (ft^2)	0.0975	(1.05)
Span, m (ft)	0.305	(1.0)
Aspect ratio	1.89	
Taper ratio	0.61	
Root chord, m (ft)	0.2121	(0.696)
Tip chord, m (ft)	0.1295	(0.425)
Mean aerodynamic chord, m (ft)	0.1786	(0.586)
Airfoil section –		
Root	NACA $64_{(112)}$A013	
Tip	NACA 64_1A012	
Tail length (0.25 wing M.A.C. to 0.25 tail M.A.C.), m (ft)	0.6730	(2.208)
Leading-edge sweep angle, deg	12.0	
Quarter-chord sweep angle, deg	7.0	
Rudder hinge line (% V.T. chord)	77.5	
Rudder area aft of hinge line (per side), m^2 (ft^2)	0.0102	(0.1104)
Centroid of rudder area to hinge line, m (ft)	0.0198	(0.0651)
Moment area (per side), m^3 (ft^3)	0.000204	(0.0072)
Wetted areas:		
Fuselage, m^2 (ft^2)	0.641	(6.90)
Wing, m^2 (ft^2)	0.777	(8.36)
Gear pods, m^2 (ft^2)	0.078	(0.84)
Horizontal tail, m^2 (ft^2)	0.186	(2.00)
Vertical tail, m^2 (ft^2)	0.186	(2.00)
Store pylon, m^2 (ft^2)	0.116	(1.25)
Nacelle:		
Inlet area, m^2 (ft^2)	0.00535	(0.0576)
Exit area, m^2 (ft^2)	0.00558	(0.0601)
Inlet diameter, m (ft)	0.0826	(0.271)
Exit diameter, m (ft)	0.084	(0.277)
Length (along axis of nozzle), m (ft)	0.331	(1.085)
Outside diameter (ellipse), m (ft) –		
Vertical plane	0.149	(0.489)
Horizontal plane	0.141	(0.464)

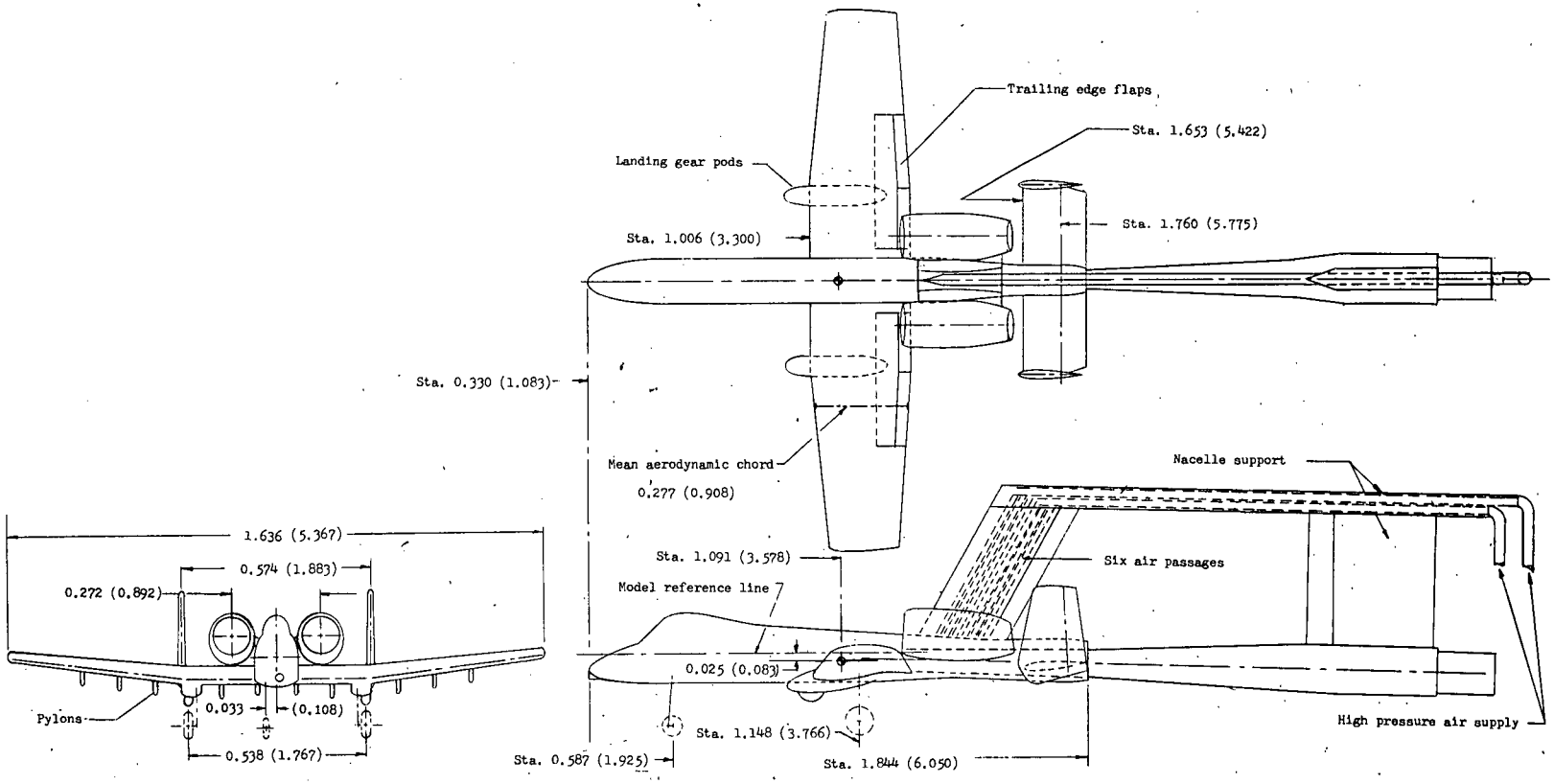

Figure 1.- Three-view drawing of test configuration. Dimensions are in meters (feet).

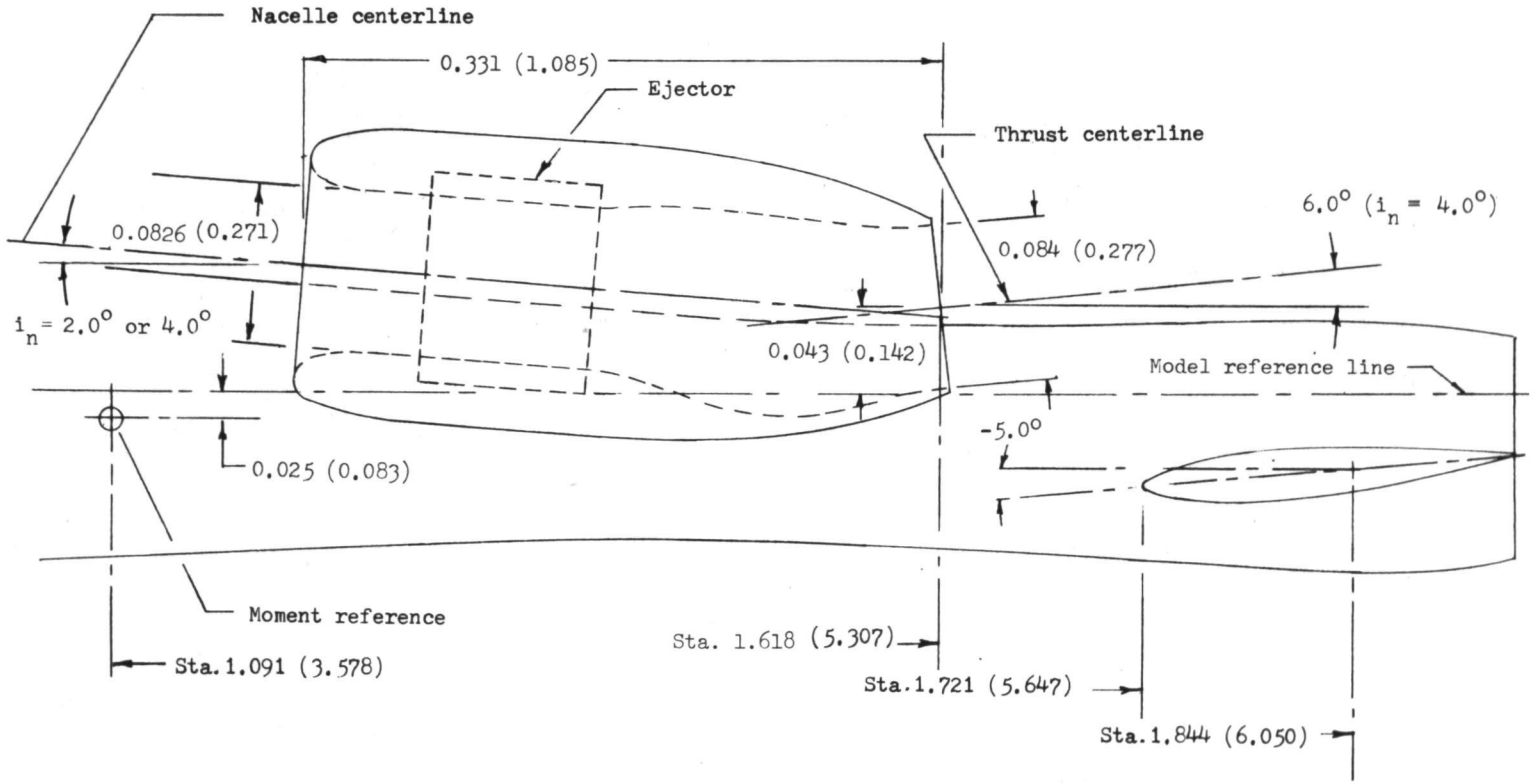

Figure 2.- Drawing showing relationship of horizontal tail, engine nacelle, and model moment reference. Dimensions are in meters (feet).

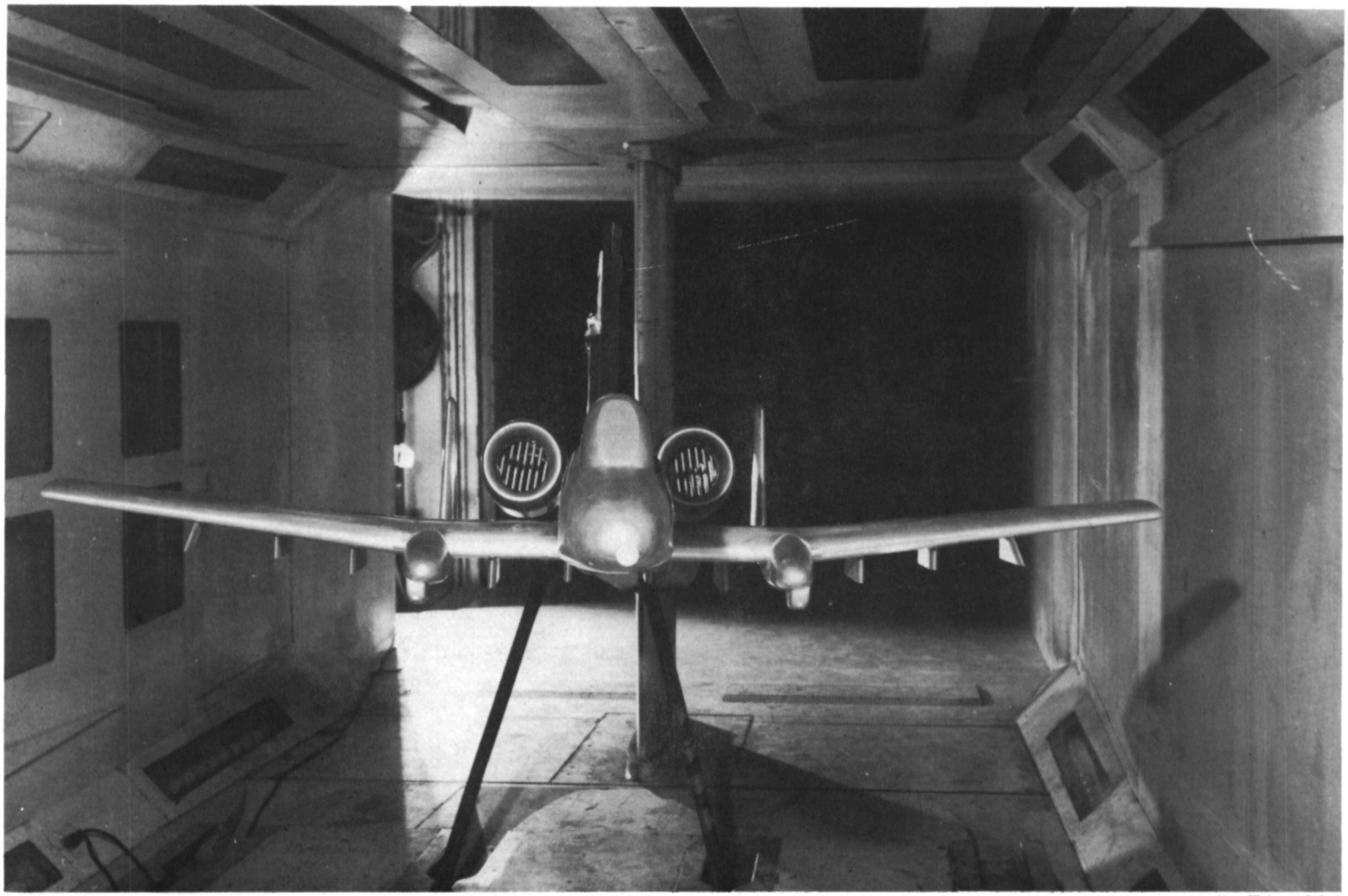

(a) Front view.

L-71-5991

Figure 3.- Photographs of the model mounted in the Langley high-speed 7- by 10-foot tunnel. $\beta = 9^{o}$; $\delta_f = 0^{o}$.

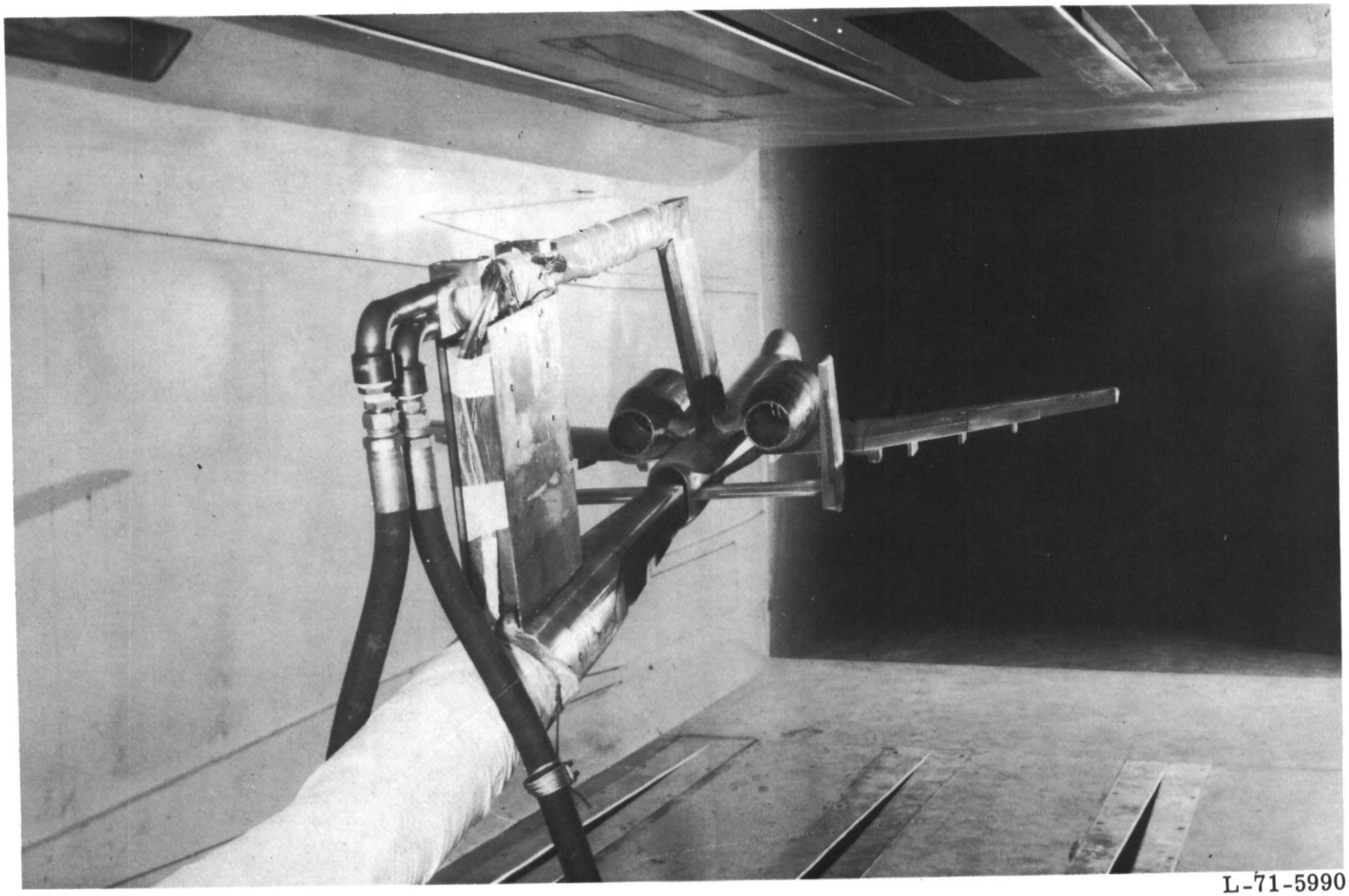

L-71-5990

(b) Rear view.

Figure 3.- Concluded.

(a) Front view.

L-71-6058

Figure 4.- Photographs of the model with ground plane in place. Landing gear on; $\beta = 0^{o}$; $\delta_f = 30^{o}$.

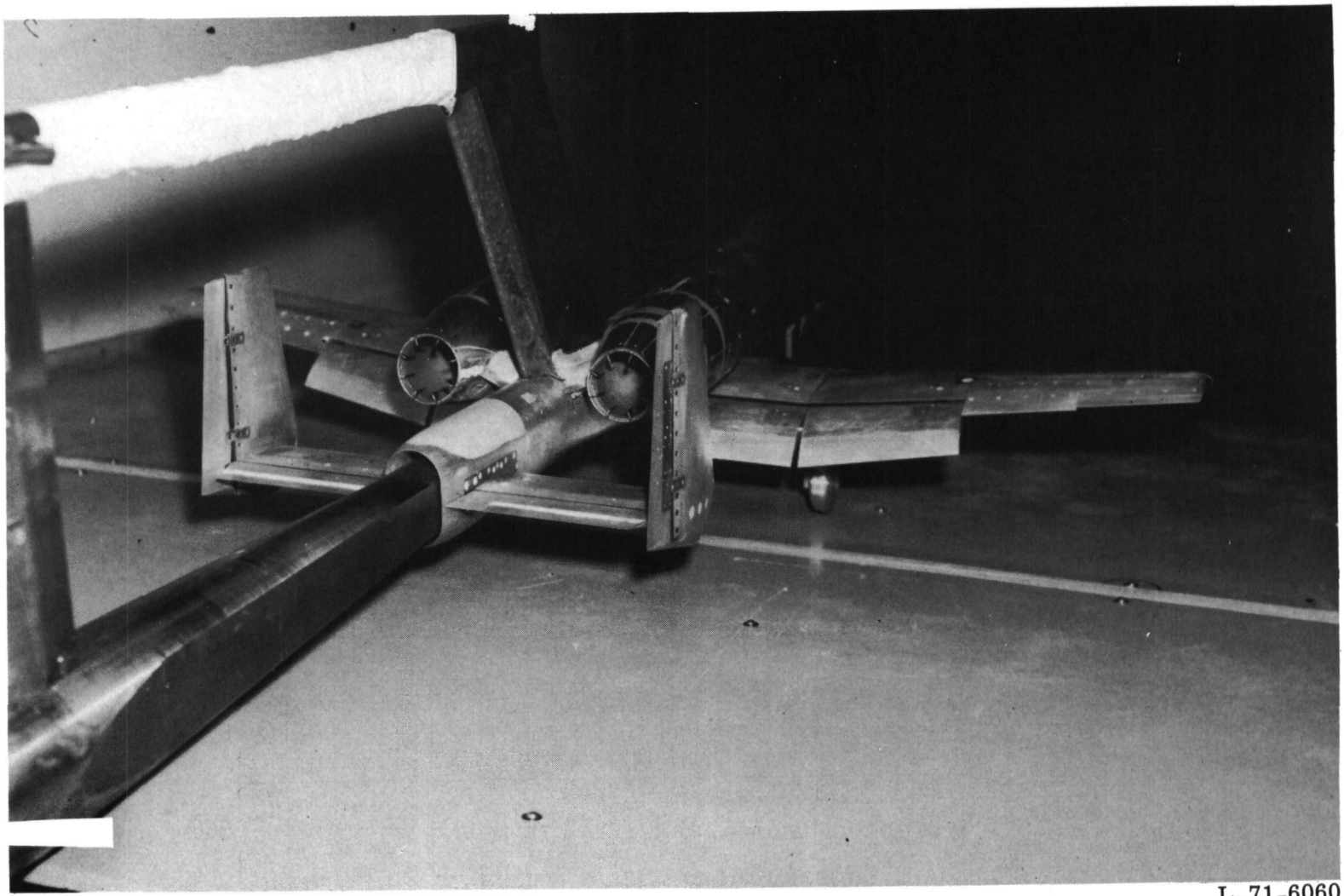

L-71-6060

(b) Rear view.

Figure 4.- Concluded.

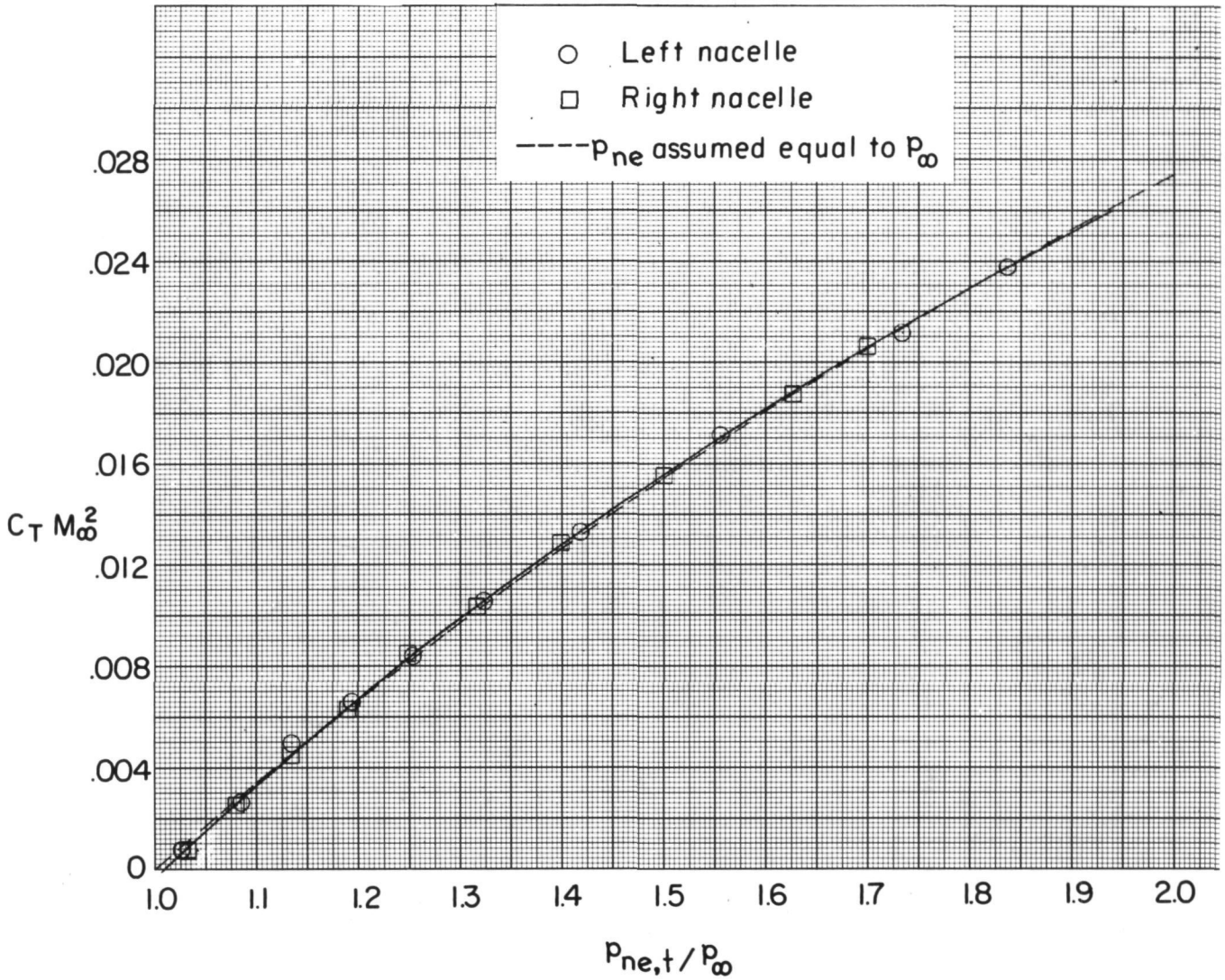

Figure 5.- Nozzle calibrations showing variation of $C_T M_\infty^2$ as a function of $p_{ne,t}/p_\infty$.

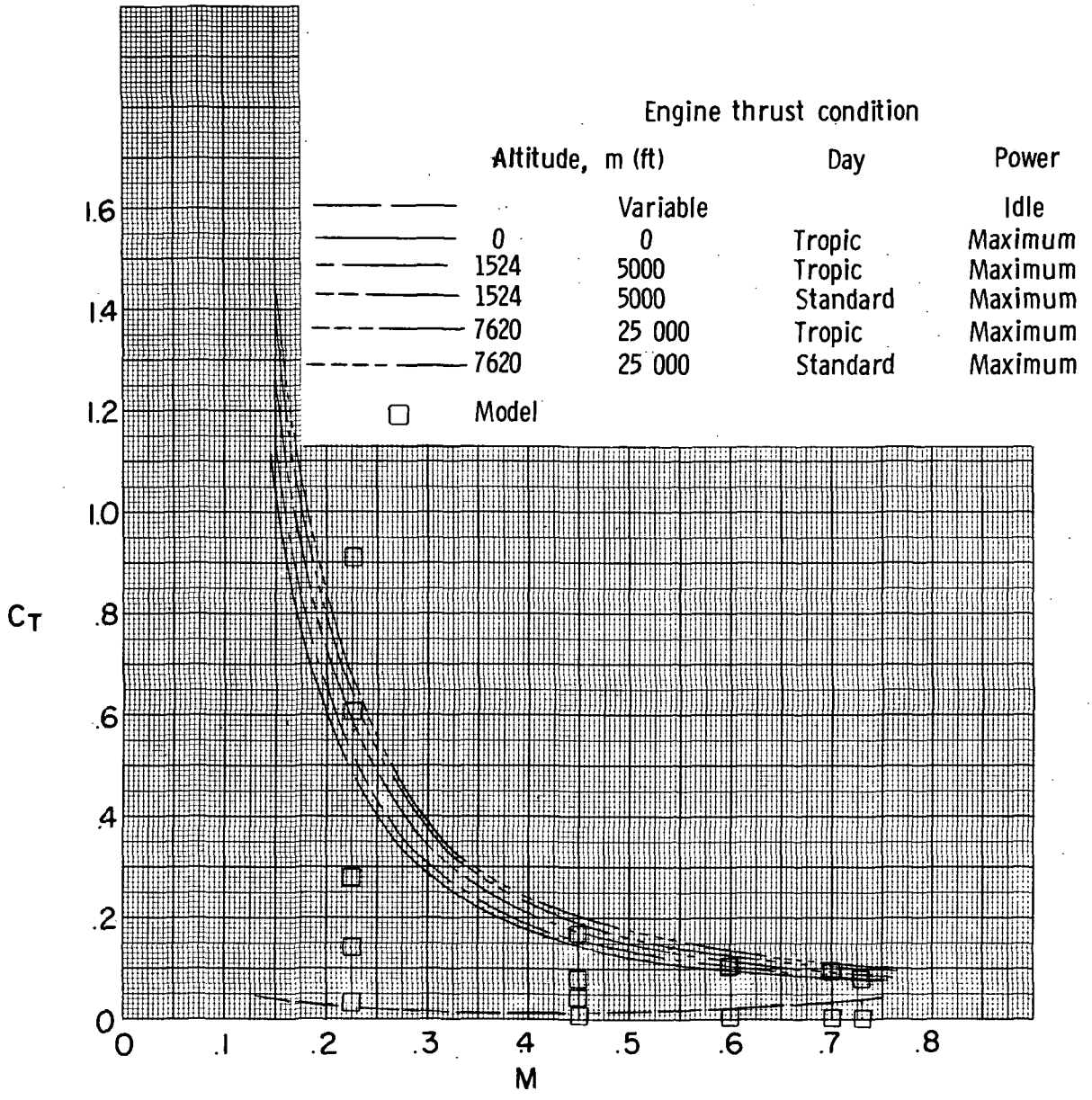

Figure 6.- Variation of airplane gross thrust coefficient with Mach number for various conditions. Square symbols indicate model thrust coefficients used.

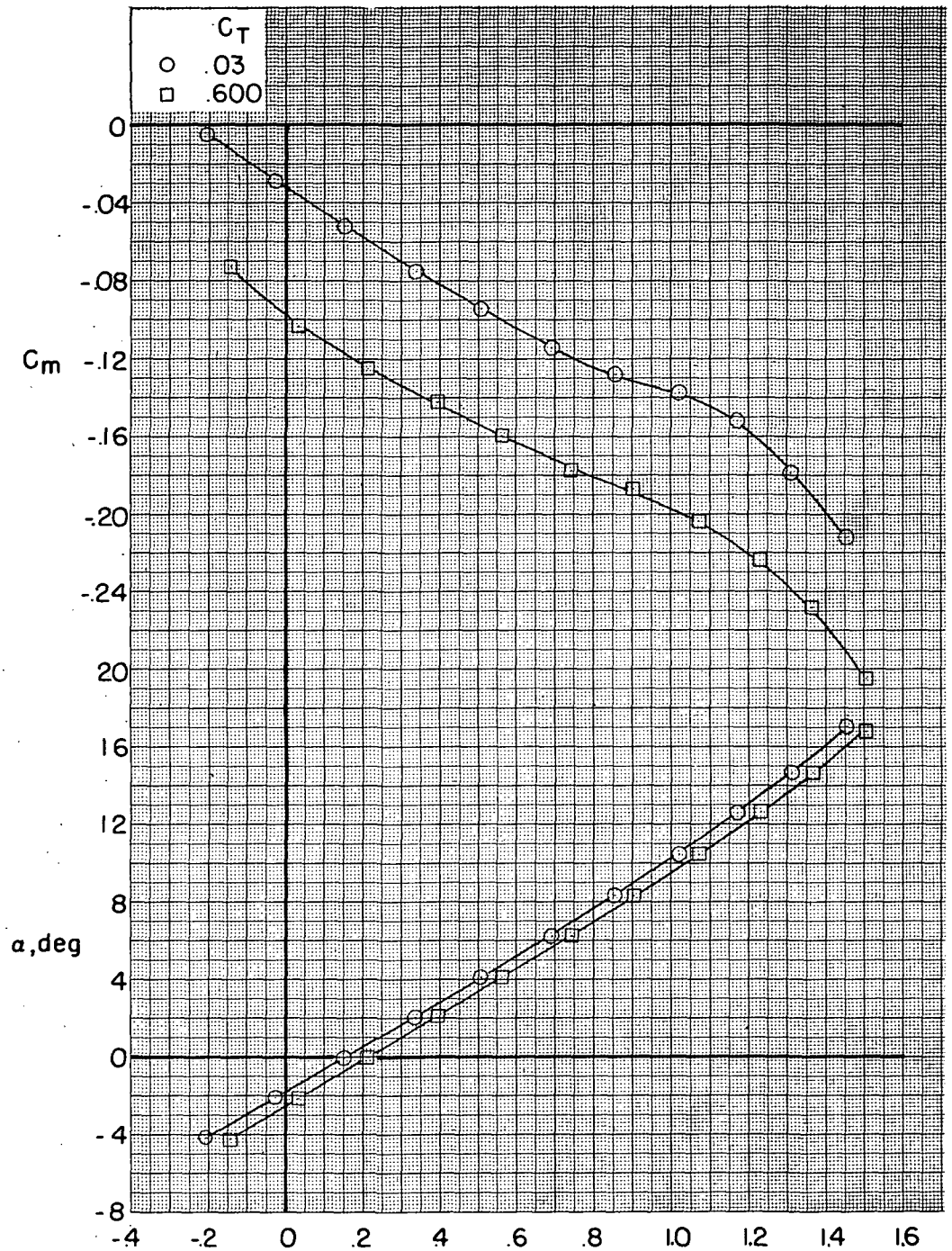

(a) $\delta_e = 0^o$.

Figure 7.- Effect of nacelle thrust coefficient on model characteristics. M = 0.225; $\delta_f = 0^o$; $\beta = 0^o$; $i_n = 4^o$; $h = \infty$.

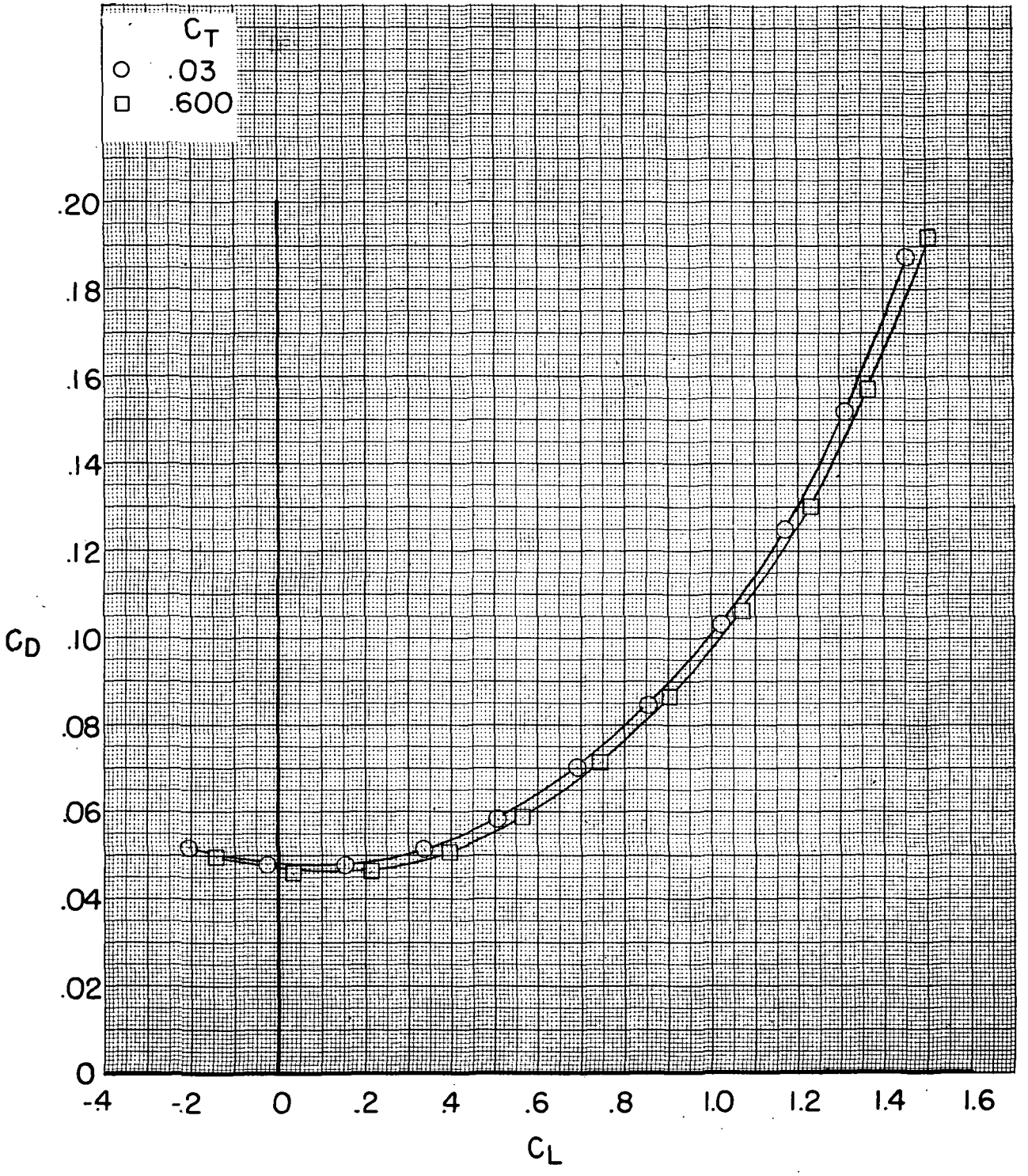

(a) Concluded.

Figure 7.- Continued.

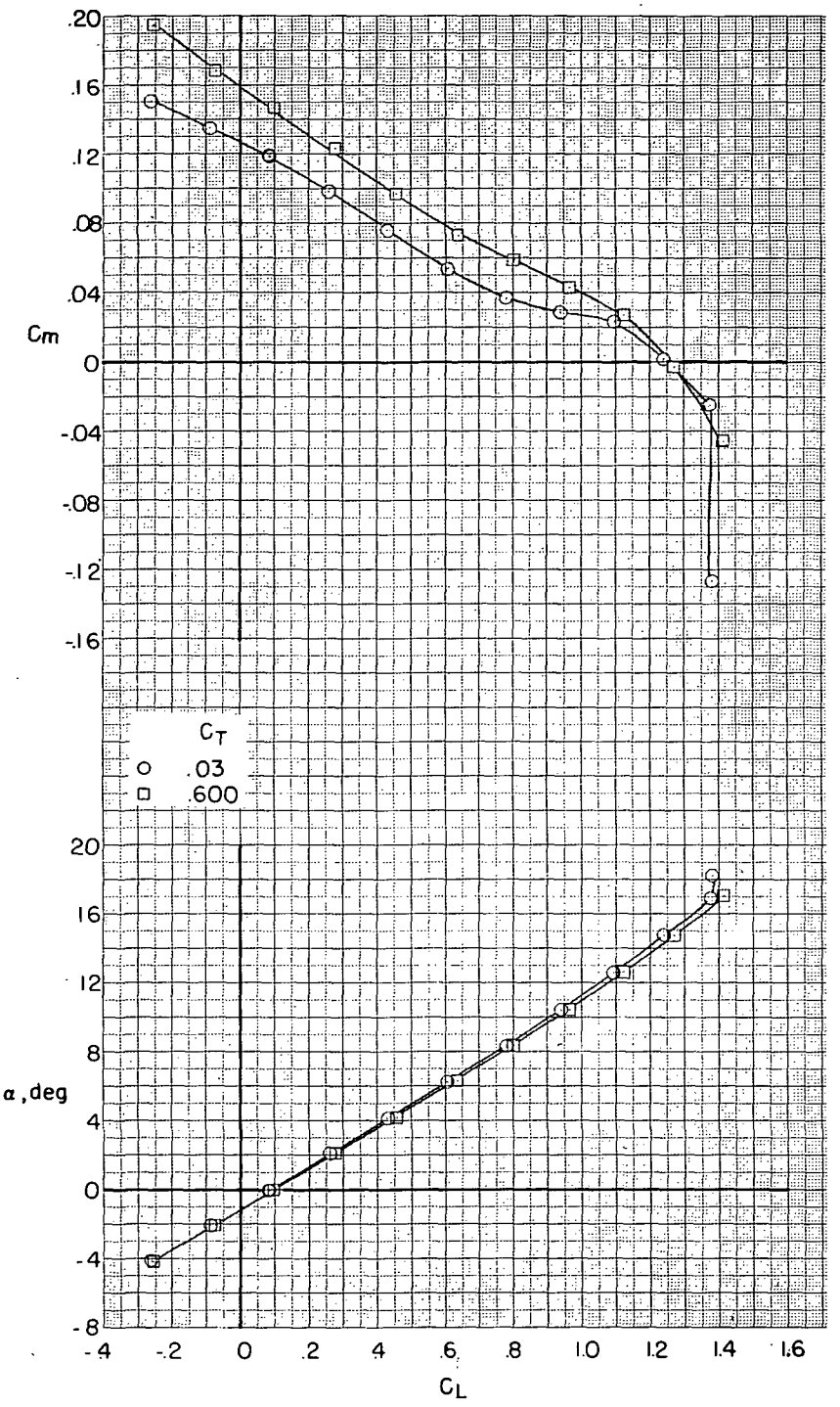

(b) $\delta_e = -15^o$.

Figure 7.- Continued.

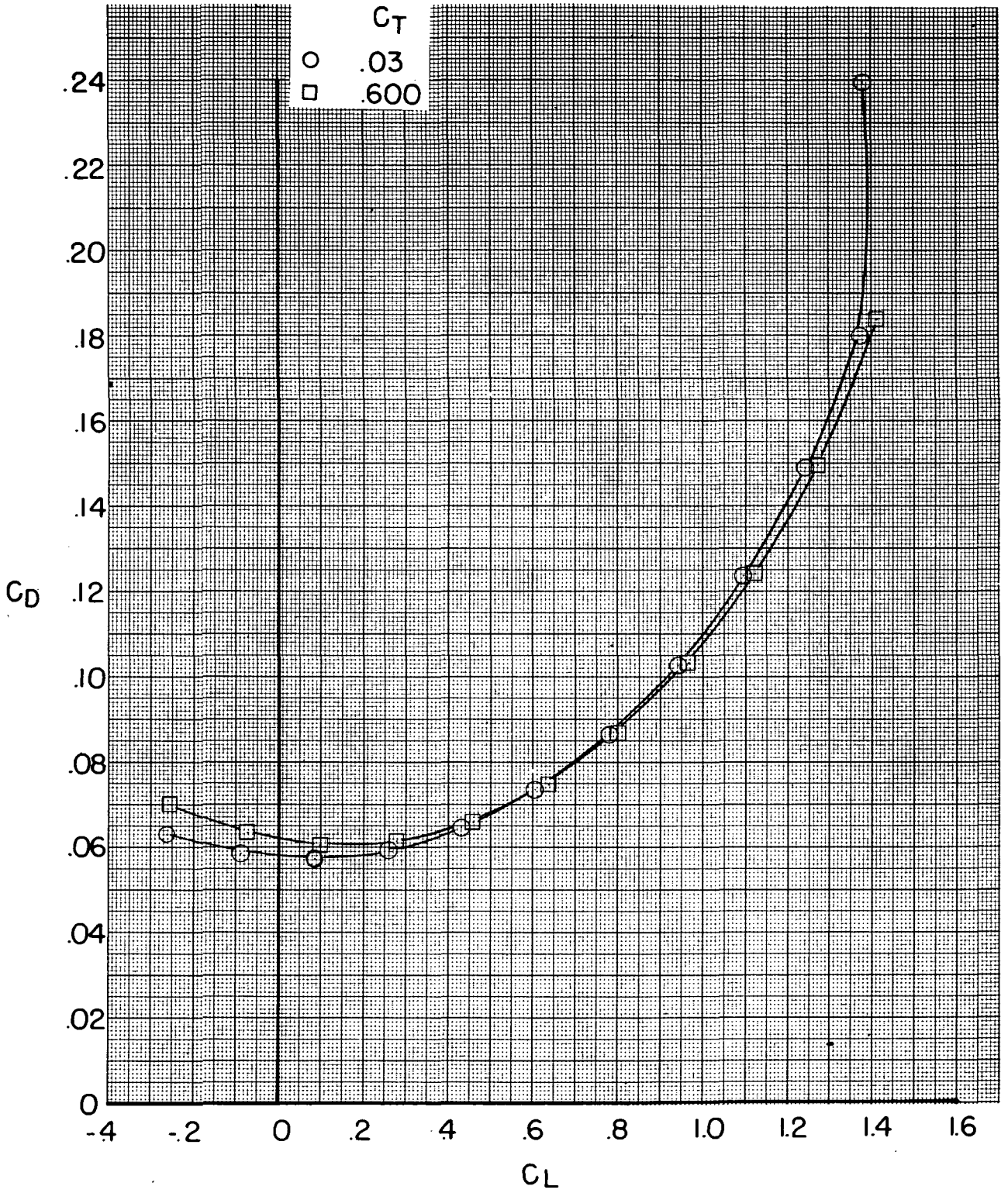

(b) Concluded.

Figure 7.- Concluded.

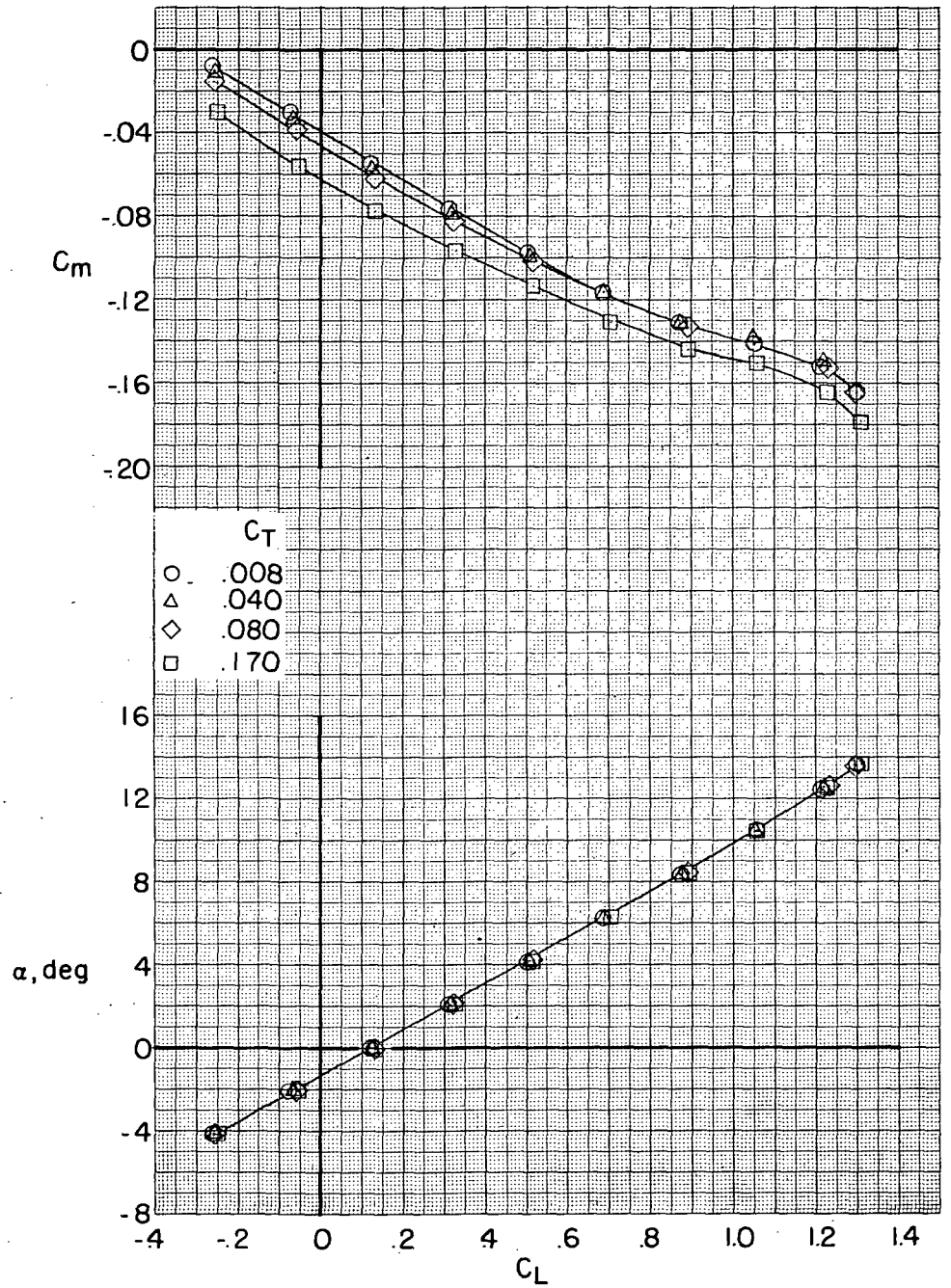

(a) $\delta_e = 0^o$.

Figure 8.- Effect of nacelle thrust coefficient on model characteristics. $M = 0.45$; $\delta_f = 0^o$; $\beta = 0^o$; $i_n = 4^o$; $h = \infty$.

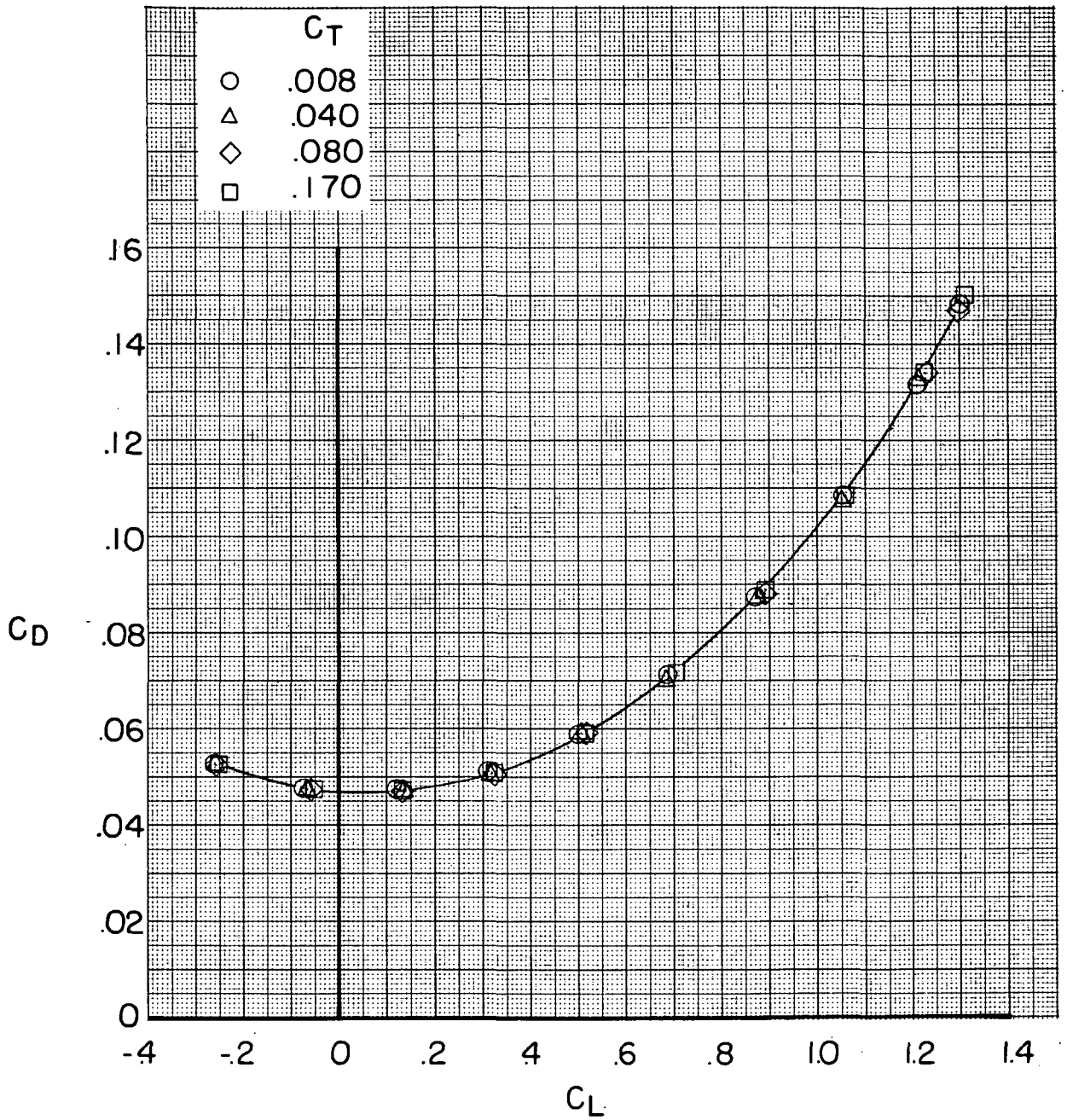

(a) Concluded.

Figure 8.- Continued.

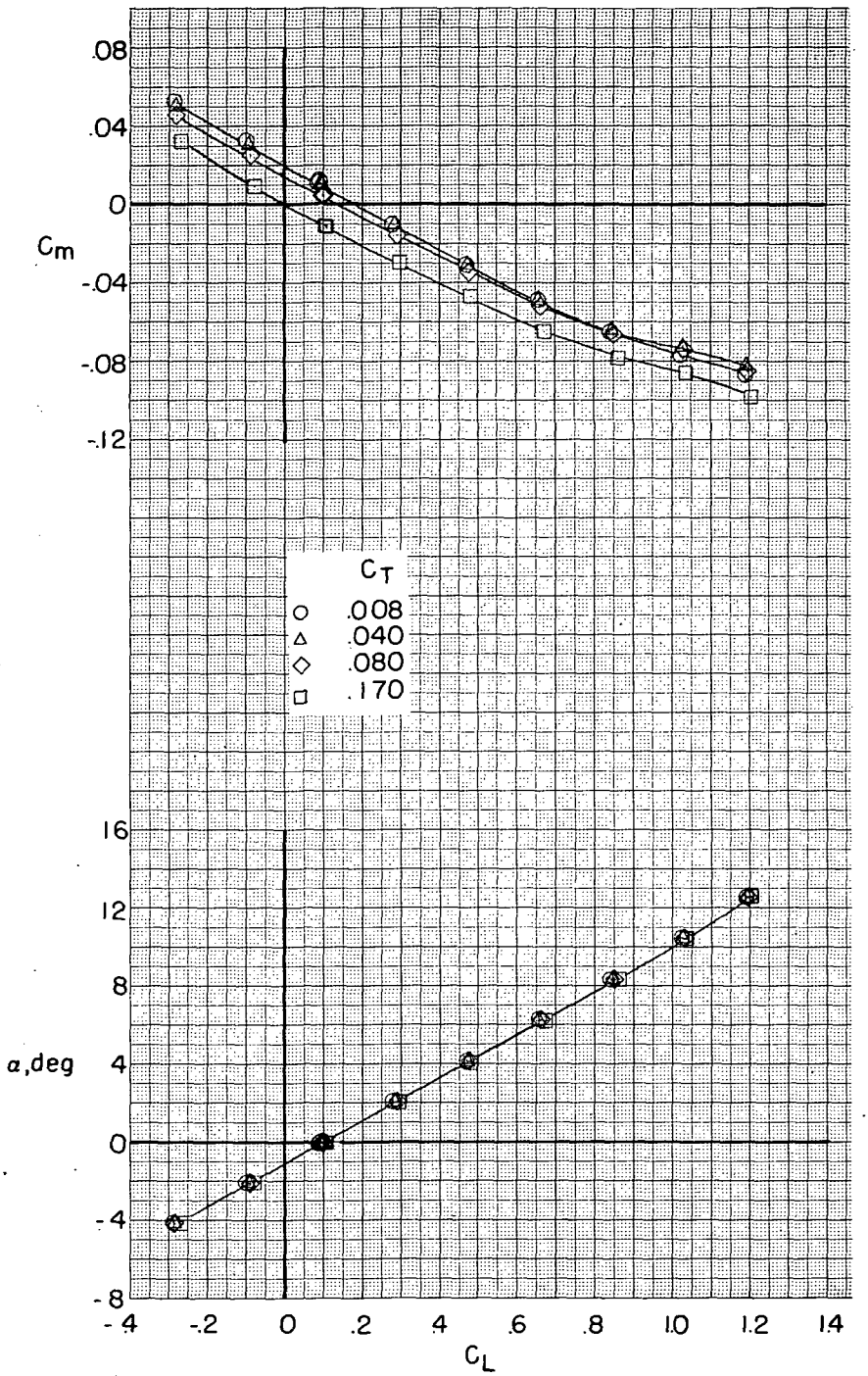

(b) $\delta_e = -5^o$.

Figure 8.- Continued.

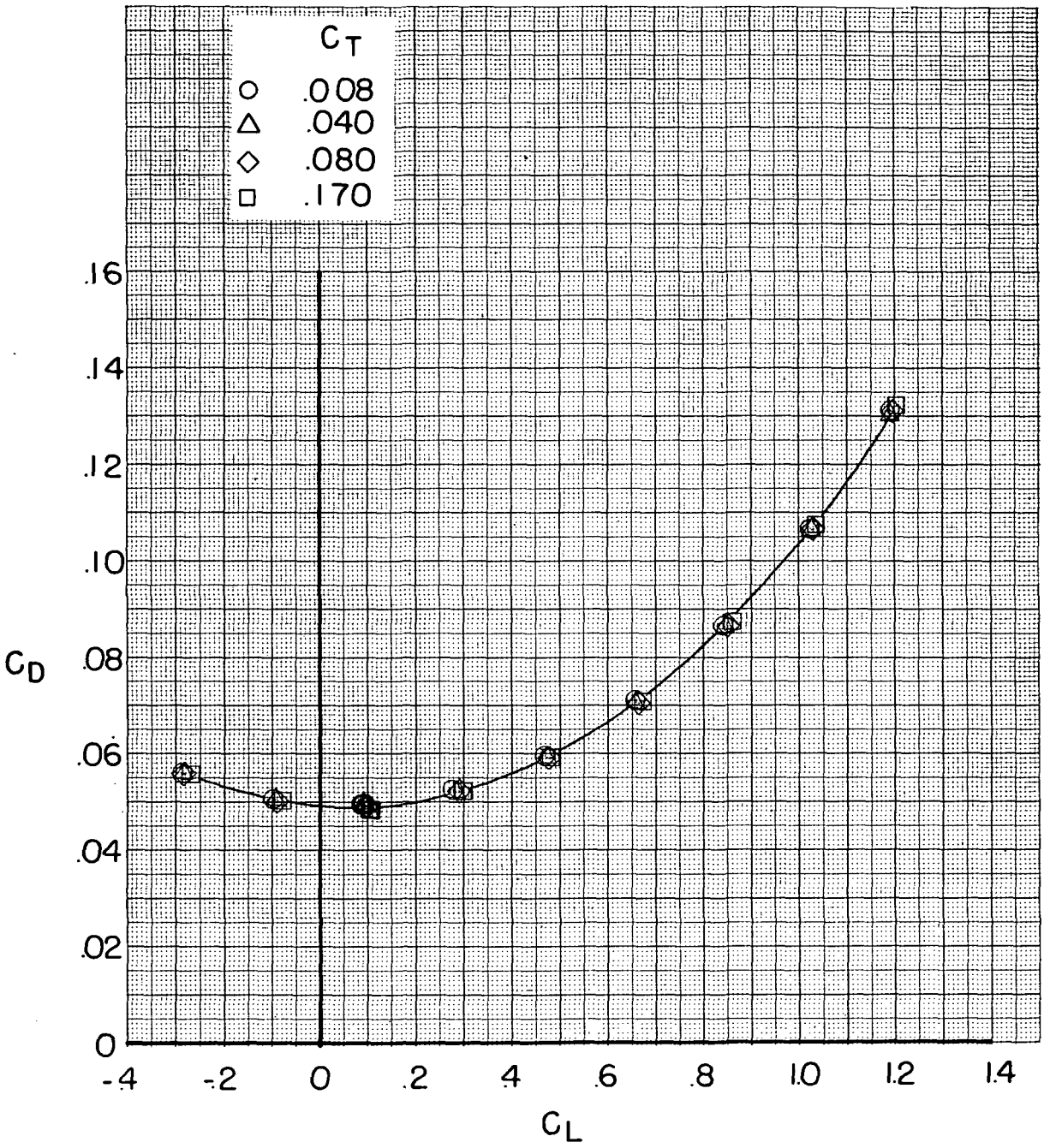

(b) Concluded.

Figure 8.- Continued.

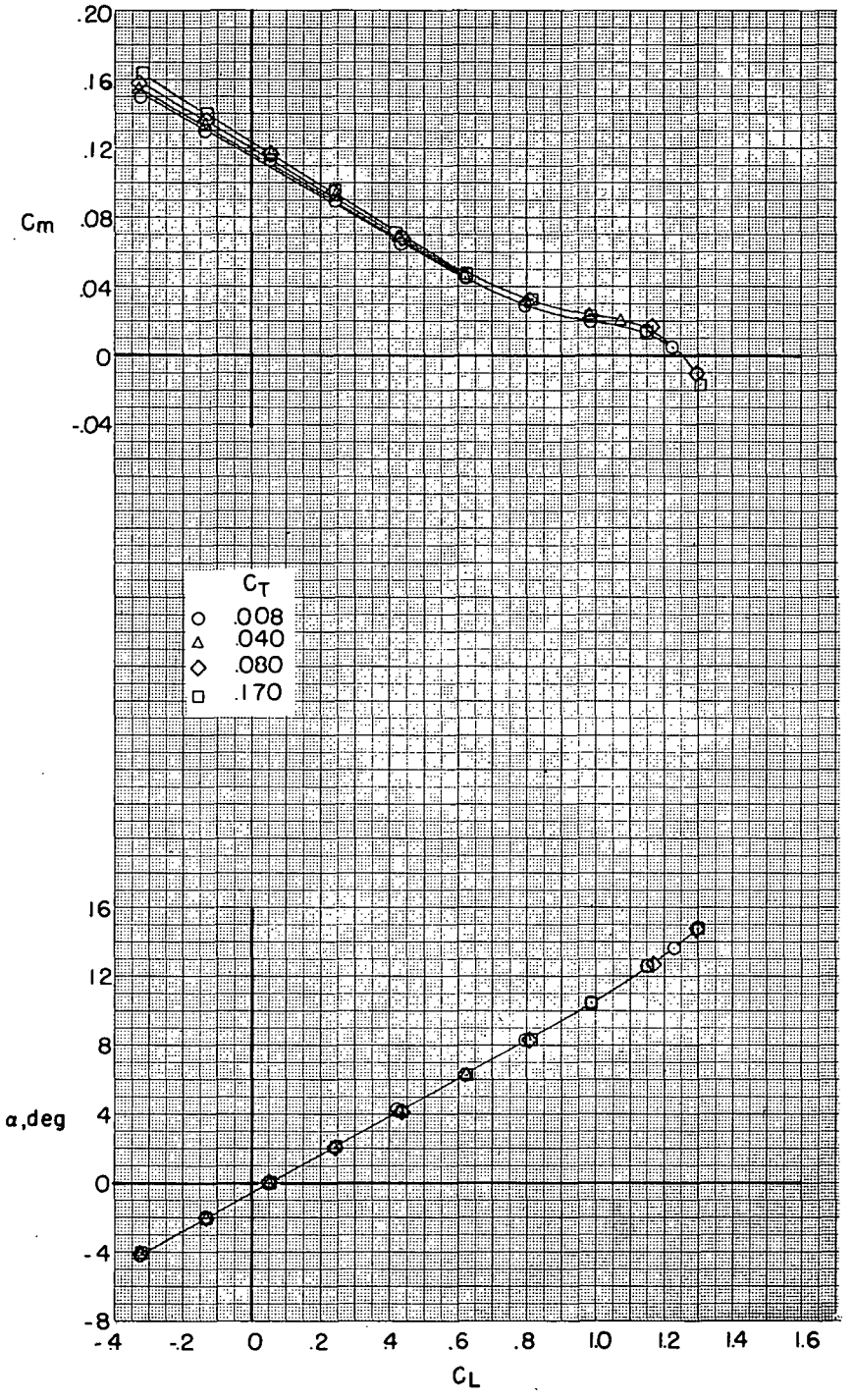

(c) $\delta_e = -15^o$.

Figure 8.- Continued.

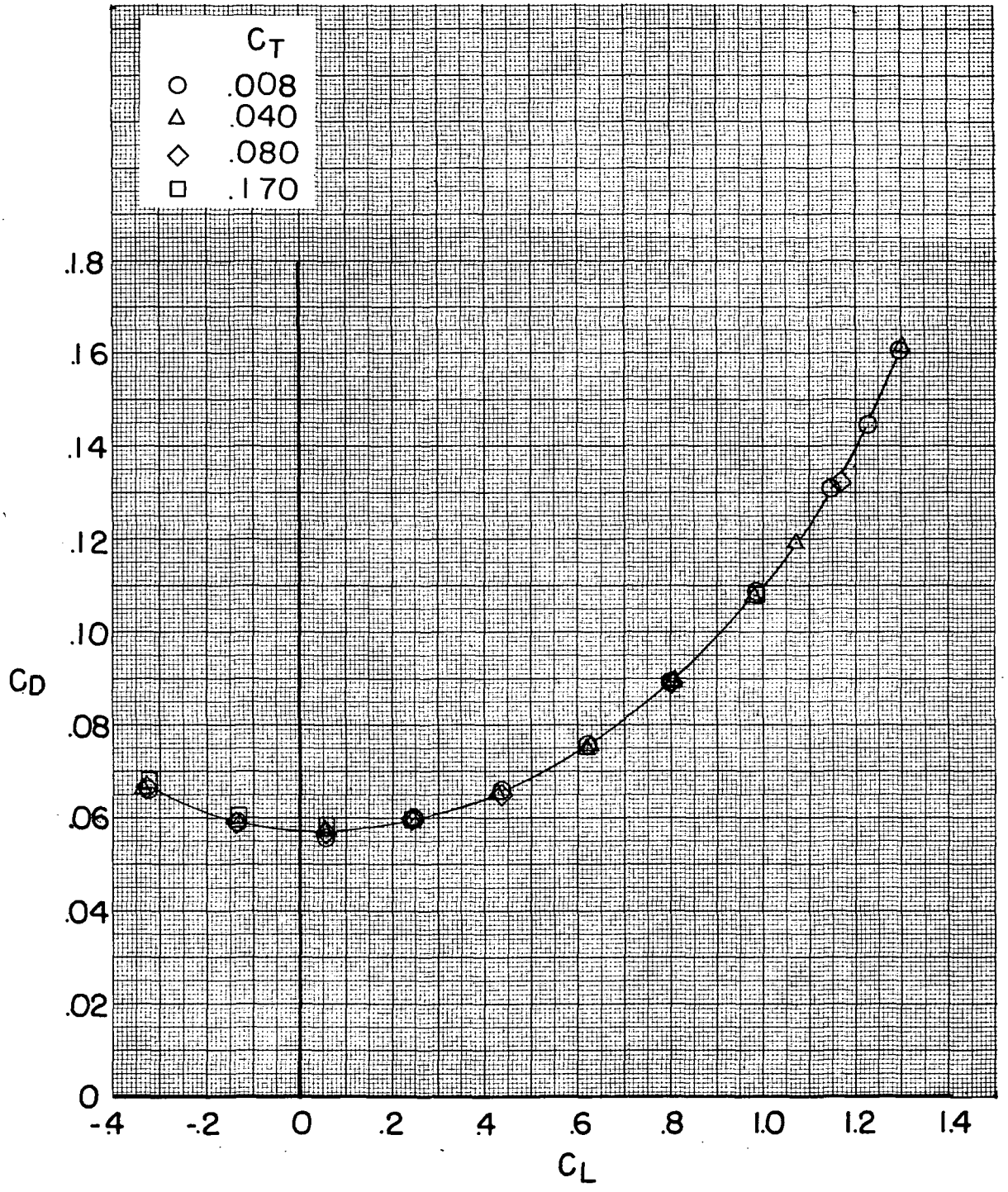

(c) Concluded.

Figure 8.- Concluded.

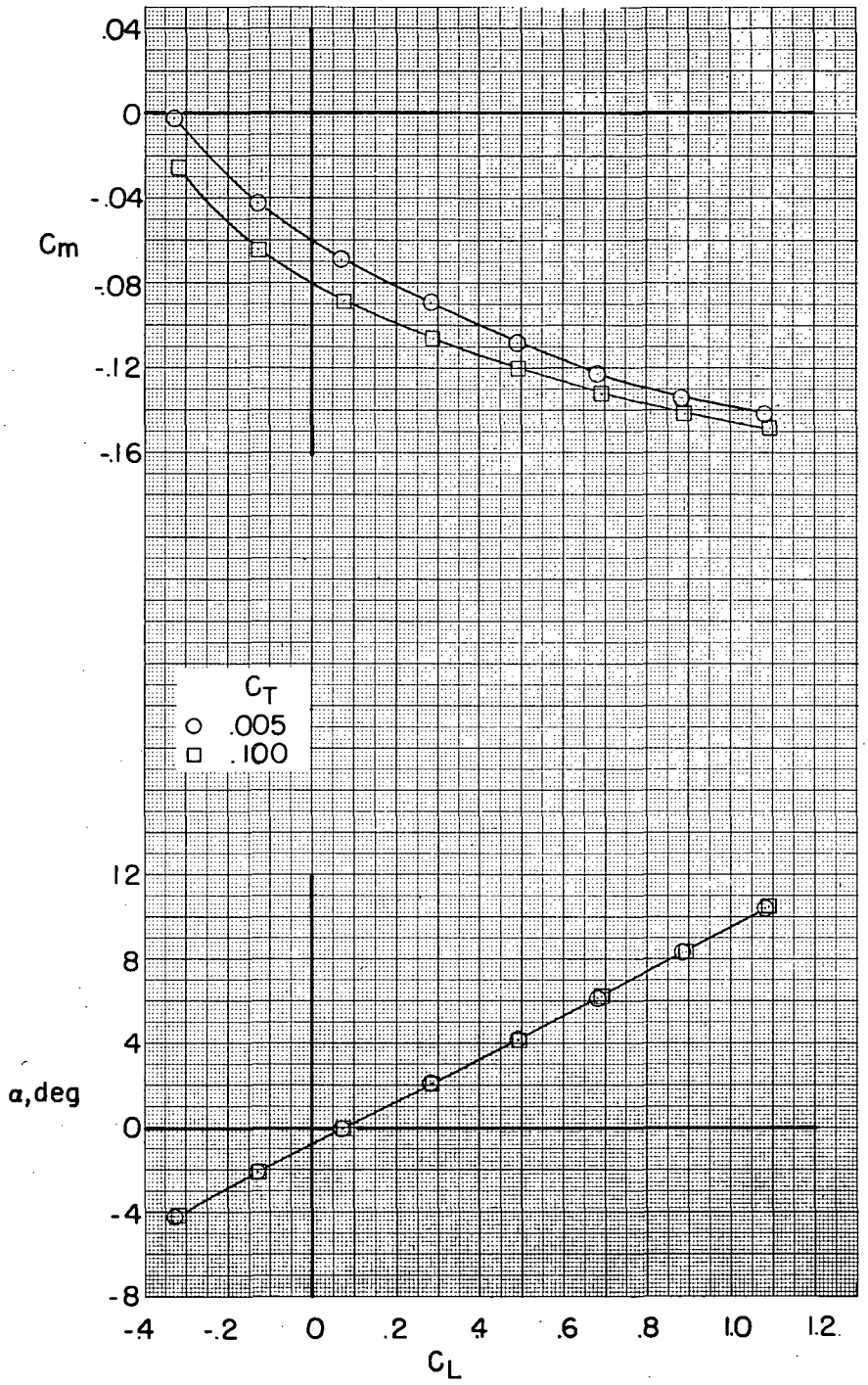

(a) $\delta_e = 0^o$.

Figure 9.- Effect of nacelle thrust coefficient on model characteristics. $M = 0.60$; $\delta_f = 0^o$; $\beta = 0^o$; $i_n = 4^o$; $h = \infty$.

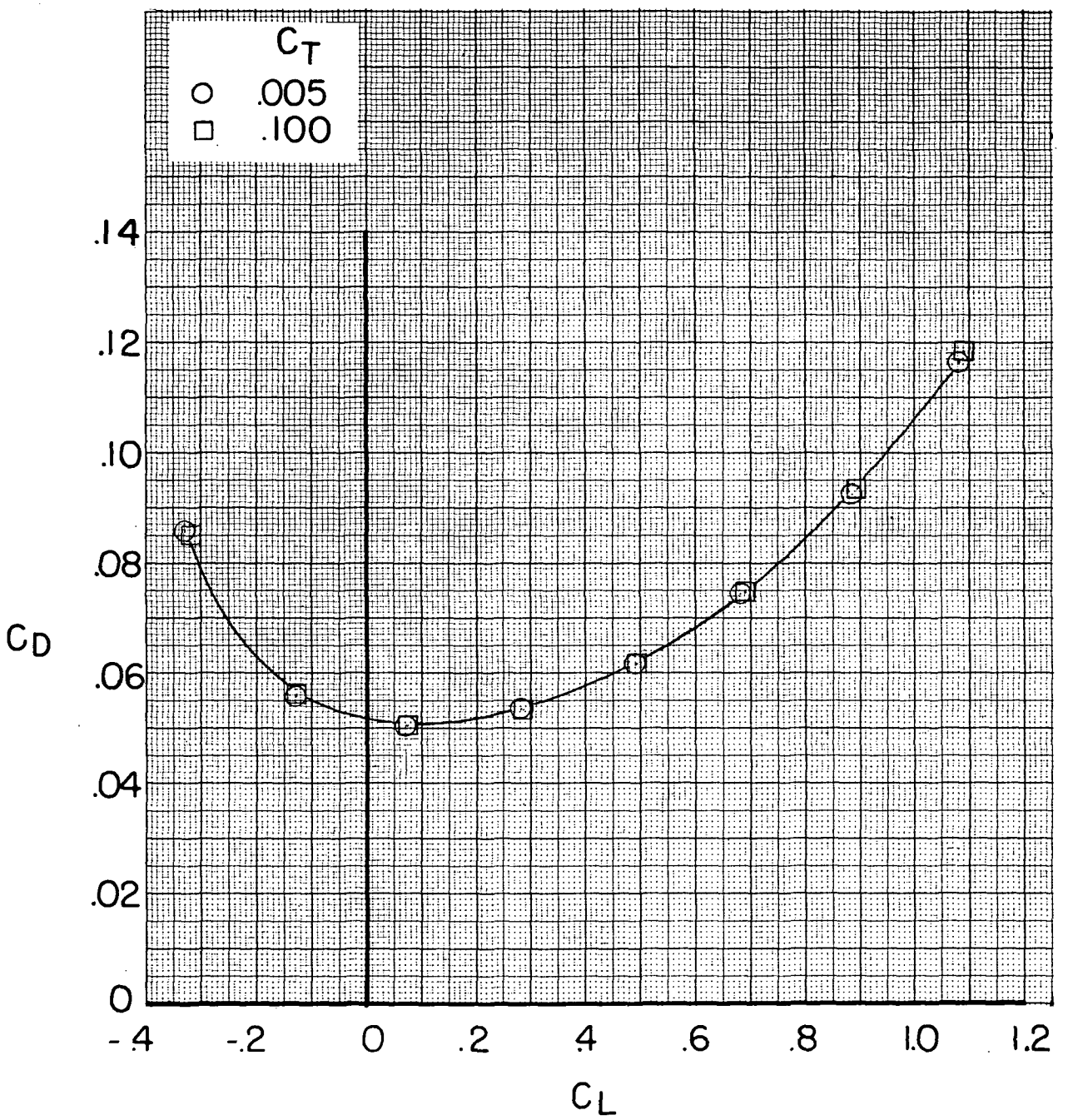

(a) Concluded.

Figure 9.- Continued.

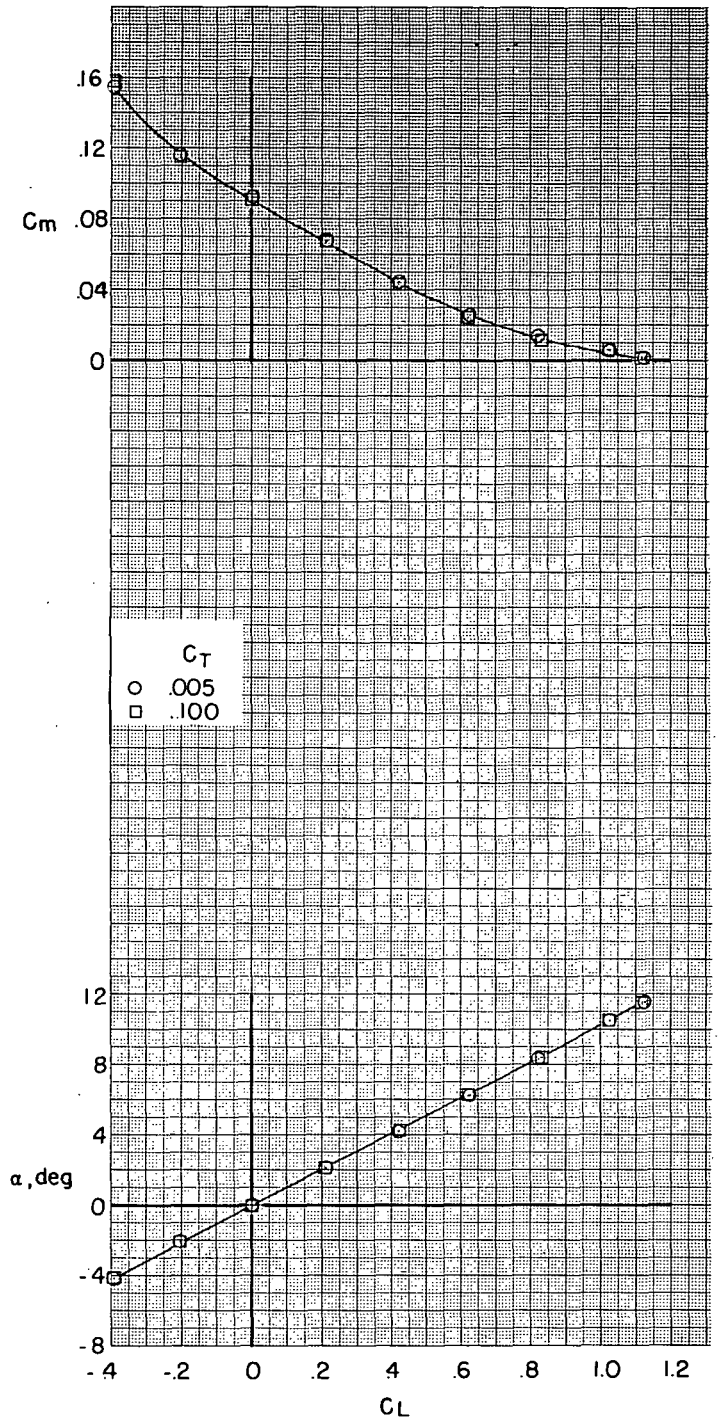

(b) $\delta_e = -15^o$.

Figure 9.- Continued.

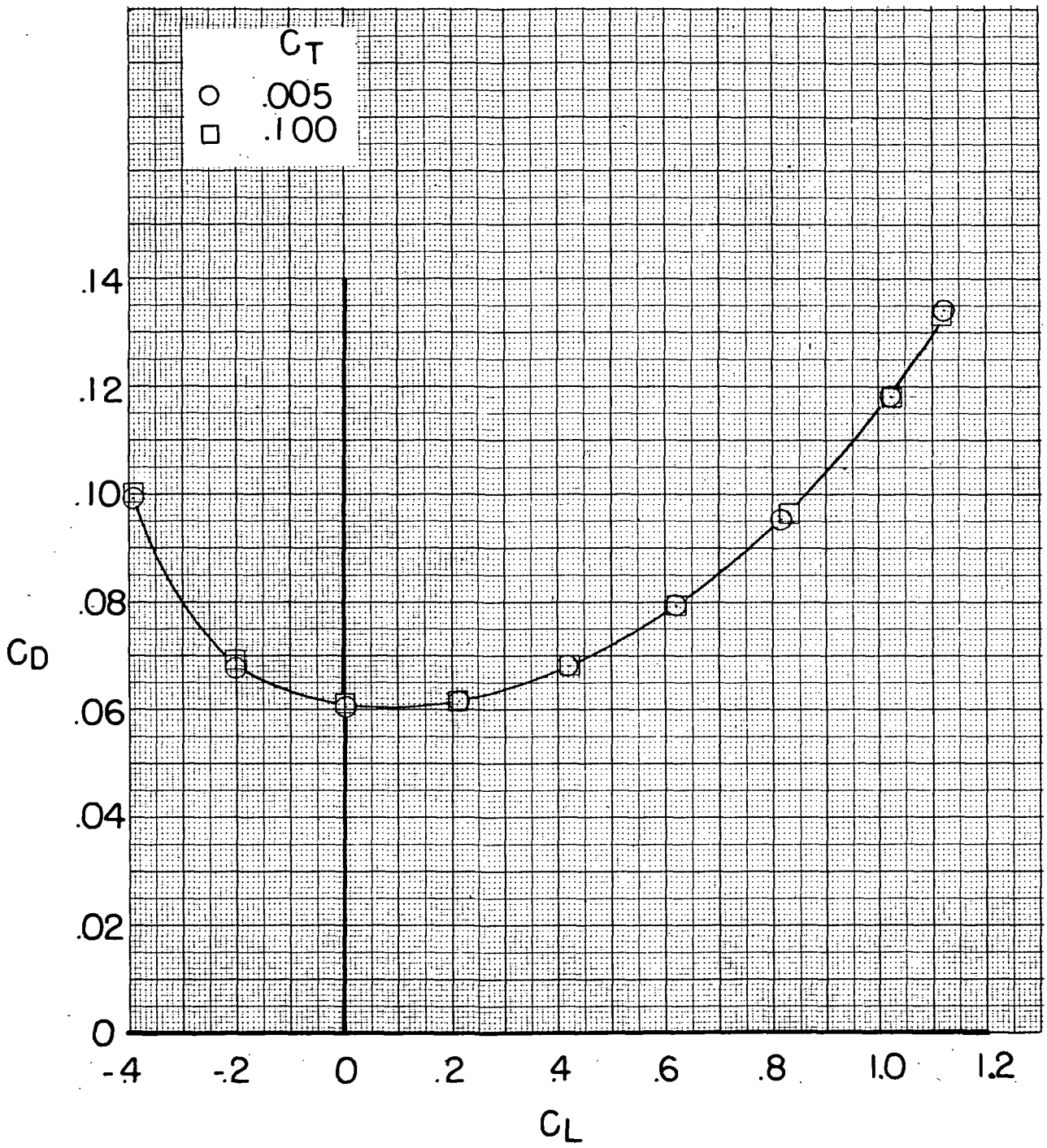

(b) Concluded.

Figure 9.- Concluded.

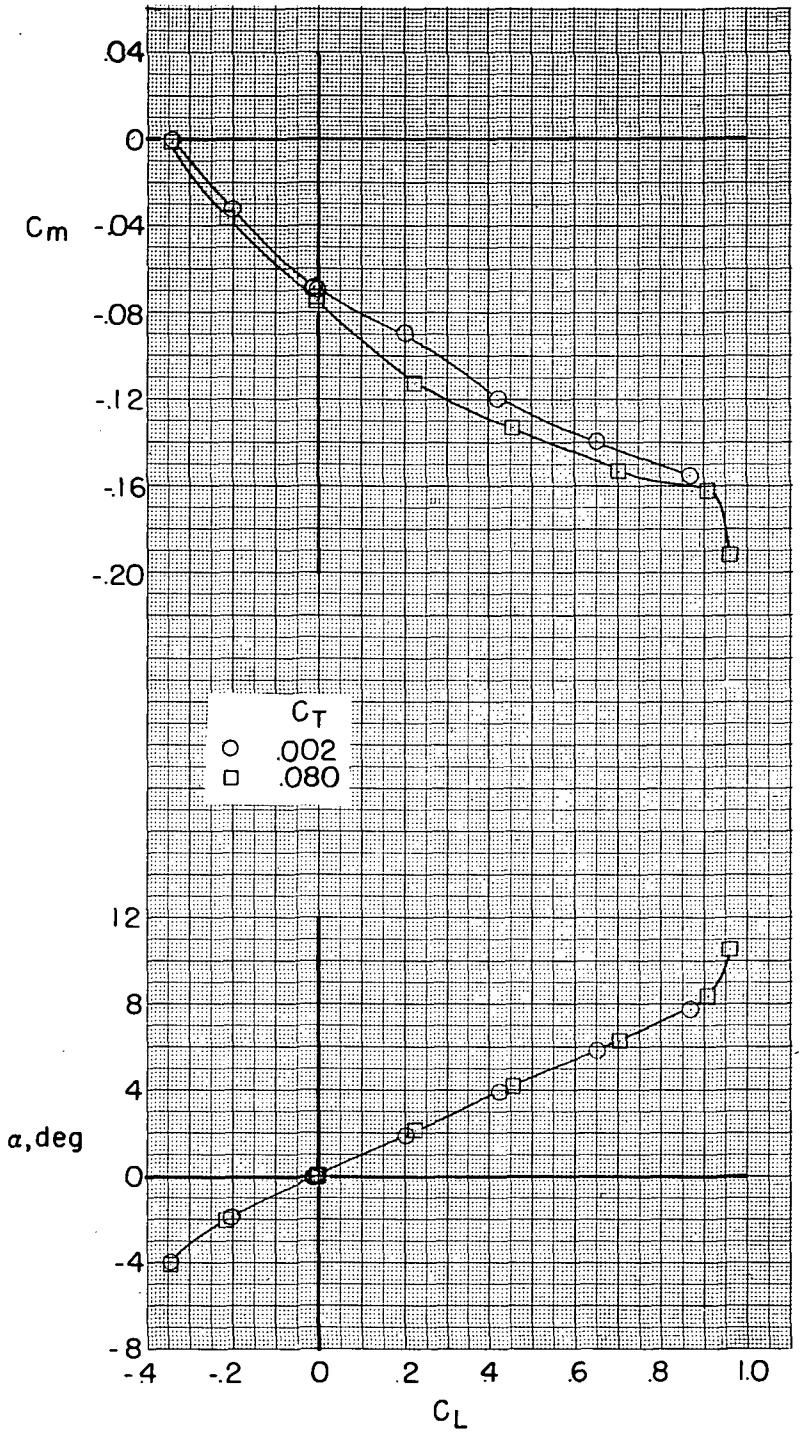

(a) $\delta_e = 0^o$.

Figure 10.- Effect of nacelle thrust coefficient on model characteristics. $M = 0.70$; $\delta_f = 0^o$; $\beta = 0^o$; $i_n = 4^o$; $h = \infty$.

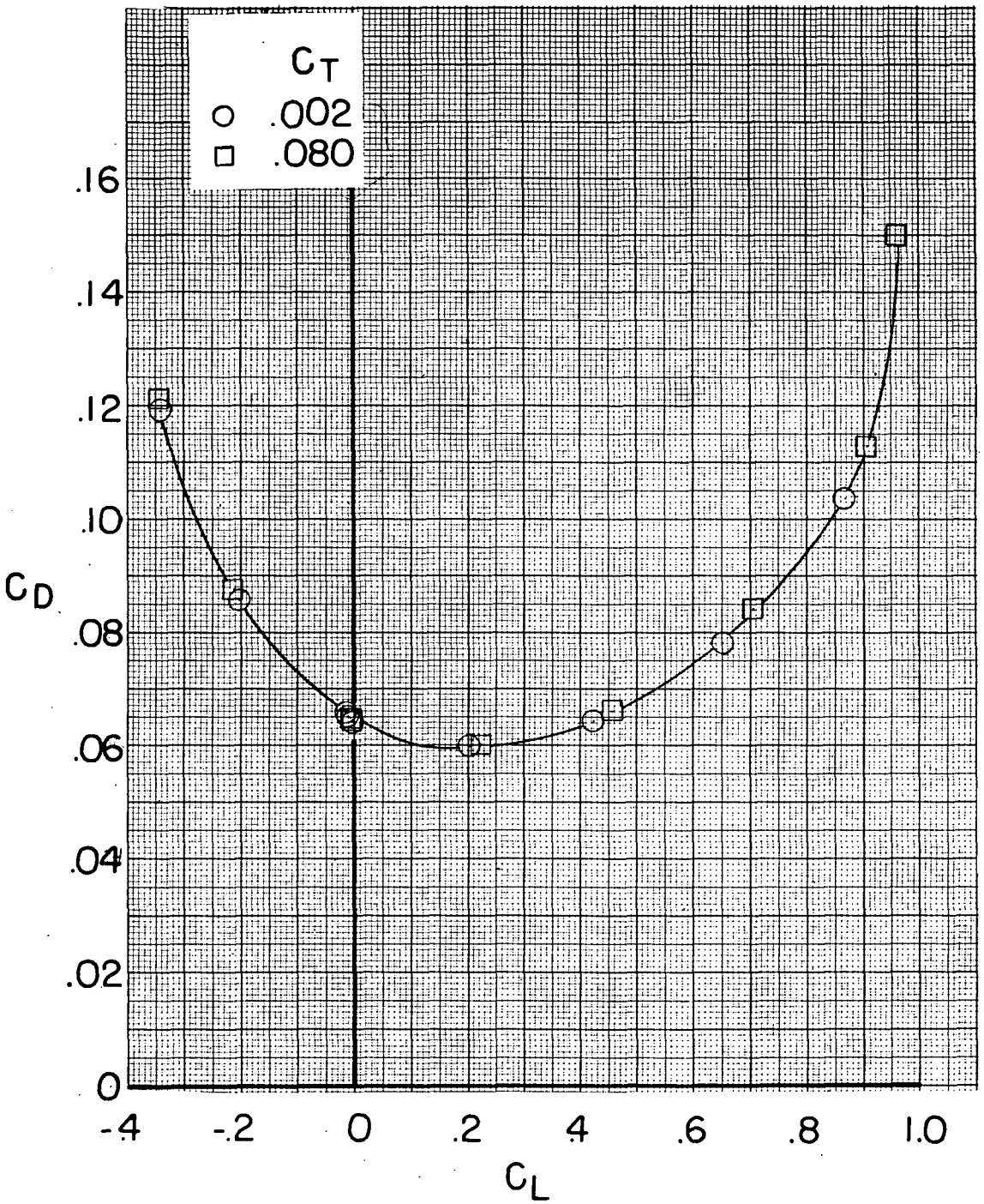

(a) Concluded.

Figure 10.- Continued.

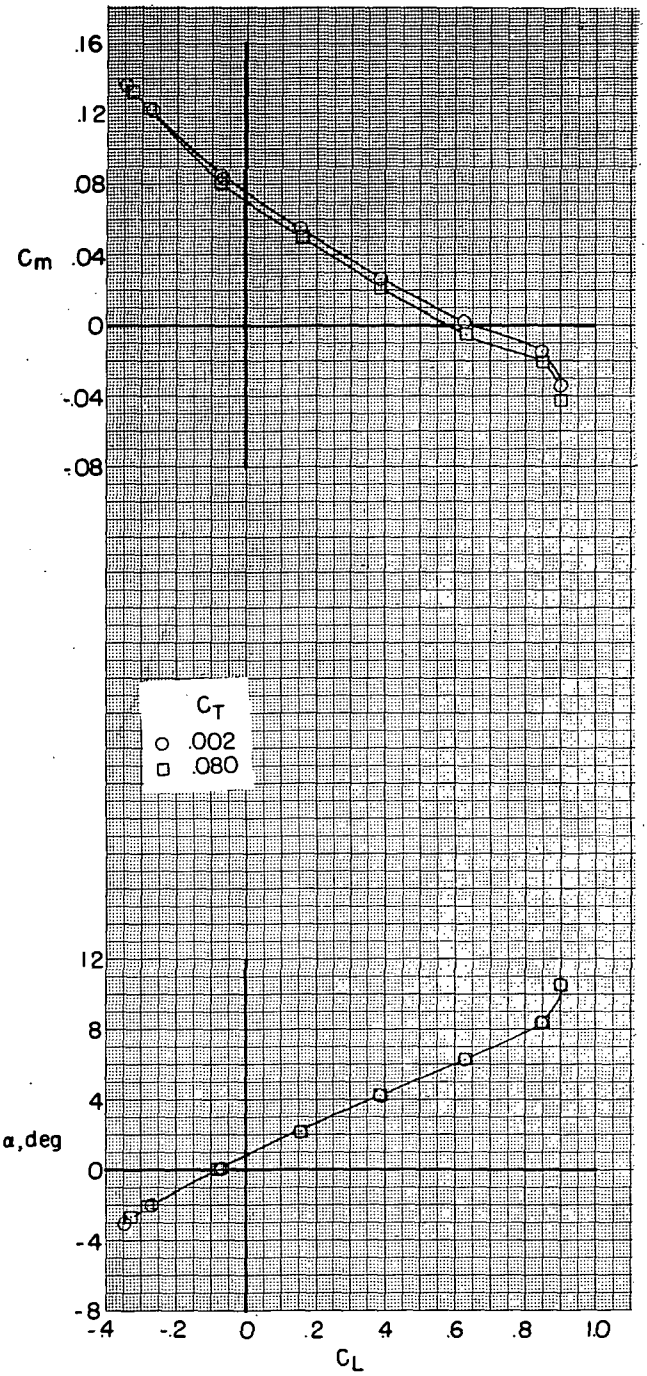

(b) $\delta_e = -15^o$.

Figure 10.- Continued.

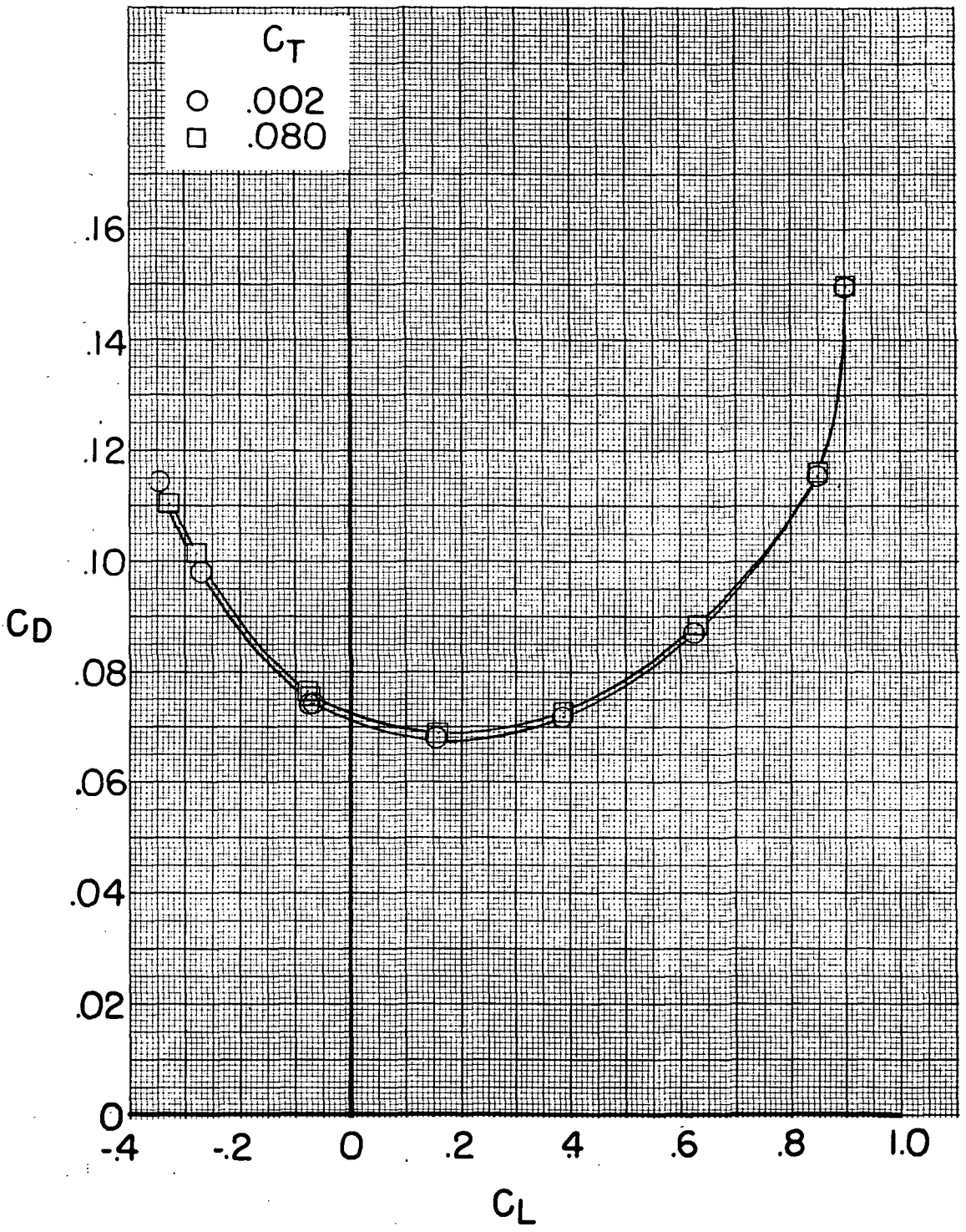

(b) Concluded.

Figure 10.- Concluded.

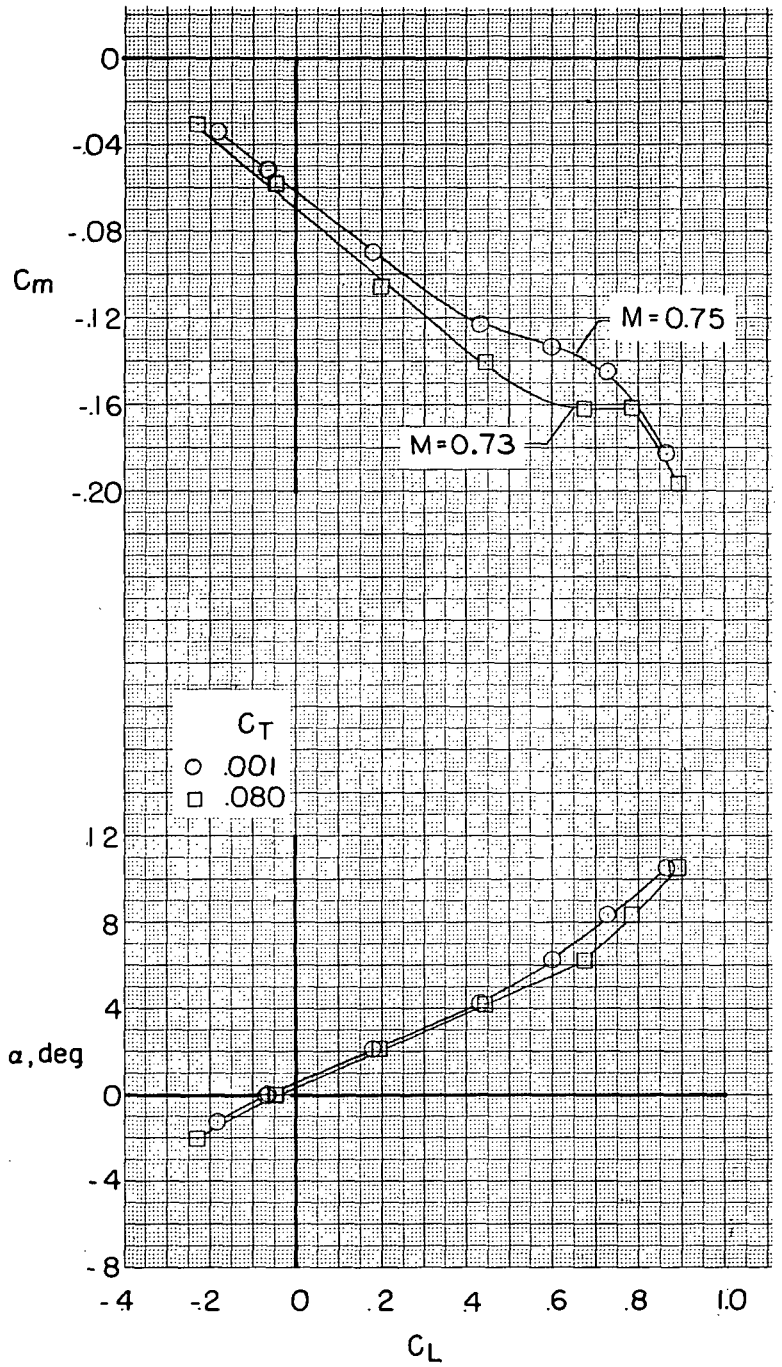

(a) $\delta_e = 0^o$.

Figure 11.- Effect of nacelle thrust coefficient on model characteristics. M = 0.73; $\delta_f = 0^o$; $\beta = 0^o$; $i_n = 4^o$; $h = \infty$.

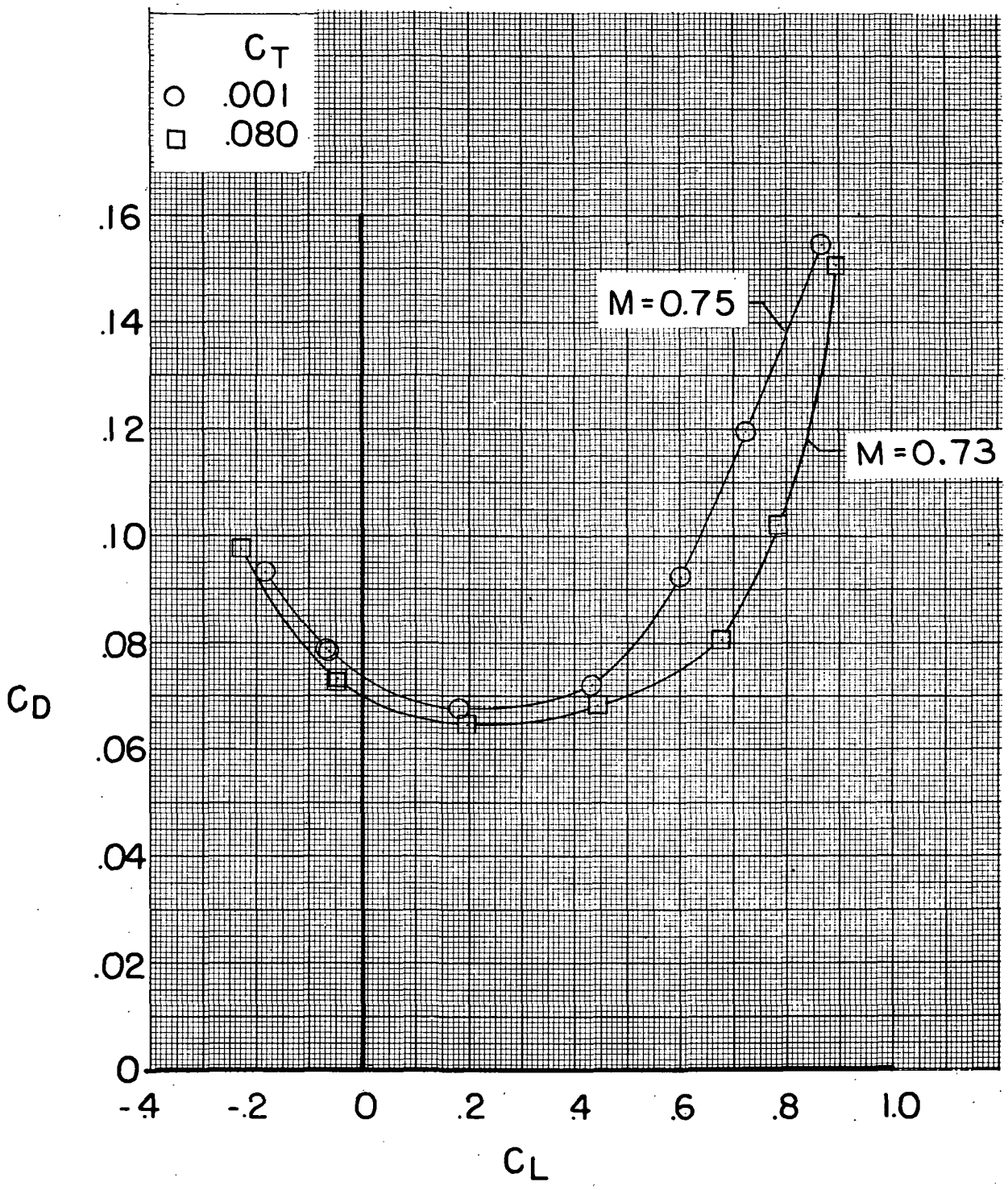

(a) Concluded.

Figure 11.- Continued.

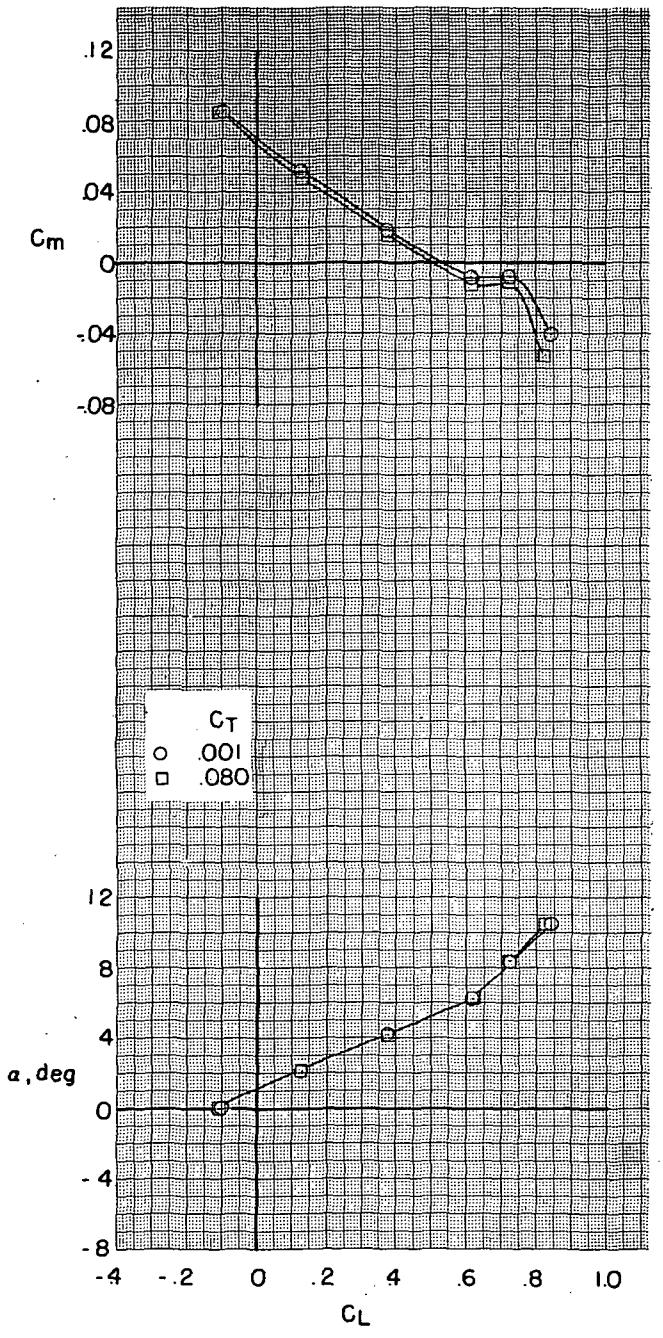

(b) $\delta_e = -15^o$.

Figure 11.- Continued.

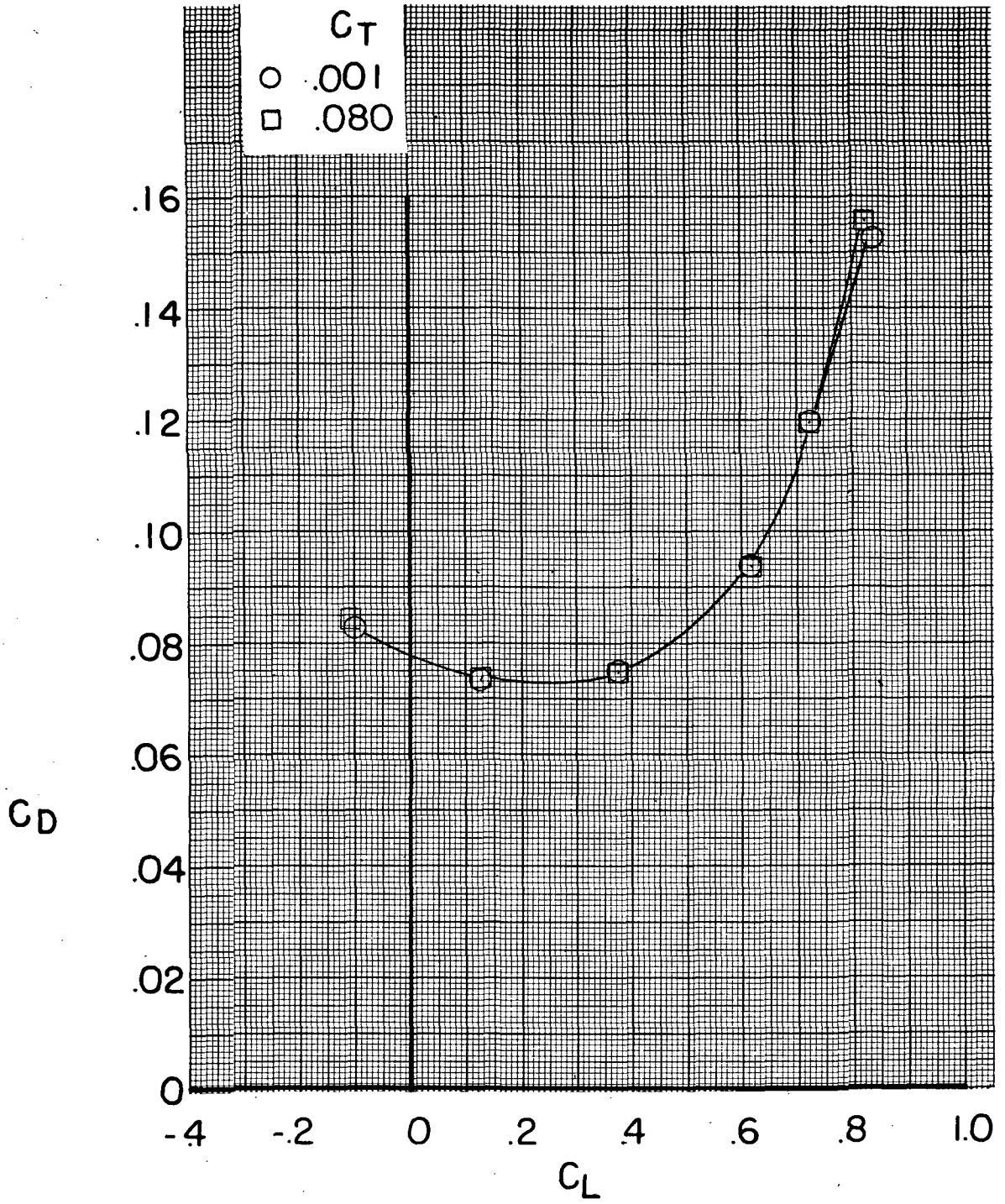

(b) Concluded.

Figure 11.- Concluded.

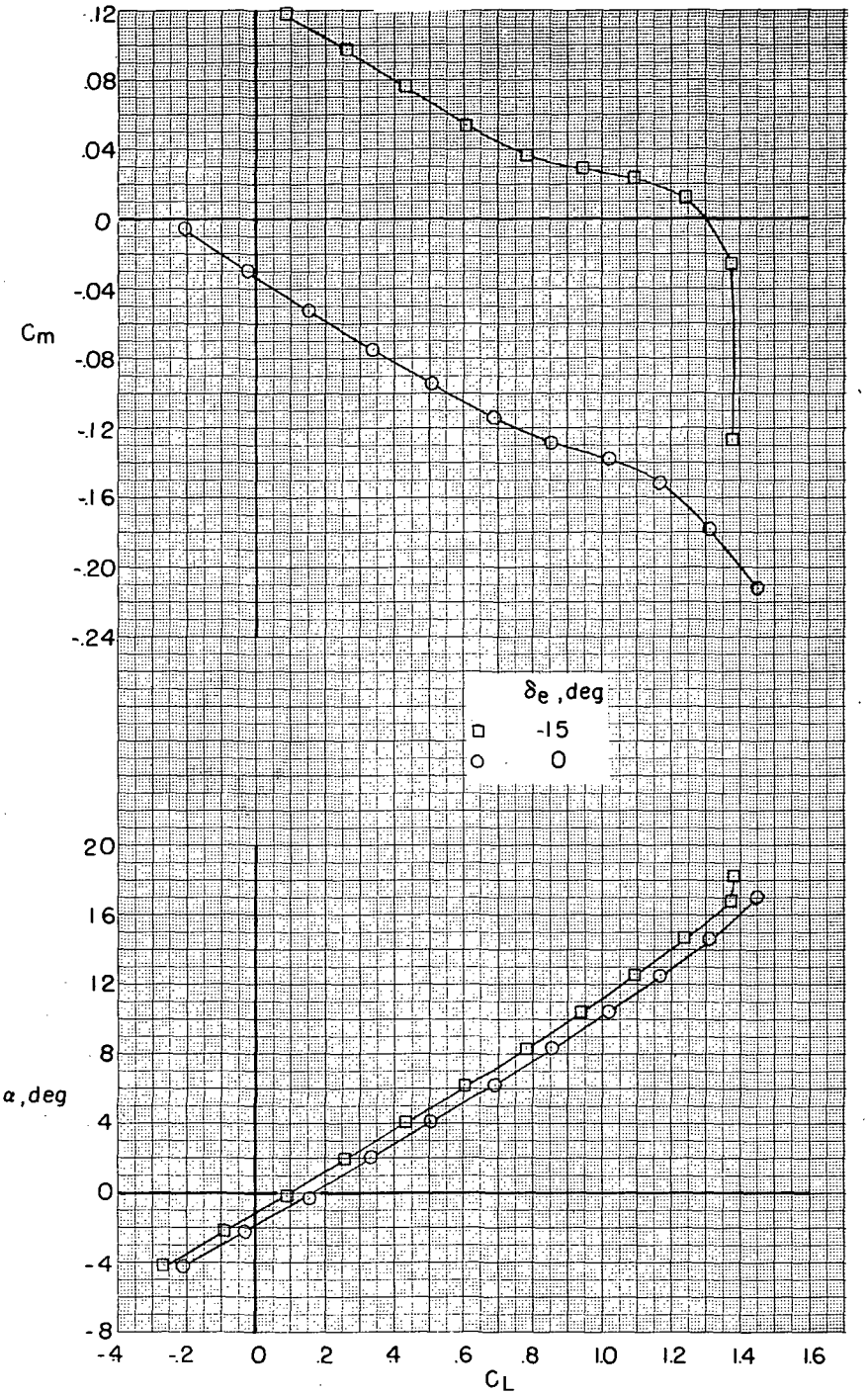

(a) $C_T = 0.030$.

Figure 12.- Effect of elevator deflection on model characteristics. $M = 0.225$; $\delta_f = 0^o$; $\beta = 0^o$; $i_n = 4^o$; $h = \infty$.

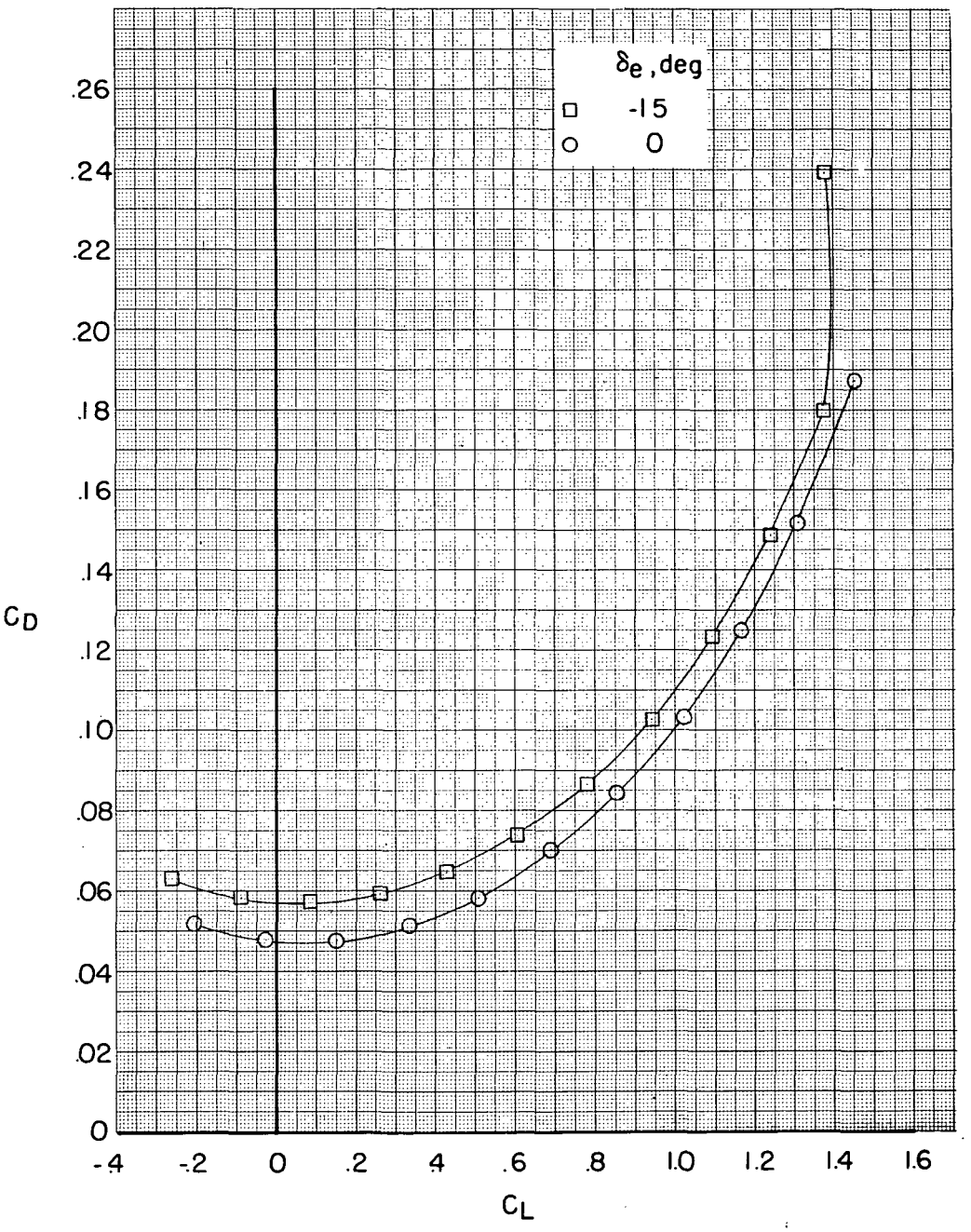

(a) Concluded.

Figure 12.- Continued.

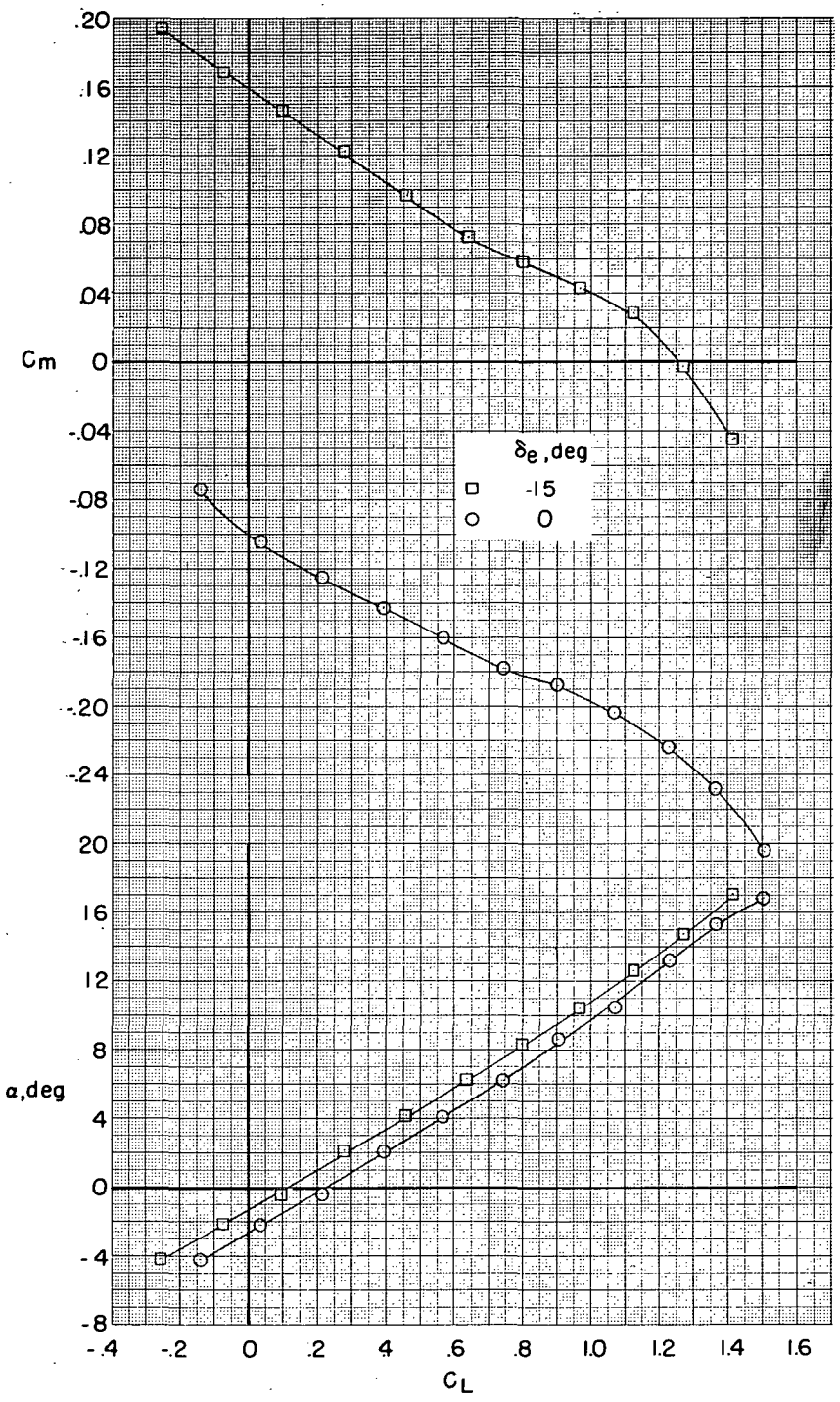

(b) $C_T = 0.600$.

Figure 12.- Continued.

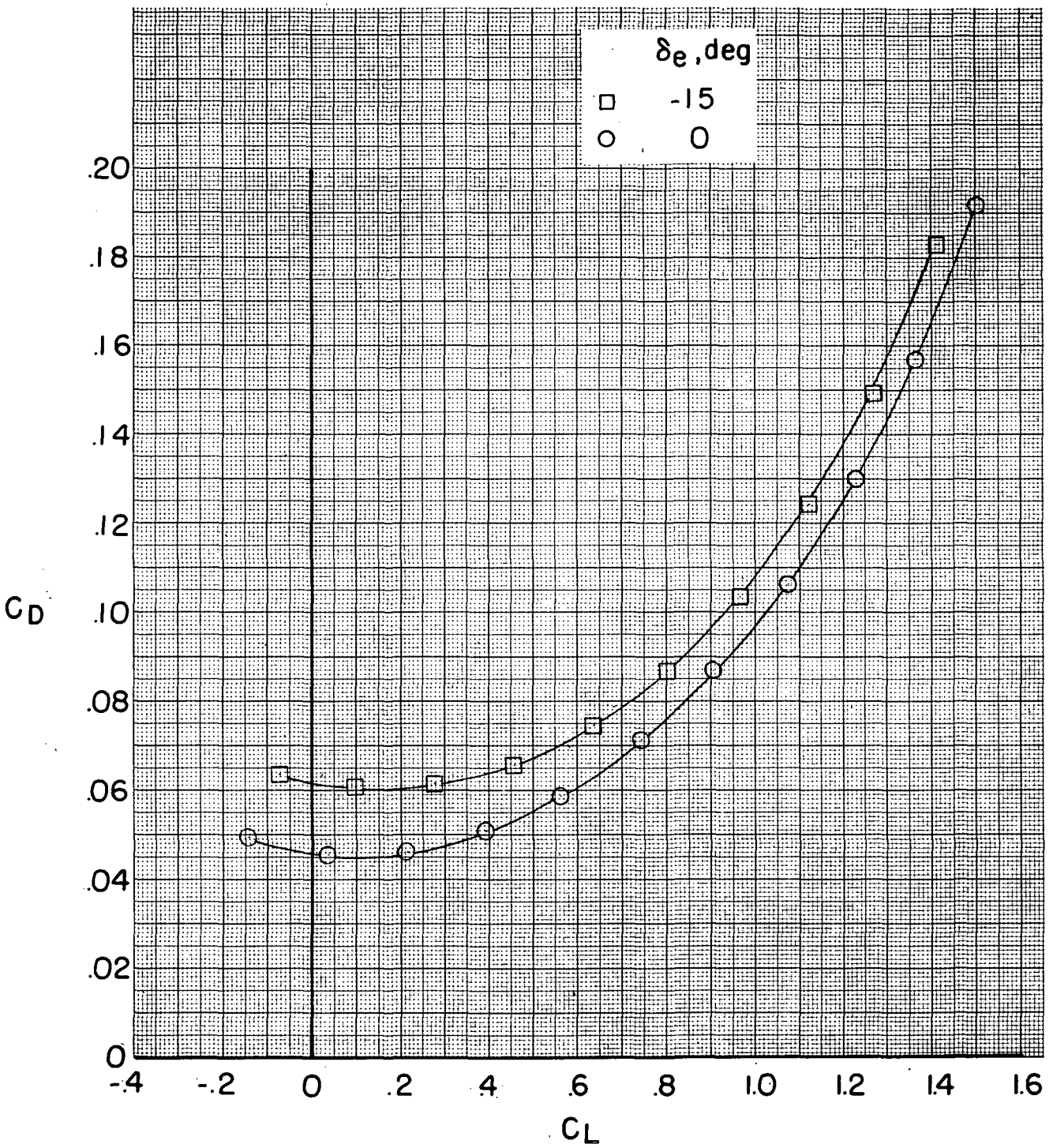

(b) Concluded.

Figure 12.- Concluded.

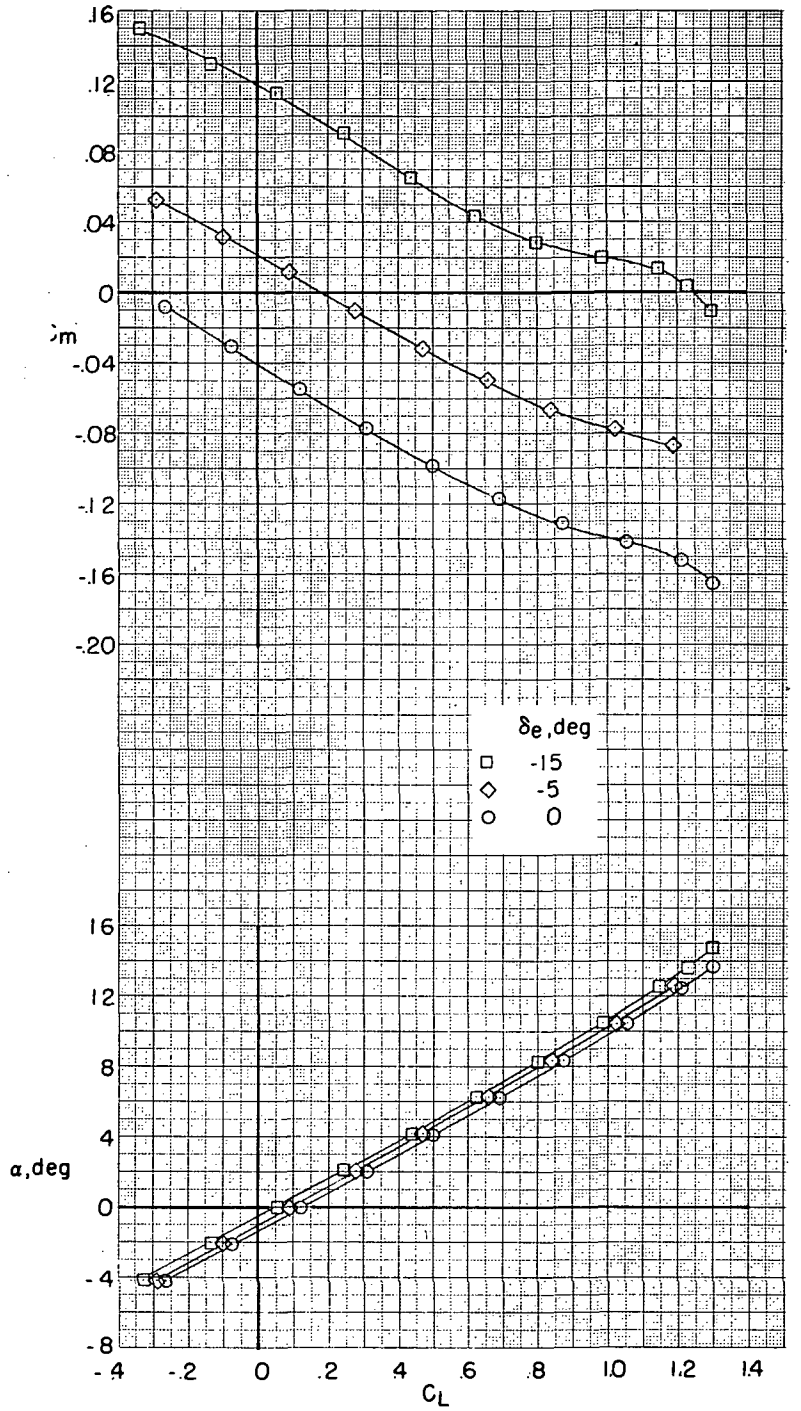

(a) $C_T = 0.008$.

Figure 13.- Effect of elevator deflection on model characteristics. $M = 0.45$; $\delta_f = 0^o$; $\beta = 0^o$; $i_n = 4^o$; $h = \infty$.

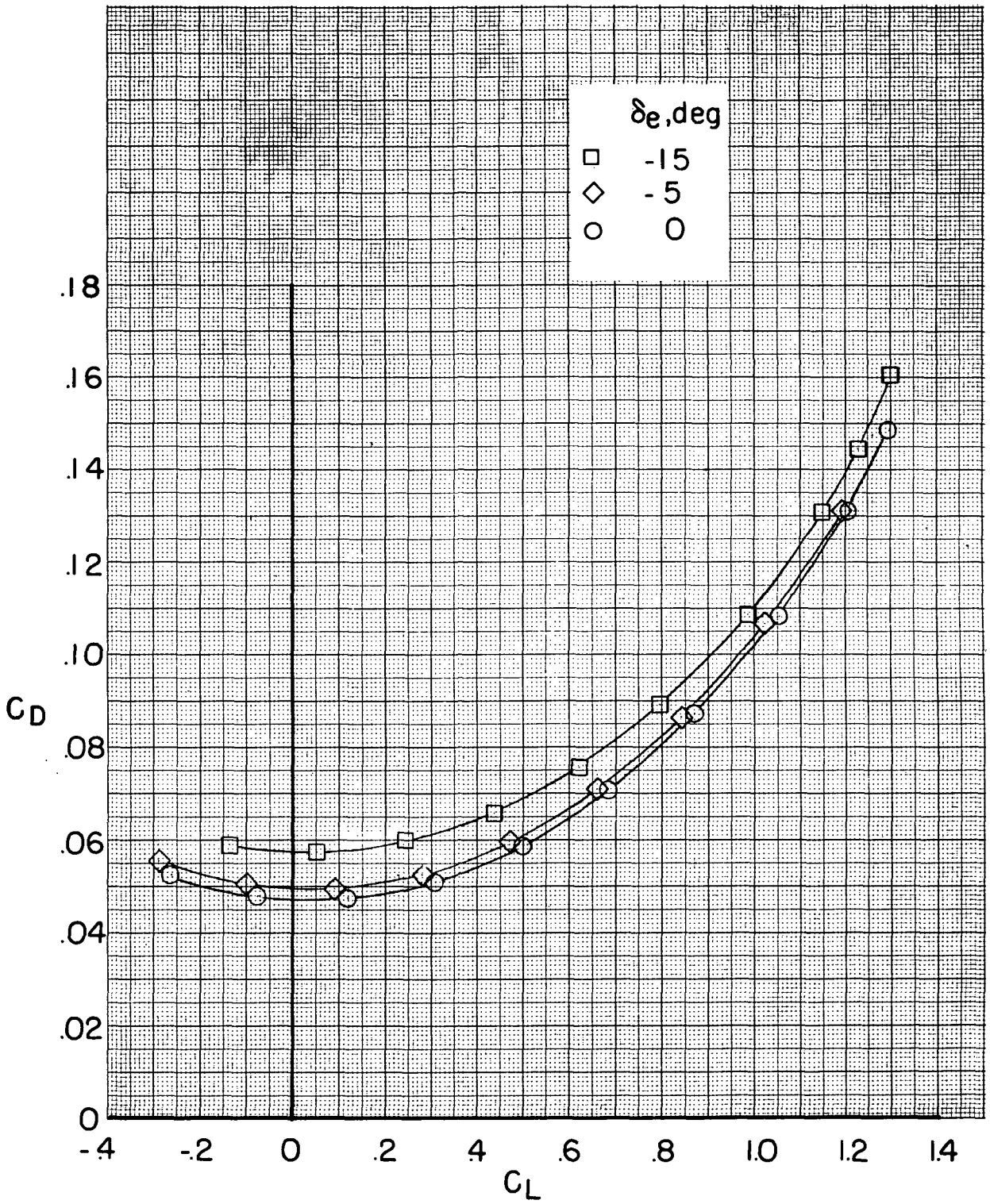

(a) Concluded.

Figure 13.- Continued.

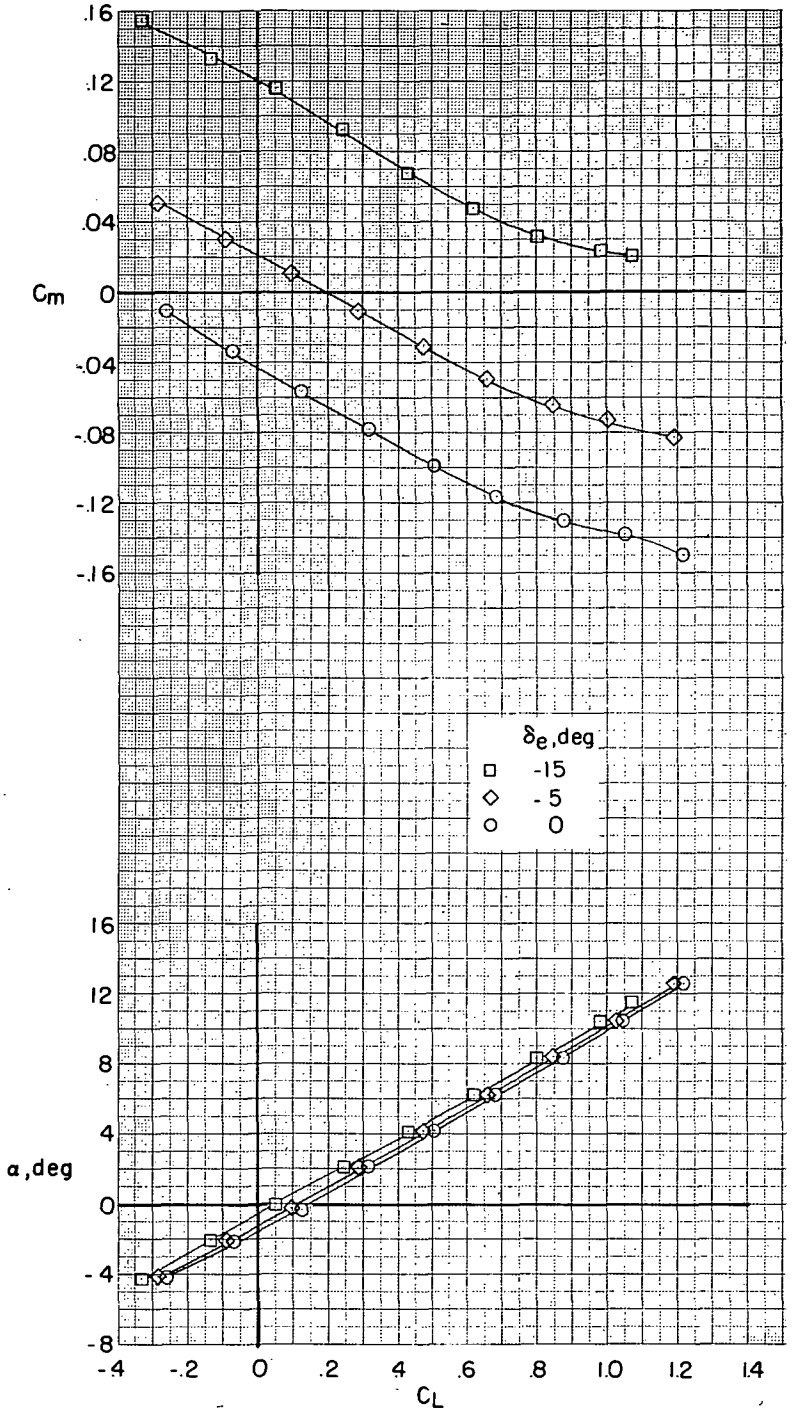

(b) $C_T = 0.040$.

Figure 13.- Continued.

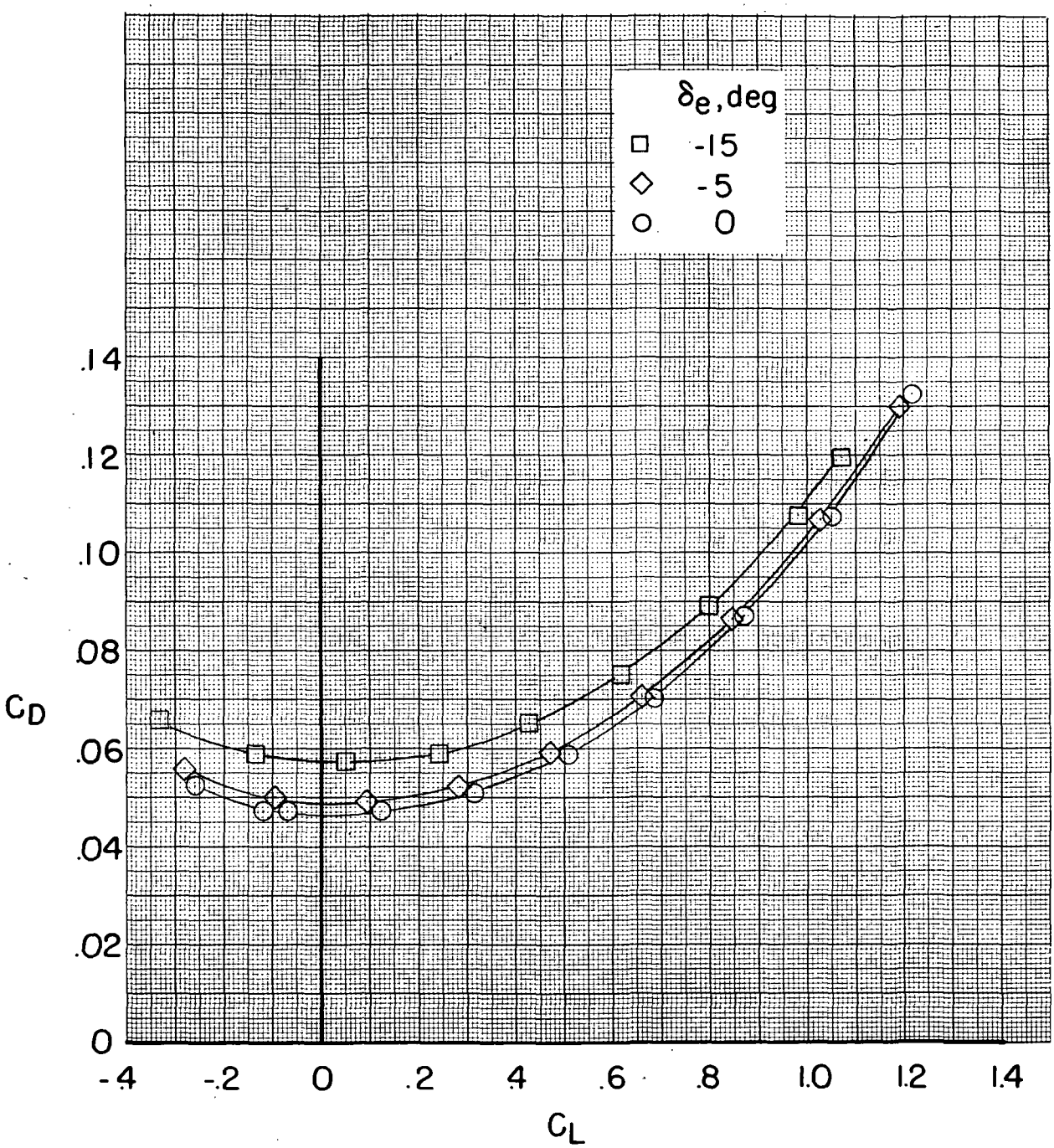

(b) Concluded.

Figure 13.- Continued.

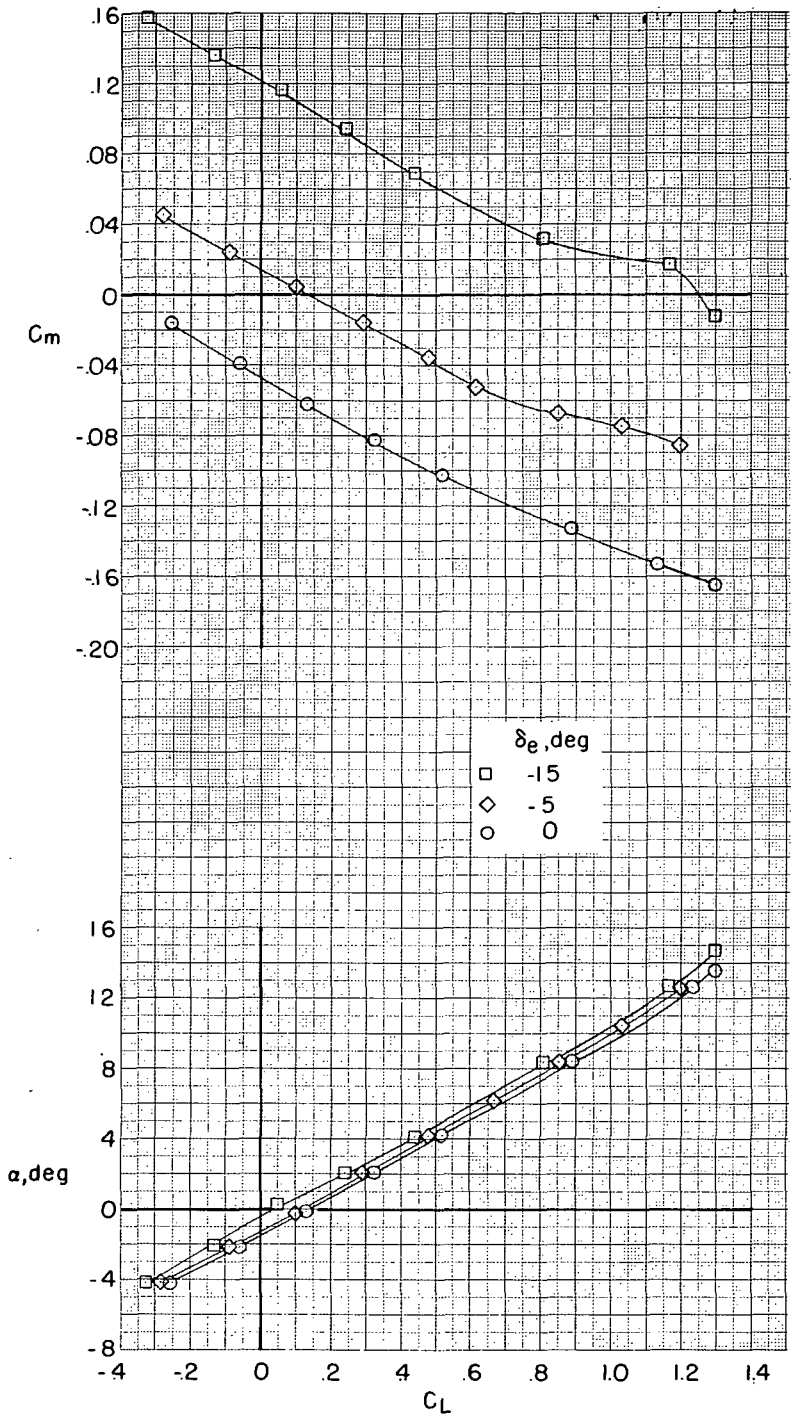

(c) $C_T = 0.080$.

Figure 13.- Continued.

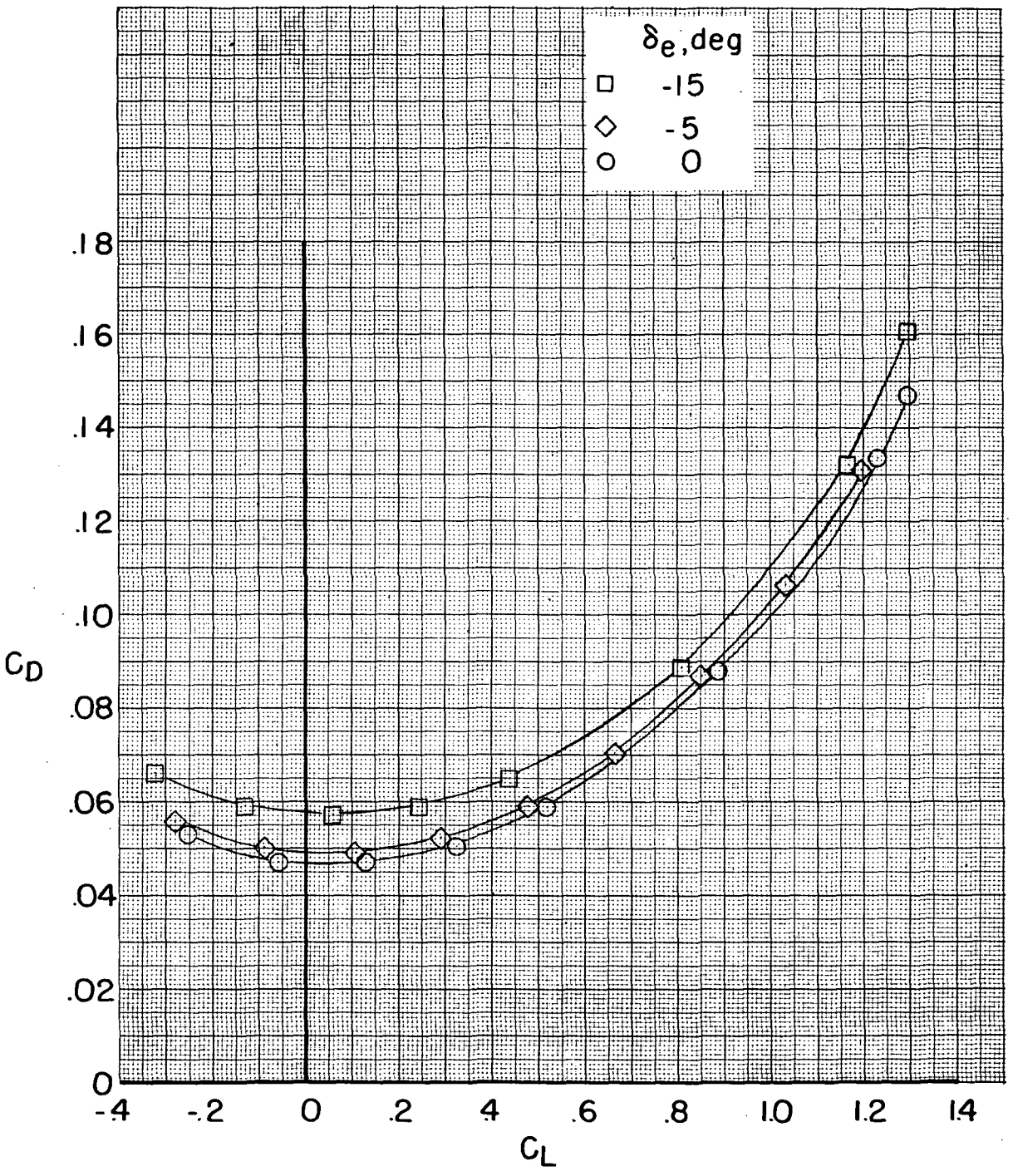

(c) Concluded.

Figure 13.- Continued.

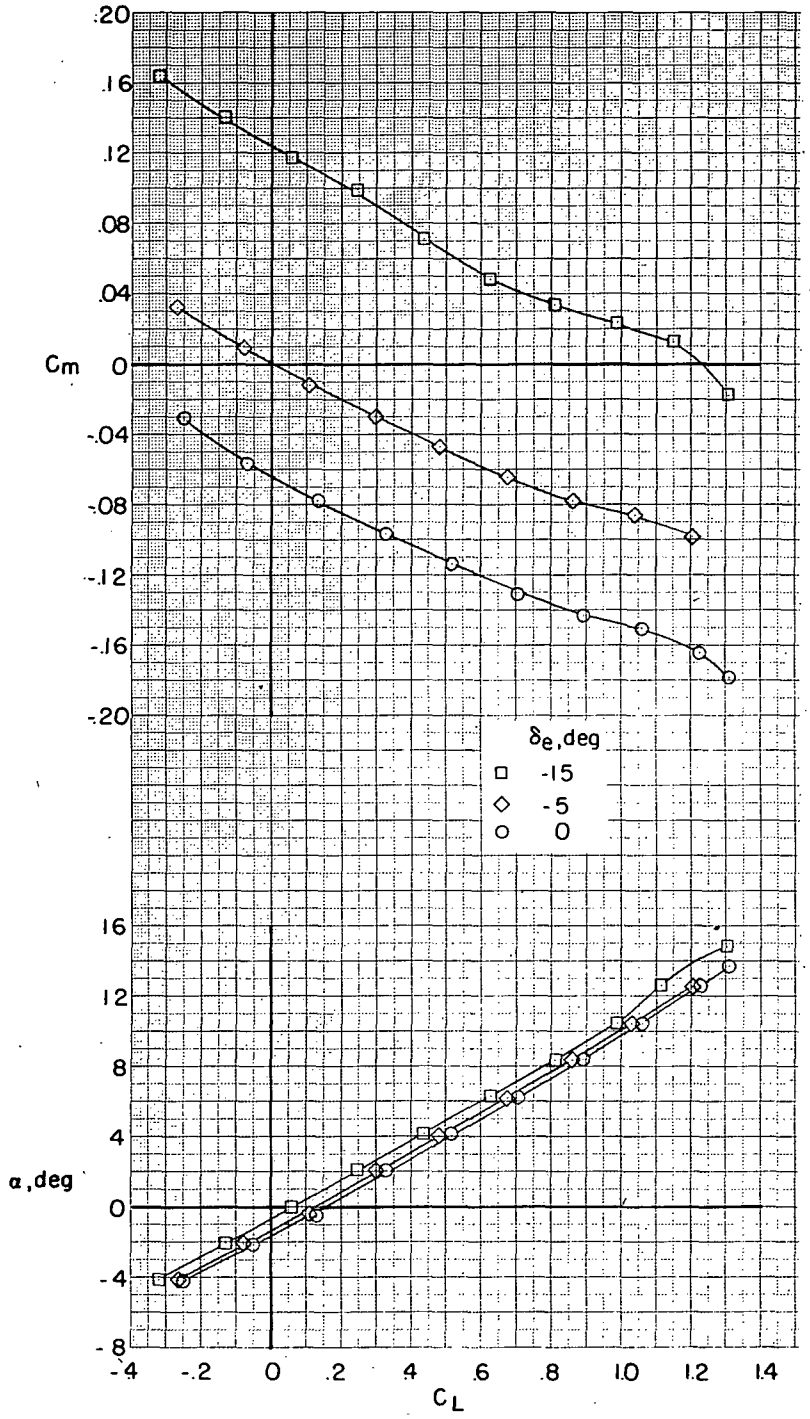

(d) $C_T = 0.170$.

Figure 13.- Continued.

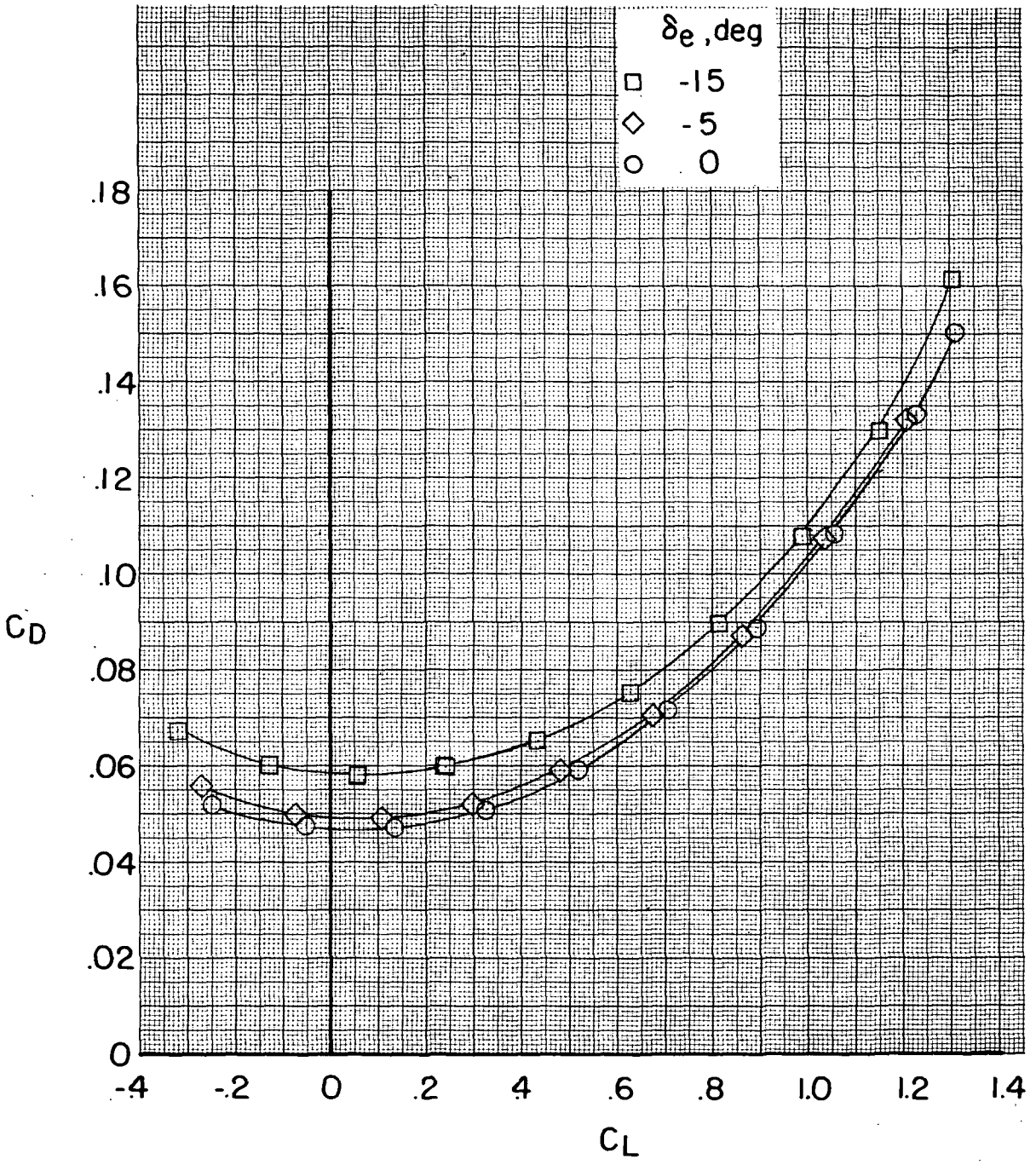

(d) Concluded.

Figure 13.- Concluded.

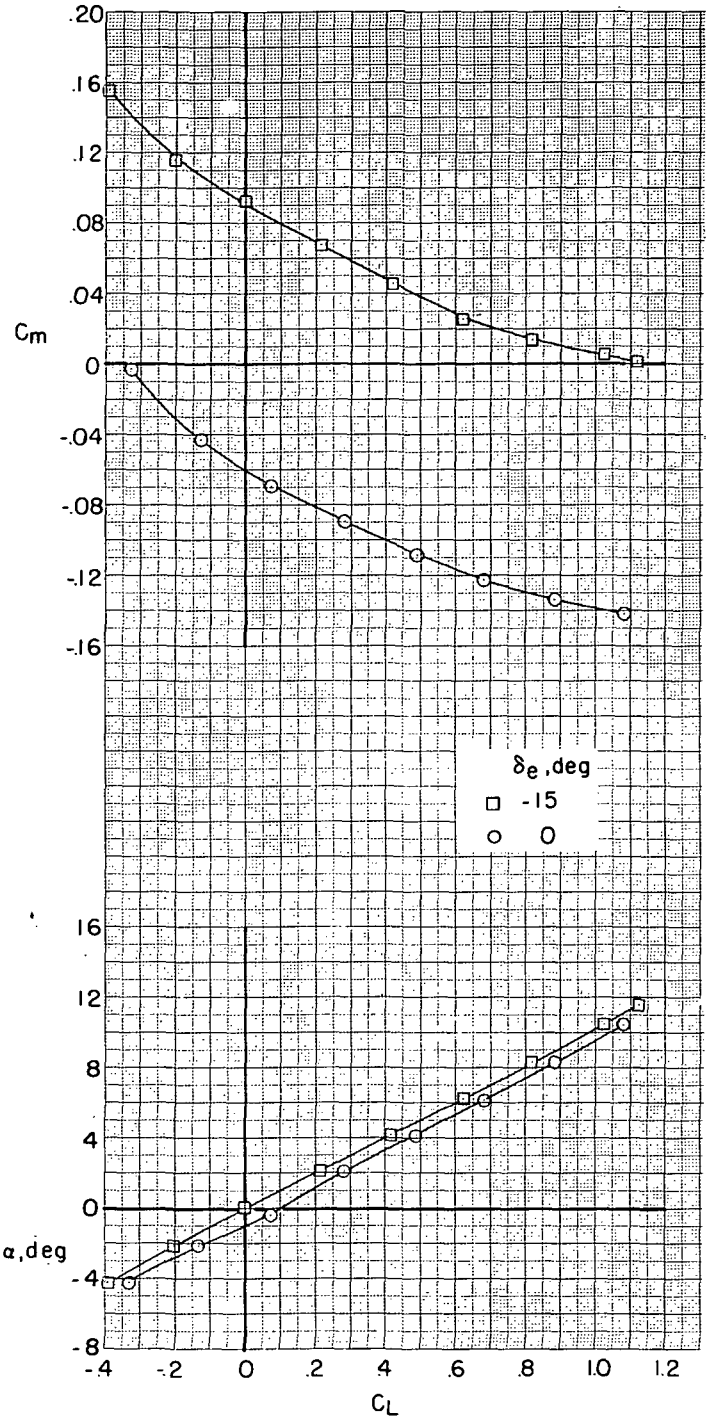

(a) $C_T = 0.005$.

Figure 14.- Effect of elevator deflection on model characteristics. $M = 0.60$; $\delta_f = 0^o$; $\beta = 0^o$; $i_n = 4^o$; $h = \infty$.

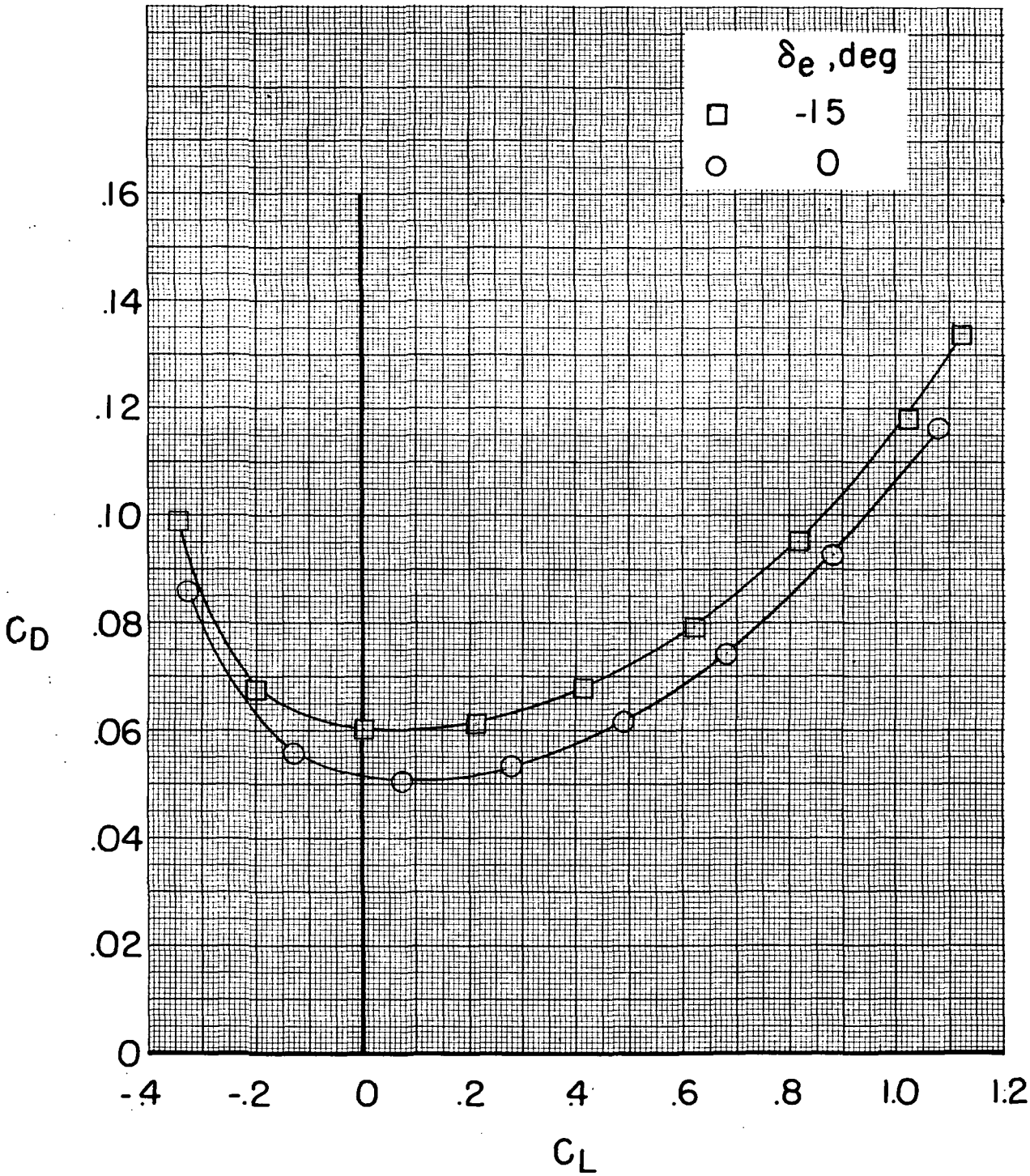

(a) Concluded.

Figure 14.- Continued.

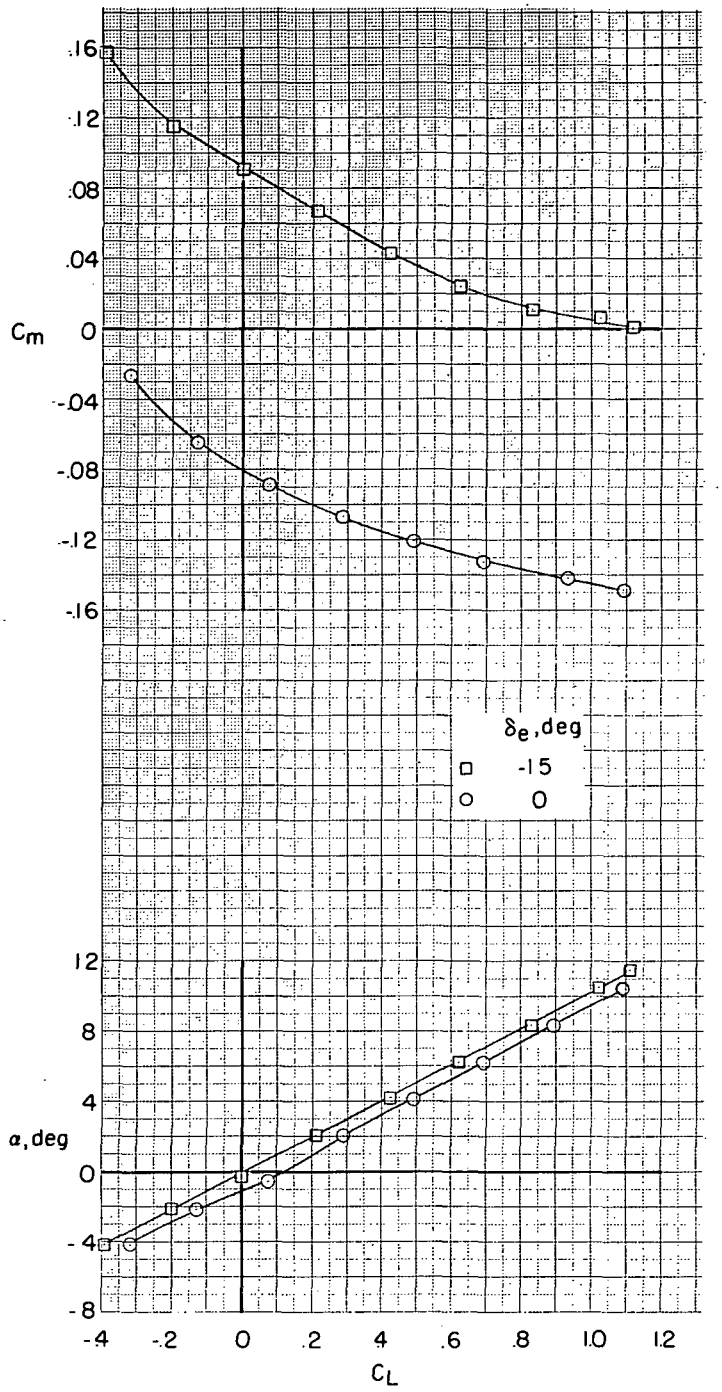

(b) $C_T = 0.100$.

Figure 14.- Continued.

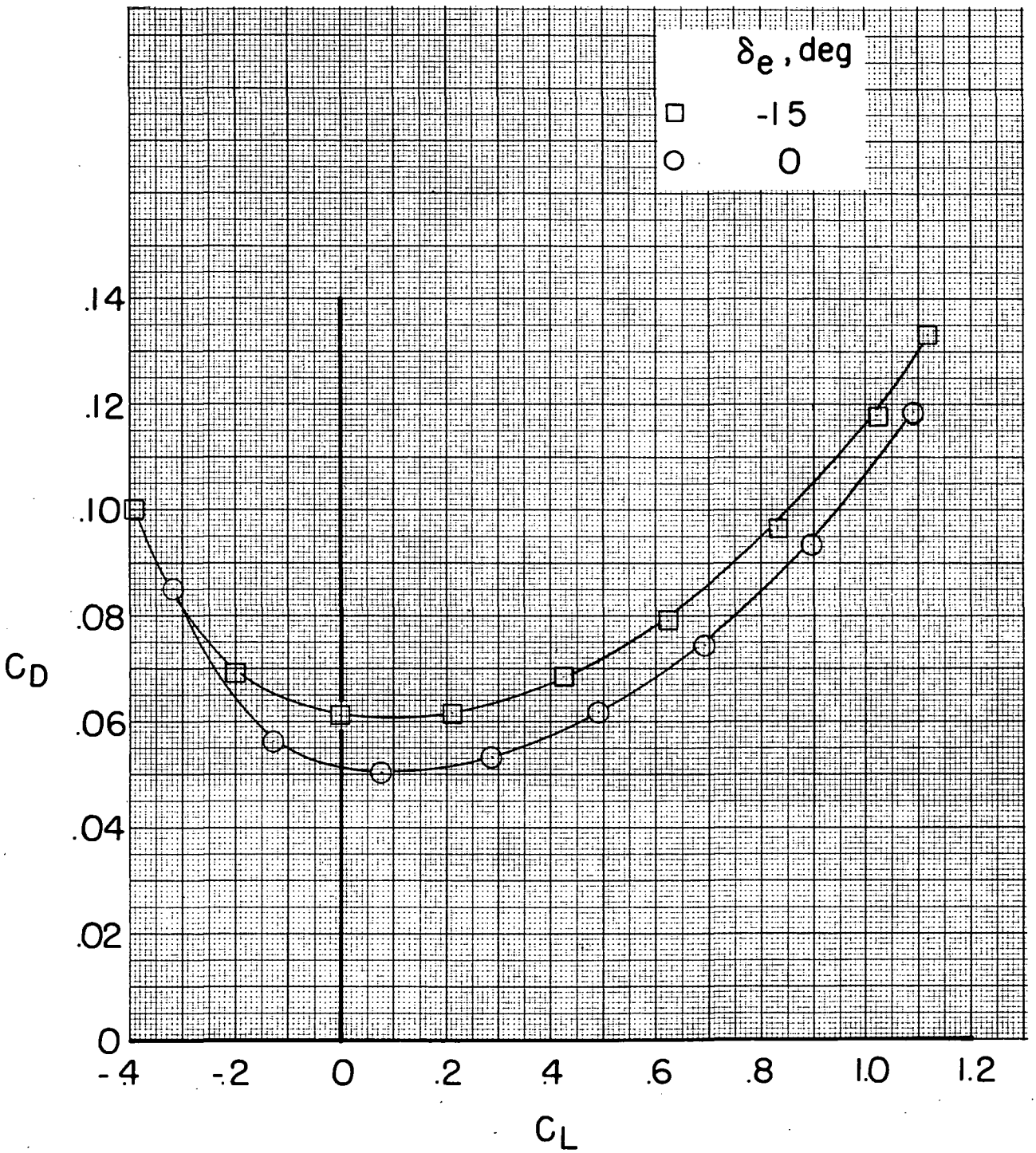

(b) Concluded.

Figure 14.- Concluded.

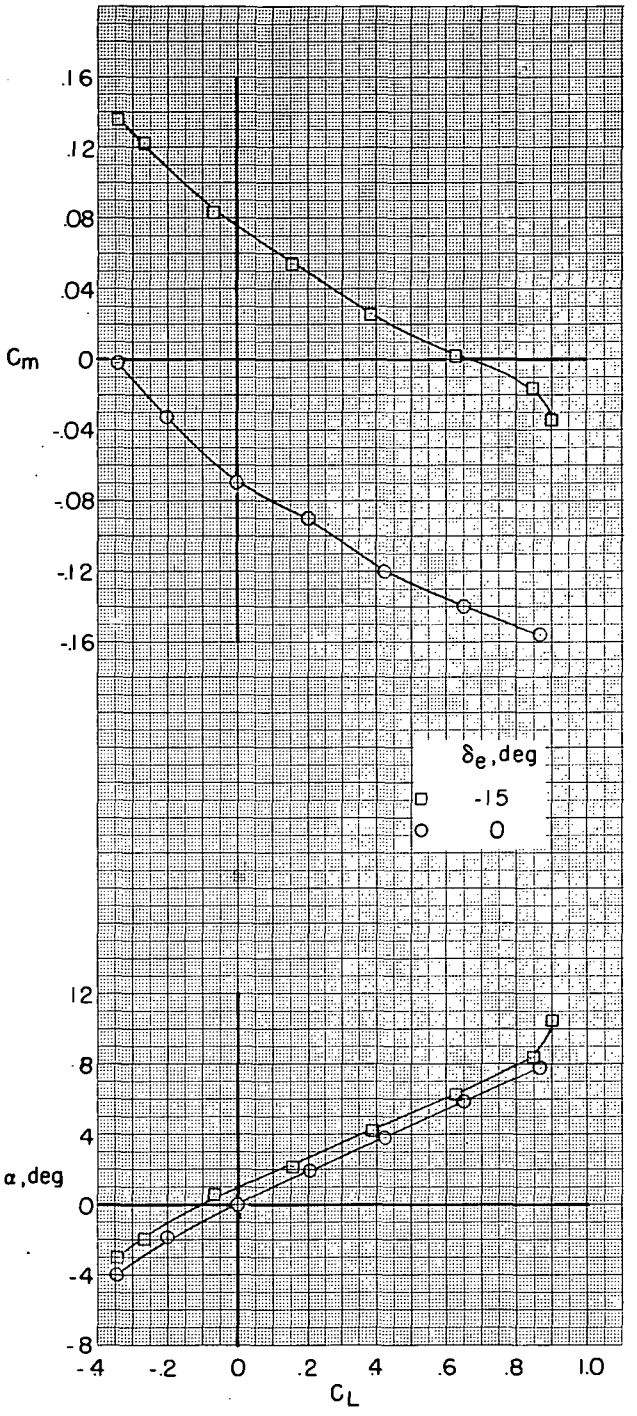

(a) $C_T = 0.002$.

Figure 15.- Effect of elevator deflection on model characteristics. $M = 0.70$; $\delta_f = 0^o$; $\beta = 0^o$; $i_n = 4^o$; $h = \infty$.

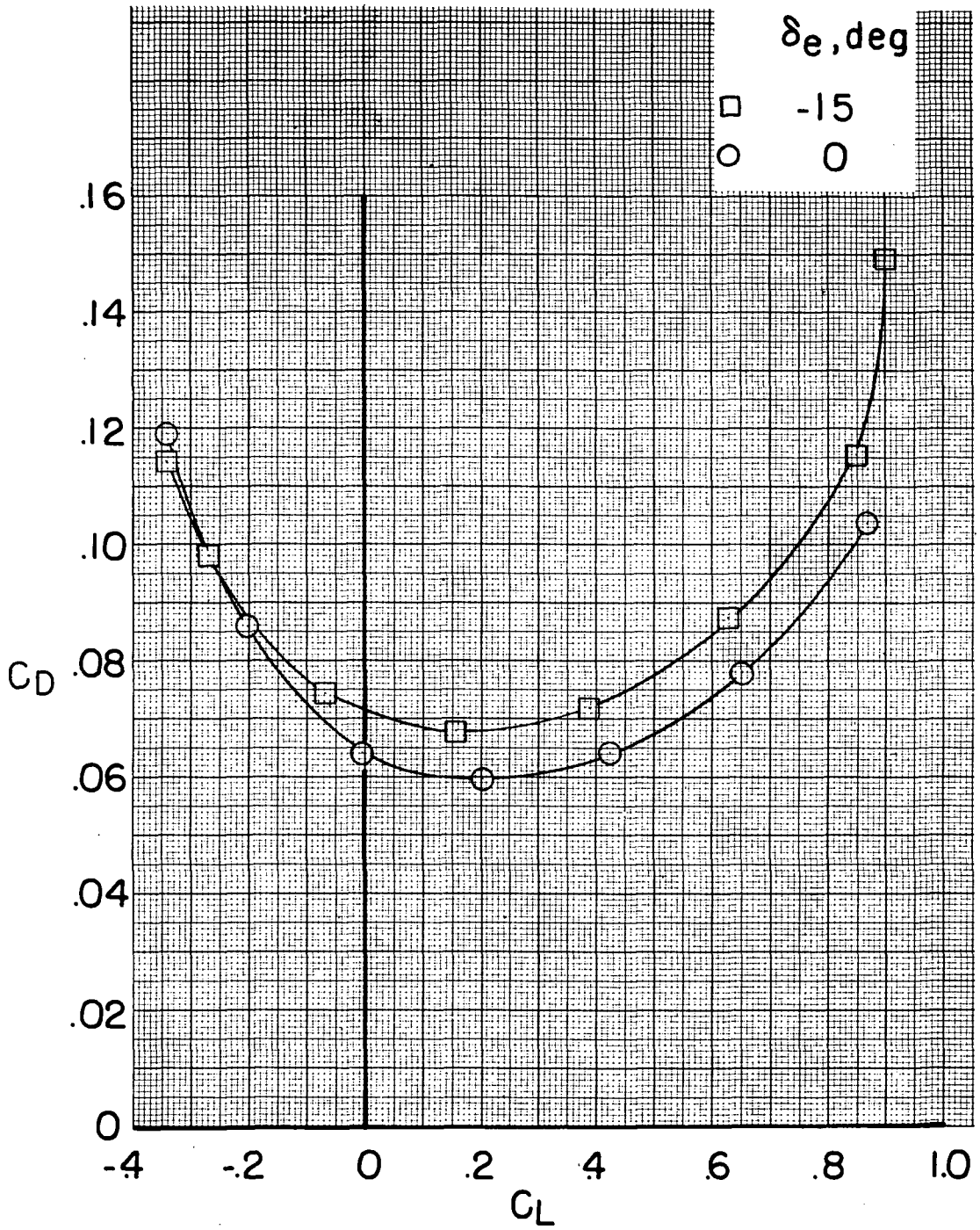

(a) Concluded.

Figure 15.- Continued.

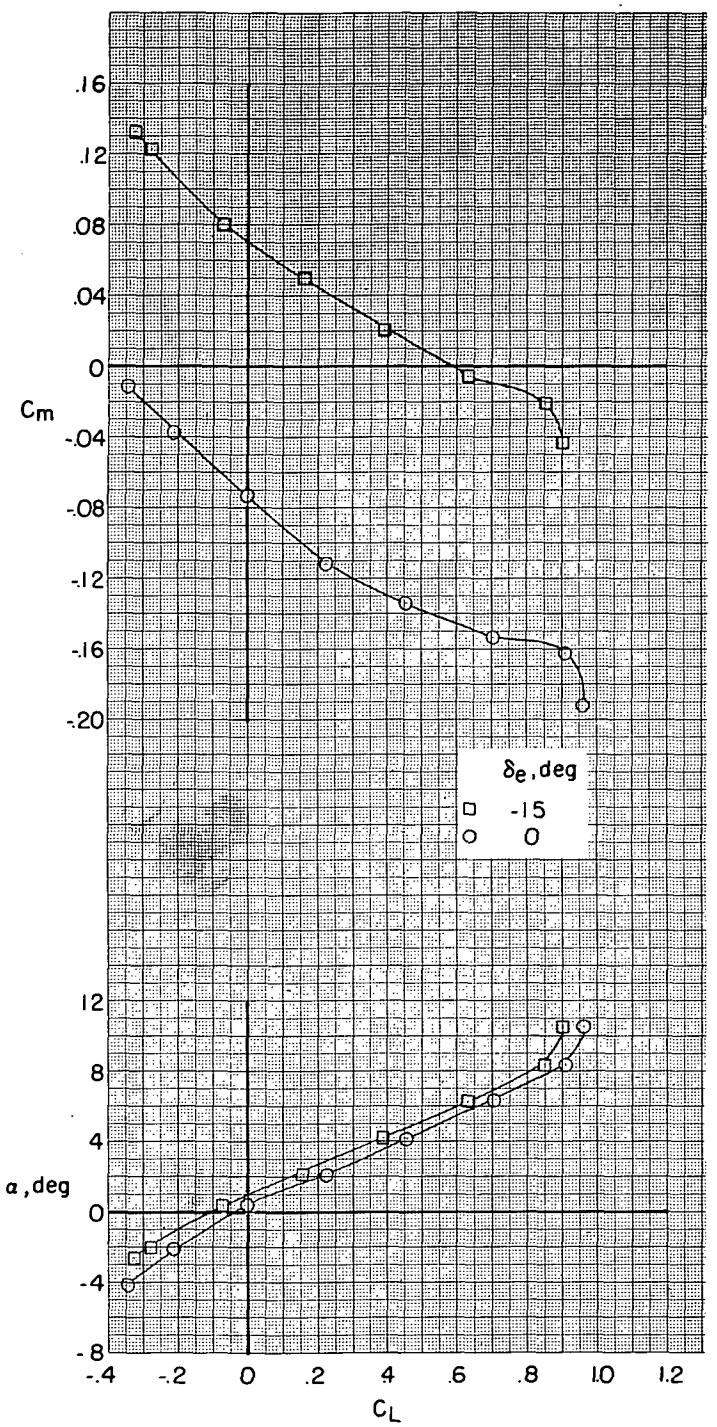

(b) $C_T = 0.080$.

Figure 15.- Continued.

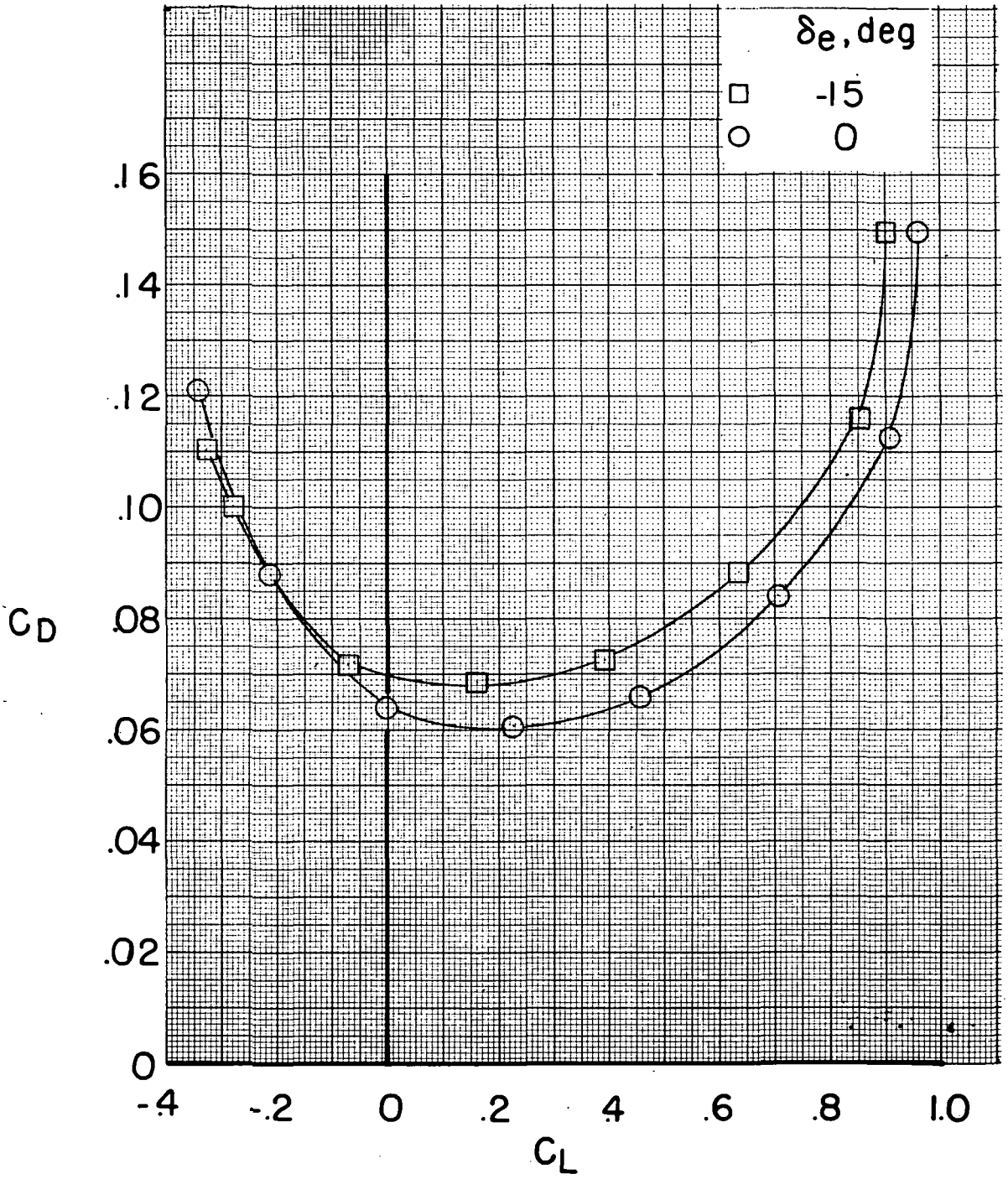

(b) Concluded.

Figure 15.- Concluded.

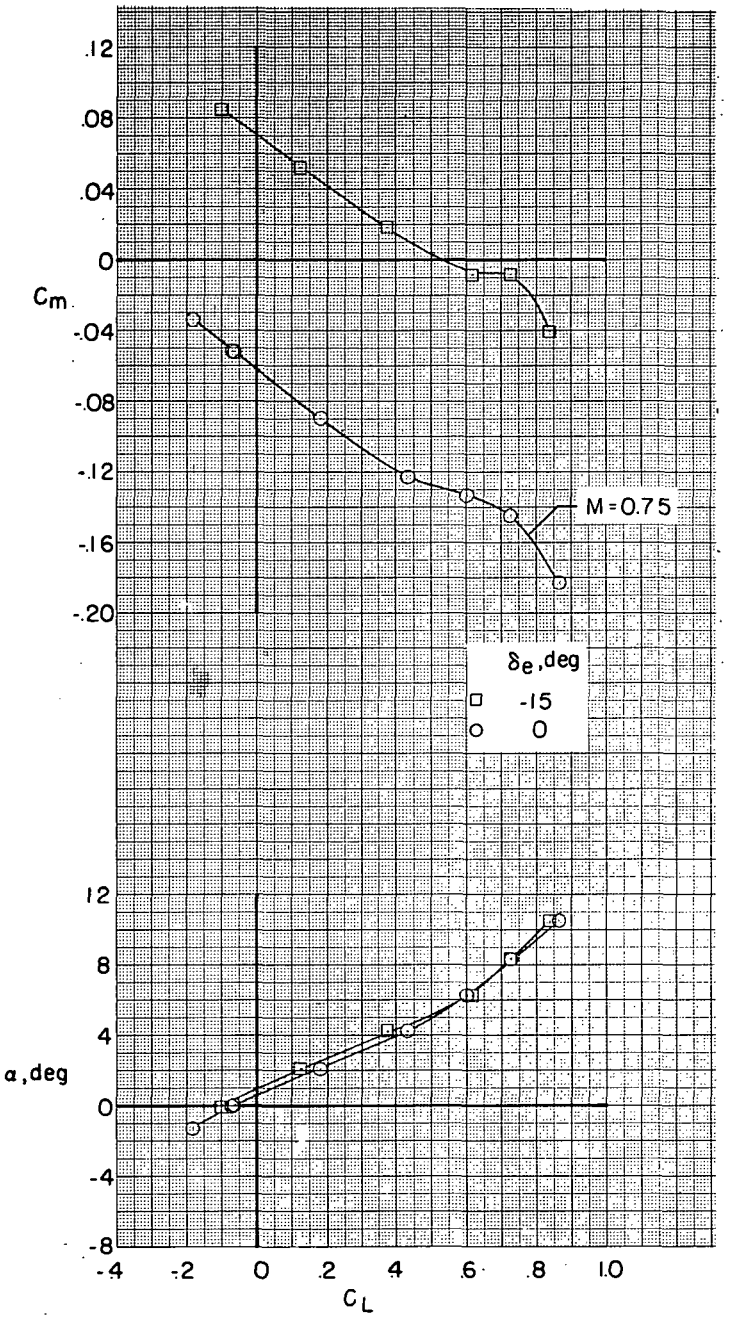

(a) $C_T = 0.001$.

Figure 16.- Effect of elevator deflection on model characteristics. $M = 0.73$; $\delta_f = 0^o$; $\beta = 0^o$; $i_n = 4^o$; $h = \infty$.

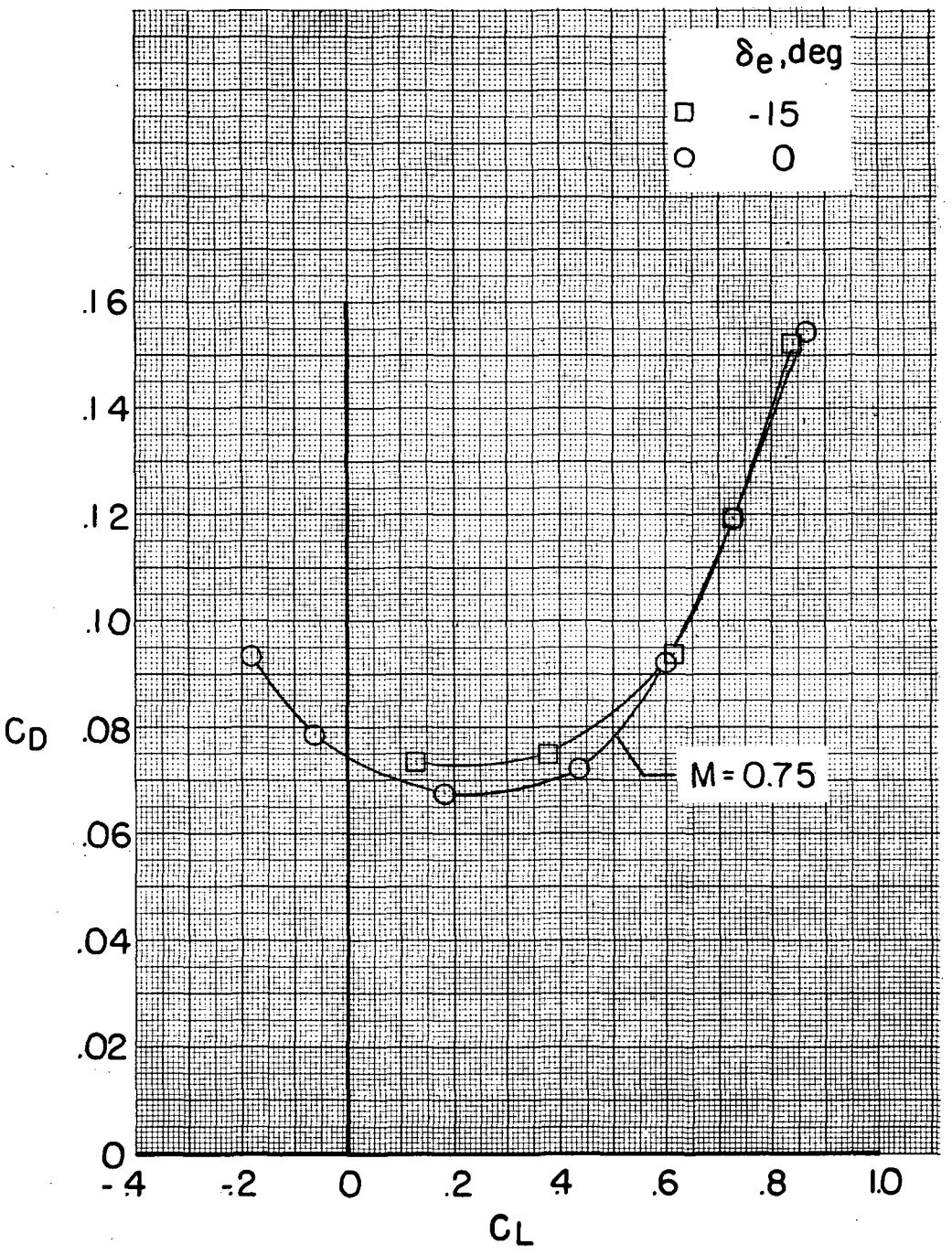

(a) Concluded.

Figure 16.- Continued.

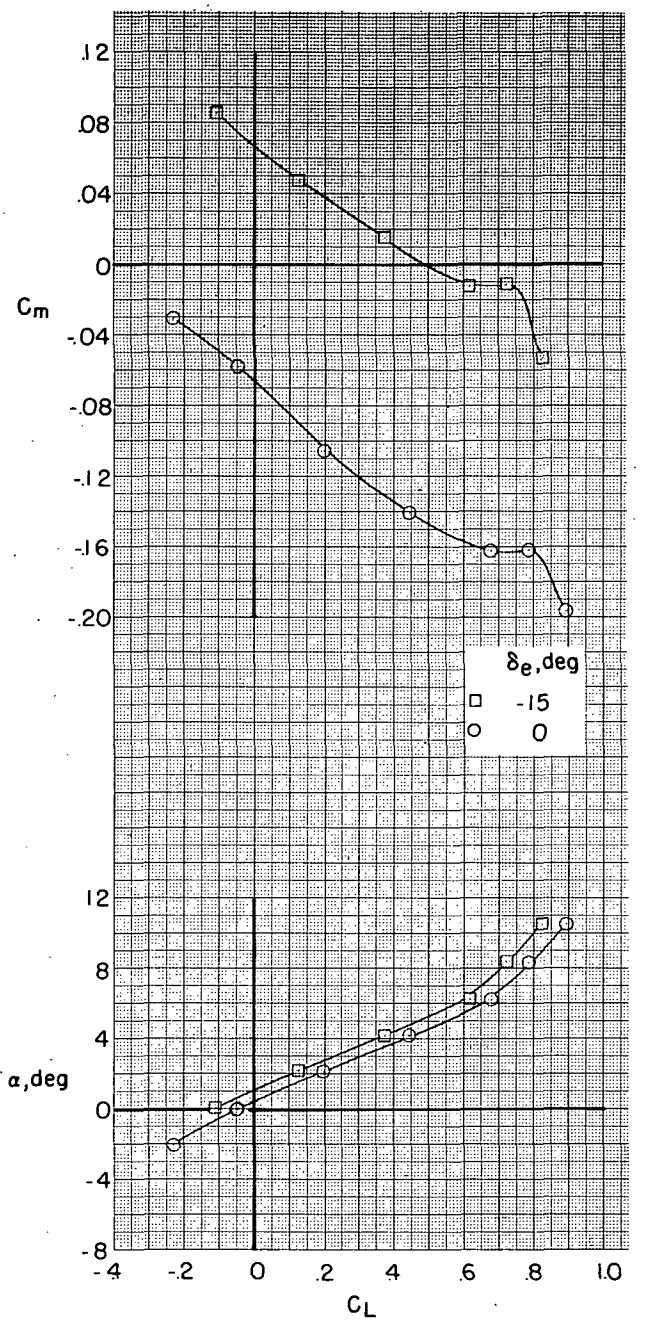

(b) $C_T = 0.080$.

Figure 16.- Continued.

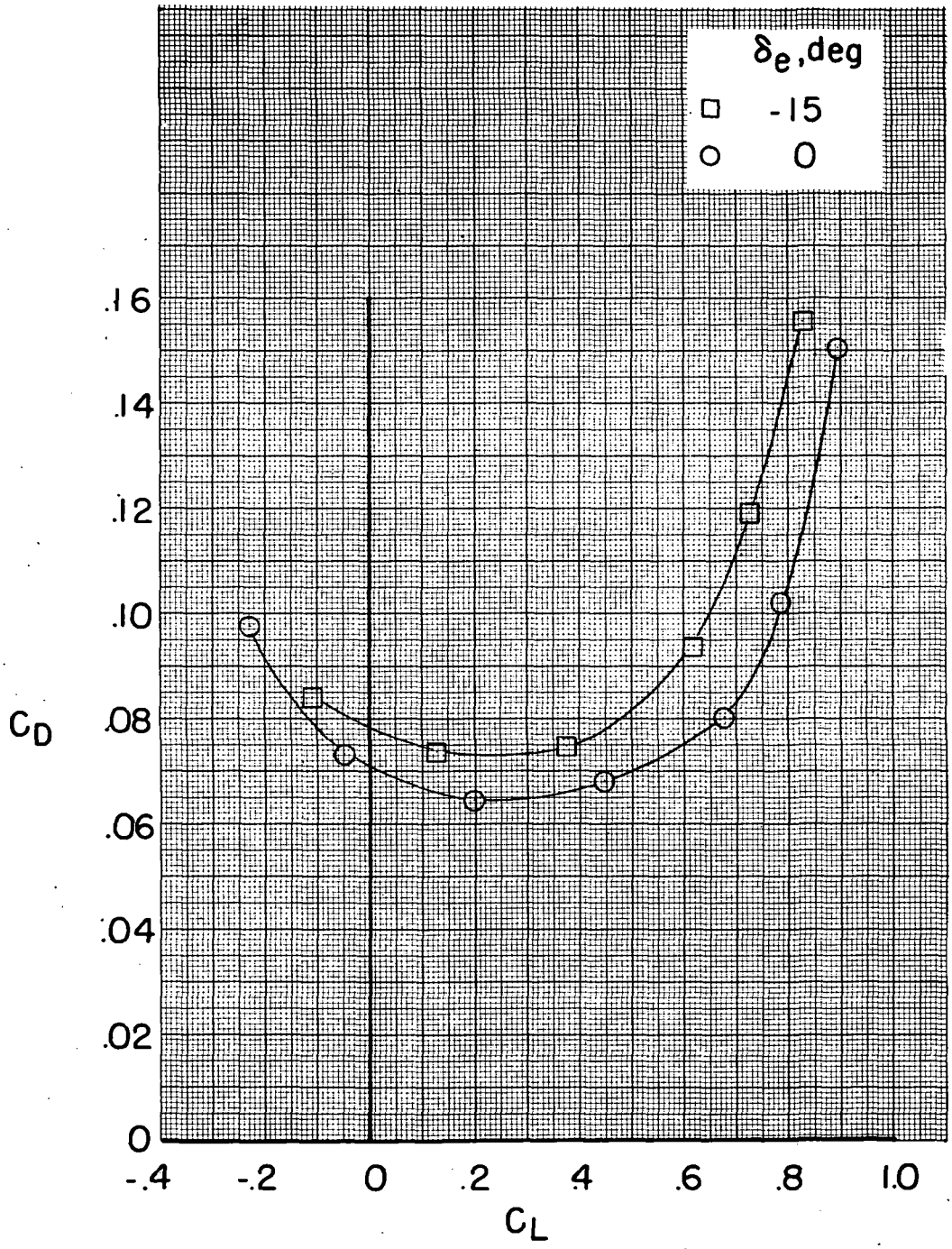

(b) Concluded.

Figure 16.- Concluded.

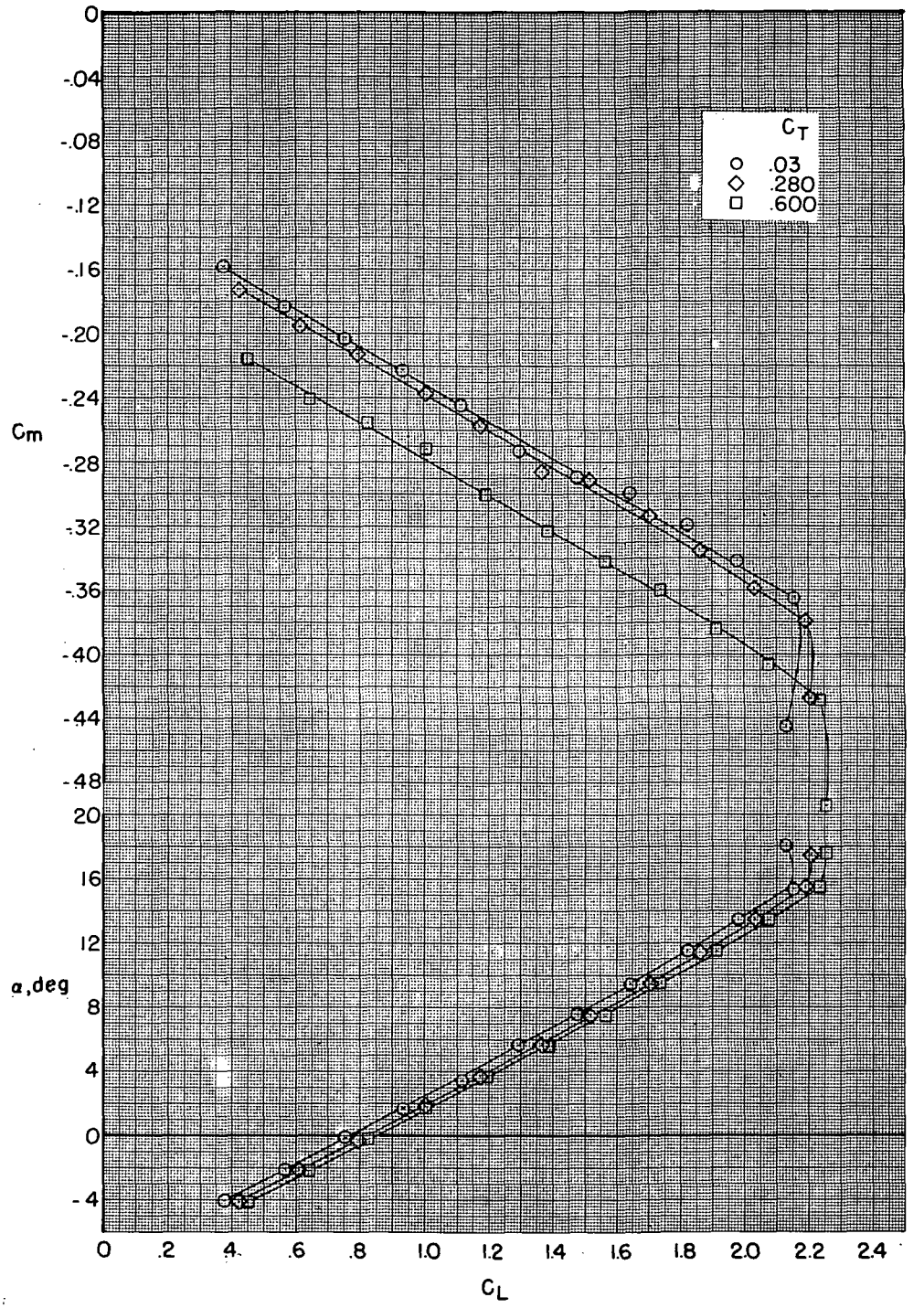

(a) $\delta_e = 0^o$.

Figure 17.- Effect of nacelle thrust coefficient on model characteristics. $M = 0.225$; $\delta_f = 30^o$; $\beta = 0^o$; $i_n = 4^o$; $h/b = \infty$.

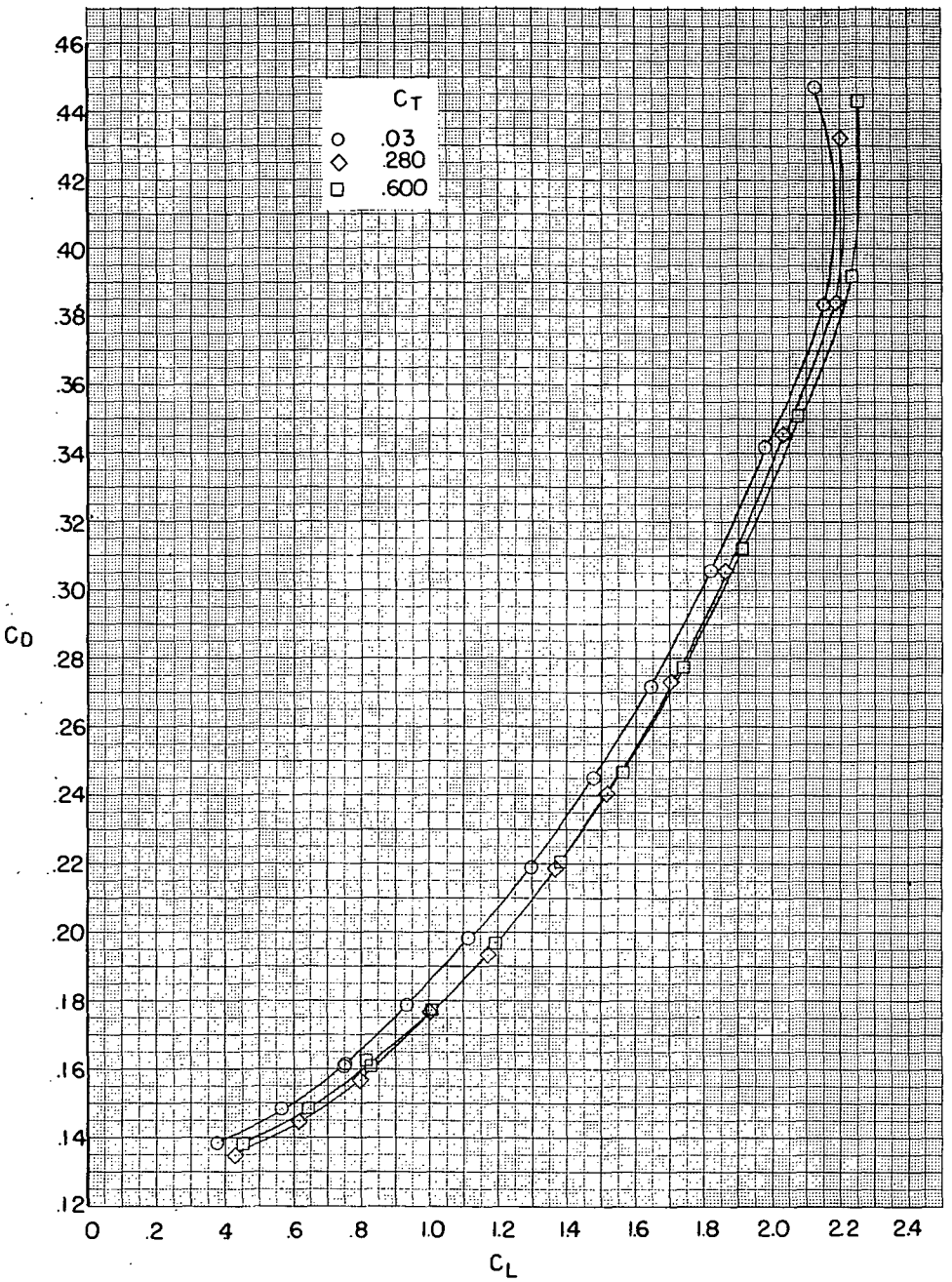

(a) Concluded.

Figure 17.- Continued.

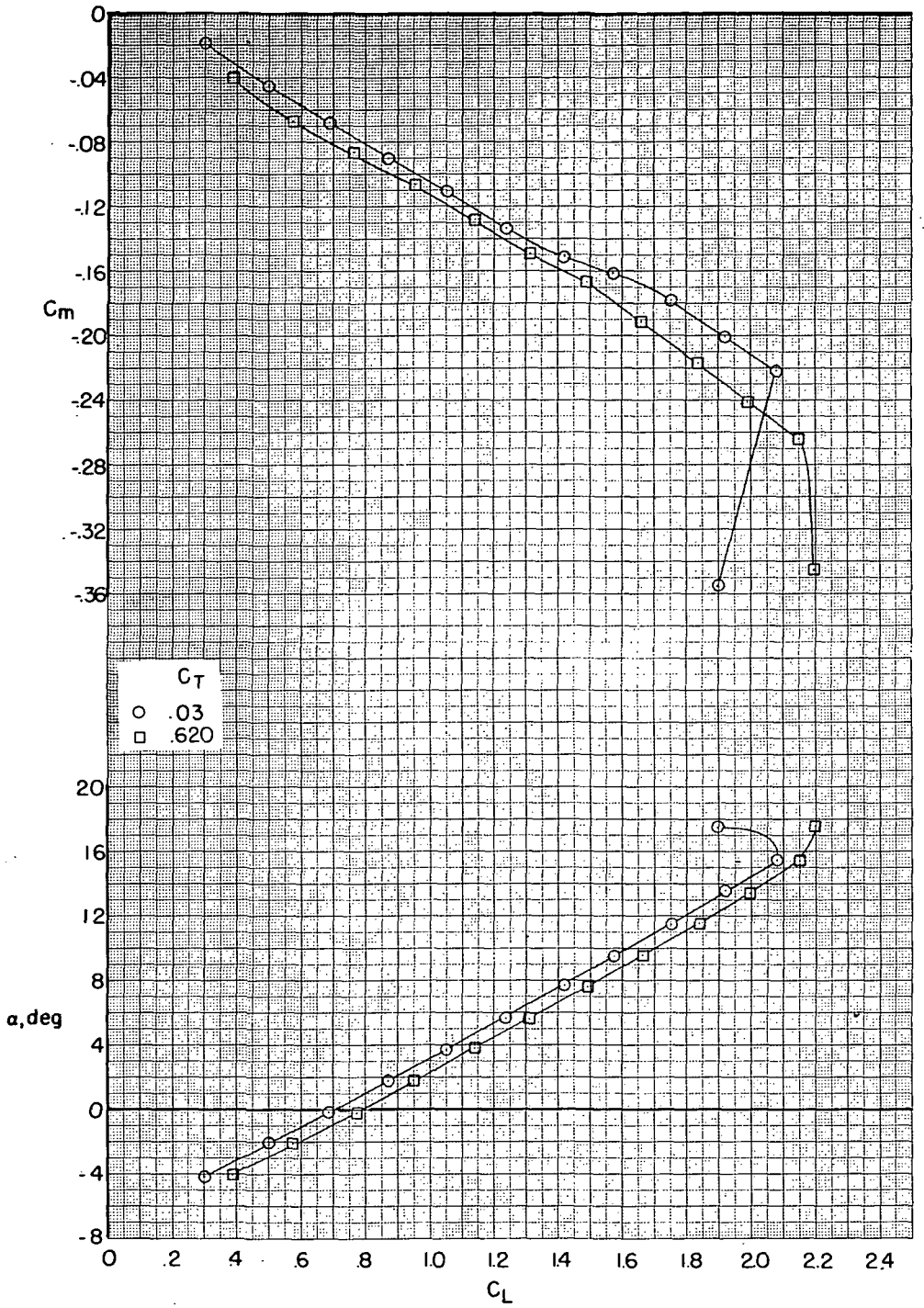

(b) $\delta_e = -10^o$.

Figure 17.- Continued.

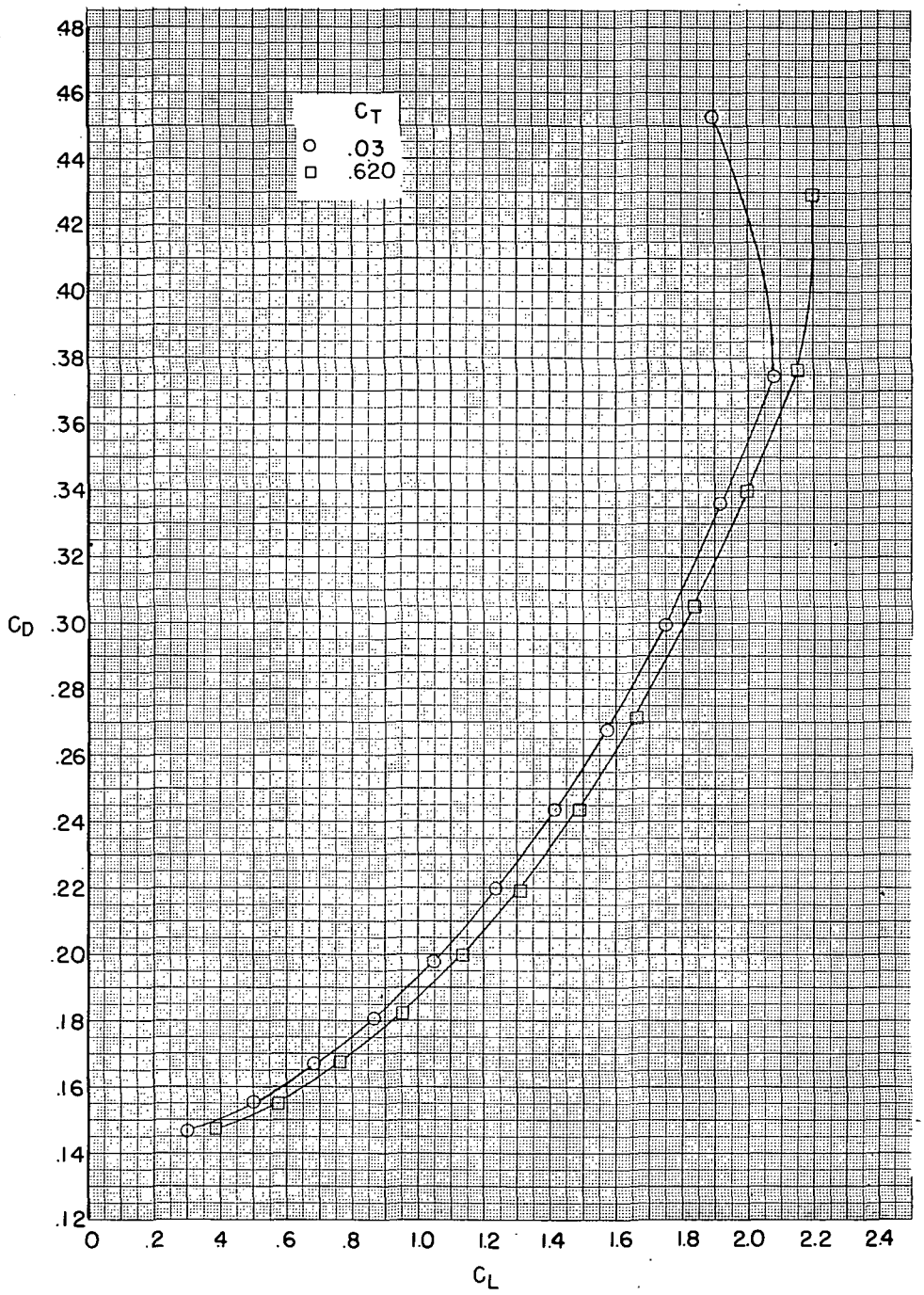

(b) Concluded.

Figure 17.- Continued.

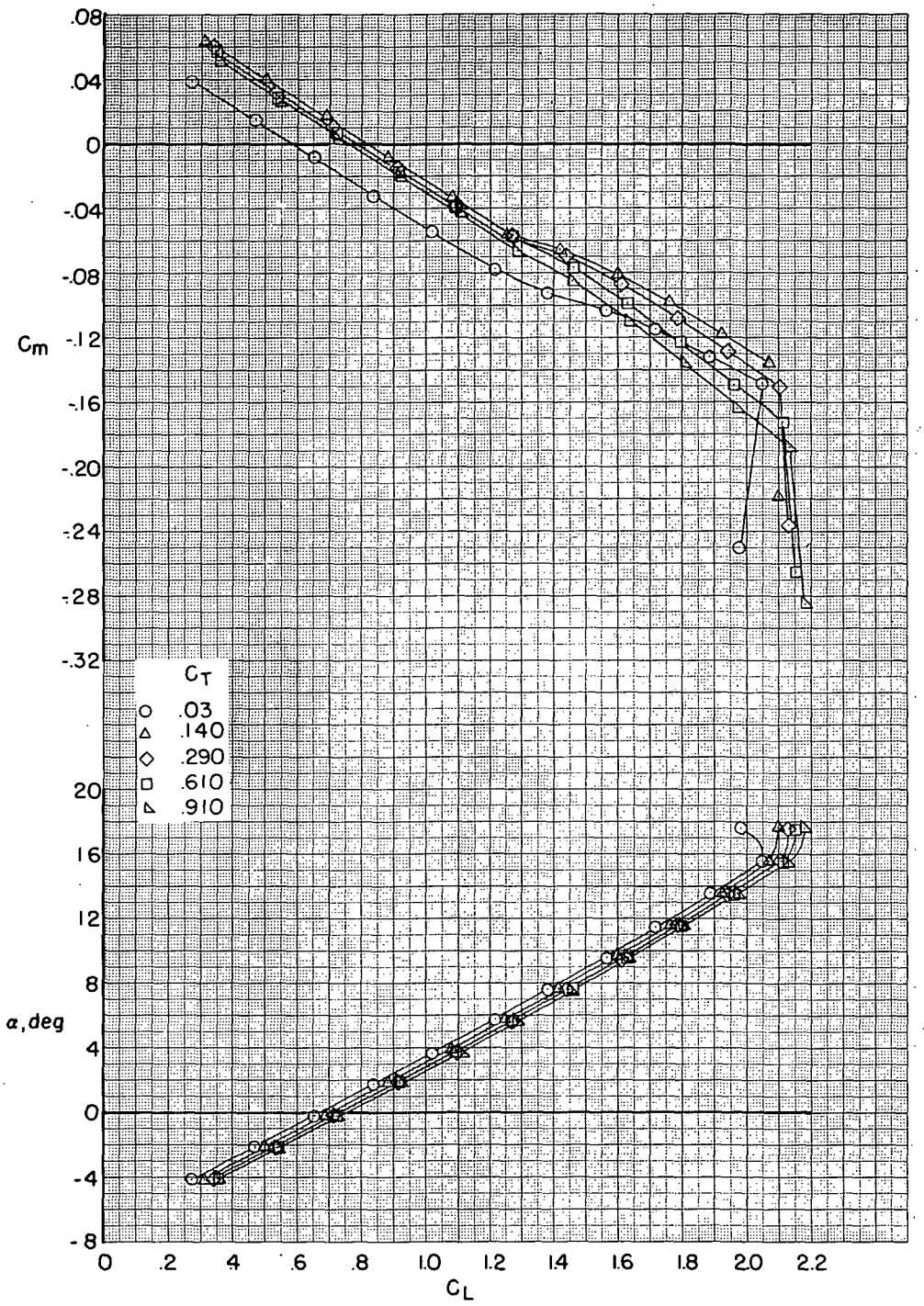

(c) $\delta_e = -15^o$.

Figure 17.- Continued.

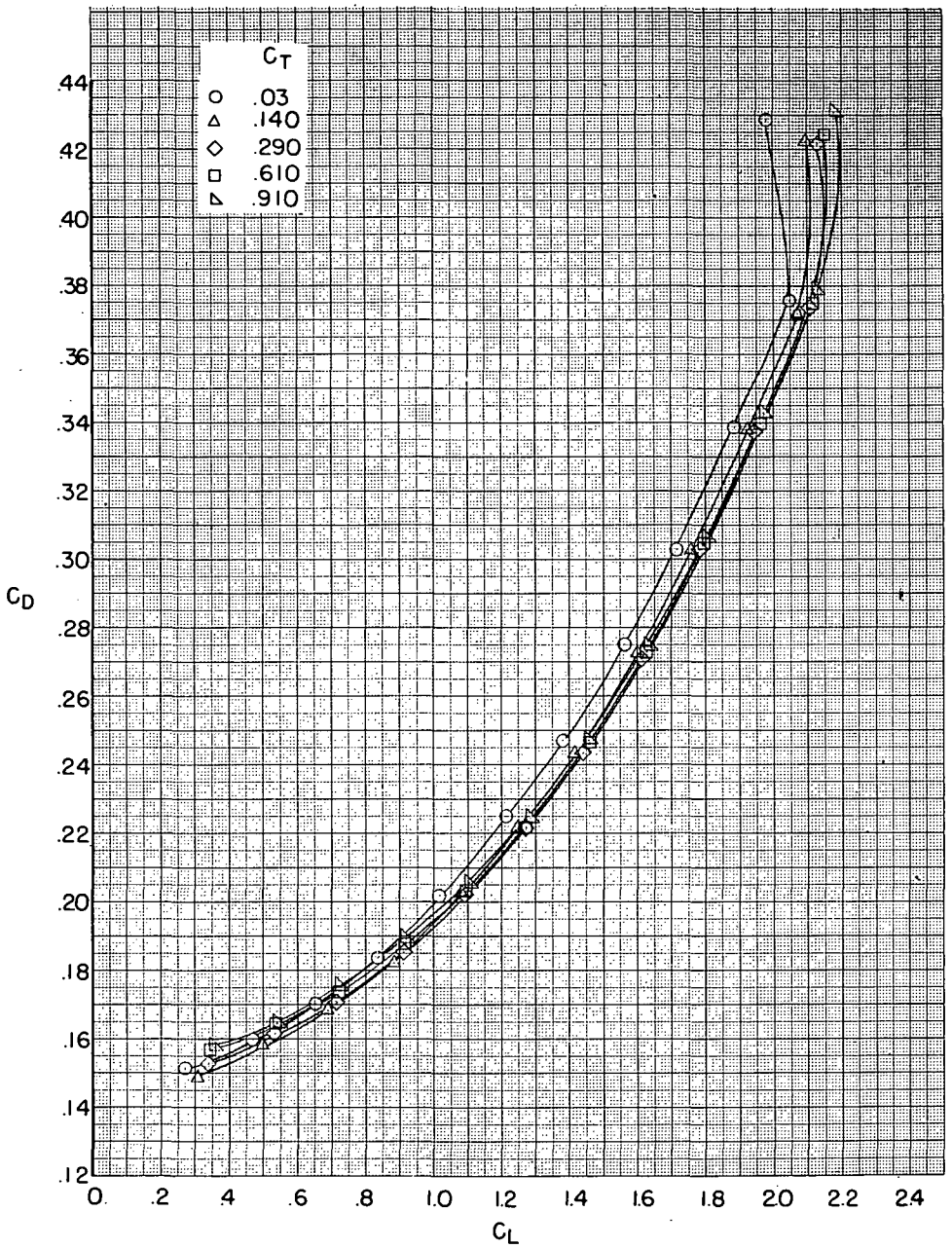

(c) Concluded.

Figure 17.- Continued.

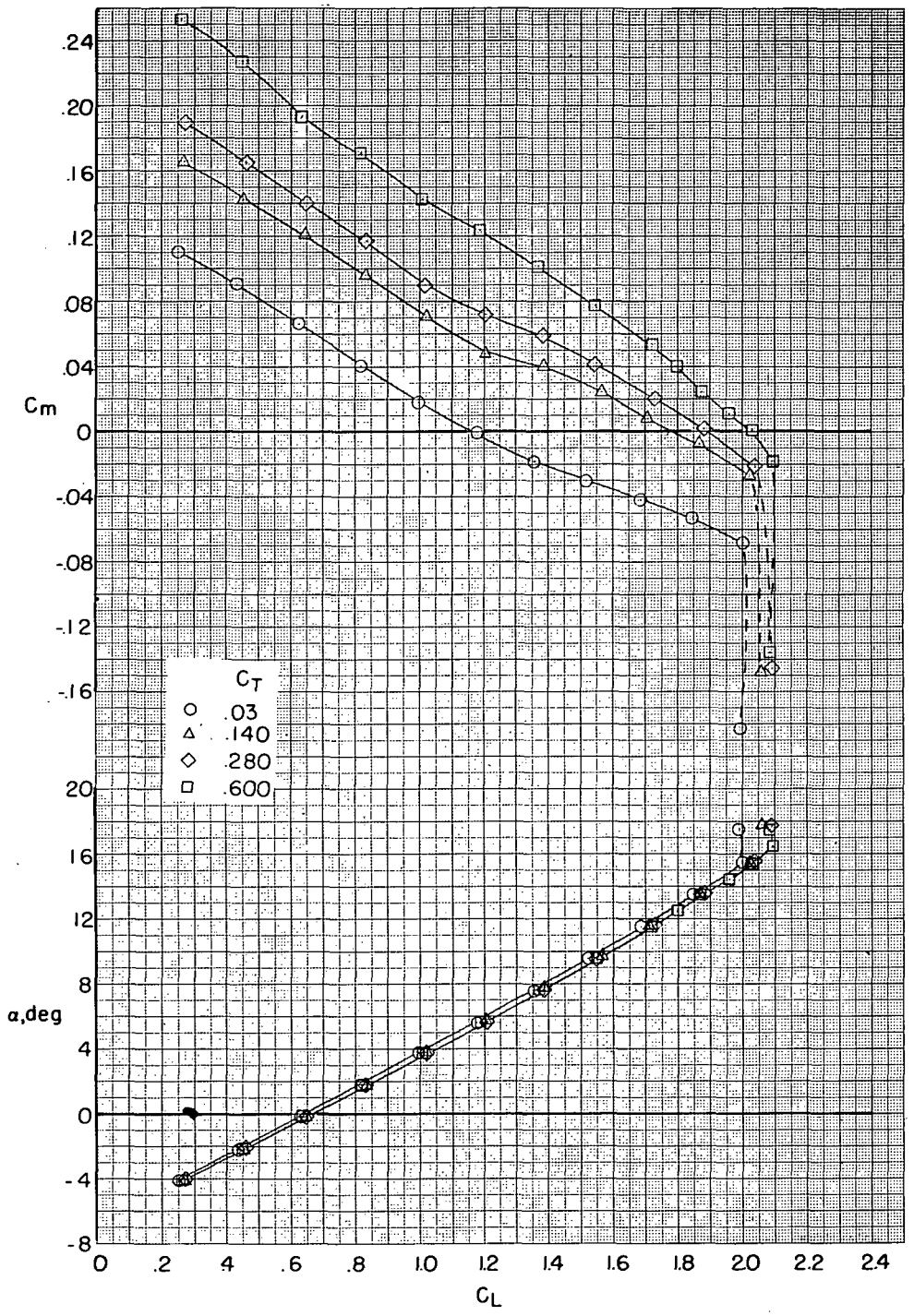

(d) $\delta_e = -25^o$.

Figure 17.- Continued.

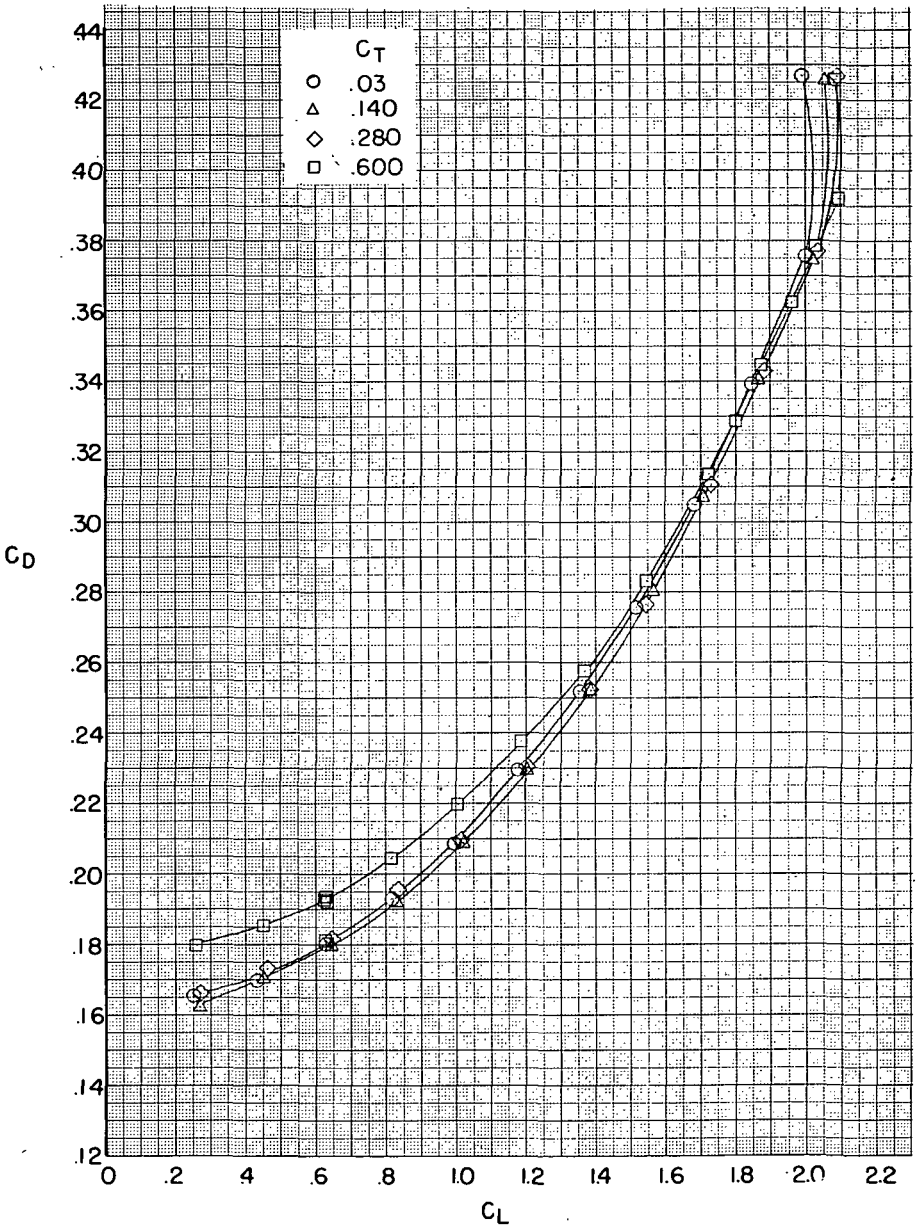

(d) Concluded.

Figure 17.- Concluded.

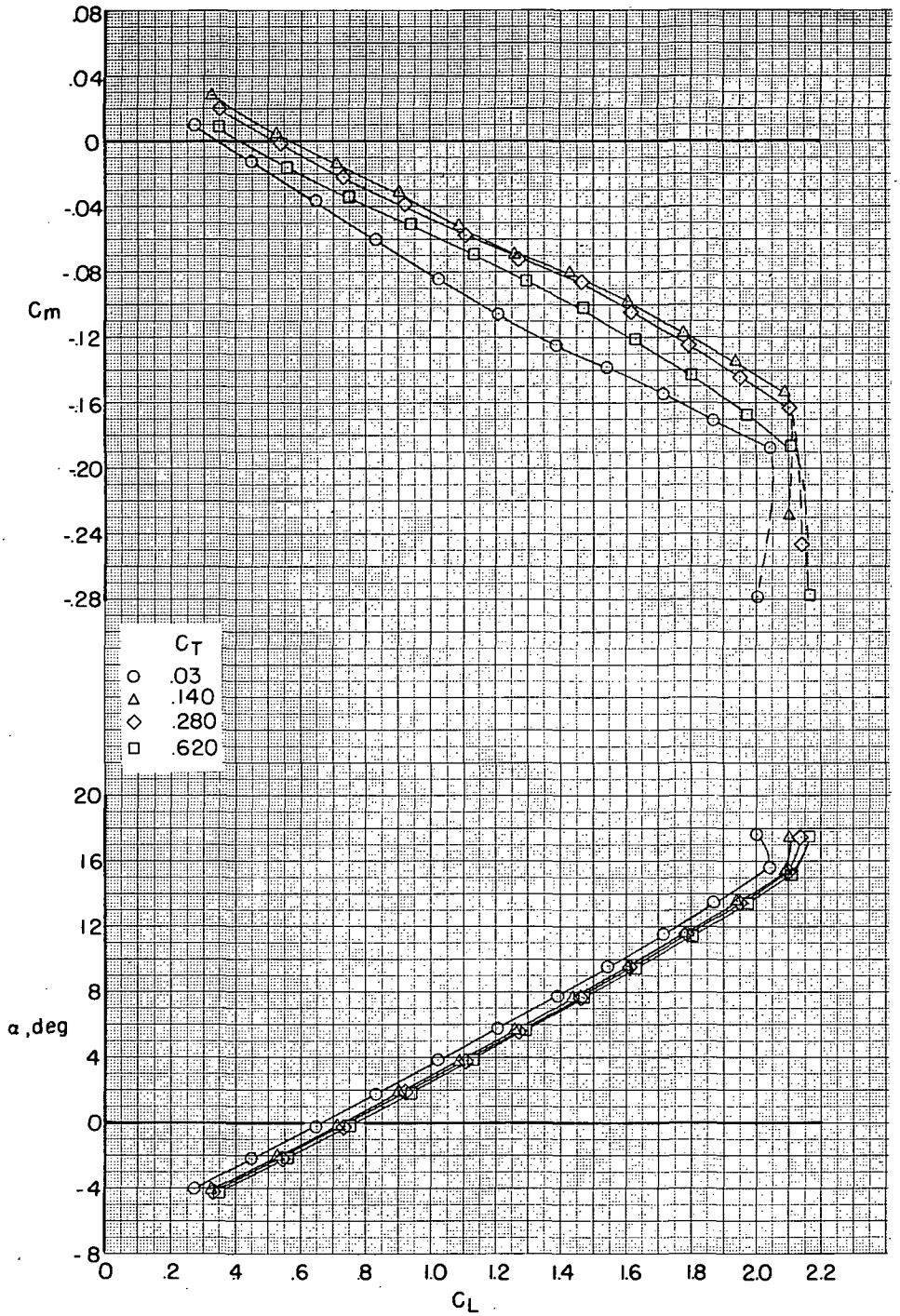

(a) $\delta_e = -15^o$.

Figure 18.- Effect of nacelle thrust coefficient on model characteristics. M = 0.225; $\delta_f = 30^o$; $\beta = 0^o$; $i_n = 2^o$; $h = \infty$.

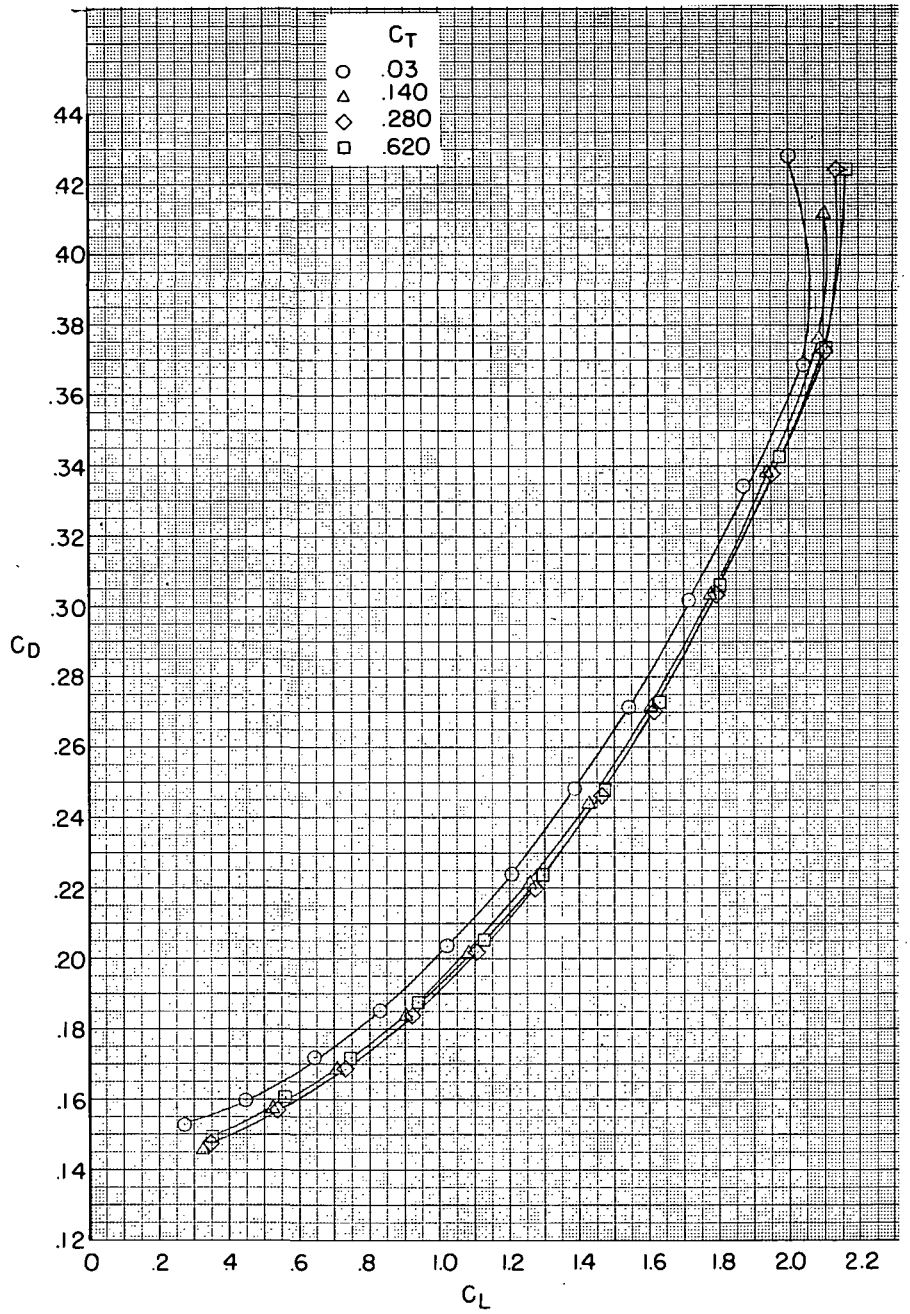

(a) Concluded.

Figure 18.- Continued.

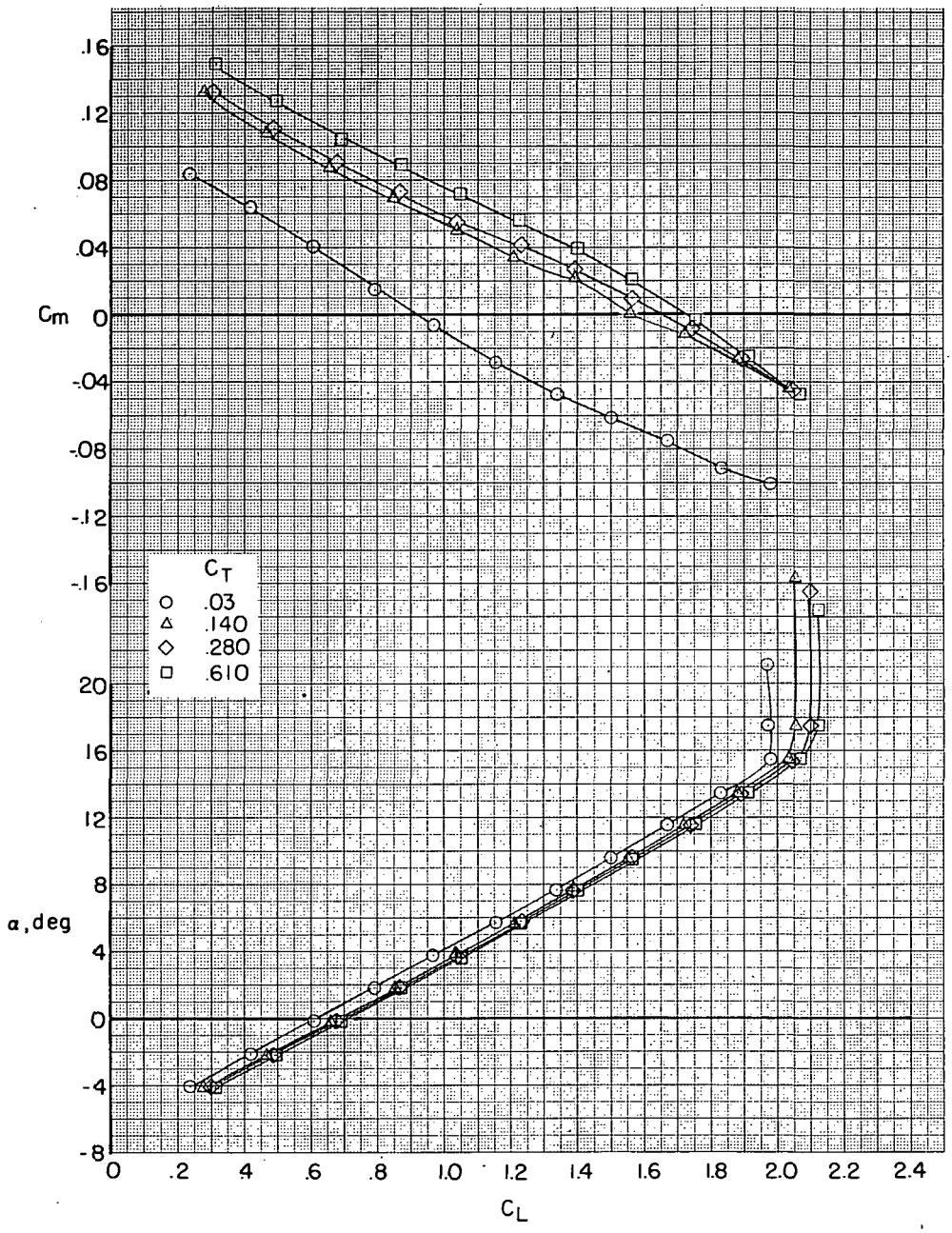

(b) $\delta_e = -25^o$.

Figure 18.- Continued.

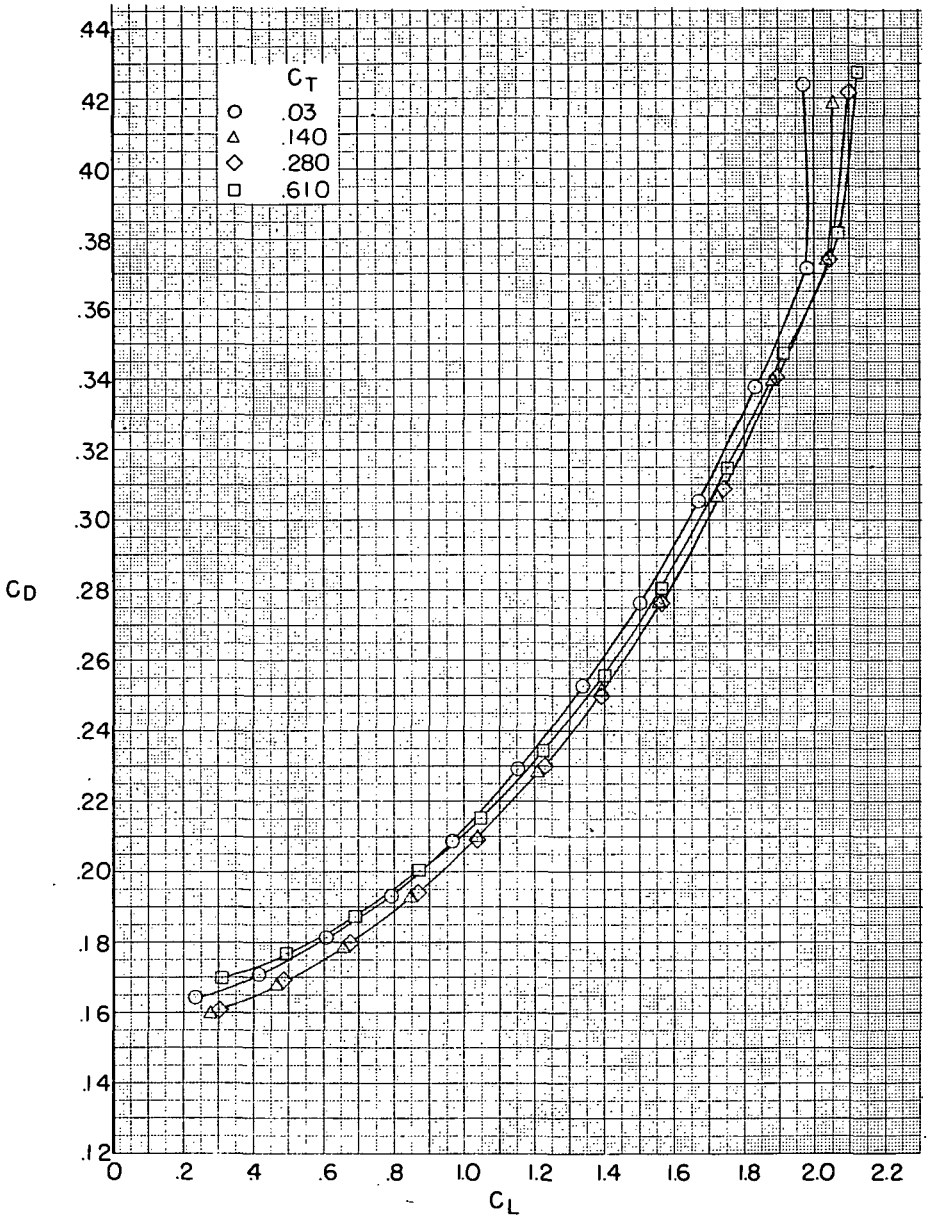

(b) Concluded.

Figure 18.- Concluded.

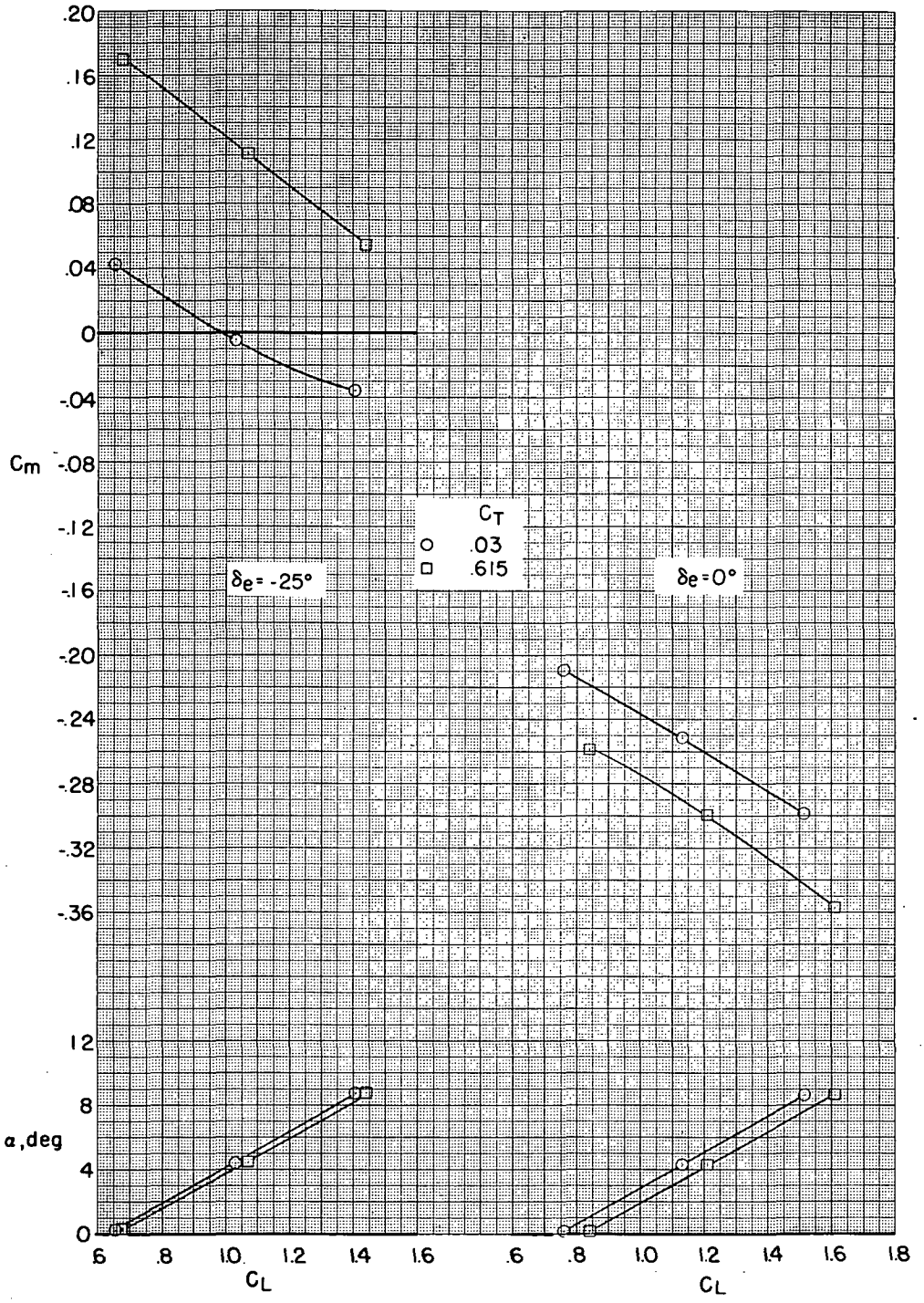

(a) h/b = 0.353.

Figure 19.- Effect of nacelle thrust coefficient on model characteristics with ground plane in place. M = 0.225; $\delta_f = 30^o$; $\beta = 0^o$; $i_n = 4^o$.

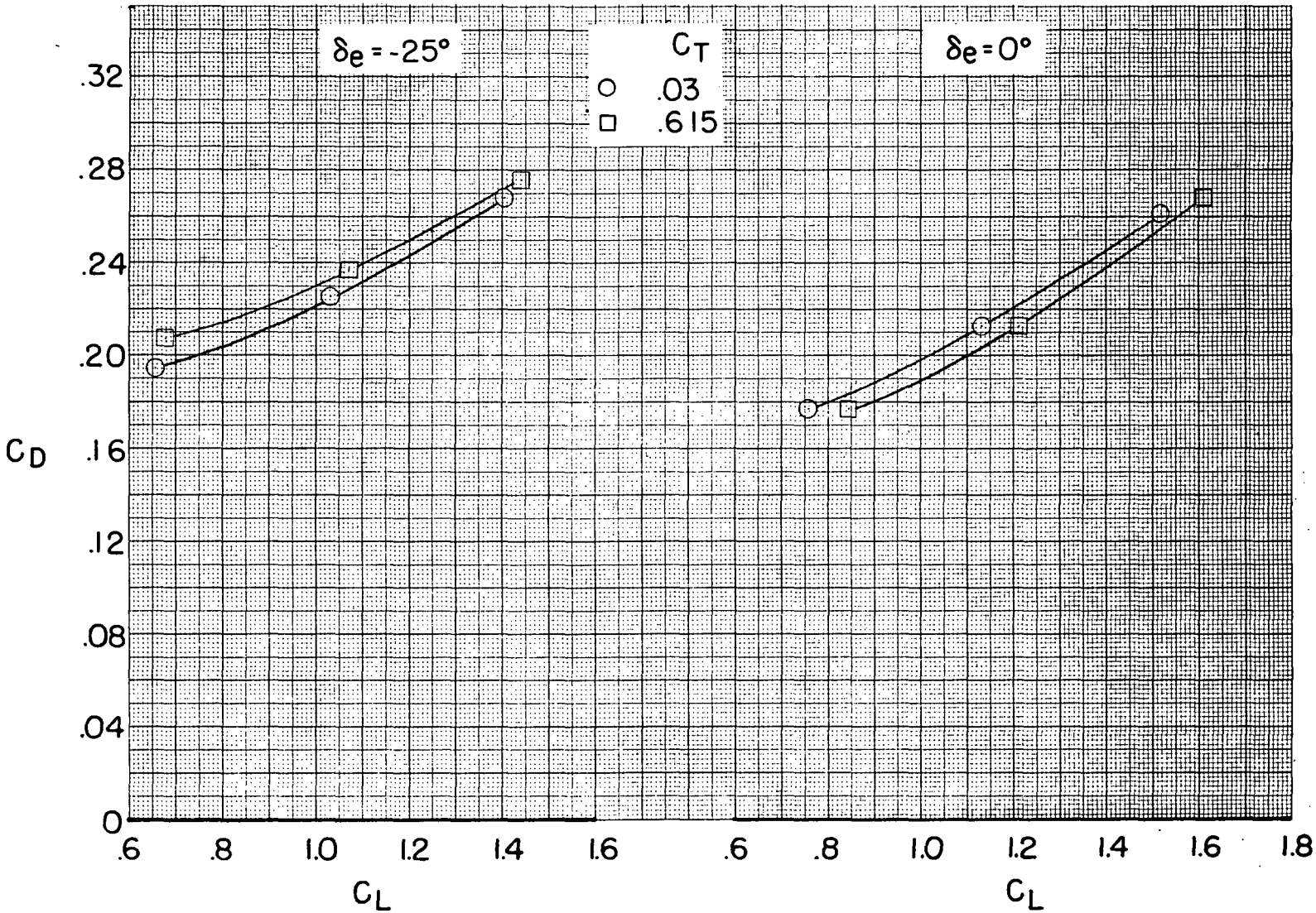

(a) Concluded.

Figure 19.- Continued.

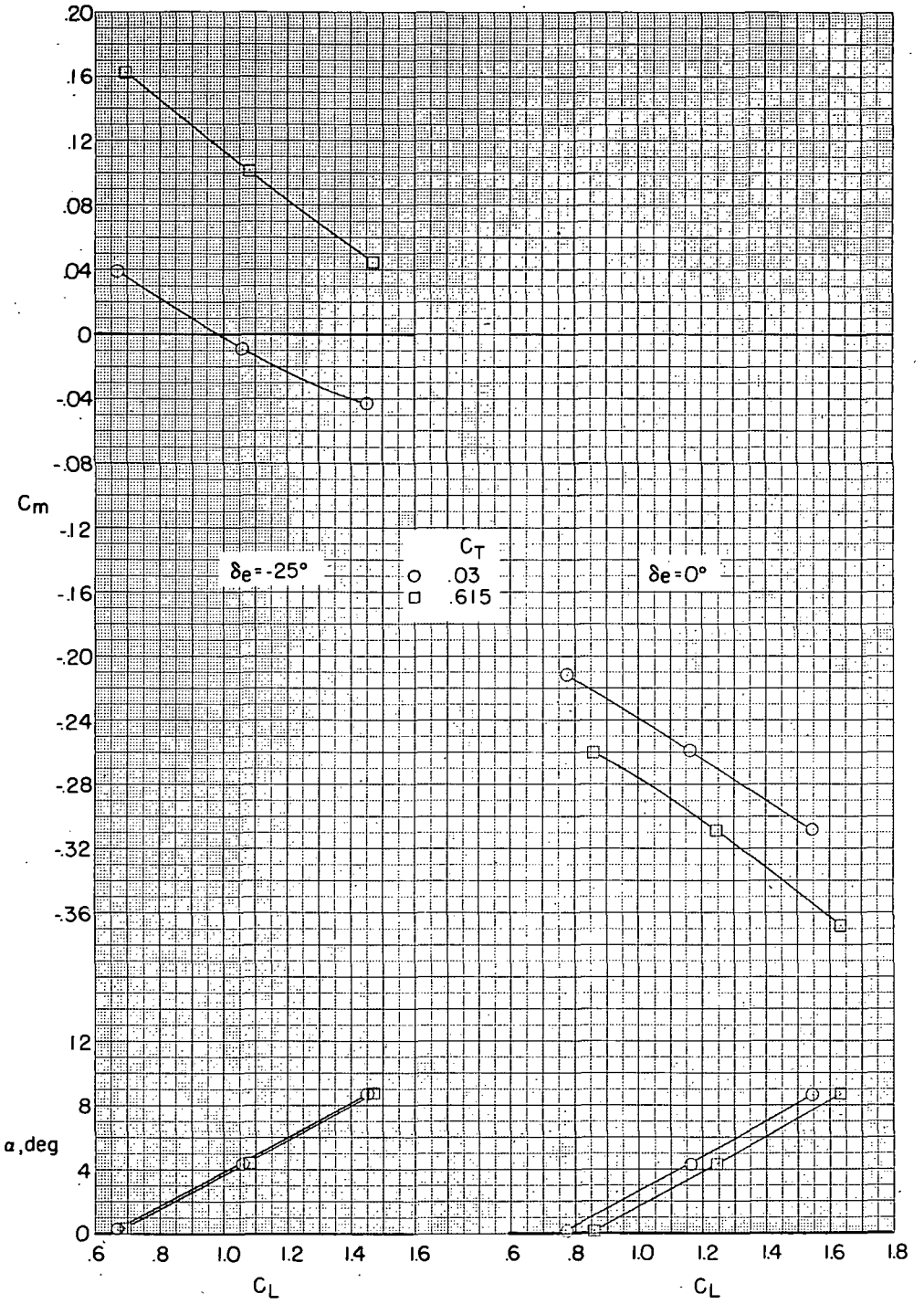

(b) h/b = 0.253.

Figure 19.- Continued.

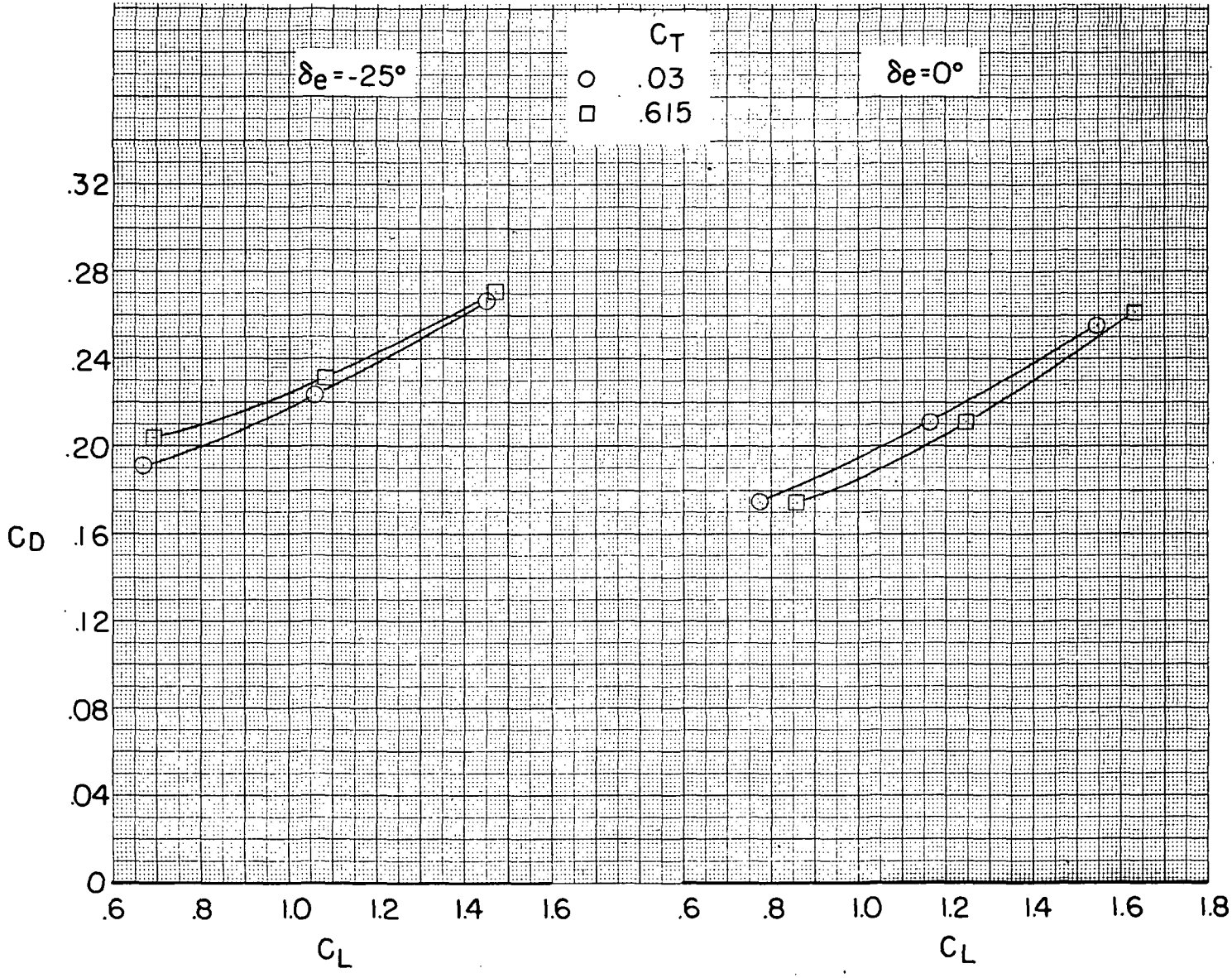

(b) Concluded.

Figure 19.- Continued.

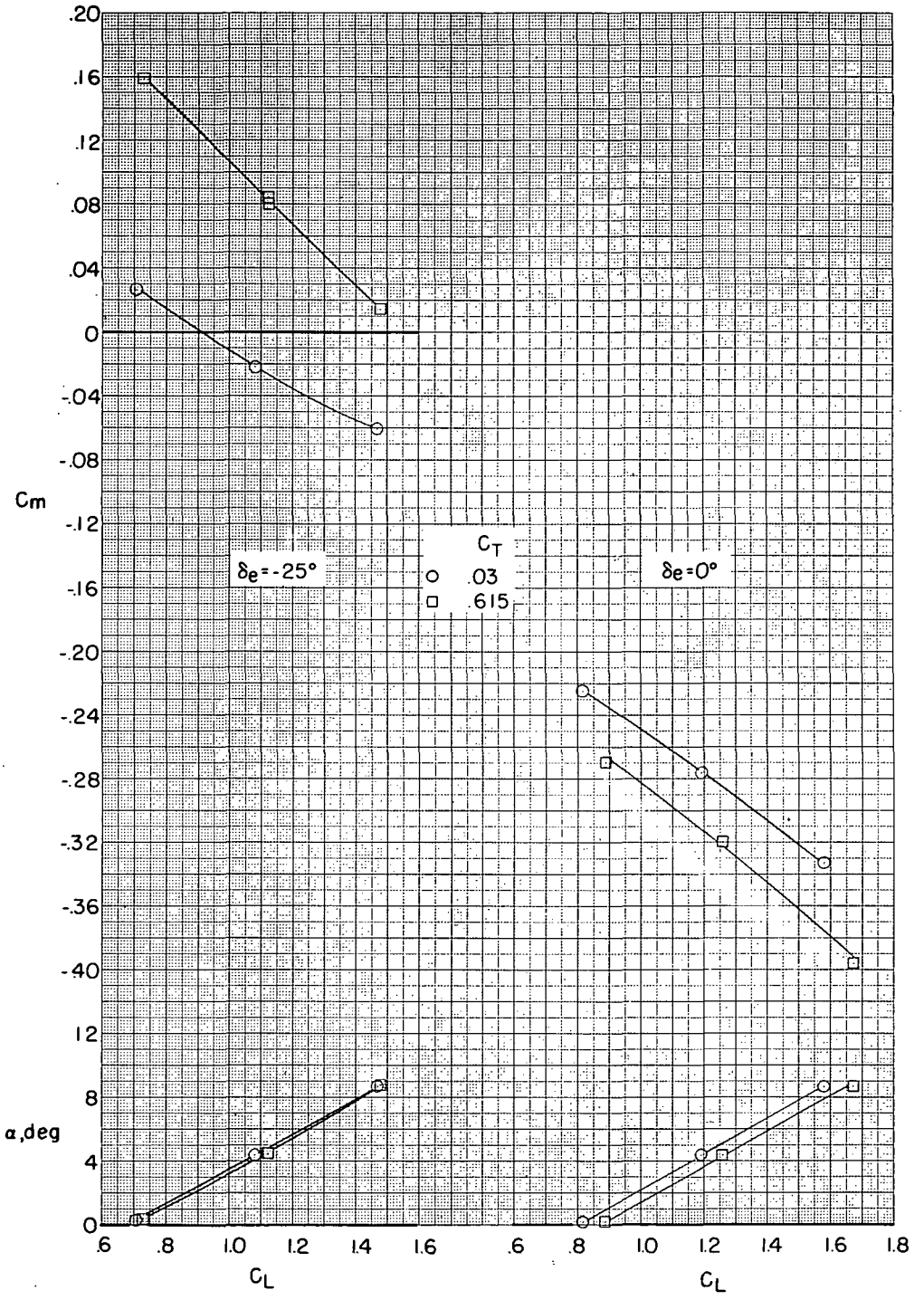

(c) h/b = 0.153.

Figure 19.- Continued.

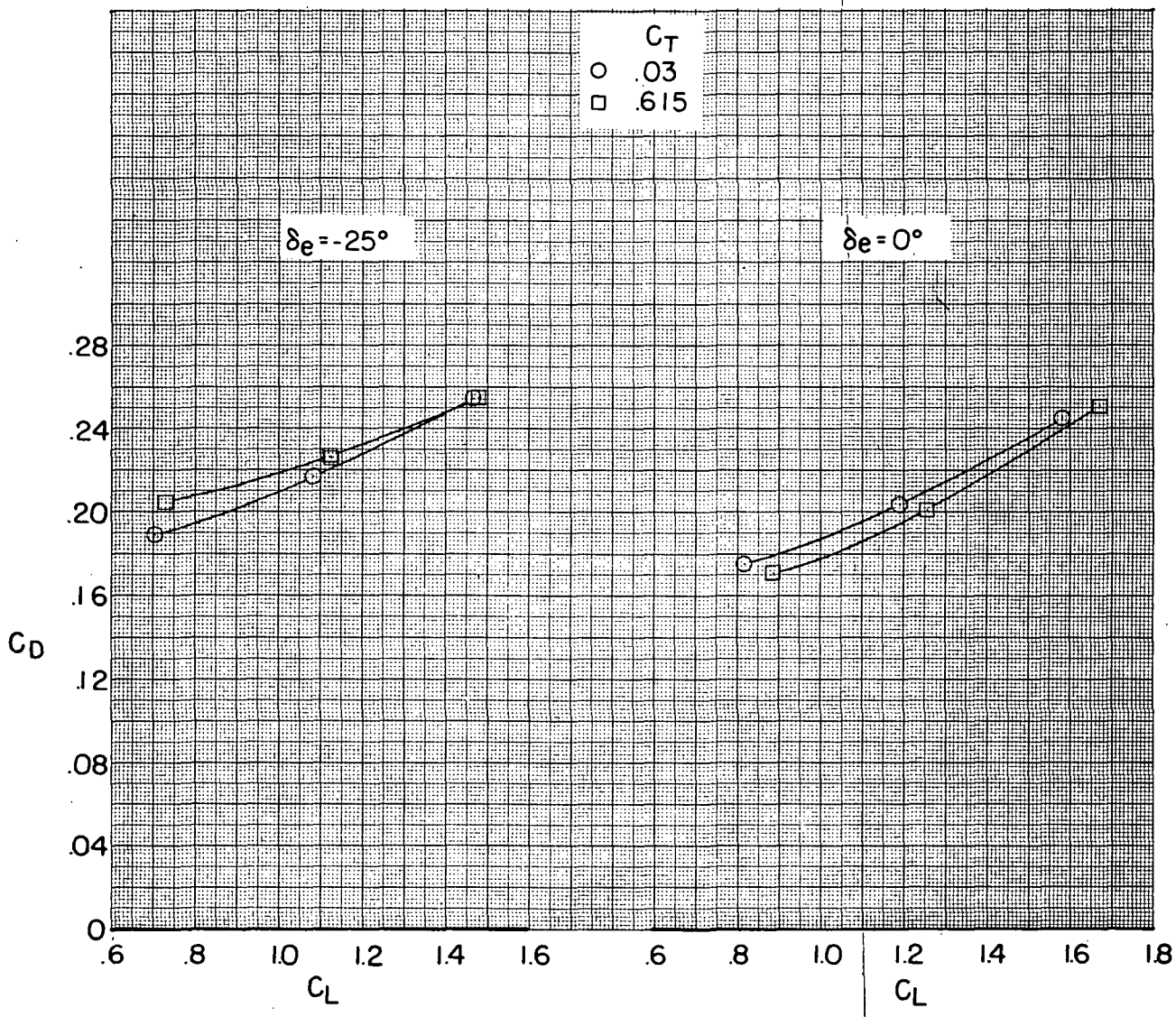

(c) Concluded.

Figure 19.- Continued.

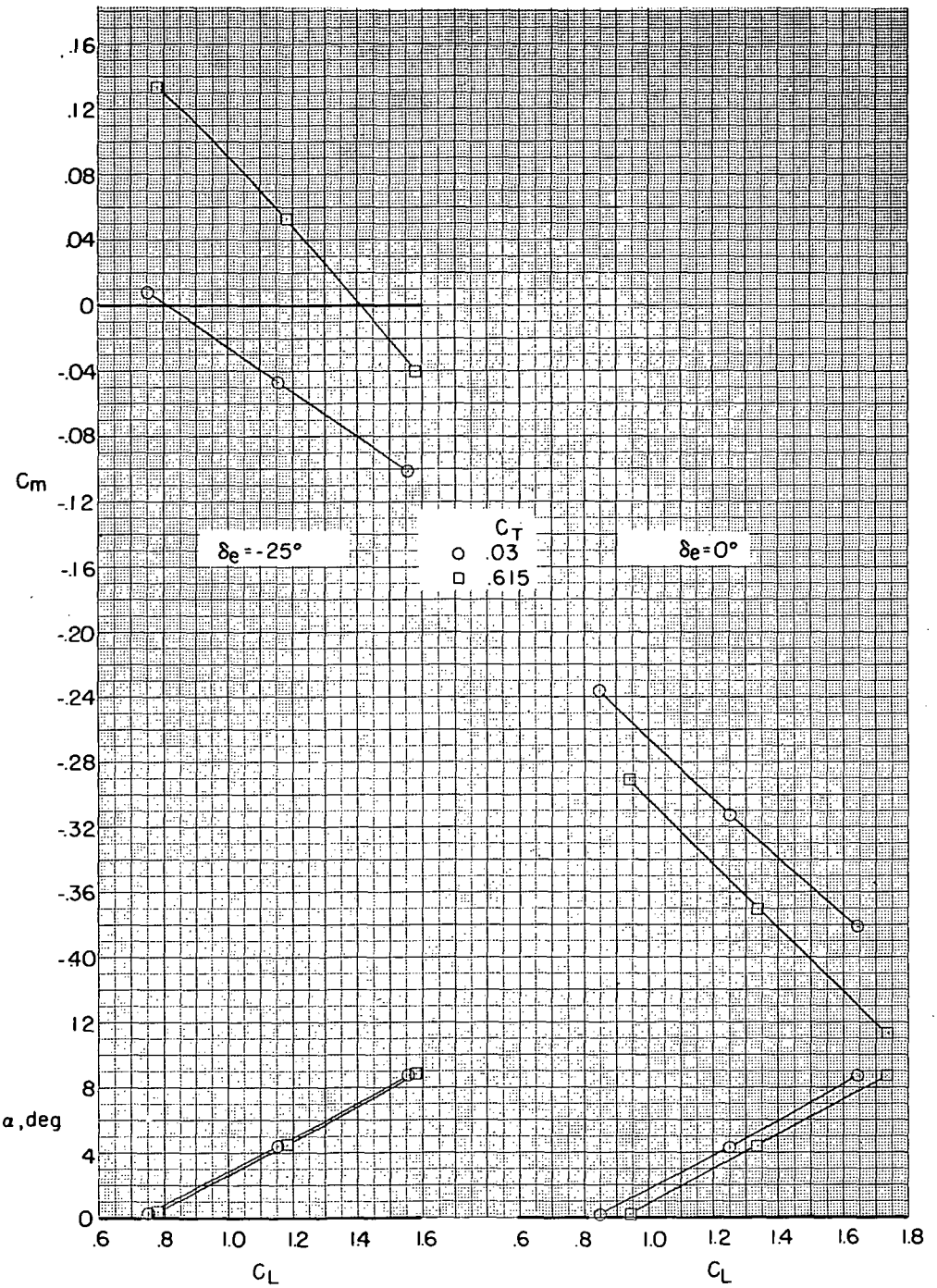

(d) h/b = 0.053.

Figure 19.- Continued.

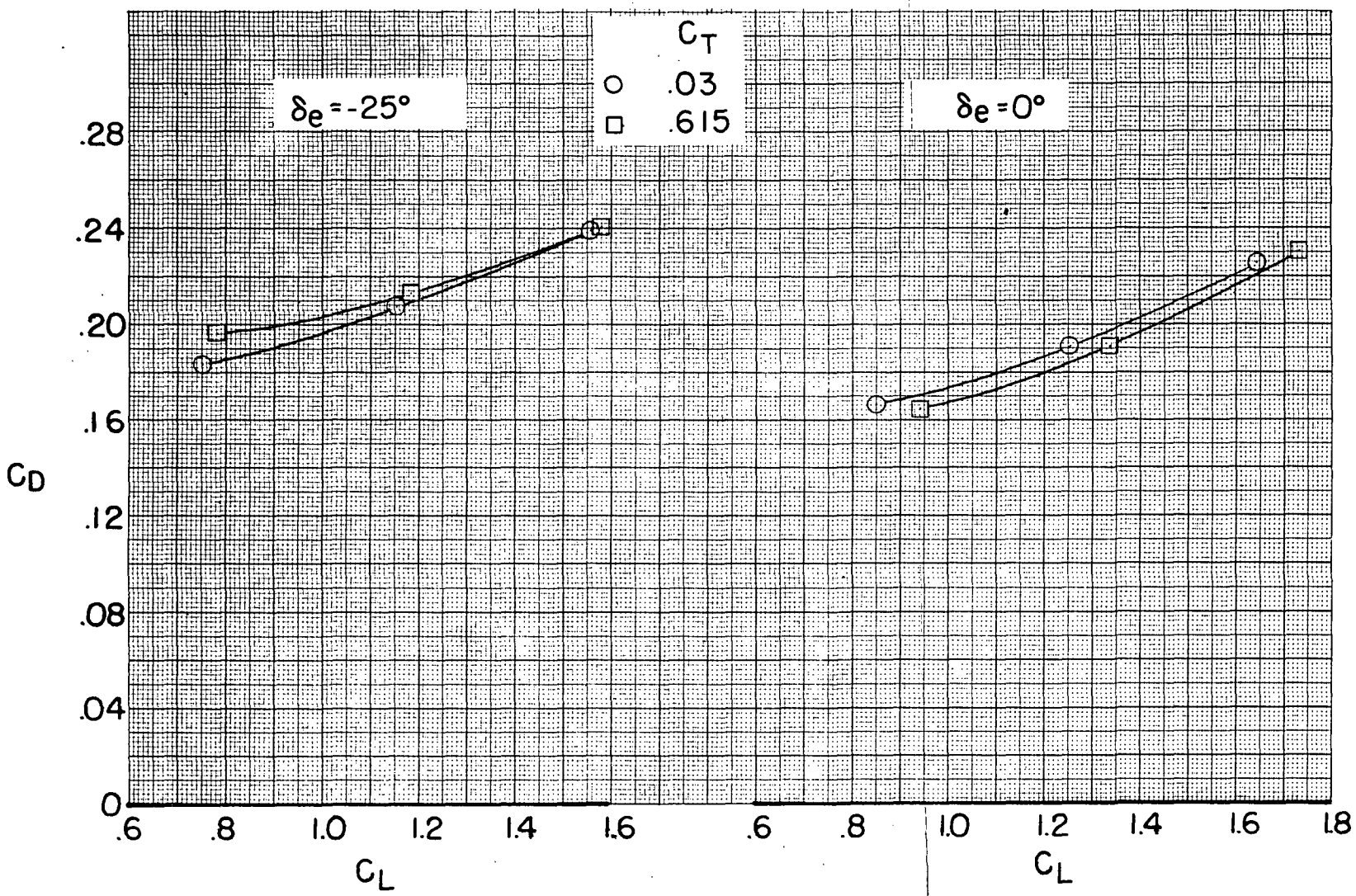

(d) Concluded.

Figure 19.- Continued.

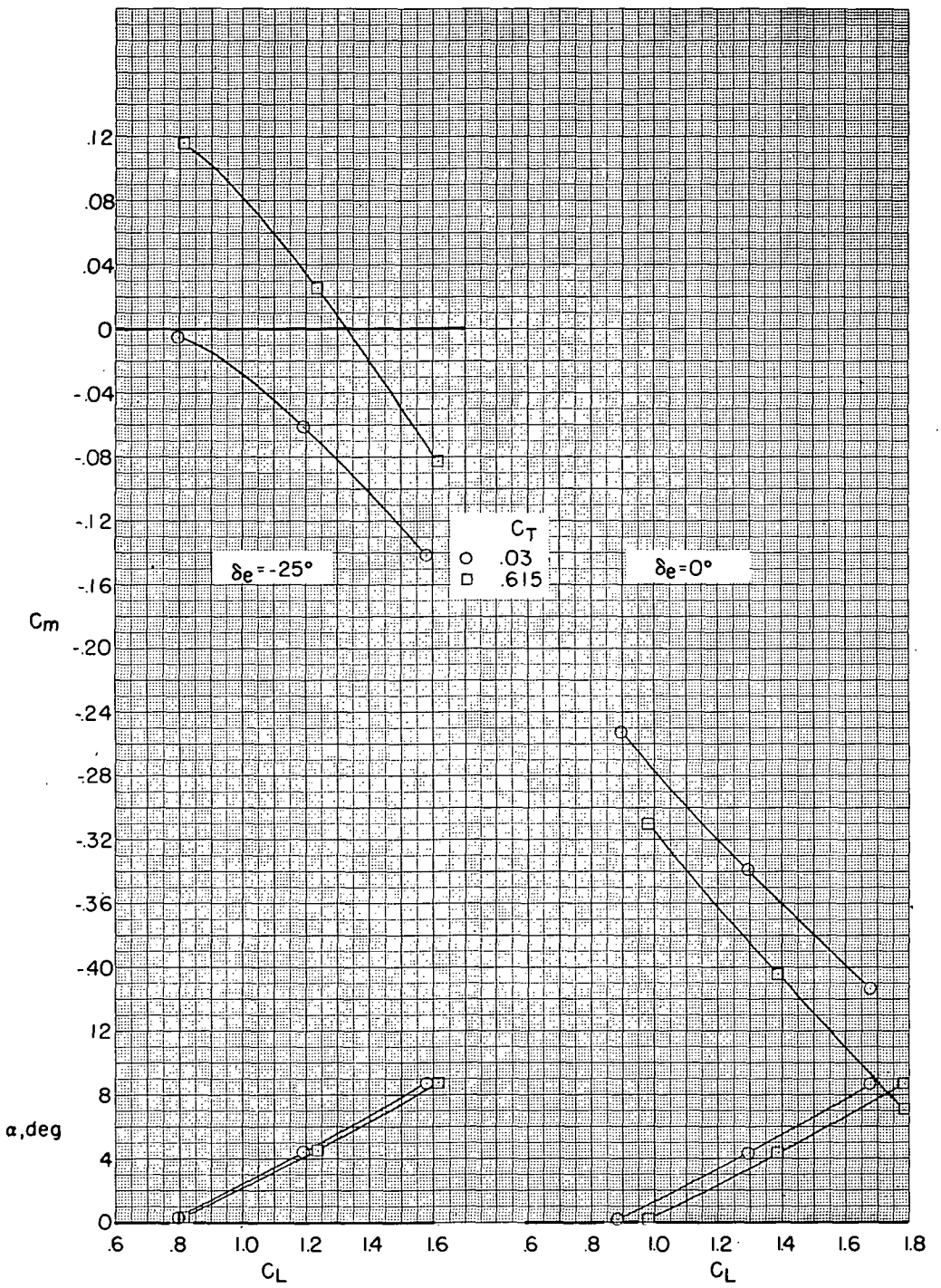

(e) h/b = 0.004.

Figure 19.- Continued.

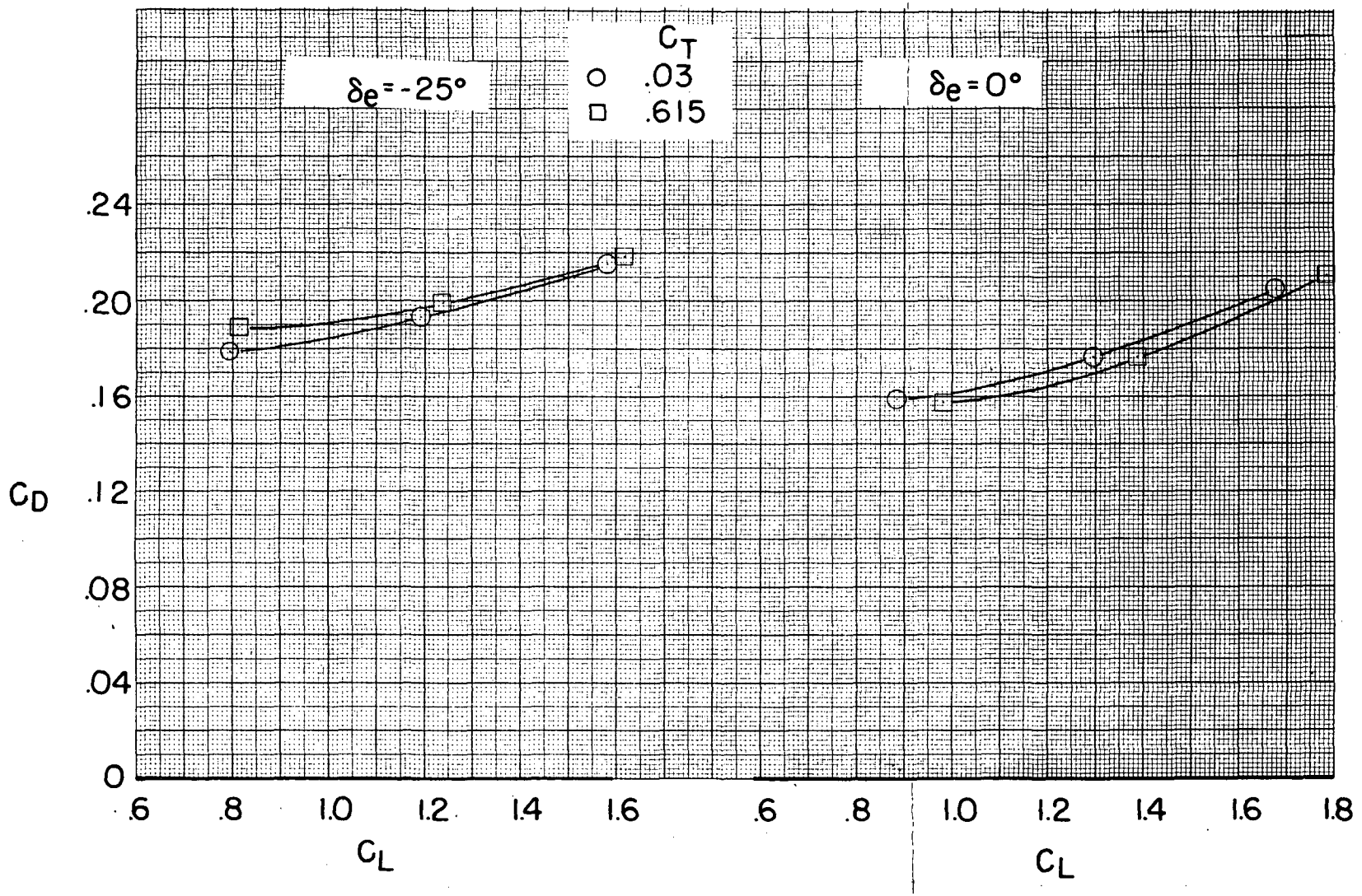

(e) Concluded.

Figure 19.- Concluded.

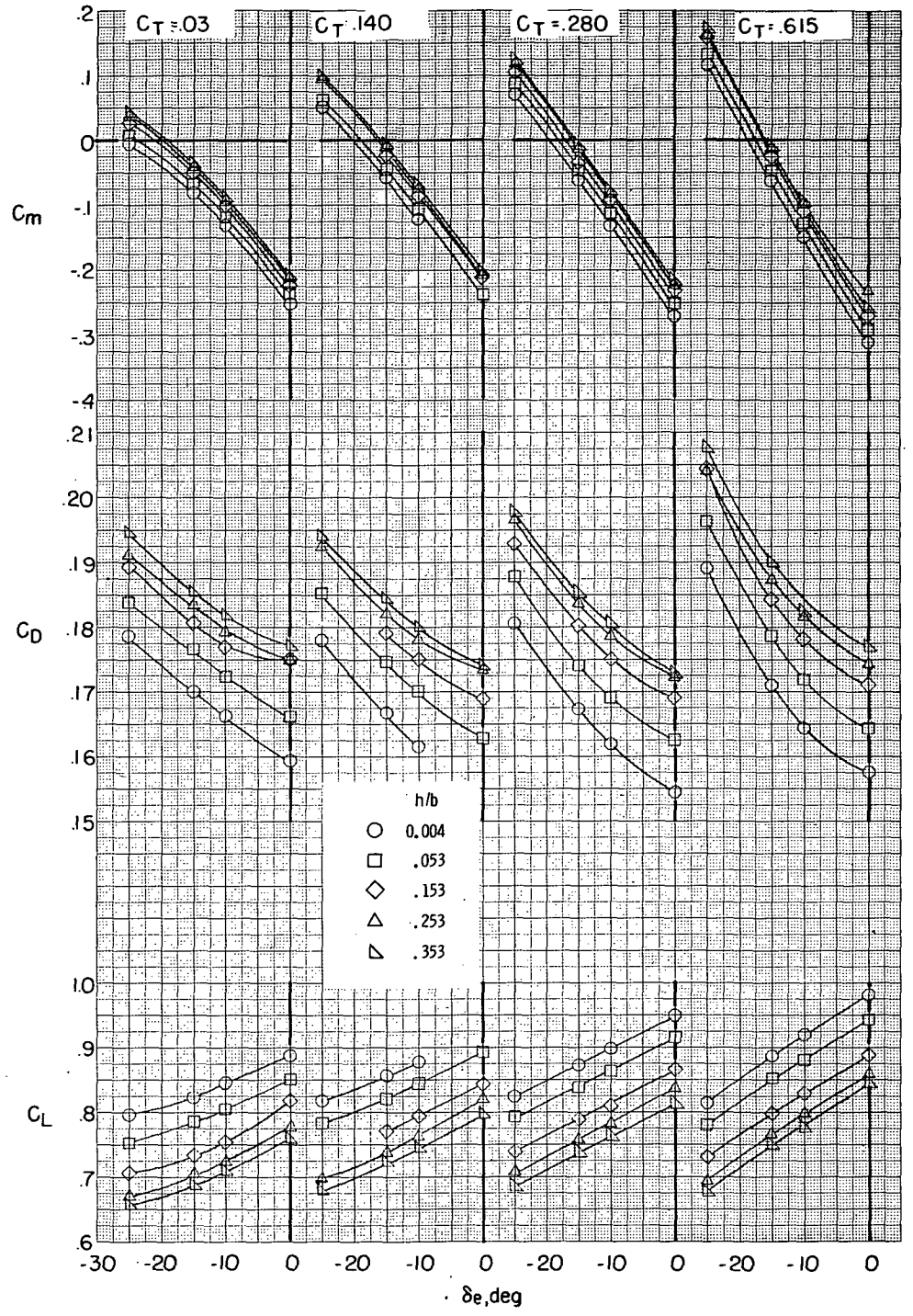

Figure 20.- Effect of nacelle thrust coefficient and model height on the characteristics with ground plane in place. M = 0.225; $\delta_f = 30^o$; $\beta = 0^o$; $i_n = 4^o$; $\alpha \approx 0^o$.

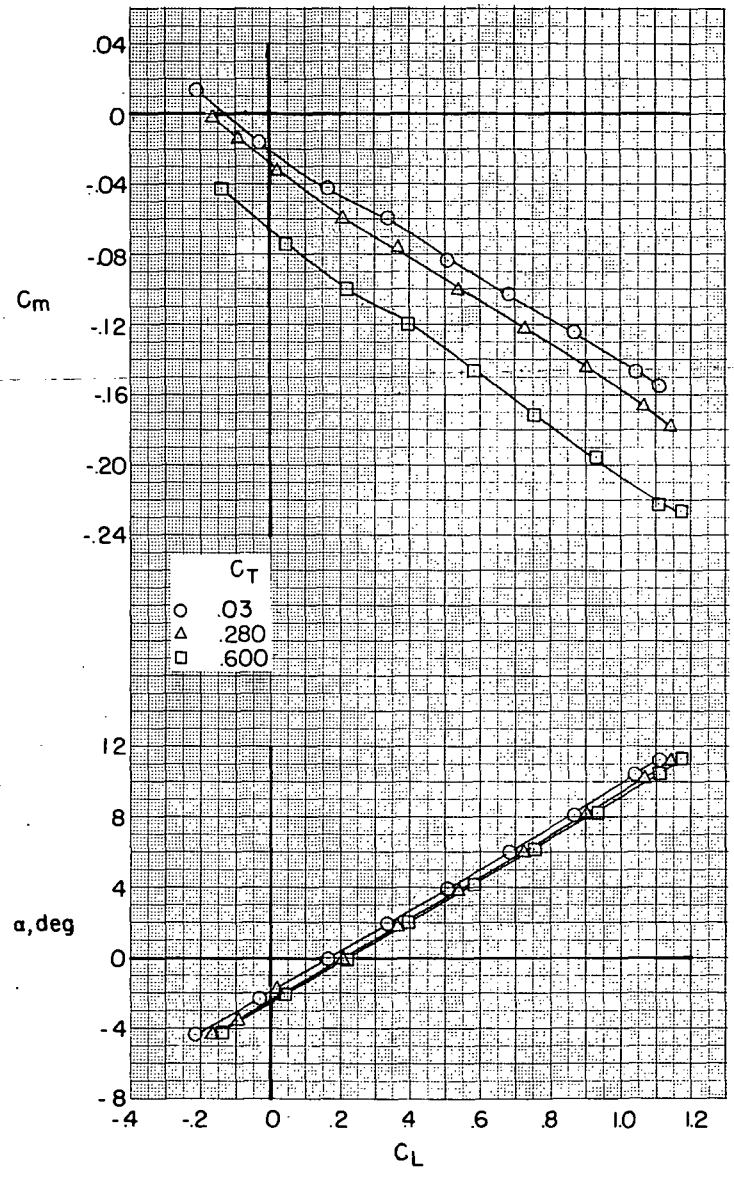

(a) $\delta_r = 10^o$.

Figure 21.- Effect of nacelle thrust coefficient on model characteristics. $M = 0.225$; $\delta_f = 0^o$; $\beta = 9^o$; $i_n = 4^o$; $h = \infty$.

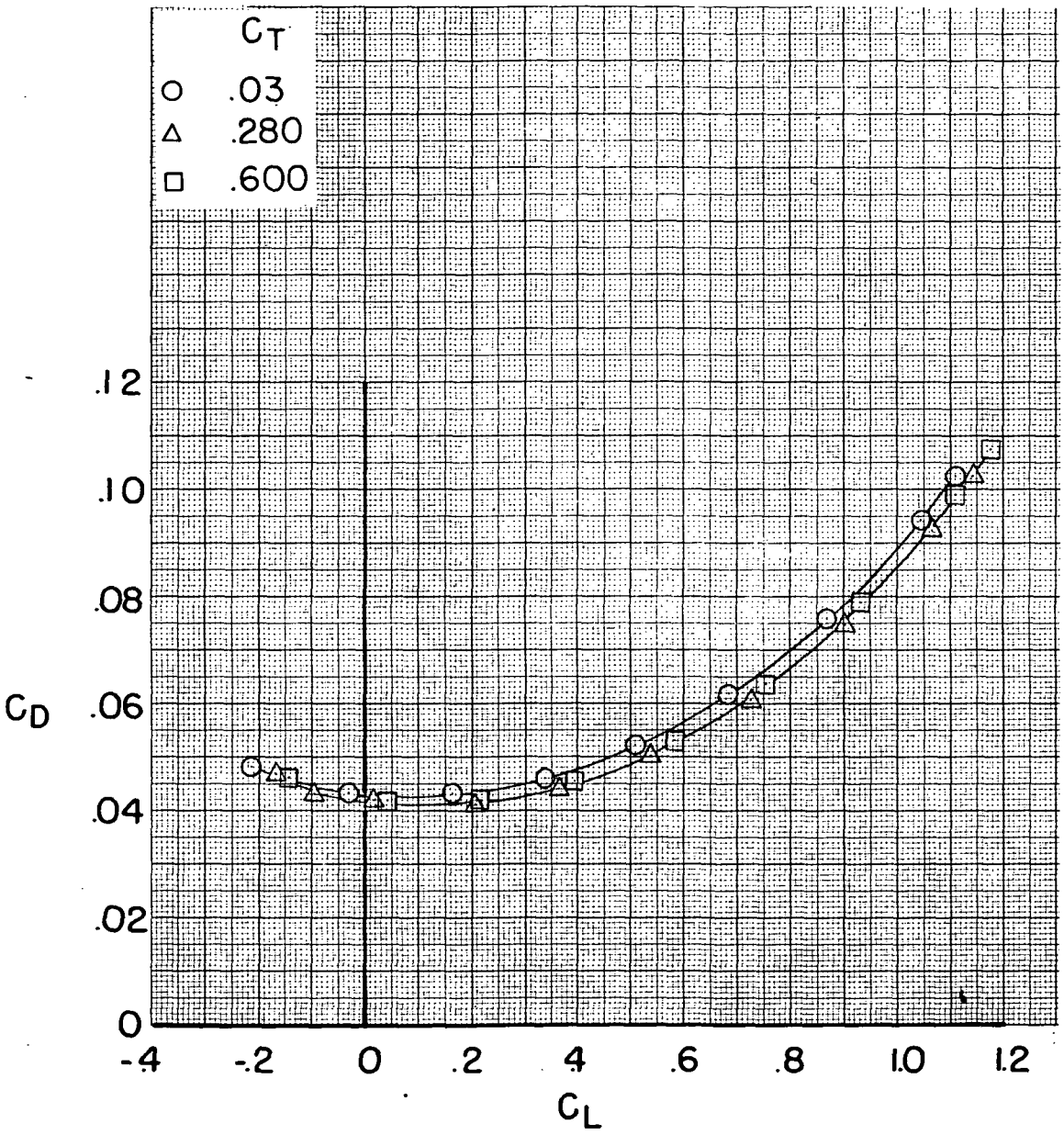

(a) Continued.

Figure 21.- Continued.

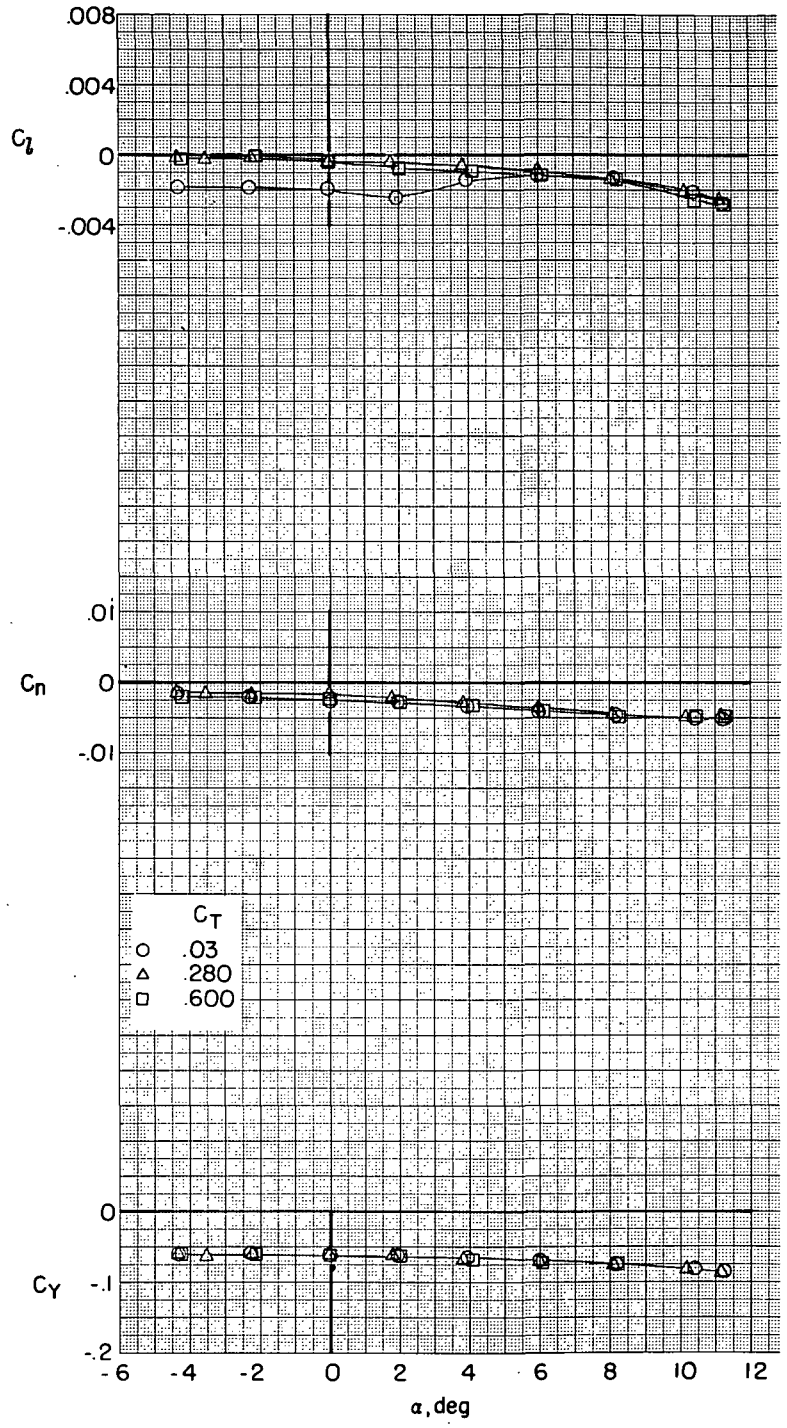

(a) Concluded.

Figure 21.- Continued.

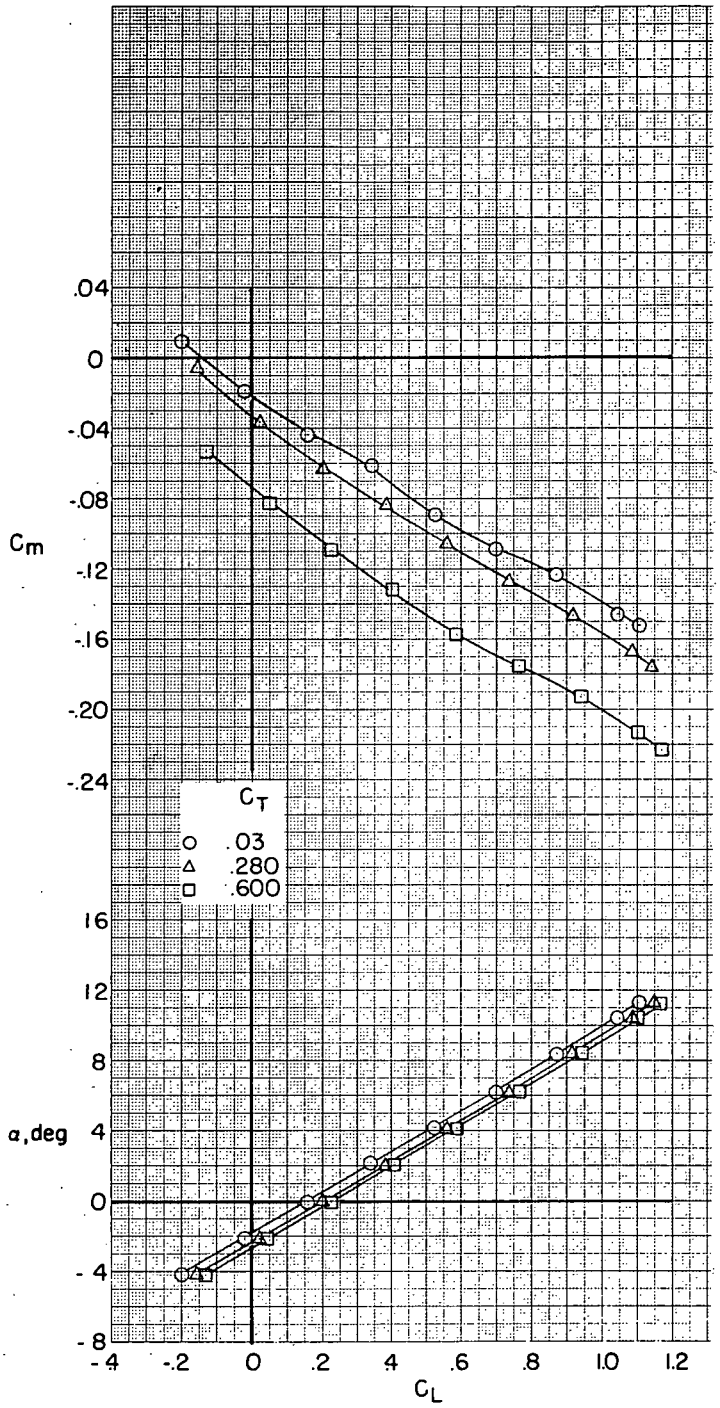

(b) $\delta_r = -10^o$.

Figure 21.- Continued.

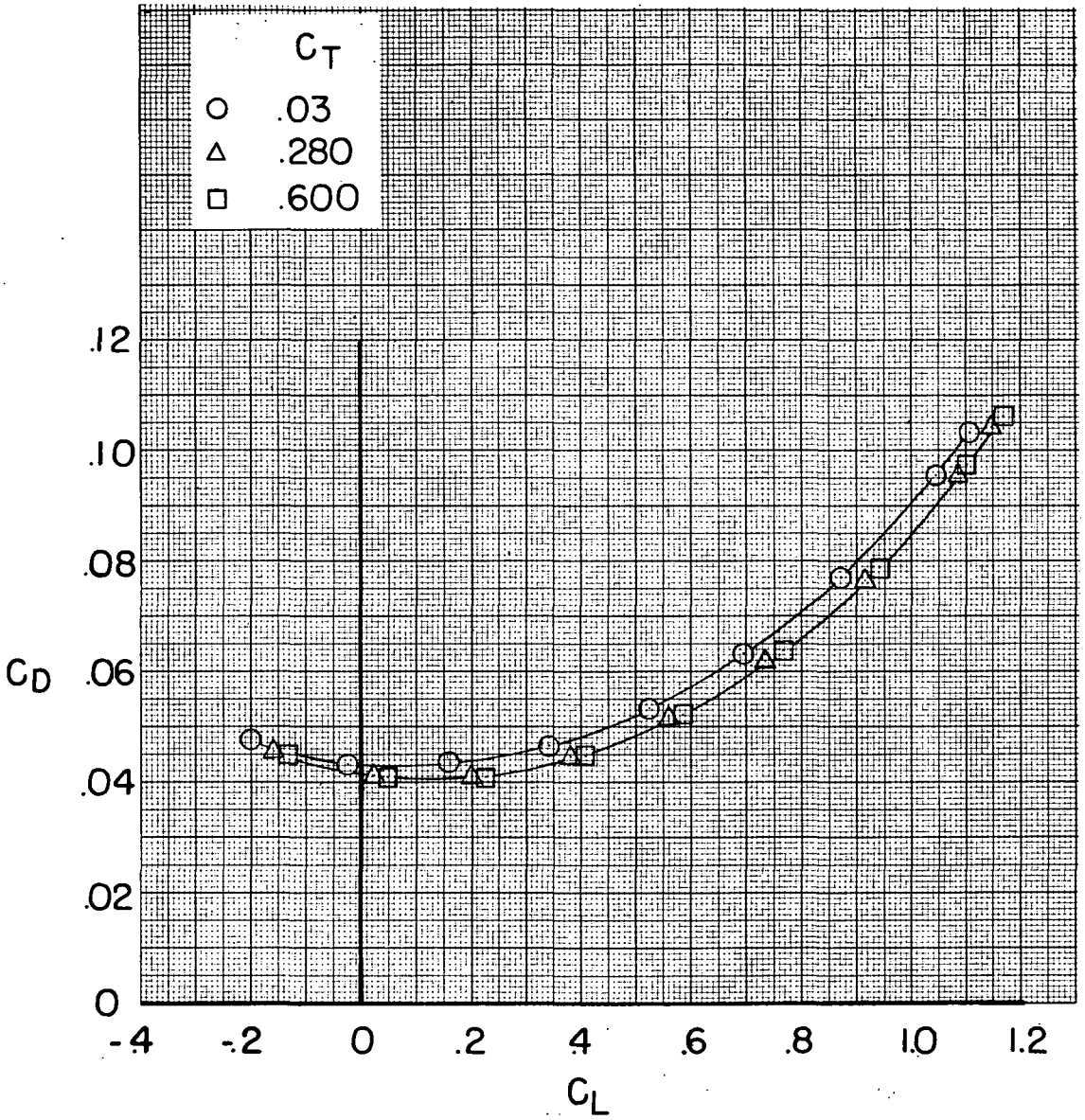

(b) Continued.

Figure 21.- Continued.

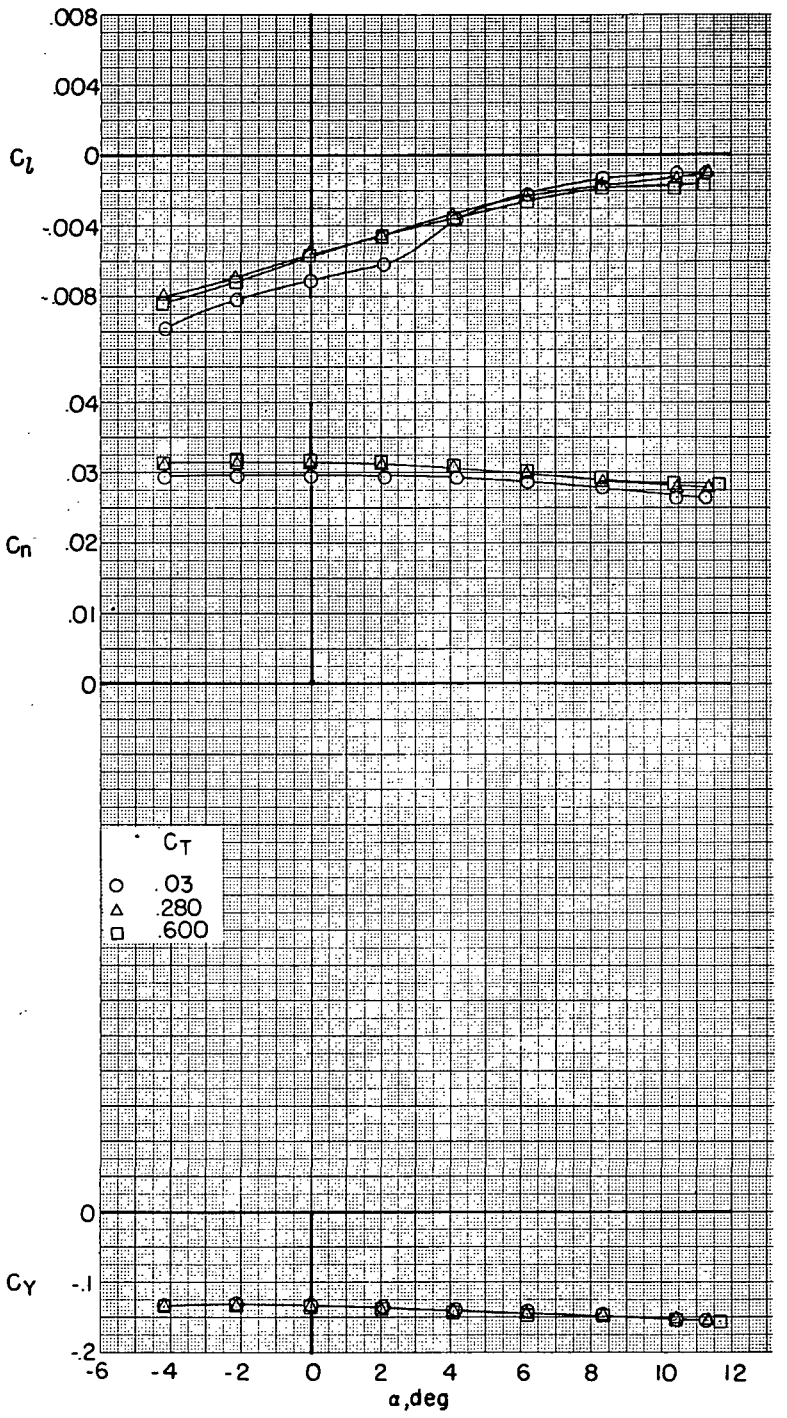

(b) Concluded.

Figure 21.- Concluded.

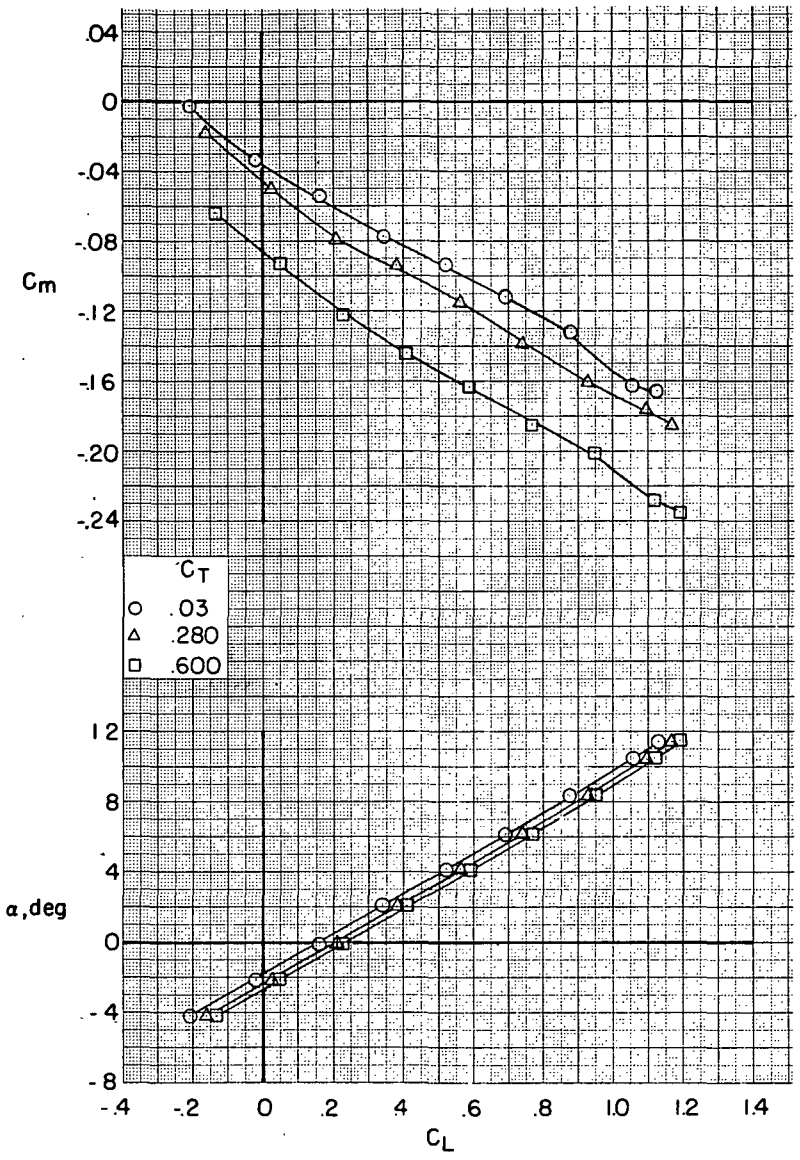

(a) $\delta_r = 10^o$.

Figure 22.- Effect of nacelle thrust coefficient on model characteristics. $M = 0.225$; $\delta_f = 0^o$; $\beta = -9^o$; $i_n = 4^o$; $h = \infty$.

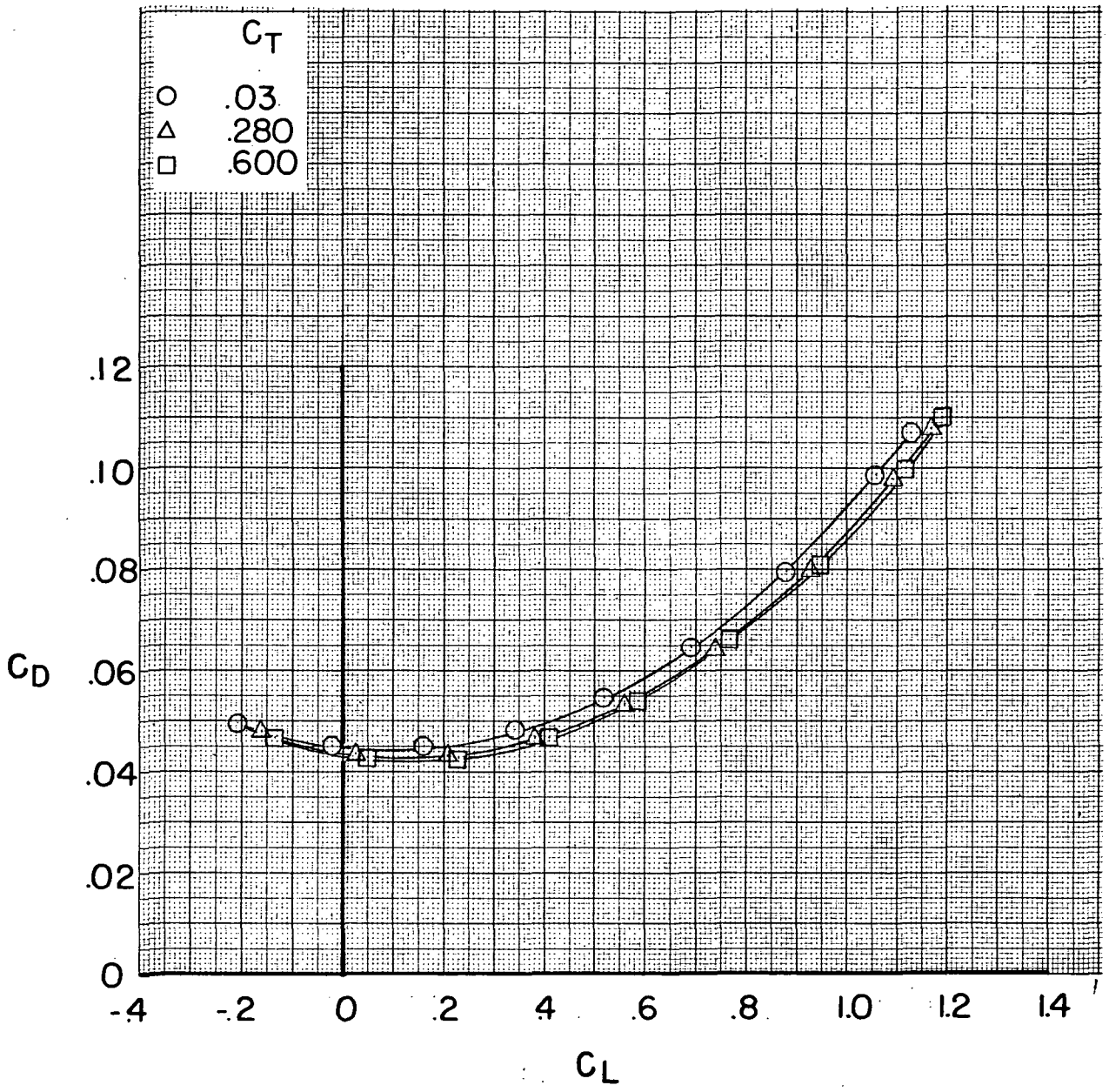

(a) Continued.

Figure 22.- Continued.

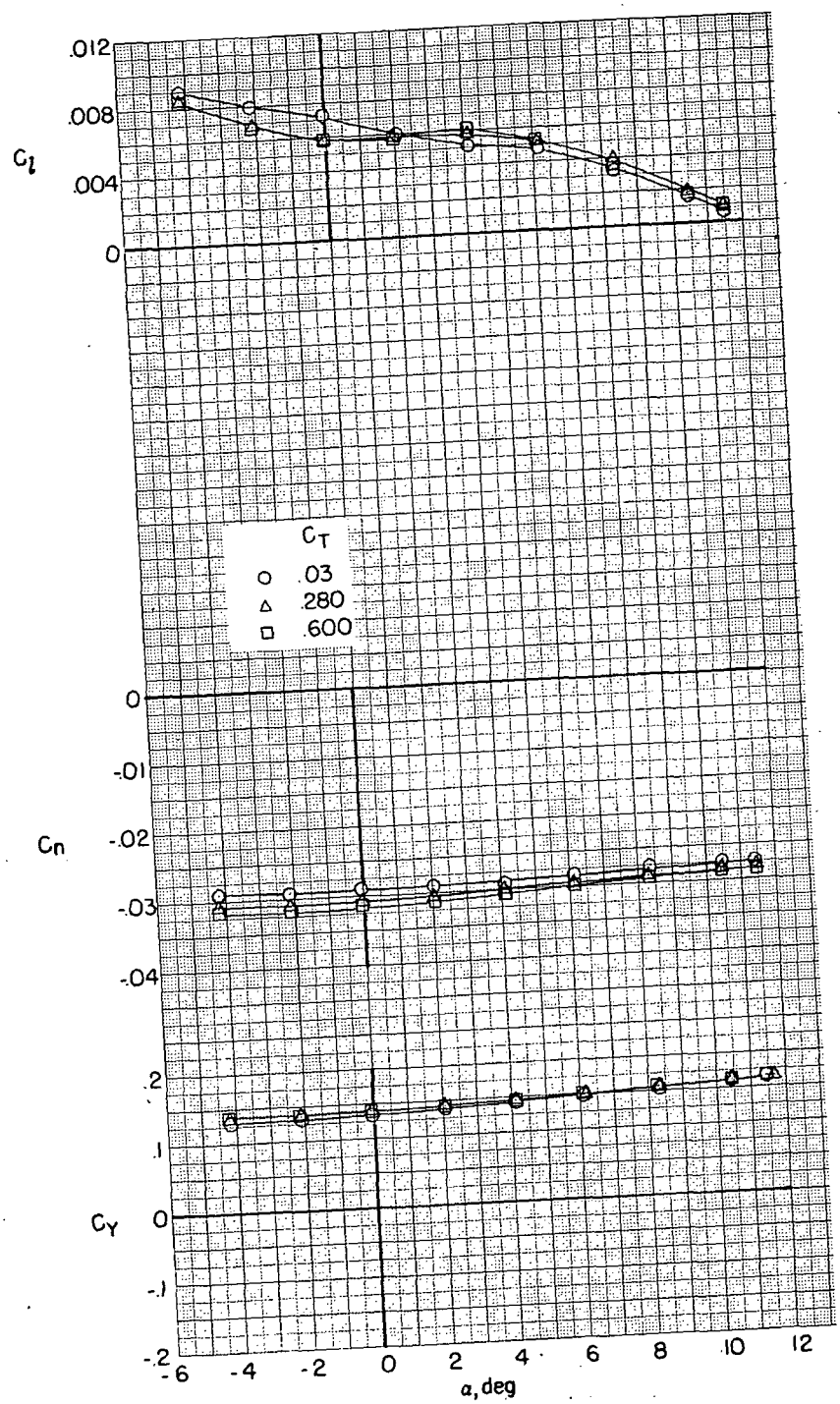

(a) Concluded.

Figure 22.- Continued.

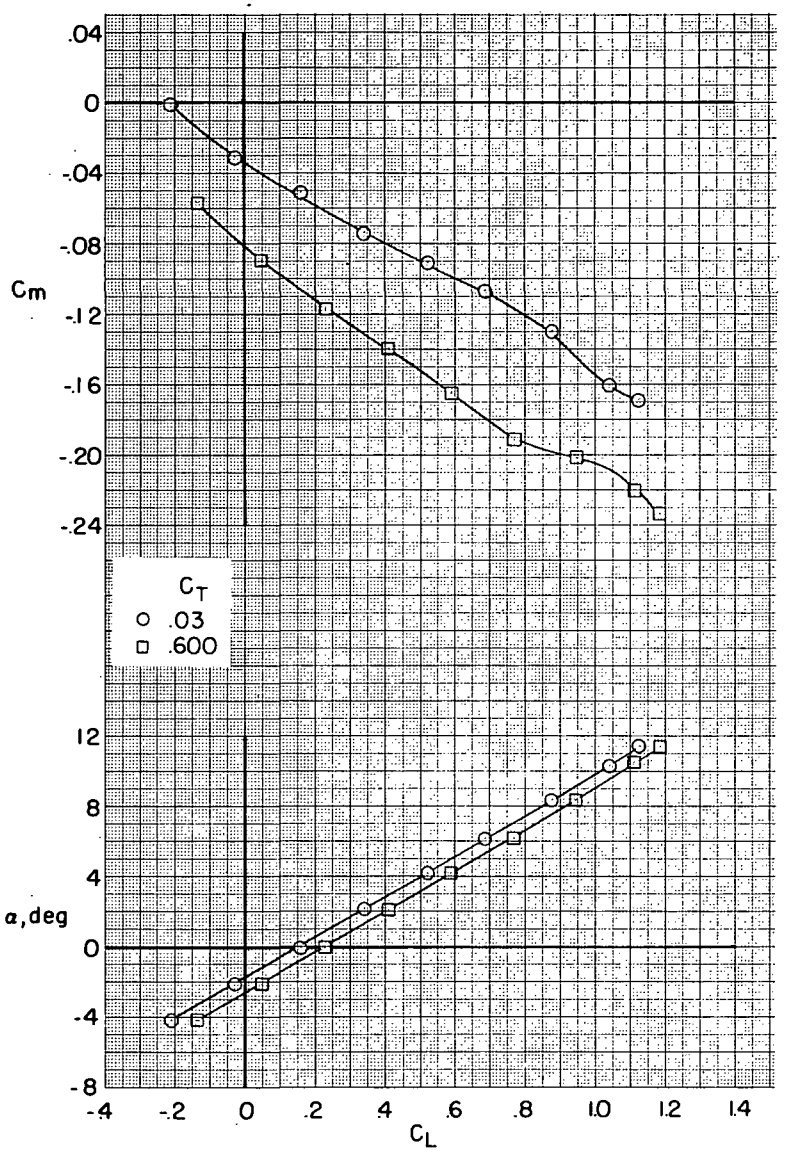

(b) $\delta_r = 0^o$.

Figure 22.- Continued.

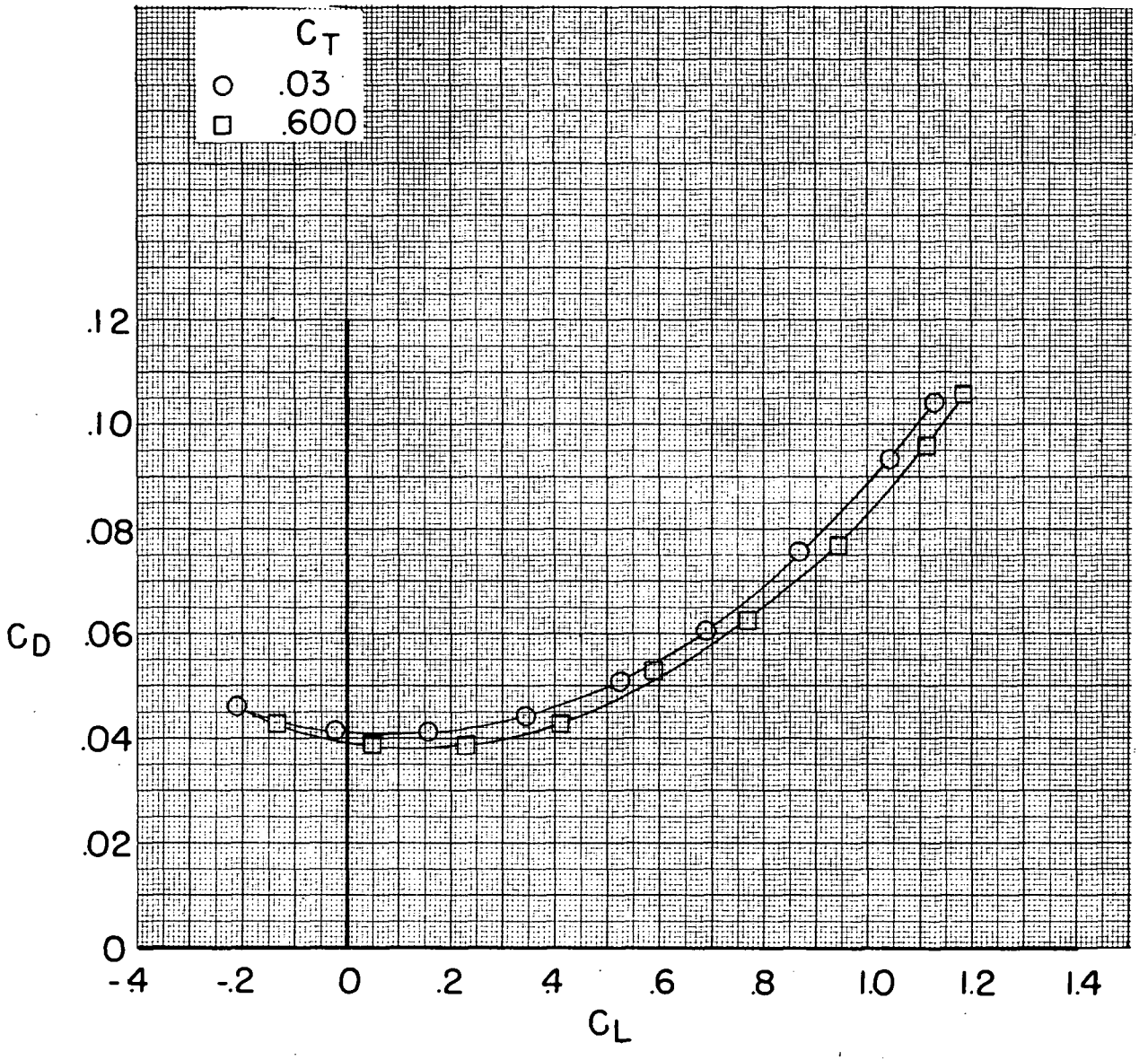

(b) Continued.

Figure 22.- Continued.

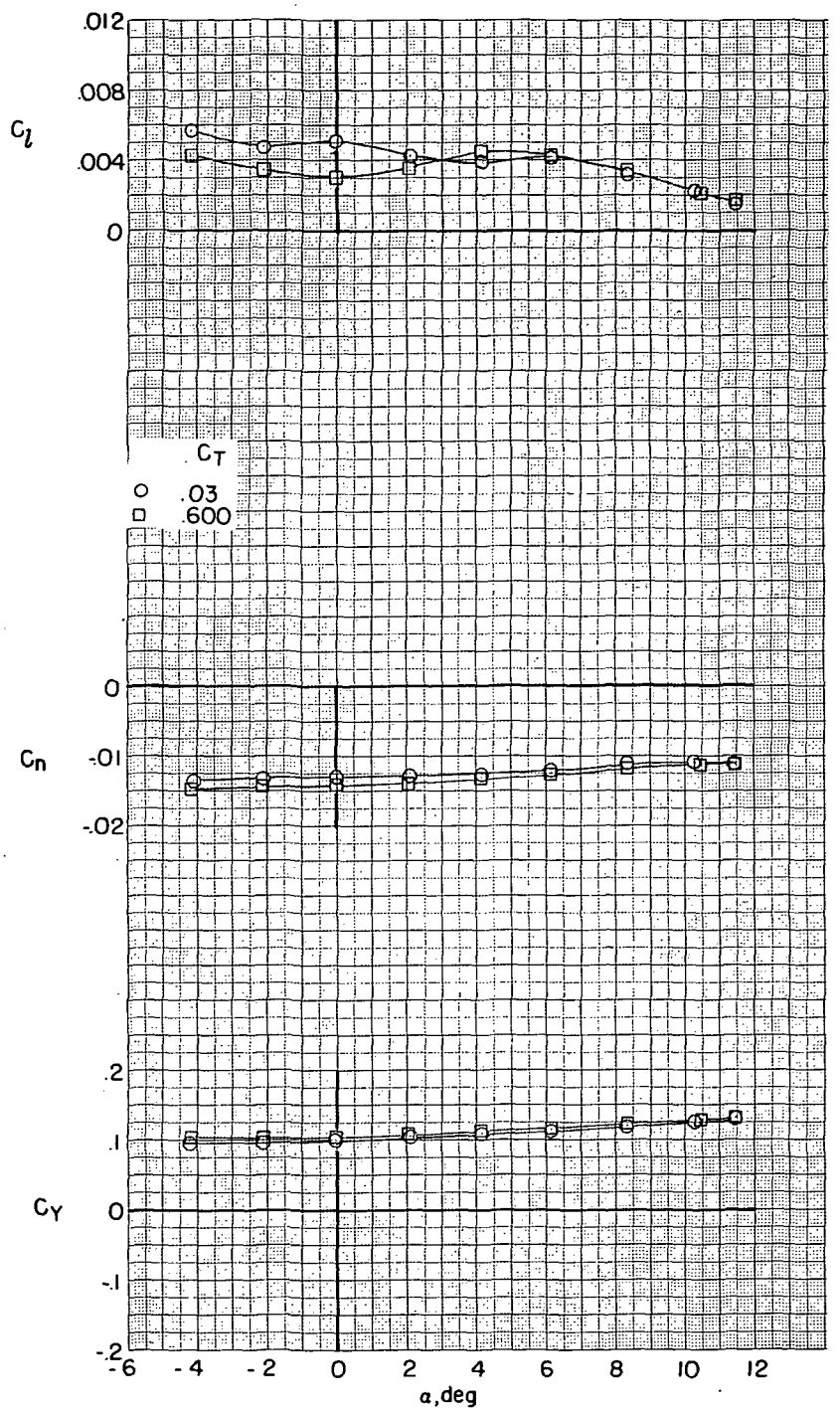

(b) Concluded.

Figure 22.- Continued.

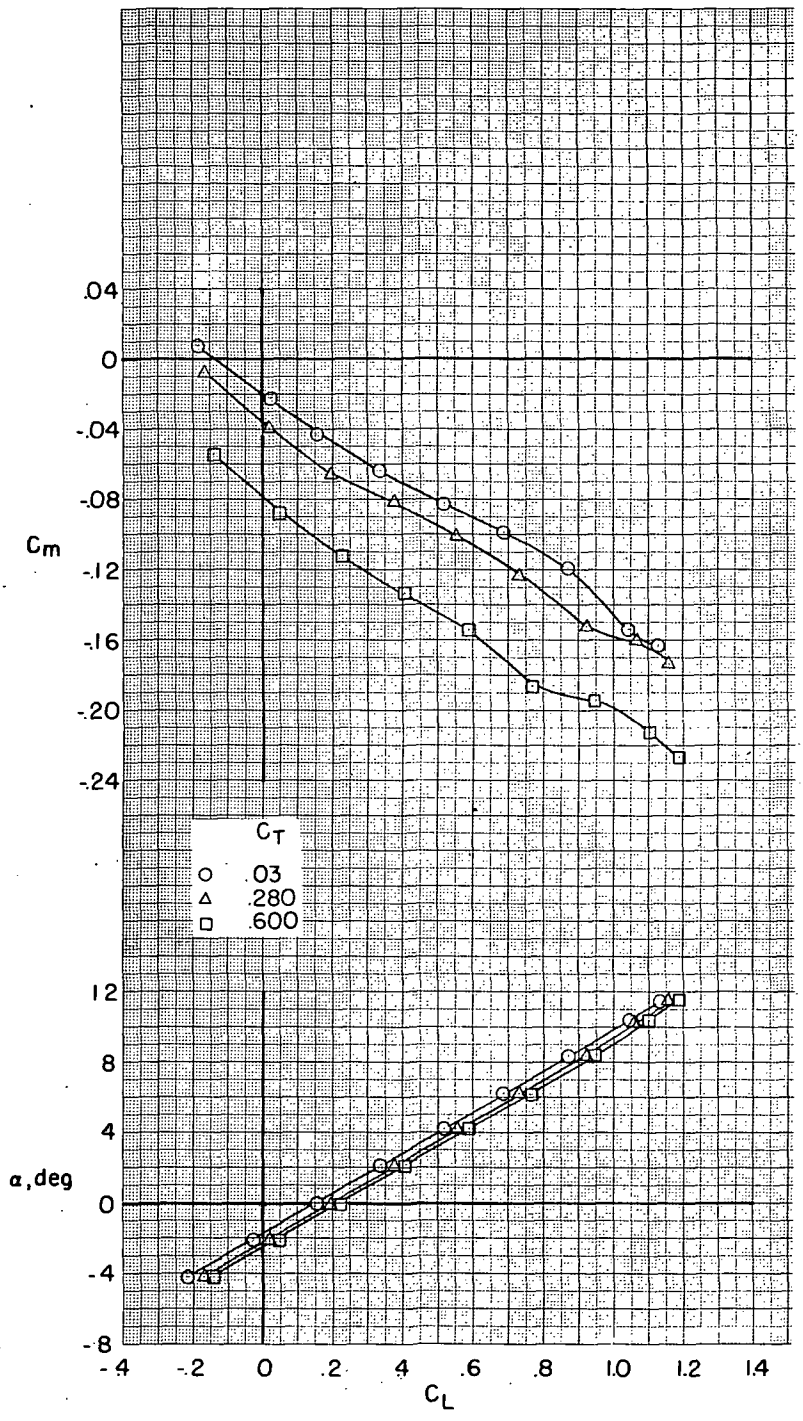

(c) $\delta_r = -10^o$.

Figure 22.- Continued.

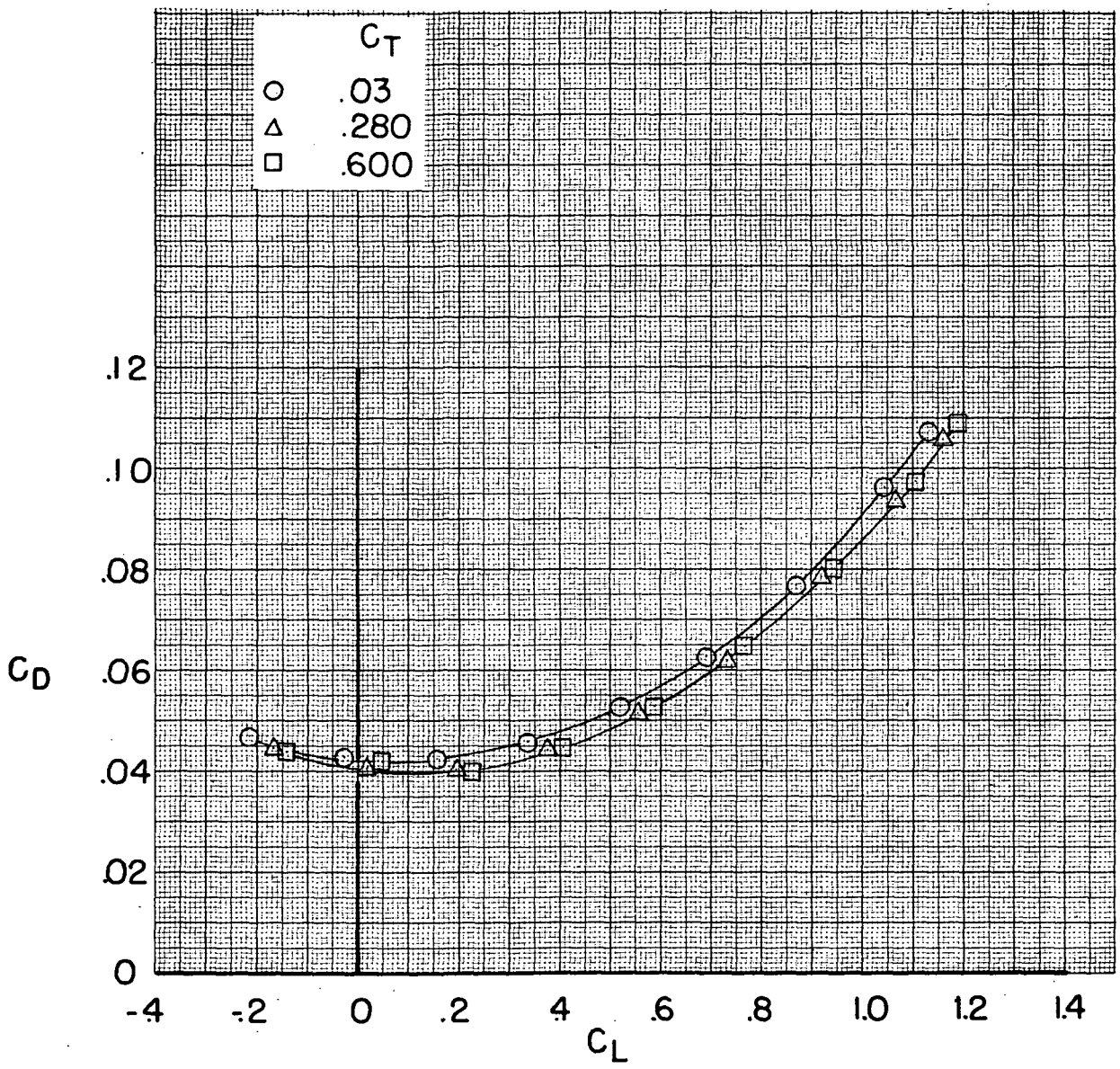

(c) Continued.

Figure 22.- Continued.

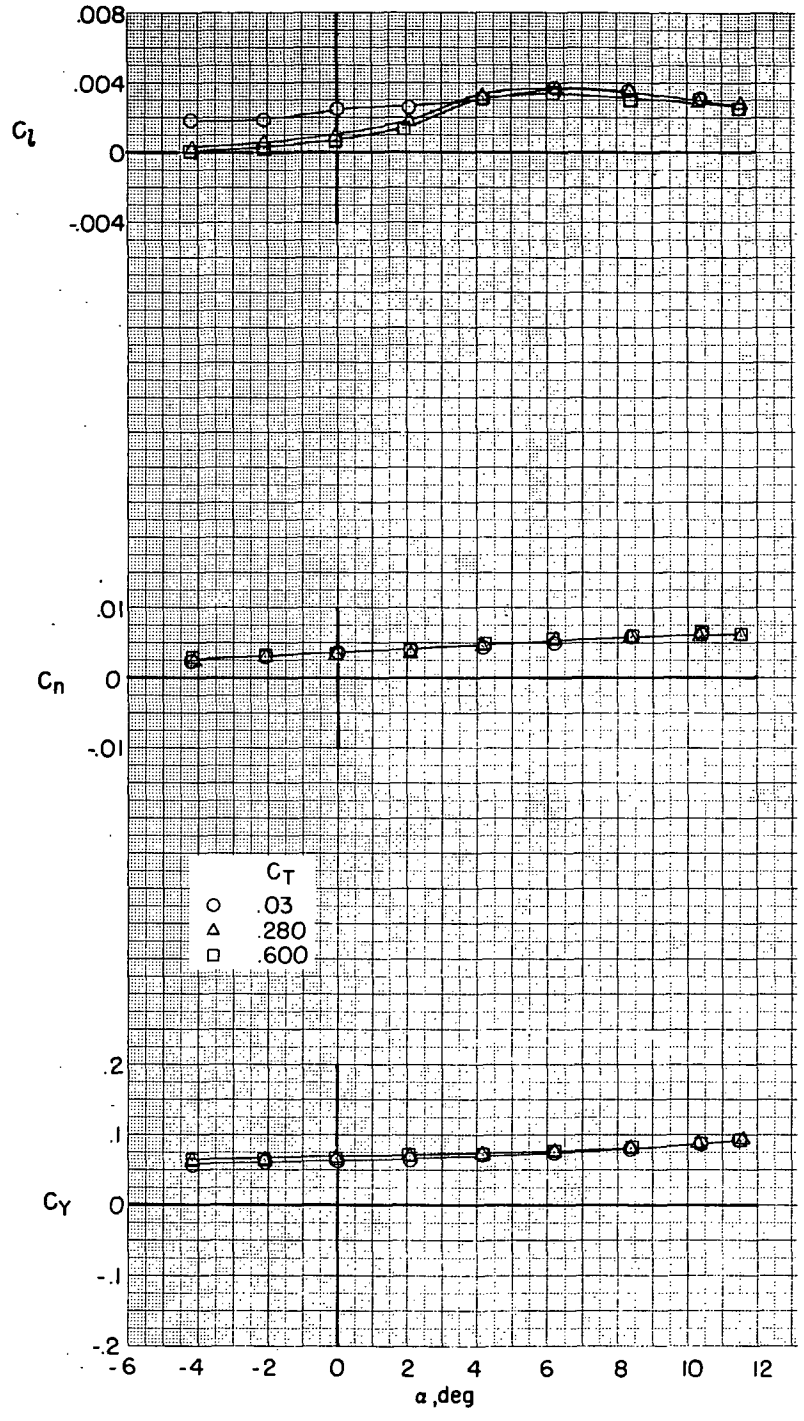

(c) Concluded.

Figure 22.- Concluded.

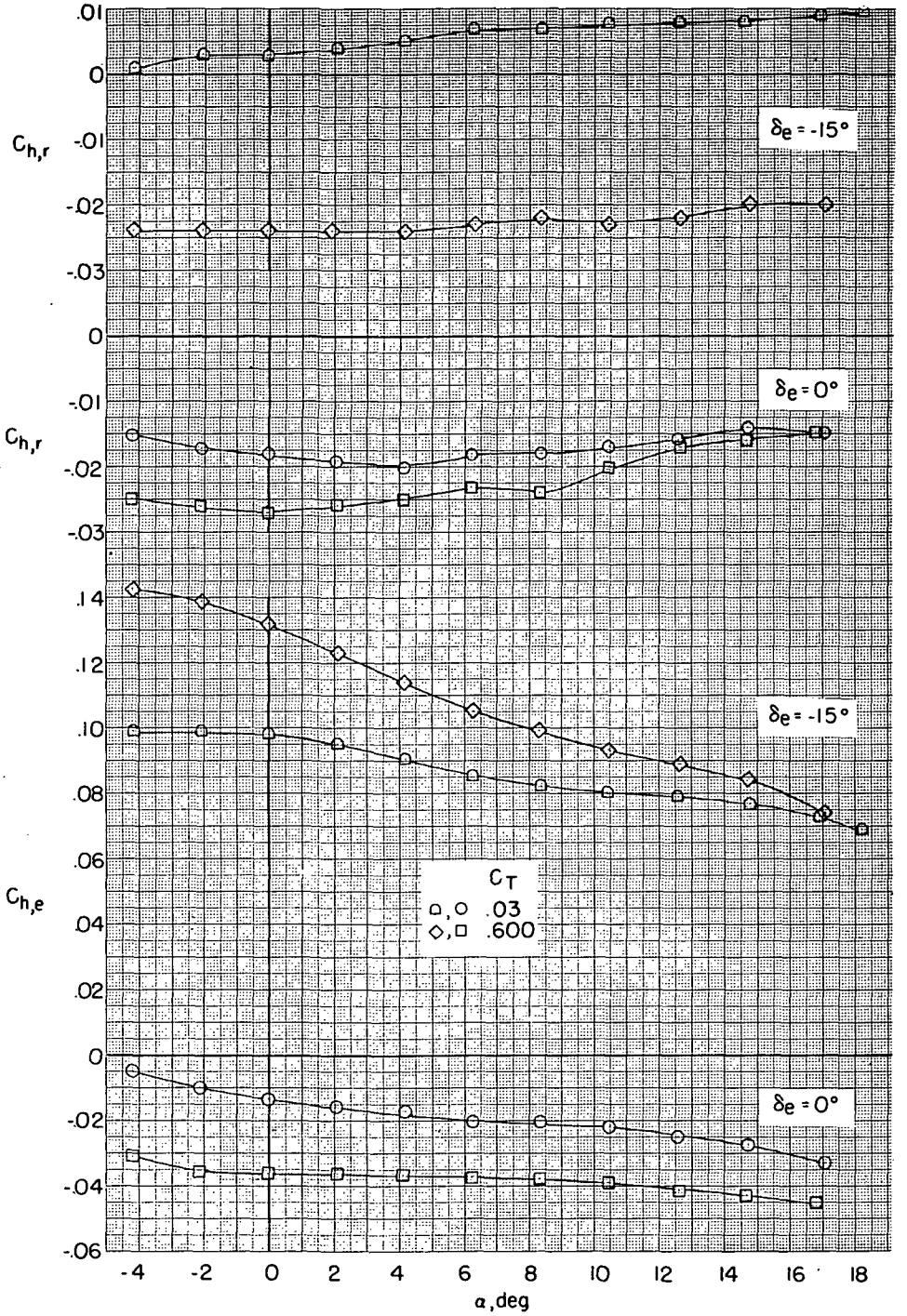

(a) M = 0.225.

Figure 23.- Effect of nacelle thrust coefficient and elevator deflection on the elevator and rudder hinge-moment coefficients. $\delta_f = 0^o$; $\beta = 0^o$; $i_n = 4^o$; $h = \infty$.

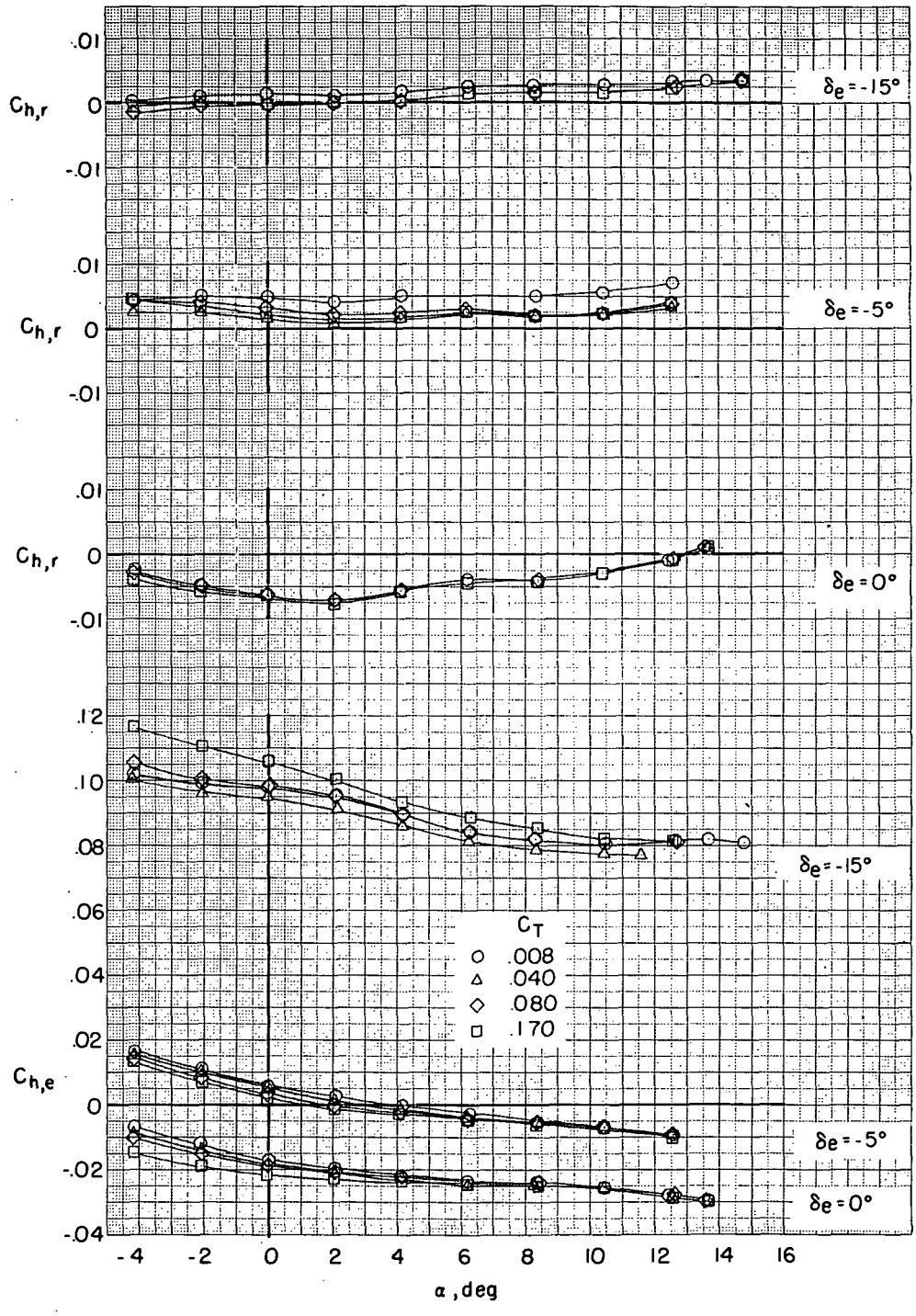

(b) M = 0.45.

Figure 23.- Continued.

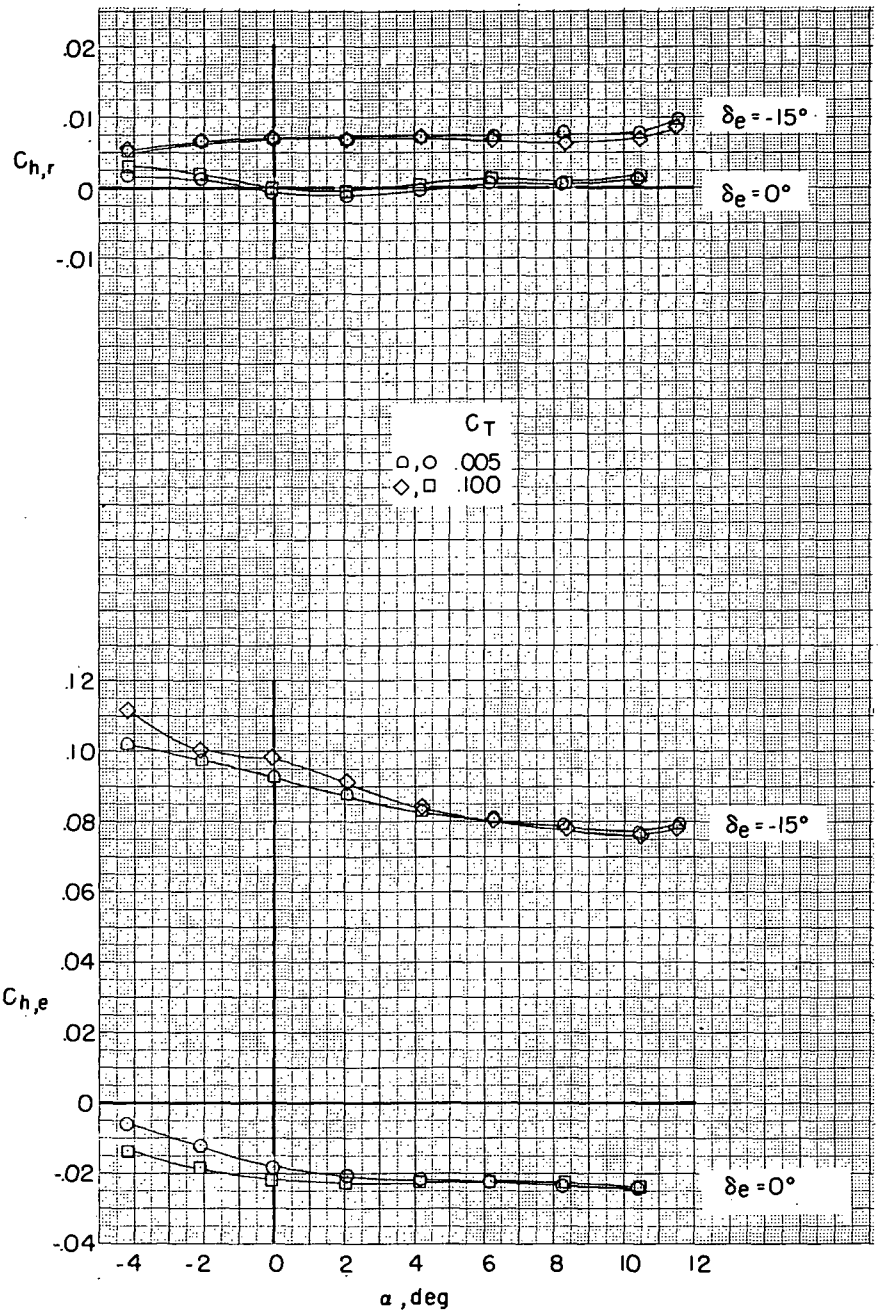

(c) M = 0.60.

Figure 23.- Continued.

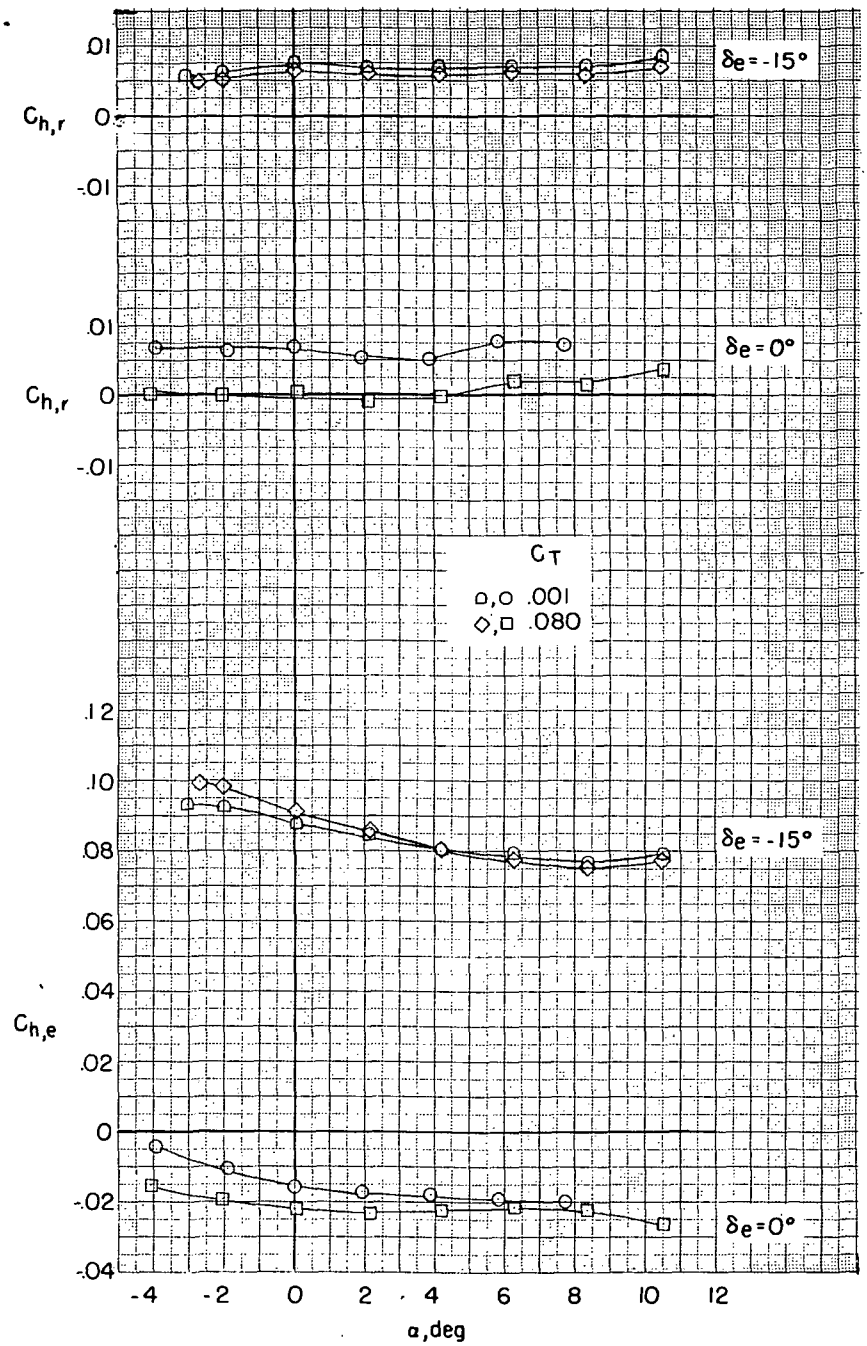

(d) M = 0.70.

Figure 23.- Continued.

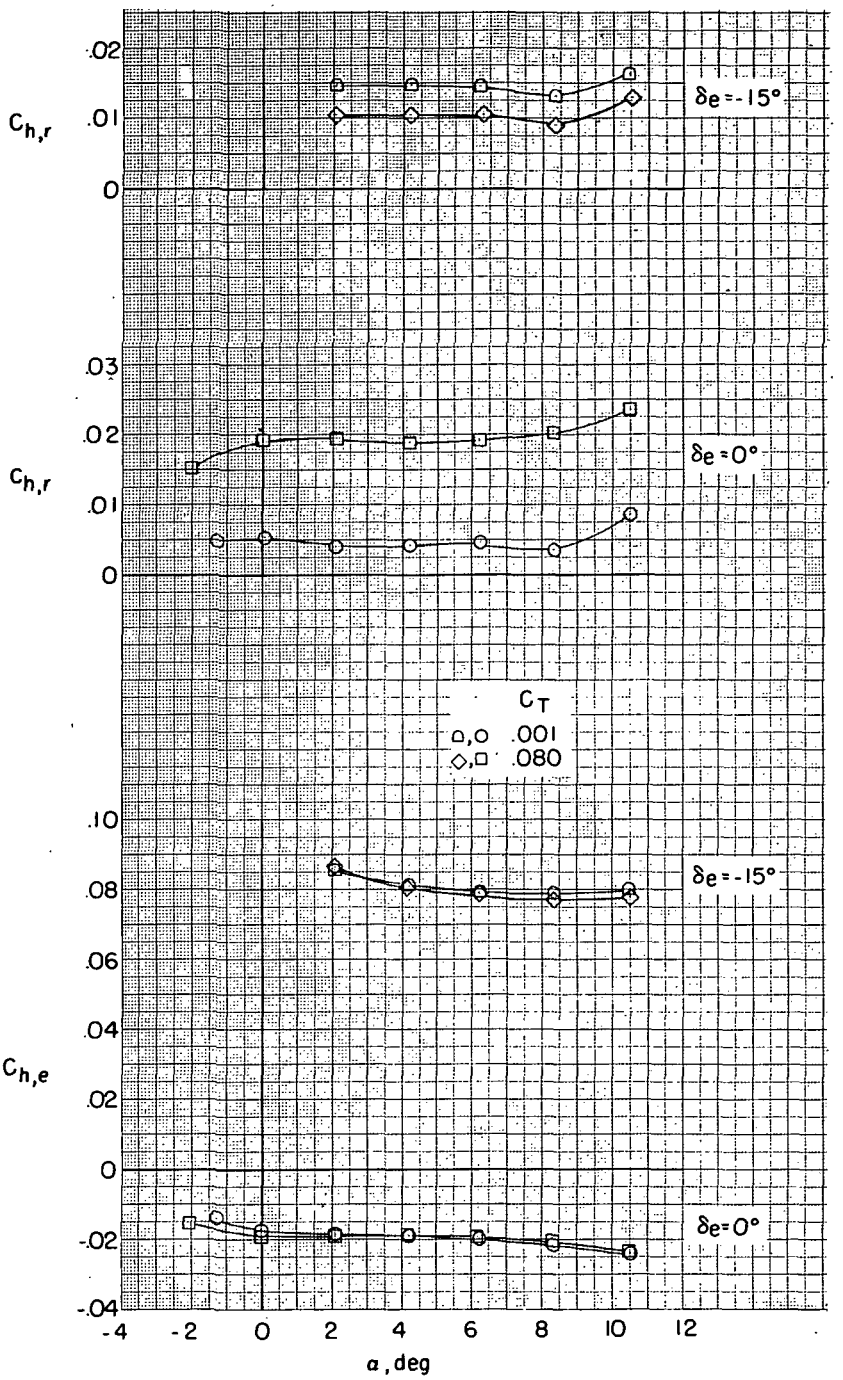

(e) M = 0.73.

Figure 23.- Concluded.

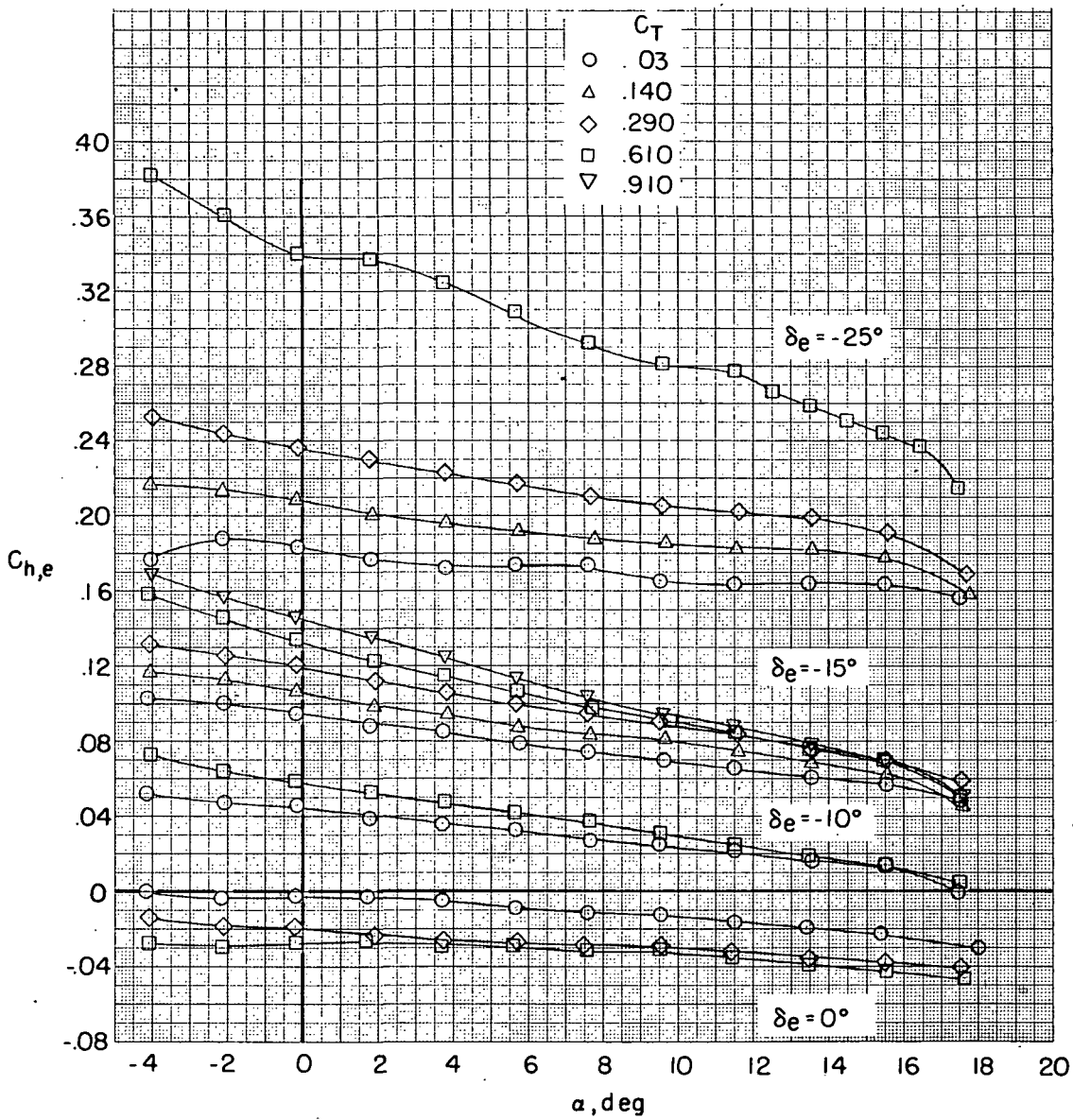

(a) $C_{h,e}$ as a function of α.

Figure 24.- Effect of nacelle thrust coefficient and elevator deflection on the elevator and rudder hinge-moment coefficients. $M = 0.225$; $\delta_f = 30^o$; $\beta = 0^o$; $i_n = 4^o$; $h = \infty$.

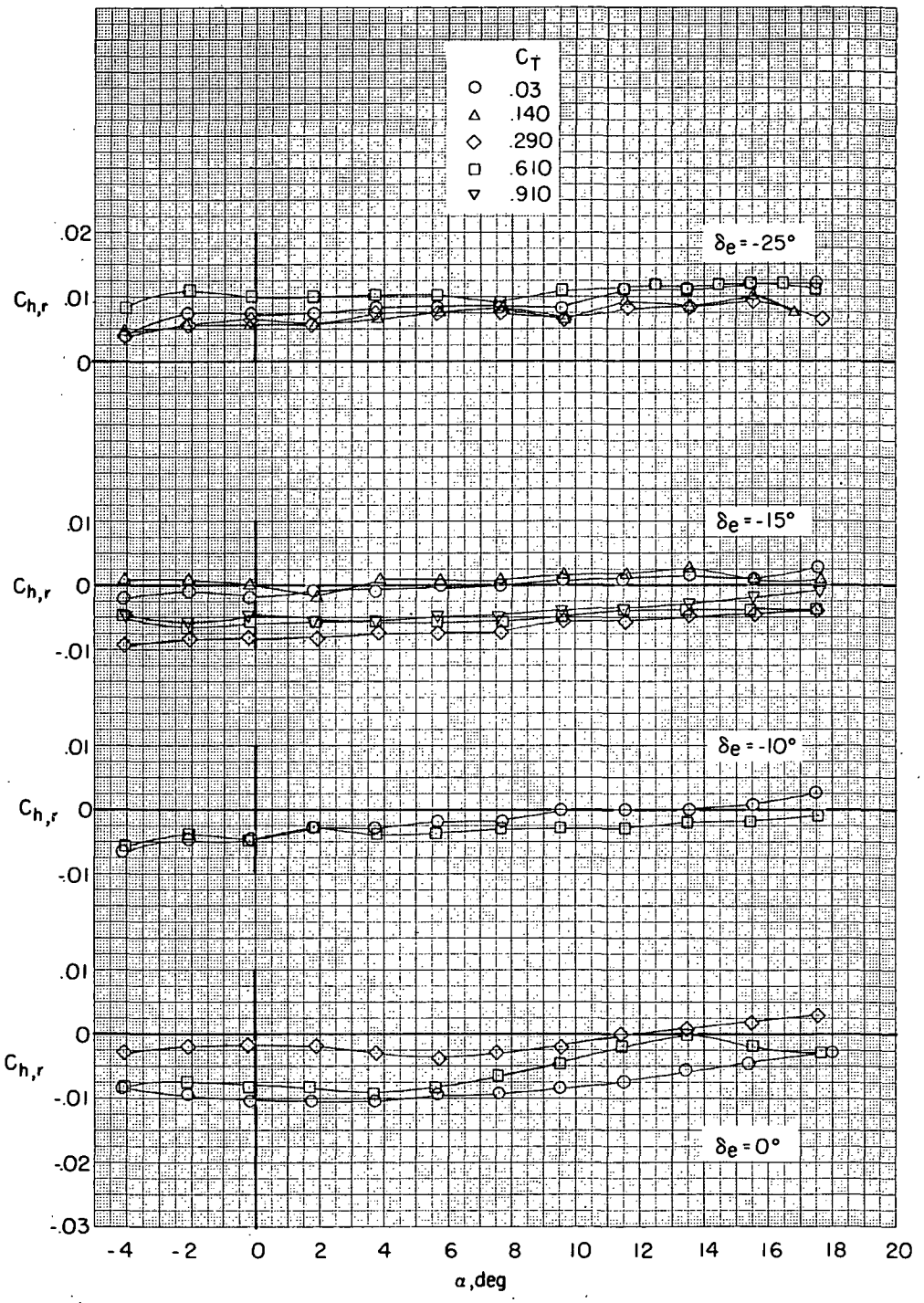

(b) $C_{h,r}$ as a function of α.

Figure 24.- Concluded.

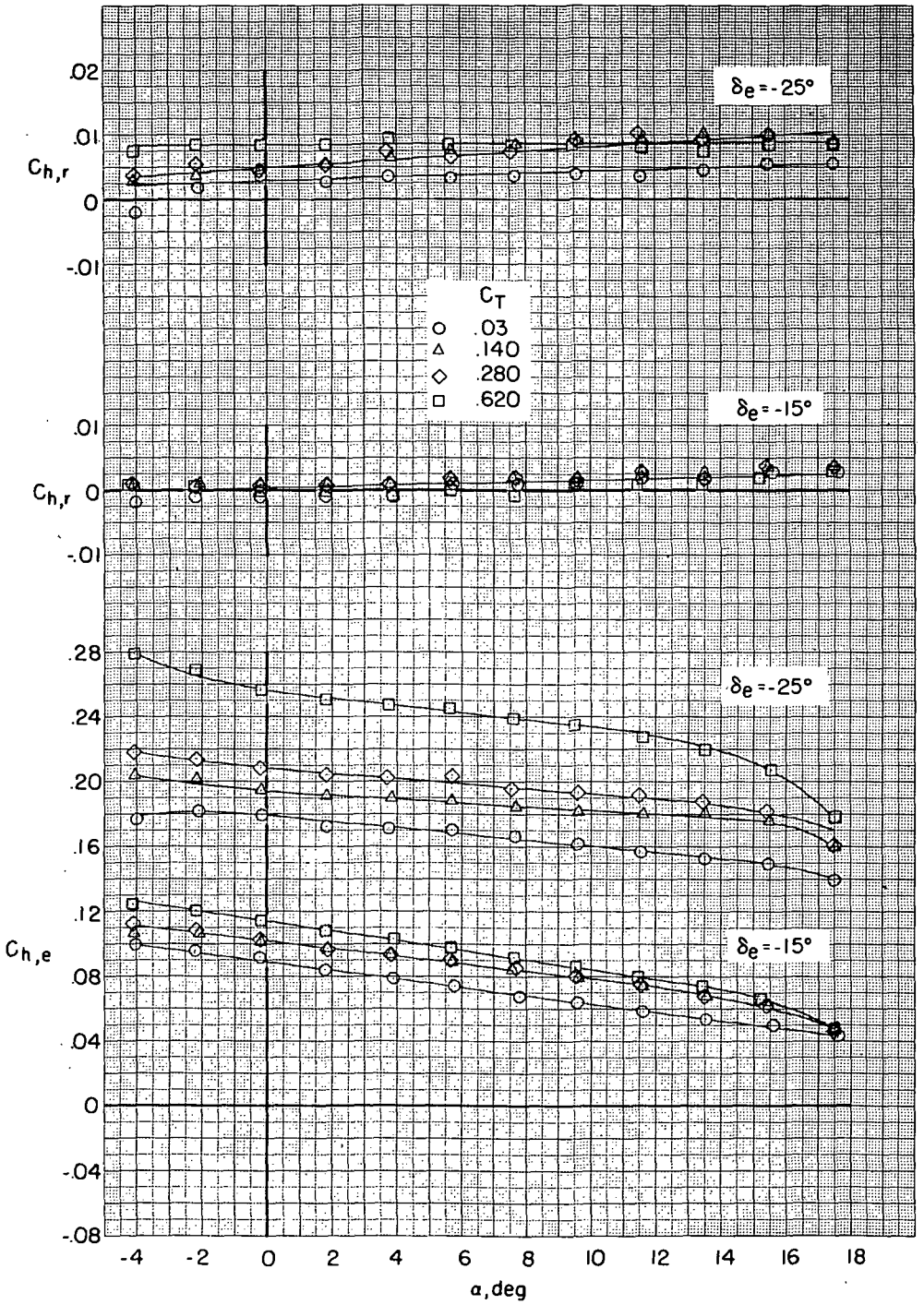

Figure 25.- Effect of nacelle thrust coefficient and elevator deflection on the elevator and rudder hinge-moment coefficients. M = 0.225; $\delta_f = 30^o$; $\beta = 0^o$; $i_n = 2^o$; h = ∞.

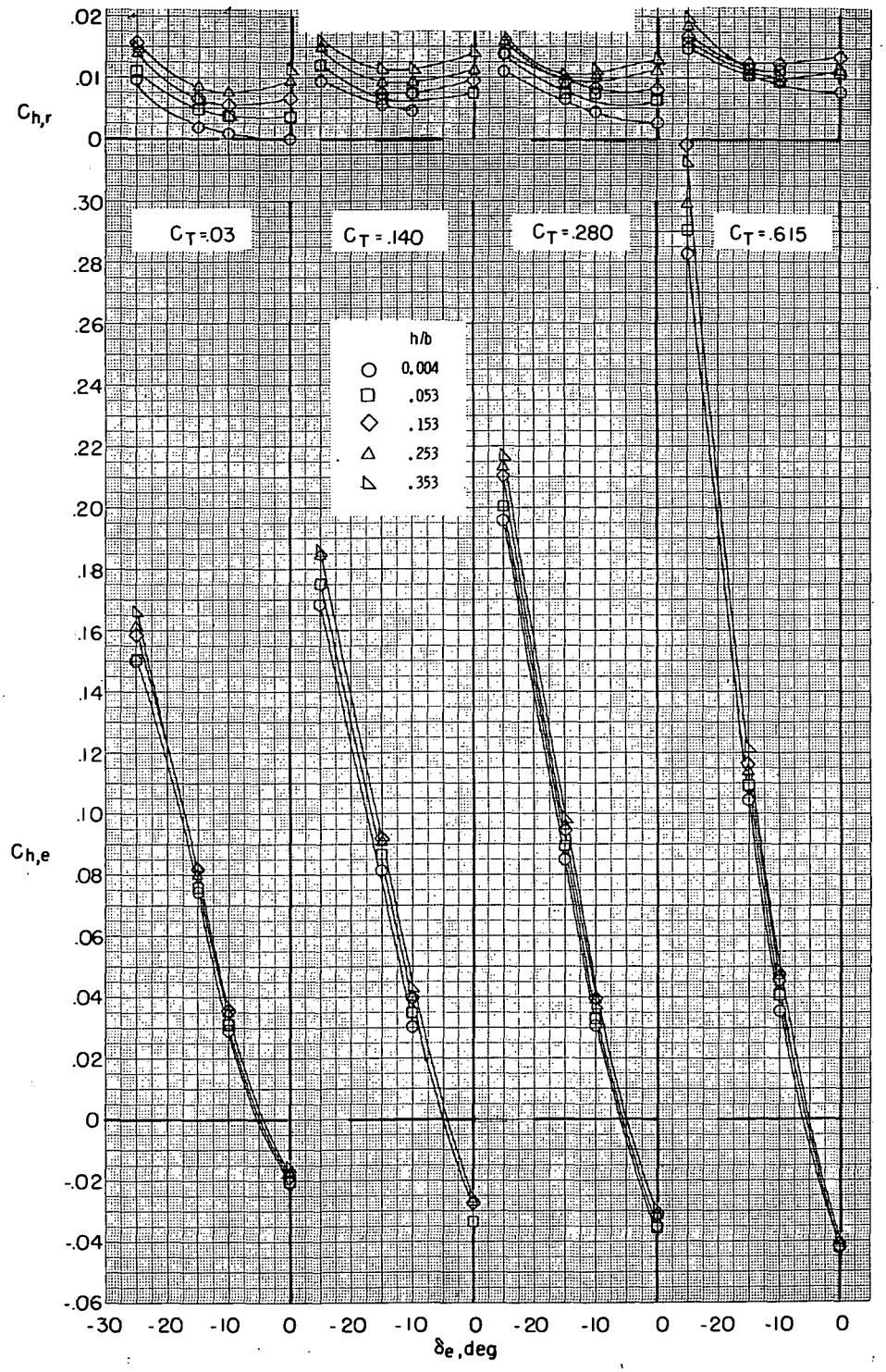

Figure 26.- Effect of nacelle thrust coefficient and model height on the elevator and rudder hinge-moment coefficients with ground plane in place. $M = 0.225$; $\delta_f = 30^o$; $\beta = 0^o$; $i_n = 4^o$; $\alpha \approx 0^o$.

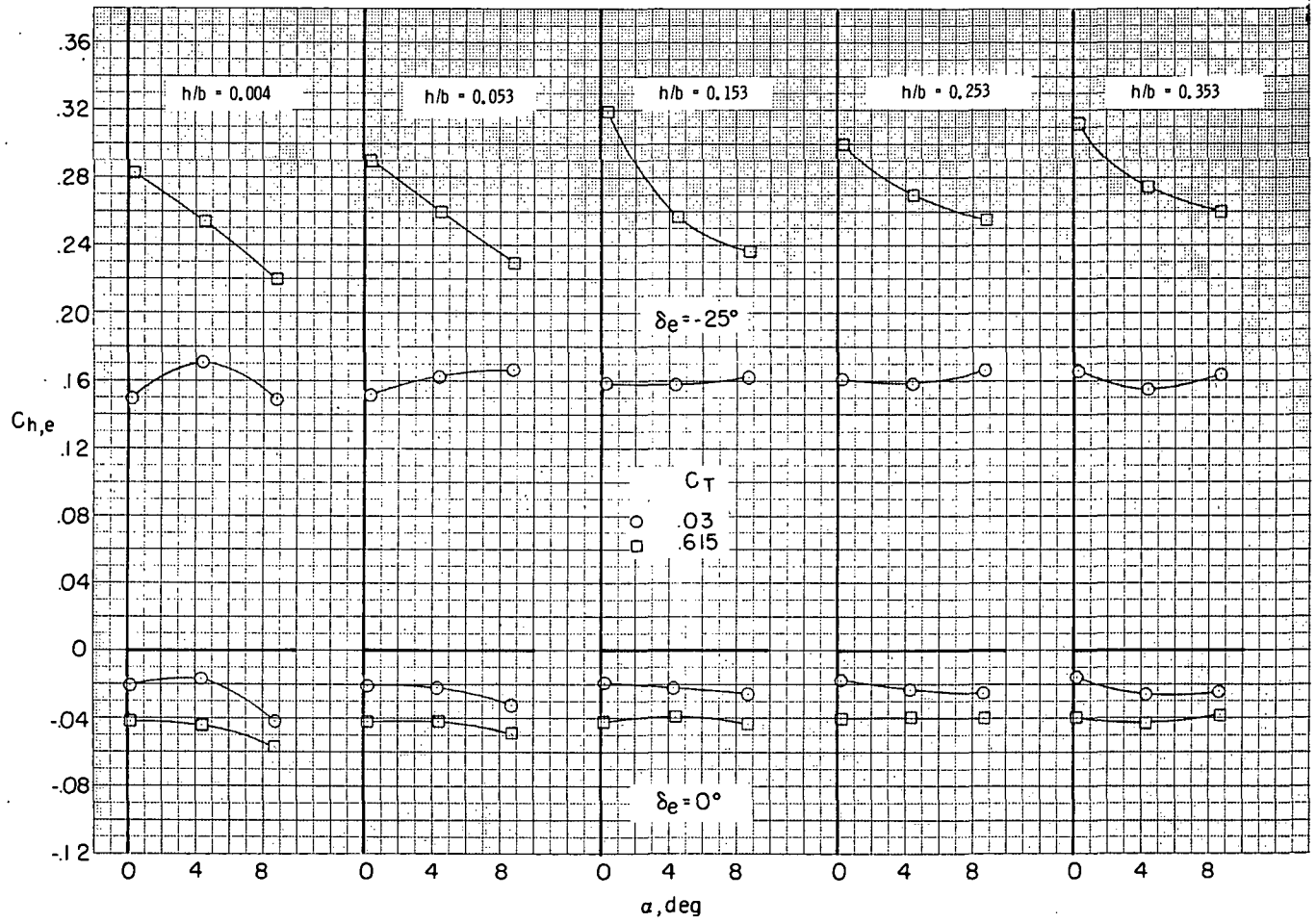

(a) $C_{h,e}$ as a function of α.

Figure 27.- Effect of nacelle thrust coefficient, elevator deflection, and model height on the elevator and rudder hinge-moment coefficients with ground plane in place. M = 0.225; $\delta_f = 30^o$; $\beta = 0^o$; $i_n = 4^o$.

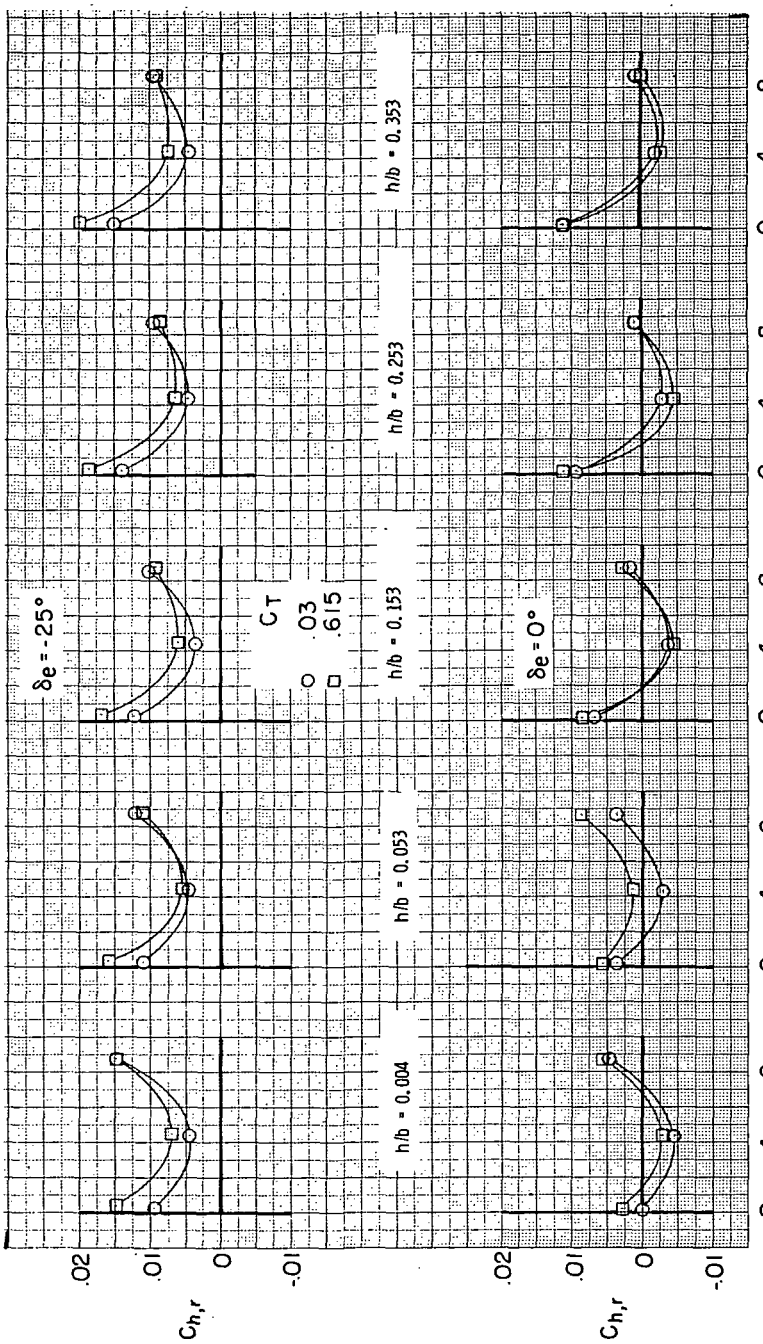

(b) $C_{h,r}$ as a function of α.

Figure 27.- Concluded.

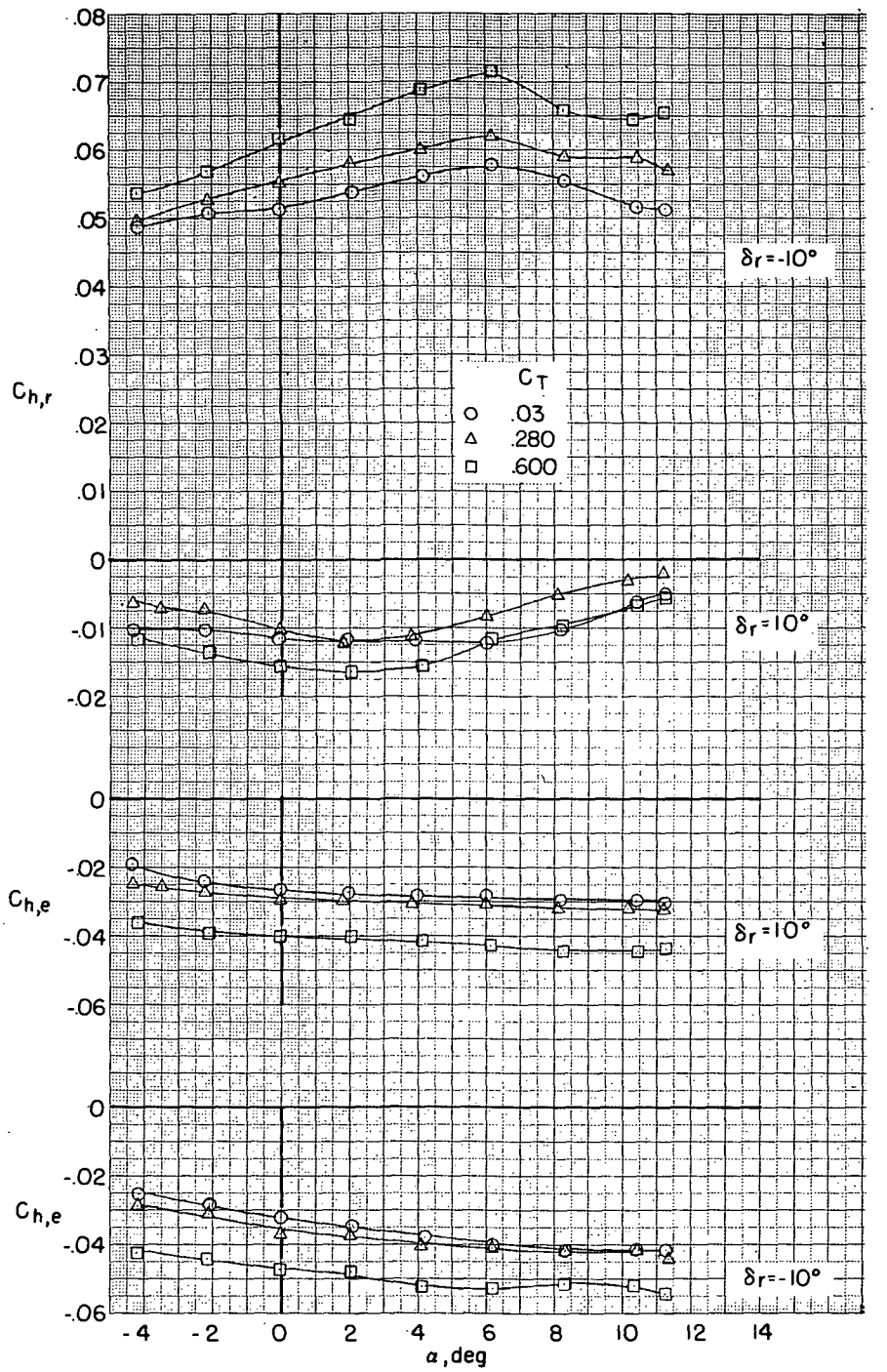

(a) $\beta = 9^{o}$.

Figure 28.- Effect of nacelle thrust coefficient and rudder deflection on the elevator and rudder hinge-moment coefficients. M = 0.225; $\delta_e = 0^{o}$; $\delta_f = 0^{o}$; $i_n = 4^{o}$; $h = \infty$.

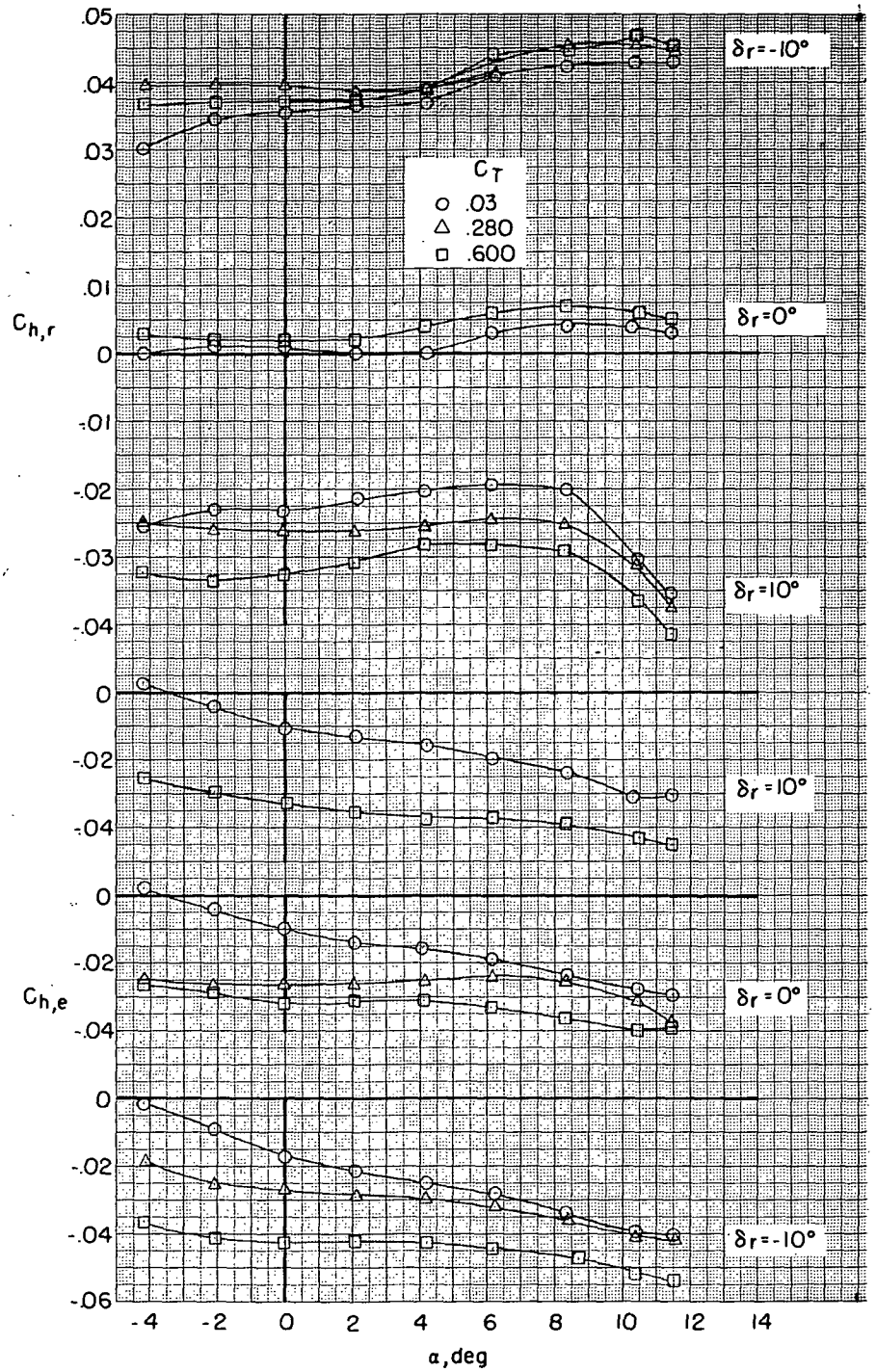

(b) $\beta = -9^{o}$.

Figure 28.- Concluded.

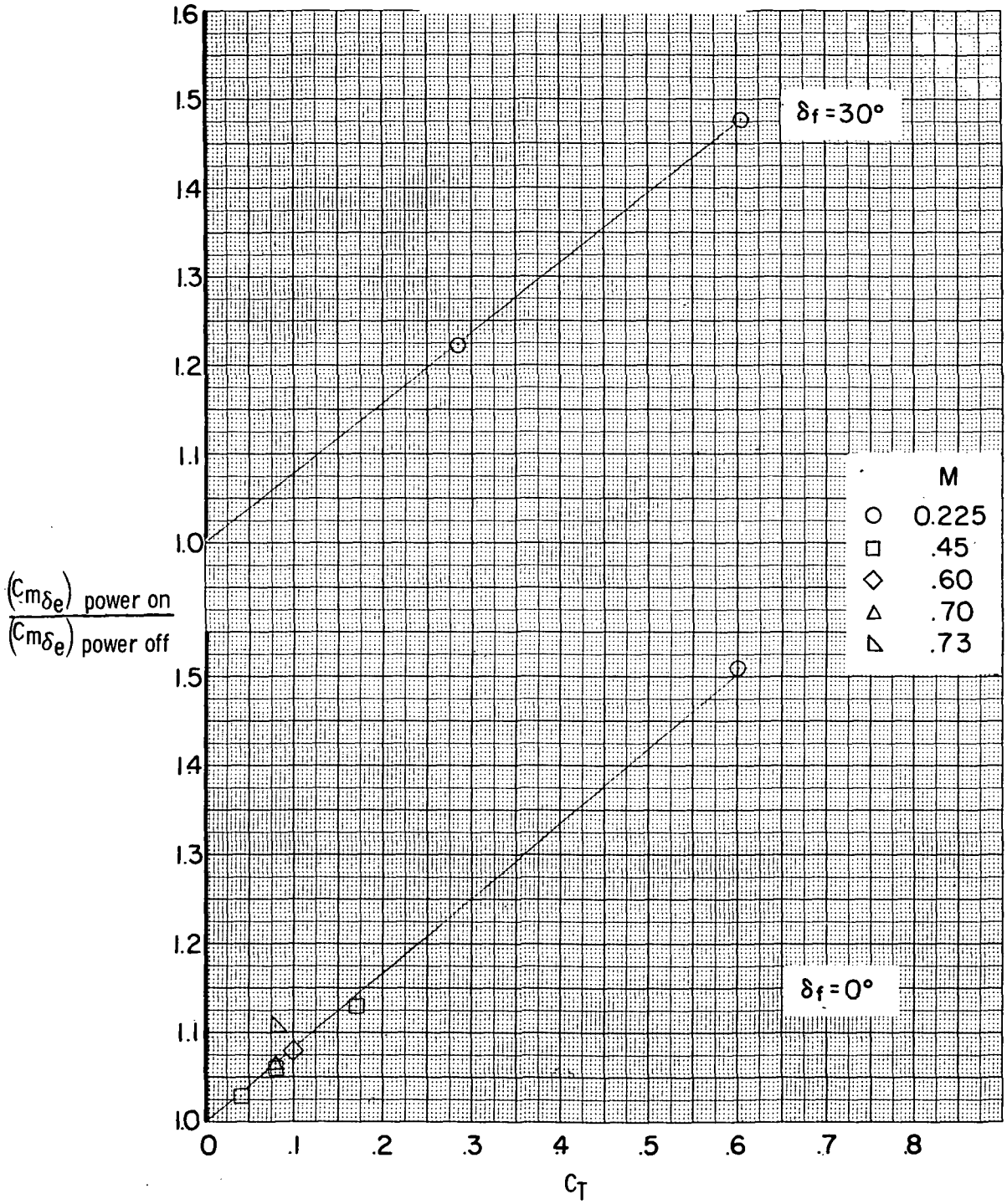

Figure 29.- Effect of Mach number and flap deflection on the longitudinal control parameter. $C_L \approx 0.5$.

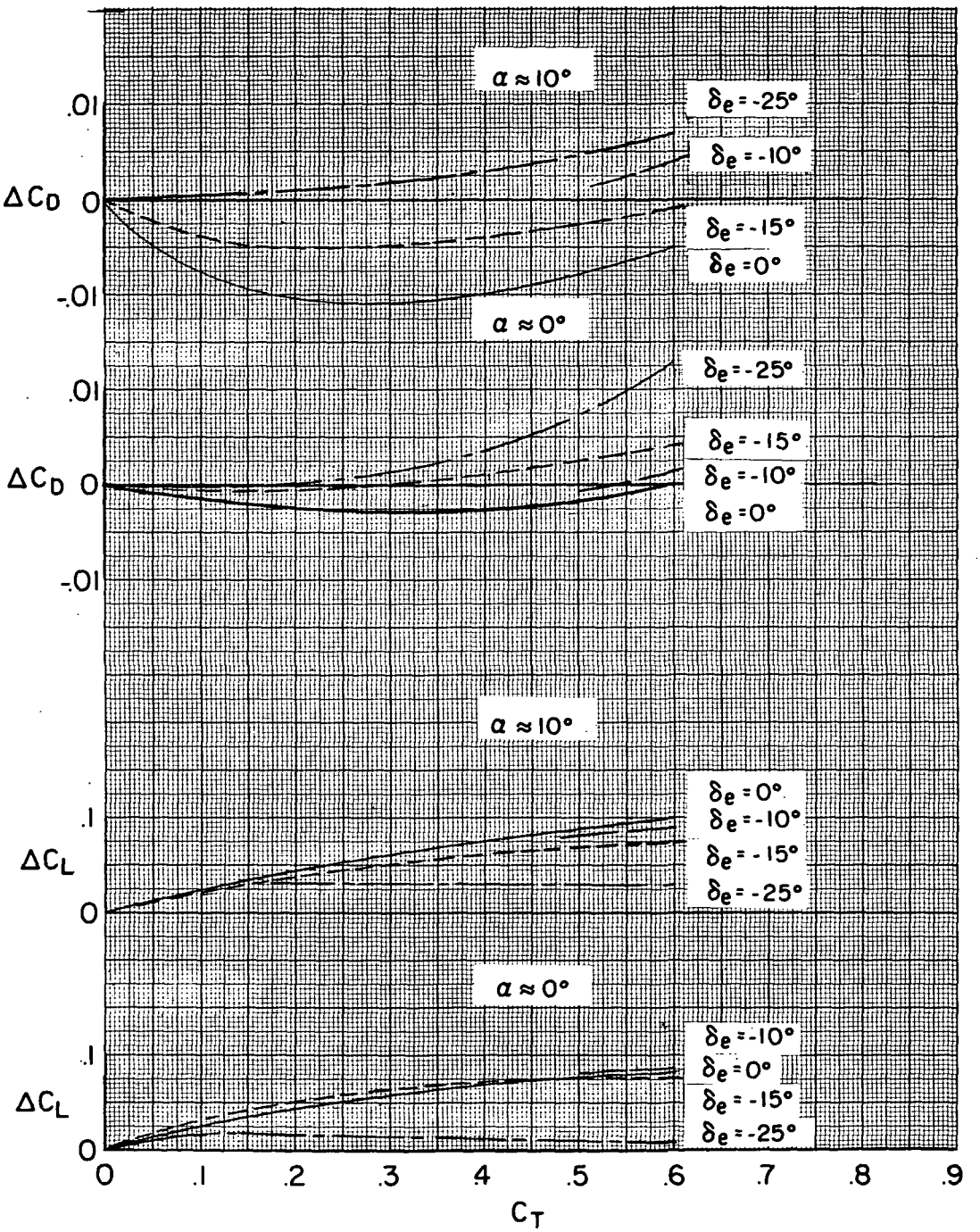

Figure 30.- Increments in lift, drag, and pitching-moment coefficients due to nacelle blowing. Data from figure 17.

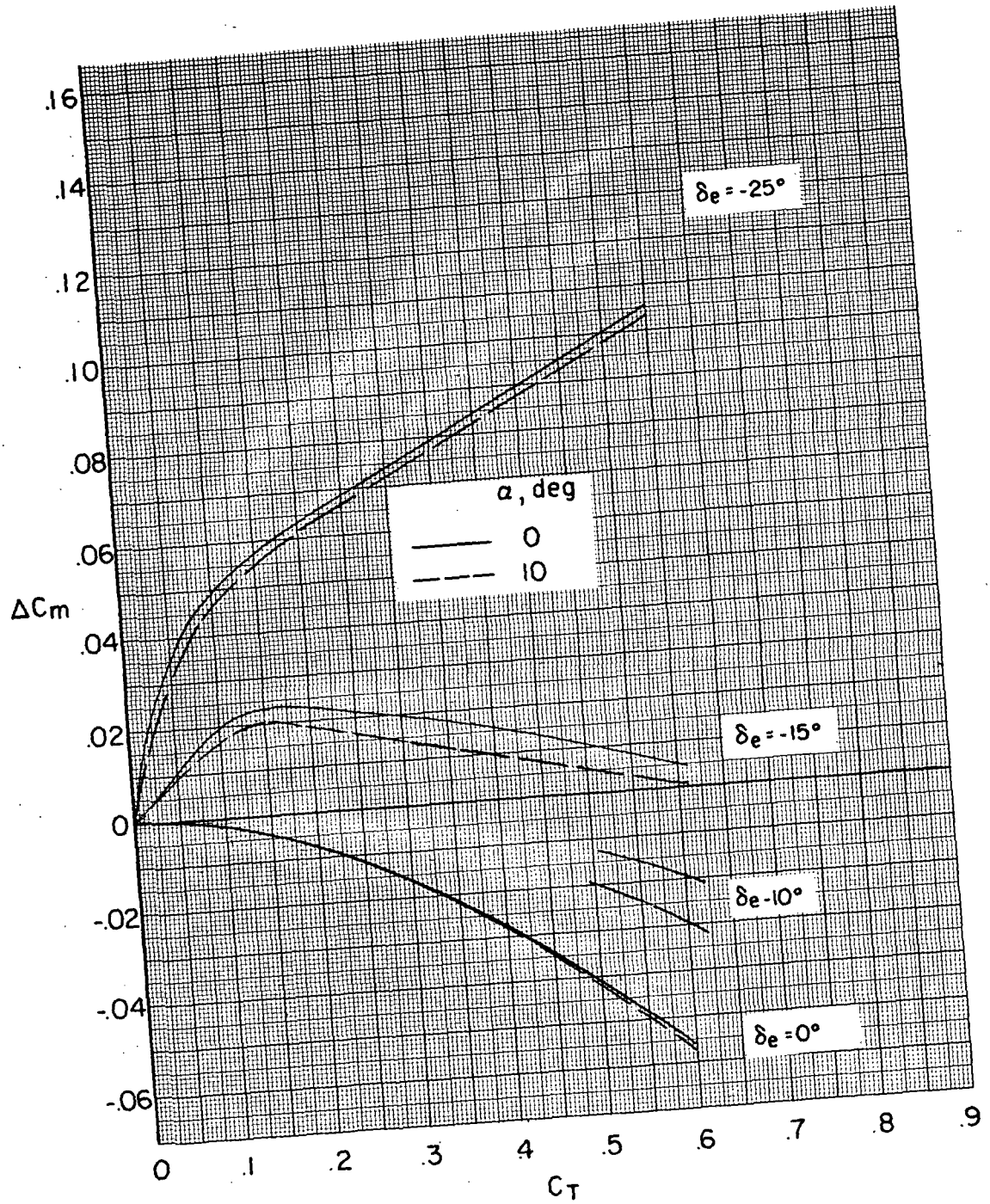

Figure 30.- Concluded.

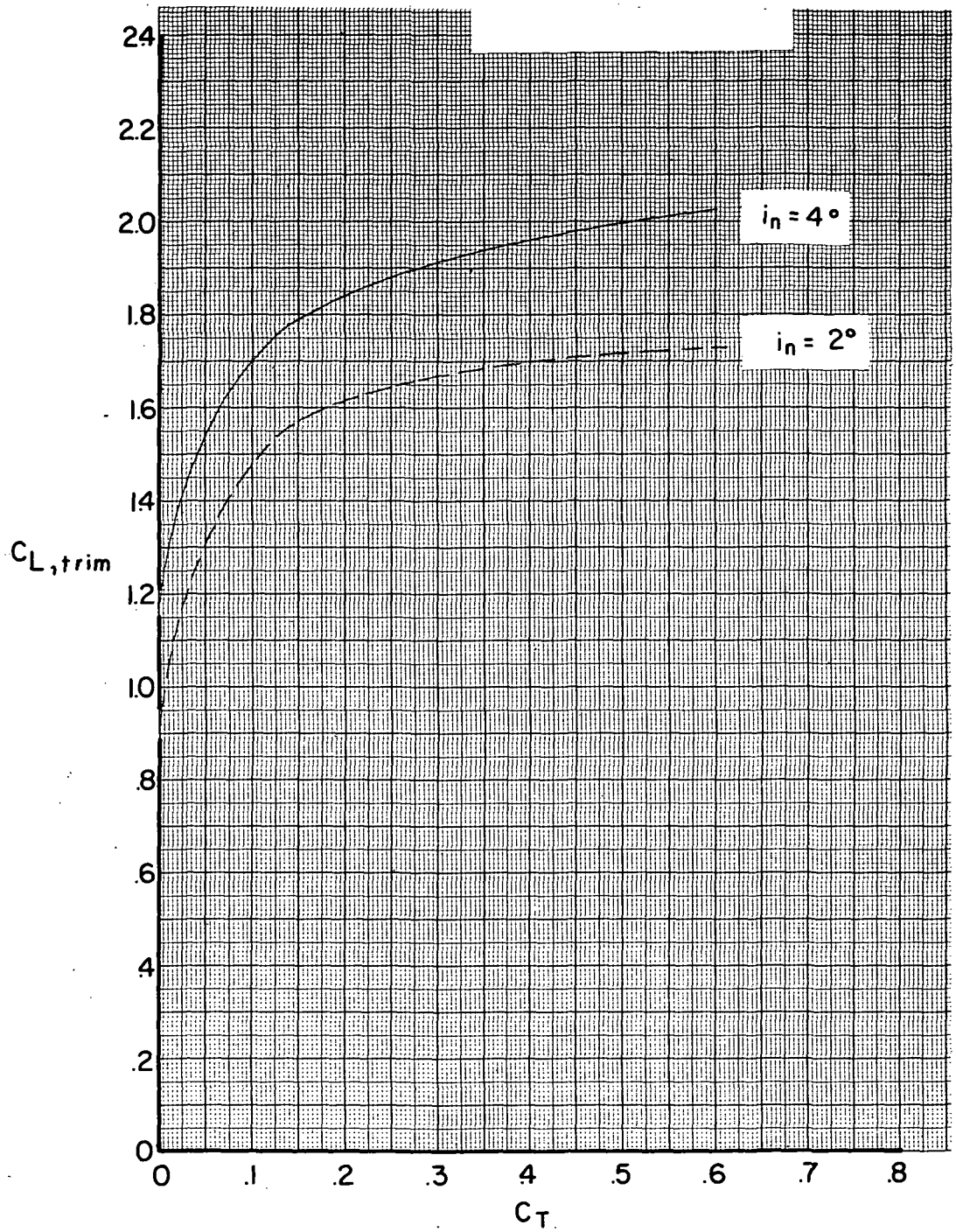

Figure 31.- Effect of nacelle incidence on the maximum trim lift coefficient. $\delta_e = -25^o$; $M = 0.225$; $\delta_f = 30^o$; $\beta = 0^o$; $h = \infty$.

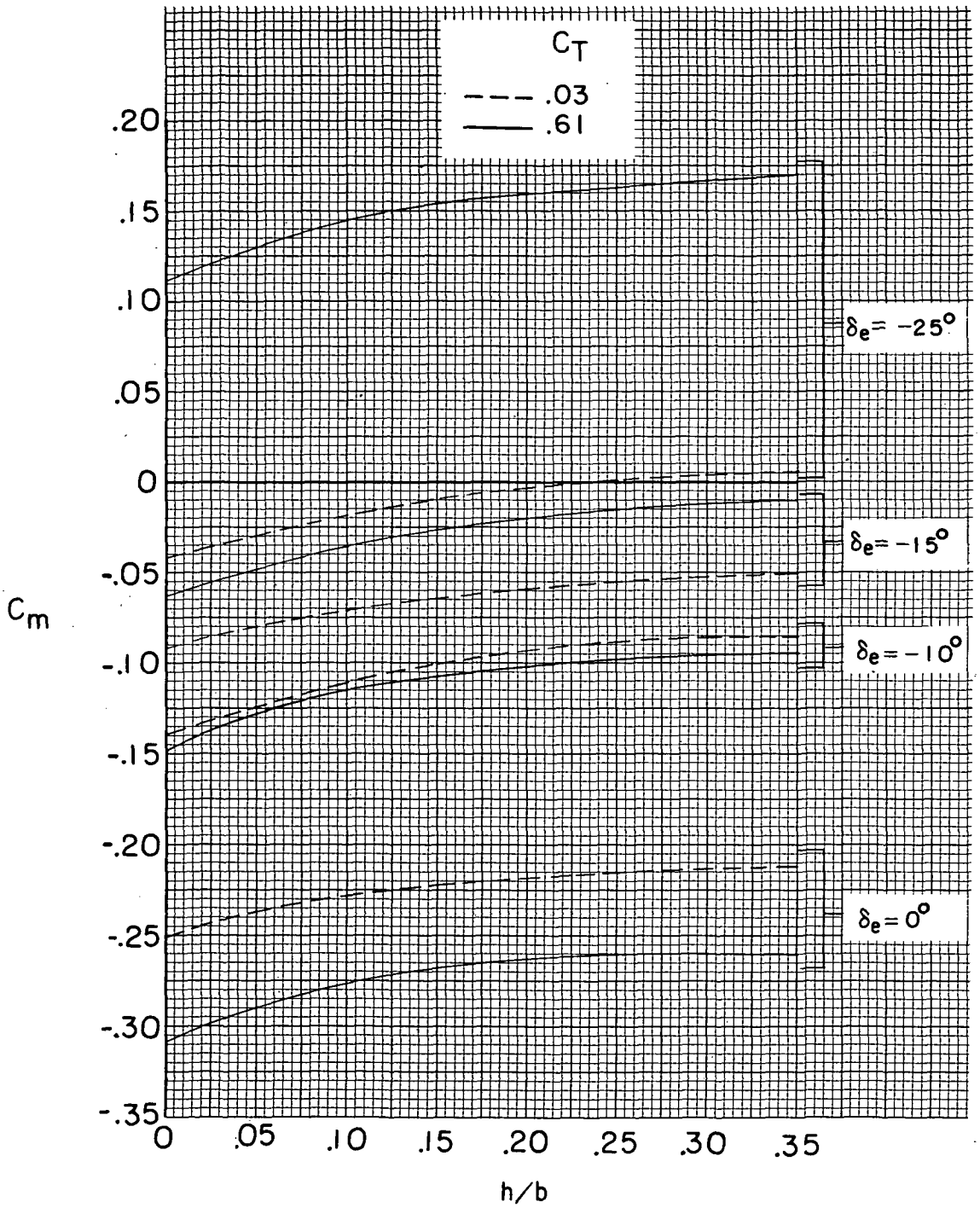

Figure 32.- Effect of thrust coefficient on the pitching-moment coefficients with the ground plane in place. $M = 0.225$; $\delta_f = 30°$; $\alpha = 0°$.

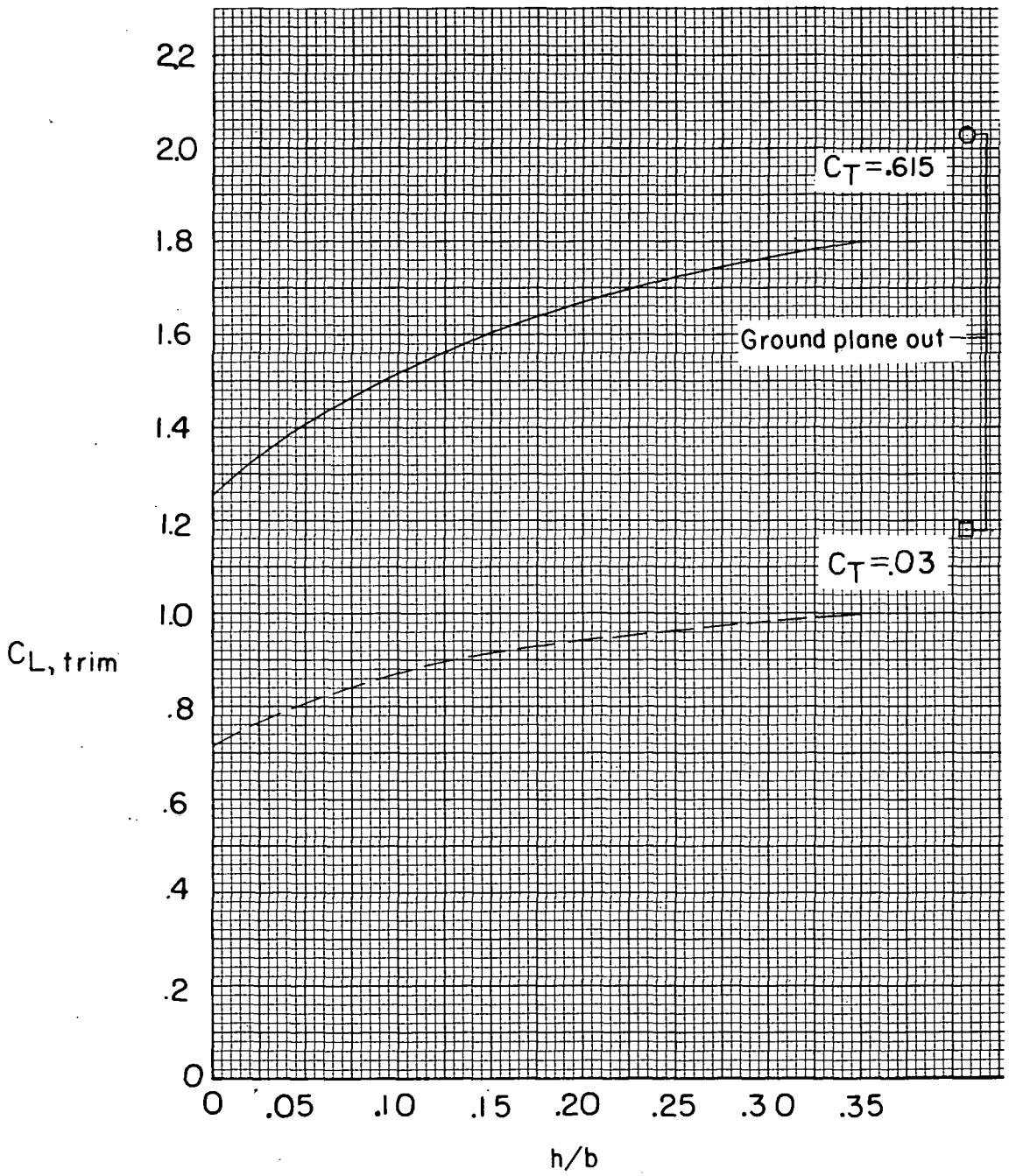

Figure 33.- Effect of nacelle thrust coefficient on the trim lift coefficient with the ground plane in place. $\delta_e = -25^o$.

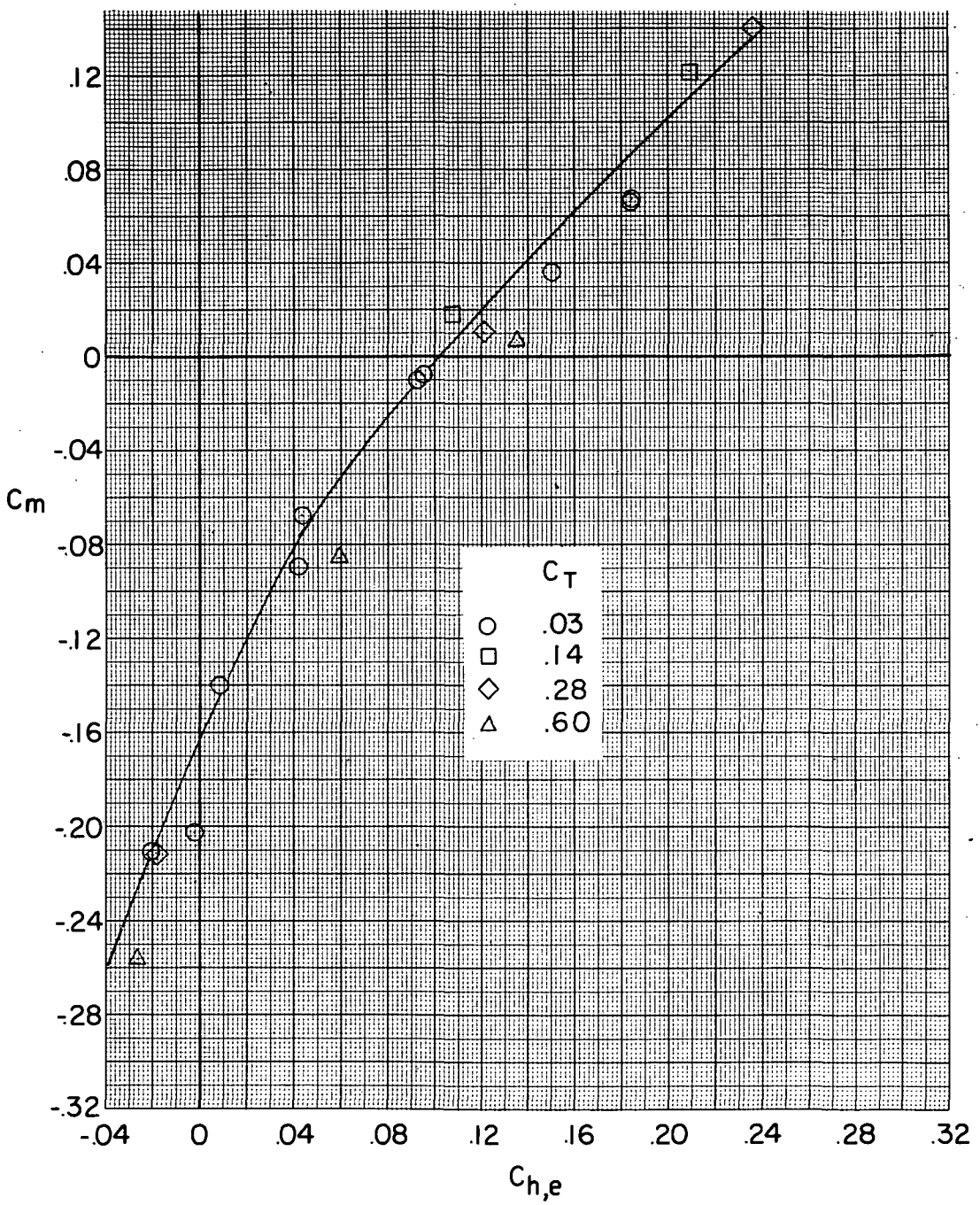

(a) h = ∞.

Figure 34.- Effect of nacelle thrust coefficient and model height on the variation of pitching-moment coefficient with elevator hinge-moment coefficient. M = 0.225; $\delta_f = 30^o$; $\beta = 0^o$; $i_n = 4^o$; $\alpha \approx 0^o$.

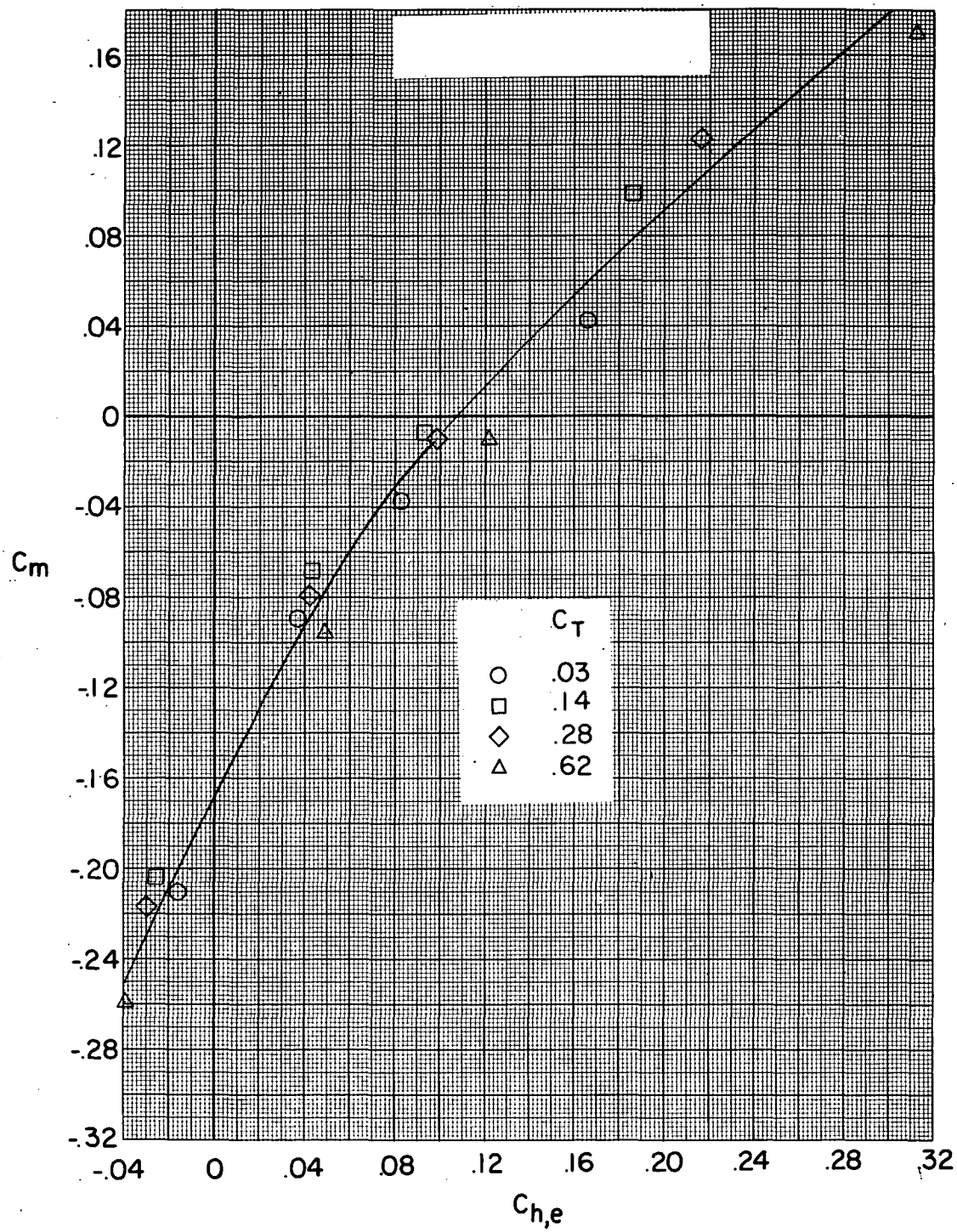

(b) h/b = 0.353.

Figure 34.- Continued.

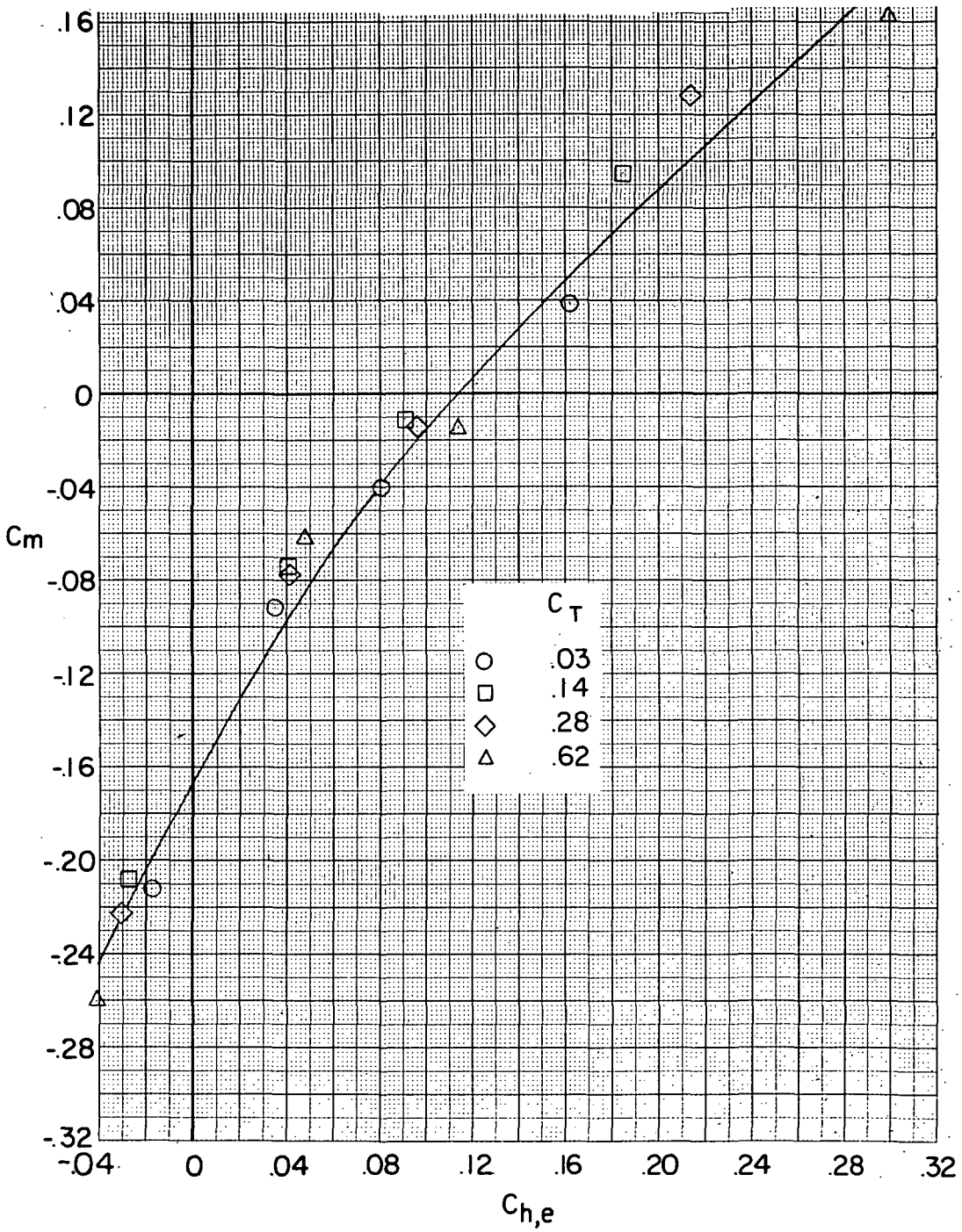

(c) h/b = 0.253.

Figure 34.- Continued.

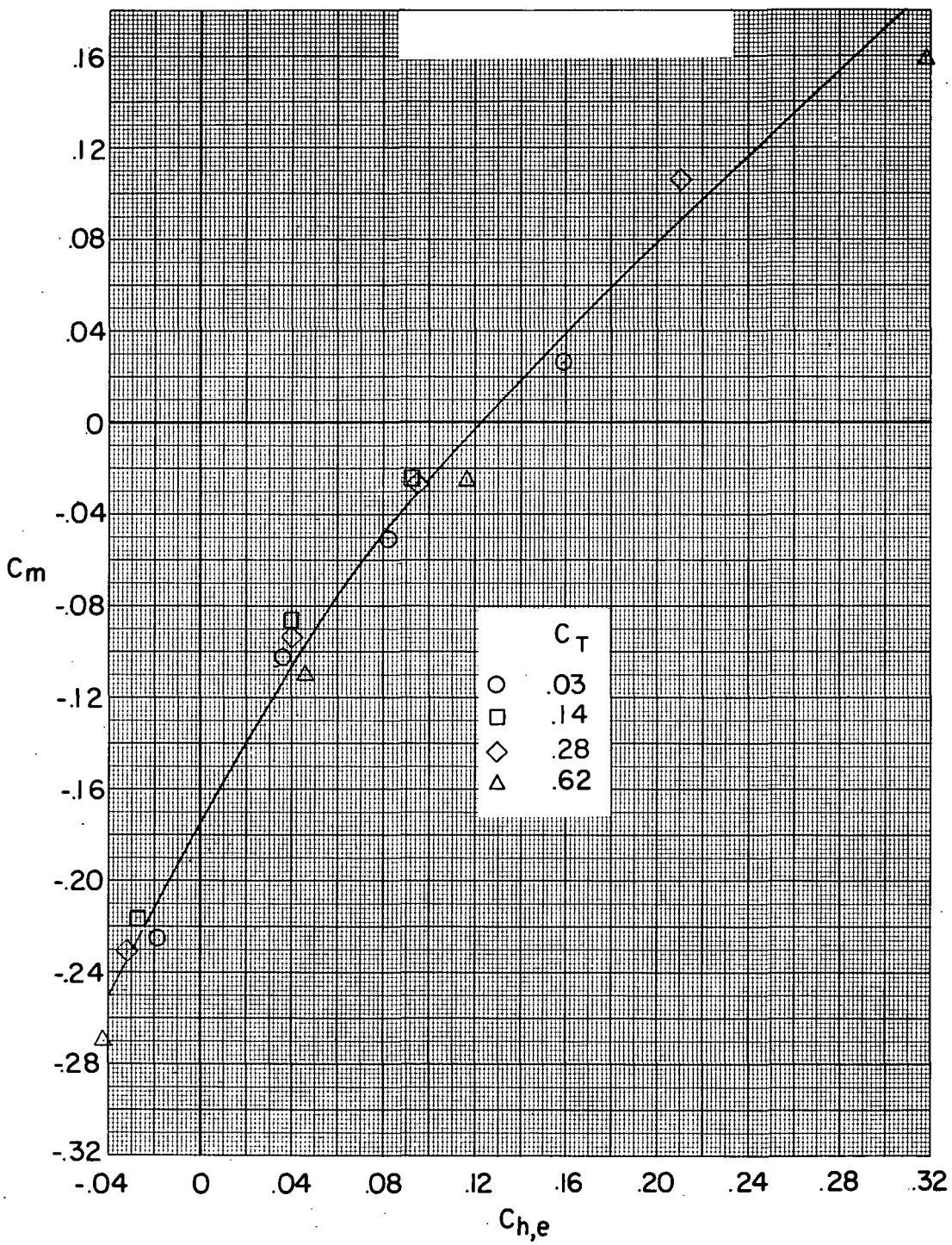

(d) h/b = 0.153.

Figure 34.- Continued.

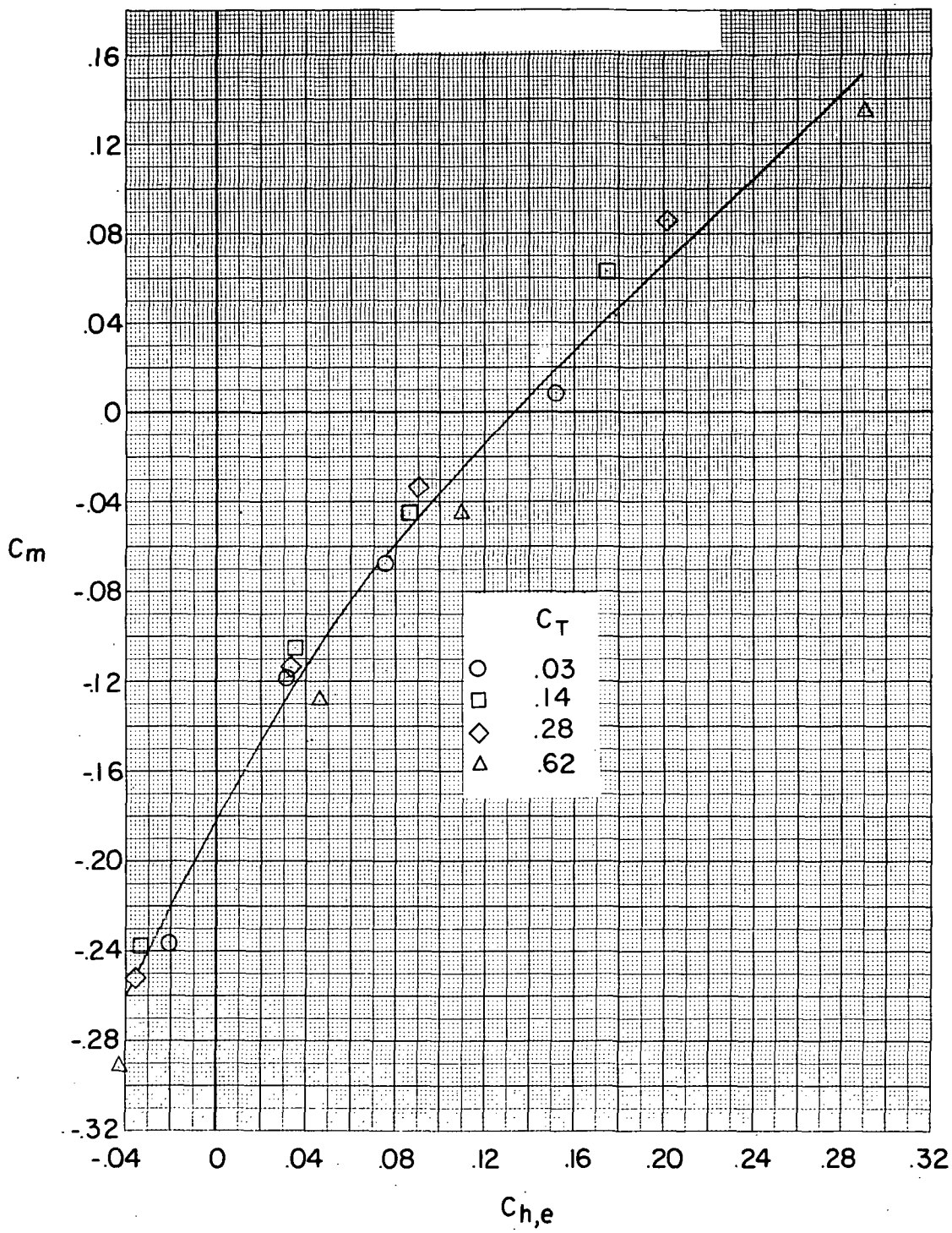

(e) h/b = 0.053.

Figure 34.- Continued.

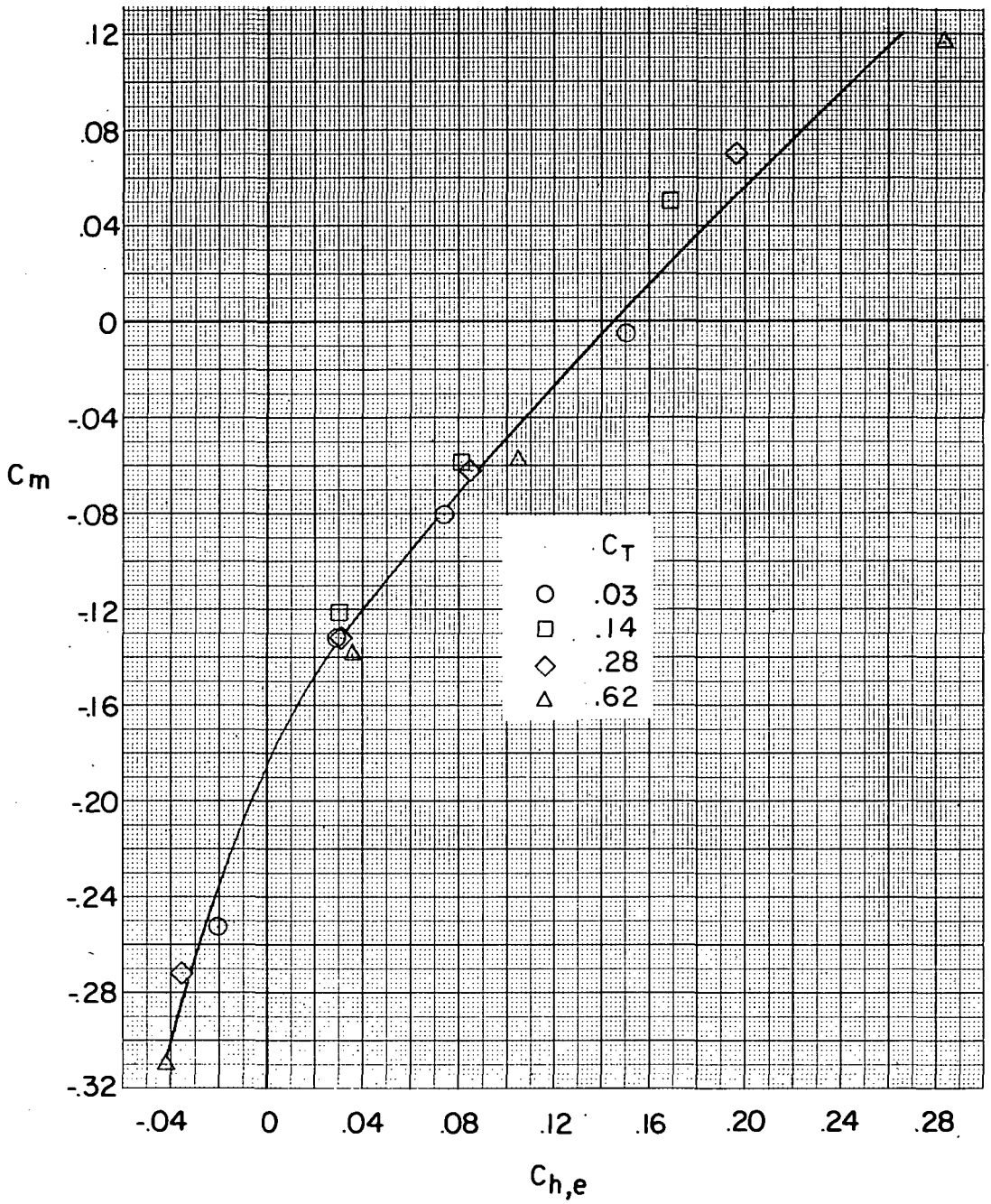

(f) h/b = 0.004.

Figure 34.- Concluded.

NASA-Langley, 1974 L-9569

"The aeronautical and space activities of the United States shall be conducted so as to contribute . . . to the expansion of human knowledge of phenomena in the atmosphere and space. The Administration shall provide for the widest practicable and appropriate dissemination of information concerning its activities and the results thereof."

—NATIONAL AERONAUTICS AND SPACE ACT OF 1958

NASA SCIENTIFIC AND TECHNICAL PUBLICATIONS

TECHNICAL REPORTS: Scientific and technical information considered important, complete, and a lasting contribution to existing knowledge.

TECHNICAL NOTES: Information less broad in scope but nevertheless of importance as a contribution to existing knowledge.

TECHNICAL MEMORANDUMS: Information receiving limited distribution because of preliminary data, security classification, or other reasons. Also includes conference proceedings with either limited or unlimited distribution.

CONTRACTOR REPORTS: Scientific and technical information generated under a NASA contract or grant and considered an important contribution to existing knowledge.

TECHNICAL TRANSLATIONS: Information published in a foreign language considered to merit NASA distribution in English.

SPECIAL PUBLICATIONS: Information derived from or of value to NASA activities. Publications include final reports of major projects, monographs, data compilations, handbooks, sourcebooks, and special bibliographies.

TECHNOLOGY UTILIZATION PUBLICATIONS: Information on technology used by NASA that may be of particular interest in commercial and other non-aerospace applications. Publications include Tech Briefs, Technology Utilization Reports and Technology Surveys.

Details on the availability of these publications may be obtained from:

SCIENTIFIC AND TECHNICAL INFORMATION OFFICE

NATIONAL AERONAUTICS AND SPACE ADMINISTRATION

Washington, D.C. 20546